14:35:17 OCA PAD INITIATION - PROJECT HEADER INFORMATION 12/06/89

Active

Project #: E-21-666 Cost share #: Rev #: 0
Center # : 10/24-6-R6860-0A0 Center shr #: OCA file #:
Work type : RES
Contract#: RP2115-24 Mod #: Document : AGR
Prime #: Contract entity: GTRC

Subprojects ? : N
Main project #:

Project unit: EE Unit code: 02.010.118
Project director(s):
MELIOPOULOS A P EE (404)894-2926

Sponsor/division names: ELECTRIC POWER RES INST /
Sponsor/division codes: 500 / 010

Award period: 891101 to 901031 (performance) 901031 (reports)

Sponsor amount	New this change	Total to date
Contract value	53,786.00	53,786.00
Funded	53,786.00	53,786.00
Cost sharing amount		0.00

Does subcontracting plan apply ?: N

Title: EFFECTS OF GEOMAGNETIC DISTURBANCES ON ELECTRIC POWER TRANSMISSION SYSTEMS

PROJECT ADMINISTRATION DATA

OCA contact: Kathleen R. Ehlinger 894-4820

Sponsor technical contact

DR. MARIO RABINOWITZ
(415)855-2000
ELECTRIC POWER RESEARCH INSTITUTE
3412 HILLVIEW AVENUE
PALO ALTO, CA. 94303

Sponsor issuing office

BARBARA BRATHWAITE
(415)855-2882
ELECTRIC POWER RESEARCH INSTITUTE
3412 HILLVIEW AVENUE
PALO ALTO, CA. 94303

Security class (U,C,S,TS) : U ONR resident rep. is ACO (Y/N): N
Defense priority rating : N/A N/A supplemental sheet
Equipment title vests with: Sponsor X GIT
NONE PROPOSED.

Administrative comments -
AGREEMENT OF 11/8/89 FUNDS PROJECT FOR $29,640 IN 1989 AND $24,146 IN 1990.

GEORGIA INSTITUTE OF TECHNOLOGY
OFFICE OF CONTRACT ADMINISTRATION

NOTICE OF PROJECT CLOSEOUT

Closeout Notice Date 05/16/91

Project No. E-21-666 Center No. 10/24-6-R6860-0A0

Project Director MELIOPOULOS A P School/Lab ELEC ENGR

Sponsor ELECTRIC POWER RES INST/

Contract/Grant No. RP2115-24 Contract Entity GTRC

Prime Contract No.

Title EFFECTS OF GEOMAGNETIC DISTURBANCES ON ELECTRIC POWER TRANSMISSION SYSTEM

Effective Completion Date 901031 (Performance) 901031 (Reports)

Closeout Actions Required:	Y/N	Date Submitted
Final Invoice or Copy of Final Invoice	Y	
Final Report of Inventions and/or Subcontracts	Y	
Government Property Inventory & Related Certificate	Y	
Classified Material Certificate	N	
Release and Assignment	Y	
Other	N	

CommentsWILL USE THE SPONSOR'S FORM 214 TO CLOSEOUT UPON RECEIPT OF IN-HOUSE DOCUMENTS.

Subproject Under Main Project No.

Continues Project No.

Distribution Required:

Project Director	Y
Administrative Network Representative	Y
GTRI Accounting/Grants and Contracts	Y
Procurement/Supply Services	Y
Research Property Managment	Y
Research Security Services	N
Reports Coordinator (OCA)	Y
GTRC	Y
Project File	Y
Other	N
	N

NOTE: Final Patent Questionnaire sent to PDPI.

EPRI

CONTRACTOR COST PERFORMANCE REPORT

EPRI 177 5/84R

EPRI CONTRACT NUMBER	EPRI DIVISION NUMBER	CONTRACTOR NAME, ADDRESS AND TELEPHONE NUMBER
RP 2115-24	4 (For EPRI Use Only)	Georgia Institute of Technology School of Electrical Engineering Atlanta, GA 30332 (404) 894-2926
EPRI PROJECT MANAGER Name M. Rabinowitz	PERIOD OF PERFORMANCE From 11/1/89 to 10/31/90	

Note:
- **Instructions for completing this form are on the reverse side.**
- **All figures are to be shown in U.S. dollars—whole thousands only.**
- **Show EPRI portion of the contract only. Do not include contractor cost sharing.**

	Jan	Feb	Mar	Apr	May	Jun	Jul	Aug	Sep	Oct	Nov	Dec	Prior Year(s) Actual	
													0	(1)
Actual (booked) cost in the current year 19 ___	8	3	8										Current Year Actual: 19	(2)
Forecast to complete the current year 19 ___				5	5	5	5	5	5	5			Current Year Forecast: 35	(3)

Unbooked liability

Please list dollar amount, description of cost, and month/year in which costs are expected to be booked.

Forecast to complete the future year(s)

19 ___	19 ___	19 ___	19 ___	Remaining Years(s)	Future Year(s) Forecast	
						(4)

Grand total of lines (1) + (2) + (3) + (4) 54

Remarks: Comments on significant items

Total Funded 1989 = 29,640
1990 = 24,146
53,786

PREPARED BY

Print name Sakis Meliopoulos Date 4/23/90

Title Professor/Project Director

GEORGIA TECH RESEARCH CORPORATION

PLEASE REMIT TO:
GEORGIA TECH RESEARCH CORPORATION
P.O. BOX 100117
ATLANTA, GEORGIA 30384

INVOICE NO. E-21-666 - 020790
246R68600A0

PAYABLE UPON RECEIPT OF INVOICE
PAYER'S ACCOUNT NUMBER:
RP2115-24

ELECTRIC POWER RESEARCH INSTITUTE
ATTN: ACCOUNTING
PO BOX 10412
PALO ALTO, CA 94303

GTRC ACCOUNTING
No. _____
Date _____
D D _____

INVOICE DATE	DESCRIPTION	CUMULATIVE AMOUNT	CURRENT AMOUNT
/01/90	EFFECTS OF GEOMAGNETIC DISTURBANCE ON ELEC POWER TRANS SYSTEMS		
TO	PERSONAL SERVICES	3,841.00	3,841.00
	FRINGE BENEFITS	1,010.18	1,010.18
	MATERIALS AND SUPPLIES		
	OTHER INDIRECT		
/31/90	EQUIPMENT		
	TRAVEL		
	CAPITAL OUTLAY		
	COMPUTER		
	SUBCONTRACTS		
	OVERHEAD	3,031.99	3,031.99
		7,883.17	7,883.17

IF YOU HAVE QUESTIONS CONCERNING THIS INVOICE
CONTACT: Ellen Scott PHONE: (404)894-6759

PLEASE PAY THIS TOTAL AMOUNT > $ 7,883.17

RETAIN THIS COPY FOR YOUR RECORDS

GEORGIA TECH RESEARCH CORPORATION

Mel Lopata

PLEASE REMIT TO:
GEORGIA TECH RESEARCH CORPORATION
P.O. BOX 100117
ATLANTA, GEORGIA 30384

INVOICE NO. E-21-666 - 030690
246R68600A0

PAYABLE UPON RECEIPT OF INVOICE
PAYER'S ACCOUNT NUMBER:
RP2115-24

ELECTRIC POWER RESEARCH INSTITUTE
ATTN: ACCOUNTING
PO BOX 10412
PALO ALTO, CA 94303

GTRC ACCOUNTING
No. _____
Date _____
D D _____
_____

NVOICE DATE	DESCRIPTION	CUMULATIVE AMOUNT	CURRENT AMOUNT
'01/90	EFFECTS OF GEOMAGNETIC DISTURBANCE ON ELEC POWER TRANS SYSTEMS		
TO	PERSONAL SERVICES	5,544.68	1,703.68
	FRINGE BENEFITS	1,458.25	448.07
	MATERIALS AND SUPPLIES		
	OTHER INDIRECT		
'28/90	EQUIPMENT		
	TRAVEL		
	CAPITAL OUTLAY		
	COMPUTER		
	SUBCONTRACTS		
	OVERHEAD	4,376.83	1,344.84
		11,379.76	3,496.59

IF YOU HAVE QUESTIONS CONCERNING THIS INVOICE
CONTACT: Ellen Scott PHONE: (404) 894-6759

PLEASE PAY THIS TOTAL AMOUNT > $ 3,496.59

RETAIN THIS COPY FOR YOUR RECORDS

GEORGIA TECH RESEARCH CORPORATION

PLEASE REMIT TO:
GEORGIA TECH RESEARCH CORPORATION
P.O. BOX 100117
ATLANTA, GEORGIA 30384

INVOICE NO. E-21-666 - 040590
246R68600A0

PAYABLE UPON RECEIPT OF INVOICE
PAYER'S ACCOUNT NUMBER:
RP2115-24

ELECTRIC POWER RESEARCH INSTITUTE
ATTN: ACCOUNTING
PO BOX 10412
PALO ALTO, CA 94303

GTRC ACCOUNTING
No. _____
Date _____
D D _____
_____

NVOICE DATE	DESCRIPTION	CUMULATIVE AMOUNT	CURRENT AMOUNT
'01/90	EFFECTS OF GEOMAGNETIC DISTURBANCE ON ELEC POWER TRANS SYSTEMS		
TO	PERSONAL SERVICES	9,456.28	3,911.60
	FRINGE BENEFITS	2,487.00	1,028.75
	MATERIALS AND SUPPLIES		
	OTHER INDIRECT		
'31/90	EQUIPMENT		
	TRAVEL		
	CAPITAL OUTLAY		
	COMPUTER		
	SUBCONTRACTS		
	OVERHEAD	7,464.55	3,087.72
		19,407.83	8,028.07

RECEIVED
[redacted] 0 1990
ELECTRICAL ENGINEERING
ACCOUNTING OFFICE

IF YOU HAVE QUESTIONS CONCERNING THIS INVOICE
CONTACT: Ellen Scott PHONE: (404) 894-6755

PLEASE PAY THIS TOTAL AMOUNT > $ 8,028.07

RETAIN THIS COPY FOR YOUR RECORDS

GEORGIA INSTITUTE OF TECHNOLOGY
SCHOOL OF ELECTRICAL ENGINEERING
ATLANTA, GEORGIA 30332

TELEPHONE: (404) 894-

June 7, 1990

Ms. Pat Lora
Sr. Financial Analyst
Electric Power Research Institute
3412 Hillview Avenue
Post Office Box 10412
Palo Alto, CA 94303

Dear Ms. Lora:

Enclosed is the Contractor Cost Performance Report (Form 177) for Project RP 2115-24. The costs indicated on the report are as of the month in which they are recorded on our accounting records, and may or may not be the month in which the service was performed or the material purchased. I believe this is in keeping with the instructions we received from EPRI when the contract was negotiated.

This report covers the months of January, February, March and April, 1990. Please excuse our delay.

Should you have questions or need additional information, you may contact me at (404)894-7337.

Sincerely,

Kathy Knighton

Enclosure

EPRI

CONTRACTOR COST PERFORMANCE REPORT

EPRI 177 5/84R

EPRI CONTRACT NUMBER	EPRI DIVISION NUMBER	CONTRACTOR NAME, ADDRESS AND TELEPHONE NUMBER
RP 2115-24	4 (For EPRI Use Only)	Georgia Institute of Technology School of Electrical Engineering Atlanta, GA 30332 (404) 894-2926
EPRI PROJECT MANAGER Name M. Rabinowitz	**PERIOD OF PERFORMANCE** From 11/1/89 to 10/31/90	

Note:
- Instructions for completing this form are on the reverse side.
- All figures are to be shown in U.S. dollars—whole thousands only.
- Show EPRI portion of the contract only. Do not include contractor cost sharing.

	Jan	Feb	Mar	Apr	May	Jun	Jul	Aug	Sep	Oct	Nov	Dec	Prior Year(s) Actual	
													0	(1)
Actual (booked) cost in the current year 19 90	8	3	8	0									Current Year Actual: 19	(2)
Forecast to complete the current year 19 90					6	6	6	6	6	5			Current Year Forecast: 35	(3)

Unbooked liability

Please list dollar amount, description of cost, and month/year in which costs are expected to be booked.

Forecast to complete the future year(s)

19 ___	19 ___	19 ___	19 ___	Remaining Years(s)	Future Year(s) Forecast	
						(4)

Grand total of lines (1) + (2) + (3) + (4) 54

Remarks: Comments on significant items

Total Funded 1989 = 29,640
1990 = 24,146

53,786

PREPARED BY

Print name Sakis Meliopoulos Date 5/28/90

Title Professor/Project Director

L-21-666

GEORGIA INSTITUTE OF TECHNOLOGY
SCHOOL OF ELECTRICAL ENGINEERING
ATLANTA, GEORGIA 30332

TELEPHONE: (404) 894-

July 13, 1990

Ms. Pat Lora
Sr. Financial Analyst
Electric Power Research Institute
3412 Hillview Avenue
Post Office Box 10412
Palo Alto, CA 94303

Dear Ms. Lora:

Enclosed is the Contractor Cost Performance Report (Form 177) for Project RP 2115-24. The costs indicated on the report are as of the month in which they are recorded on our accounting records, and may or may not be the month in which the service was performed or the material purchased. I believe this is in keeping with the instructions we received from EPRI when the contract was negotiated.

This report covers the months of May, 1990.

Should you have questions or need additional information, you may contact me at (404)894-7337.

Sincerely,

Kathy Knighton

Enclosure

EPRI

CONTRACTOR COST PERFORMANCE REPORT

EPRI 177 5/84R

EPRI CONTRACT NUMBER	EPRI DIVISION NUMBER	CONTRACTOR NAME, ADDRESS AND TELEPHONE NUMBER
RP 2115-24	4 (For EPRI Use Only)	Georgia Institute of Technology School of Electrical Engineering Atlanta, GA 30332 (404) 894-2926
EPRI PROJECT MANAGER Name M. Rabinowitz	PERIOD OF PERFORMANCE From 11/1/89 to 10/31/90	

Note:
- Instructions for completing this form are on the reverse side.
- All figures are to be shown in U.S. dollars—whole thousands only.
- Show EPRI portion of the contract only. Do not include contractor cost sharing.

Actual (booked) cost in the current year 19 90

Jan	Feb	Mar	Apr	May	Jun	Jul	Aug	Sep	Oct	Nov	Dec	Prior Year(s) Actual	Current Year Actual
8	3	8	0	0								0 (1)	19 (2)

Forecast to complete the current year 19 90

Jan	Feb	Mar	Apr	May	Jun	Jul	Aug	Sep	Oct	Nov	Dec	Current Year Forecast
					7	7	7	7	7			35 (3)

Unbooked liability

Please list dollar amount, description of cost, and month/year in which costs are expected to be booked.

Forecast to complete the future year(s)

19 ___	19 ___	19 ___	19 ___	Remaining Years(s)	Future Year(s) Forecast
					(4)

Grand total of lines (1) + (2) + (3) + (4) 54

Remarks: Comments on significant items

Total Funded 1989 = 29,640
1990 = 24,146

53,786

PREPARED BY

Print name Sakis Meliopoulos Date 7/13/90

Title Professor/Project Director

E21-466

GEORGIA INSTITUTE OF TECHNOLOGY
SCHOOL OF ELECTRICAL ENGINEERING
ATLANTA, GEORGIA 30332

TELEPHONE: (404) 894-

September 5, 1990

Ms. Pat Lora
Sr. Financial Analyst
Electric Power Research Institute
3412 Hillview Avenue
Post Office Box 10412
Palo Alto, CA 94303

Dear Ms. Lora:

Enclosed is the Contractor Cost Performance Report (Form 177) for Project RP 2115-24. The costs indicated on the report are as of the month in which they are recorded on our accounting records, and may or may not be the month in which the service was performed or the material purchased. I believe this is in keeping with the instructions we received from EPRI when the contract was negotiated.

This report covers the months of June and July, 1990.

Should you have questions or need additional information, you may contact me at (404)894-7337.

Sincerely,

Kathy Knighton

Enclosure

EPRI

CONTRACTOR COST PERFORMANCE REPORT

EPRI 177 5/84R

EPRI CONTRACT NUMBER	EPRI DIVISION NUMBER (For EPRI Use Only)	CONTRACTOR NAME, ADDRESS AND TELEPHONE NUMBER
RP 2115-24	4	Georgia Institute of Technology School of Electrical Engineering Atlanta, GA 30332 (404) 894-2926
EPRI PROJECT MANAGER Name M. Rabinowitz	**PERIOD OF PERFORMANCE** From 11/1/89 to 10/31/90	

Note:
- **Instructions for completing this form are on the reverse side.**
- **All figures are to be shown in U.S. dollars—whole thousands only.**
- **Show EPRI portion of the contract only. Do not include contractor cost sharing.**

	Jan	Feb	Mar	Apr	May	Jun	Jul	Aug	Sep	Oct	Nov	Dec	Prior Year(s) Actual	
													0	(1)
Actual (booked) cost in the current year 19 90	8	3	8	0	0	0	0						Current Year Actual: 19	(2)
Forecast to complete the current year 19 90								12	12	11			Current Year Forecast: 35	(3)

	19 ___	19 ___	19 ___	19 ___	Remaining Years(s)	Future Year(s) Forecast	
Forecast to complete the future year(s)							(4)
Grand total of lines (1) + (2) + (3) + (4)						54	

Unbooked liability

Please list dollar amount, description of cost, and month/year in which costs are expected to be booked.

Remarks: Comments on significant items

Total Funded 1989 = 29,640
1990 = 24,146

53,786

PREPARED BY

Print name Sakis Meliopoulos Date 9/5/90

Title Professor/Project Director

GEORGIA TECH RESEARCH CORPORATION

PLEASE REMIT TO:
GEORGIA TECH RESEARCH CORPORATION
P.O. BOX 100117
ATLANTA, GEORGIA 30384

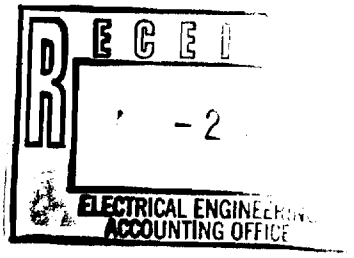

INVOICE NO. E-21-666 - 071890
246R68600A0

PAYABLE UPON RECEIPT OF INVOICE
PAYER'S ACCOUNT NUMBER:
RP2115-24

ELECTRIC POWER RESEARCH INSTITUTE
ATTN: ACCOUNTING
PO BOX 10412
PALO ALTO, CA 94303

GTRC ACCOUNTING
No. _____
Date _____
D D _____
_____

INVOICE DATE	DESCRIPTION	CUMULATIVE AMOUNT	CURRENT AMOUNT
01/90	EFFECTS OF GEOMAGNETIC DISTURBANCE ON ELEC POWER TRANS SYSTEMS		
TO	PERSONAL SERVICES	9,456.28	
	FRINGE BENEFITS	2,487.00	
	MATERIALS AND SUPPLIES	42.00	42.00
	OTHER INDIRECT		
30/90	EQUIPMENT		
	TRAVEL		
	CAPITAL OUTLAY		
	COMPUTER		
	SUBCONTRACTS		
	OVERHEAD	7,490.80	26.25
		19,476.08	68.25

IF YOU HAVE QUESTIONS CONCERNING THIS INVOICE
CONTACT: Ellen Scott PHONE: (404) 894-6151

PLEASE PAY THIS TOTAL AMOUNT > $ 68.25

RETAIN THIS COPY FOR YOUR RECORDS

E-21-666

GEORGIA INSTITUTE OF TECHNOLOGY
SCHOOL OF ELECTRICAL ENGINEERING
ATLANTA, GEORGIA 30332

TELEPHONE: (404) 894-

October 25, 1990

Ms. Pat Lora
Sr. Financial Analyst
Electric Power Research Institute
3412 Hillview Avenue
Post Office Box 10412
Palo Alto, CA 94303

Dear Ms. Lora:

Enclosed is the Contractor Cost Performance Report (Form 177) for Project RP 2115-24. The costs indicated on the report are as of the month in which they are recorded on our accounting records, and may or may not be the month in which the service was performed or the material purchased. I believe this is in keeping with the instructions we received from EPRI when the contract was negotiated.

This report covers the month of August, 1990.

Should you have questions or need additional information, you may contact me at (404)894-7337.

Sincerely,

Kathy Knighton

Enclosure

cc: Dr. Meliopoulos
E21-666 File

EPRI

CONTRACTOR COST PERFORMANCE REPORT

EPRI 177 5/84R

EPRI CONTRACT NUMBER	EPRI DIVISION NUMBER	CONTRACTOR NAME, ADDRESS AND TELEPHONE NUMBER
RP 2115-24	4 (For EPRI Use Only)	Georgia Institute of Technology School of Electrical Engineering Atlanta, GA 30332 (404) 894-2926
EPRI PROJECT MANAGER Name M. Rabinowitz	**PERIOD OF PERFORMANCE** From 11/1/89 to 10/31/90	

Note:
- Instructions for completing this form are on the reverse side.
- All figures are to be shown in U.S. dollars—whole thousands only.
- Show EPRI portion of the contract only. Do not include contractor cost sharing.

	Jan	Feb	Mar	Apr	May	Jun	Jul	Aug	Sep	Oct	Nov	Dec	
Actual (booked) cost in the current year 19 90	8	3	8	0	0	0	0	15					
Forecast to complete the current year 19 90									10	10			

Prior Year(s) Actual		Current Year Actual		Current Year Forecast		Future Year(s) Forecast	
0	(1)		34	(2)	20	(3)	(4)

Unbooked liability

Please list dollar amount, description of cost, and month/year in which costs are expected to be booked.

Forecast to complete the future year(s)

19 ___	19 ___	19 ___	19 ___	Remaining Years(s)

Grand total of lines (1) + (2) + (3) + (4) 54

Remarks: Comments on significant items

Total Funded 1989 = 29,640
1990 = 24,146
53,786

PREPARED BY

Print name Sakis Meliopoulos Date 10/25/90

Title Professor/Project Director

GEORGIA TECH RESEARCH CORPORATION

PLEASE REMIT TO:
GEORGIA TECH RESEARCH CORPORATION
P.O. BOX 100117
ATLANTA, GEORGIA 30384

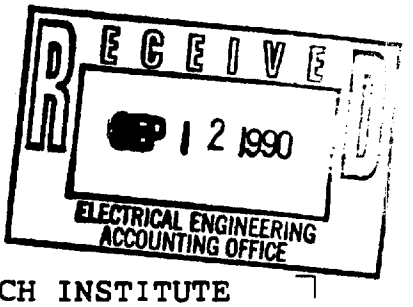

INVOICE NO. E-21-666 - 090790
246R68600A0

PAYABLE UPON RECEIPT OF INVOICE
PAYER'S ACCOUNT NUMBER:
RP2115-24

ELECTRIC POWER RESEARCH INSTITUTE
ATTN: ACCOUNTING
PO BOX 10412
PALO ALTO, CA 94303

GTRC ACCOUNTING
No. _____
Date _____
D D _____
_____

INVOICE DATE	DESCRIPTION	CUMULATIVE AMOUNT	CURRENT AMOUNT
/01/90	EFFECTS OF GEOMAGNETIC DISTURBANCE ON ELEC POWER TRANS SYSTEMS		
TO	PERSONAL SERVICES	9,456.28	
	FRINGE BENEFITS	2,487.00	
	MATERIALS AND SUPPLIES	42.00	
	OTHER INDIRECT		
/31/90	EQUIPMENT		
	TRAVEL		
	CAPITAL OUTLAY		
	COMPUTER		
	SUBCONTRACTS	9,286.50	9,286.50
	OVERHEAD	13,294.86	5,804.06
		34,566.64	15,090.56

IF YOU HAVE QUESTIONS CONCERNING THIS INVOICE
CONTACT: Allen Scott PHONE: (404) 894-6759

PLEASE PAY THIS TOTAL AMOUNT > $ 15,090.56

RETAIN THIS COPY FOR YOUR RECORDS

E-21-666

GEORGIA INSTITUTE OF TECHNOLOGY
SCHOOL OF ELECTRICAL ENGINEERING
ATLANTA, GEORGIA 30332

TELEPHONE: (404) 894-

March 16, 1990

Dr. Mario Rabinowitz

Dear Mario,

Enclosed please find the first quarterly technical report on "Effects of Geomagnetic Disturbances on Electric Power Transmission Systems."

Sincerely,

A. P. Sakis Meliopoulos

APM/pk
Enclosure
cc: Ms. Kathy Knighton, GIT

EPR90-1L

EFFECTS OF GEOMAGNETIC DISTURBANCES ON ELECTRIC POWER TRANSMISSION SYSTEMS

Prepared for

ELECTRIC POWER RESEARCH INSTITUTE
3412 Hillview Avenue
Palo Alto, California 94304

EPRI Project Manager
Dr. Mario Rabinowitz

Prepared by

A. P. Sakis Meliopoulos
E. N. Glytsis
Electric Power Laboratory
School of Electrical Engineering
Georgia Institute of Technology
Atlanta, Georgia 30332-0250

G. J. Cokkinides
Department of Electrical Engineering
University of South Carolina
Columbia, South Carolina 29208

February 1990

EPRI PERSPECTIVE

(to be added)

ABSTRACT

(to be added)

SUMMARY

(to be added)

ACKNOWLEDGEMENTS

(to be added)

TABLE OF CONTENTS

LIST OF ILLUSTRATIONS

(to be added)

LIST OF TABLES

(to be added)

Section 1

INTRODUCTION AND OBJECTIVE

1.1 INTRODUCTION

The objective of this project is to investigate the level of induced and/or transferred voltages and currents to an electric power system from (1) geomagnetic disturbances due to MHD-EMP and (2) GIC due to solar storms, SS-GIC. Subsequently, a comparison of the effects of MHD-EMP and SS-GIC have been performed.

MHD-EMP is an electromagnetic pulse with very low amplitude which results from geomagnetic disturbances caused by high altitude nuclear detonation. The electric field magnitude is on the order of 100 V/km, low frequency and lasts for several minutes. Similar geomagnetic disturbances are caused by solar storms and result in electric field magnitudes on the order of 10 V/km, low frequency and last from minutes to an hour. Both phenomena cause the flow of almost DC current in the windings of power transformers through the grounding system. Because of the nonlinear magnetization characteristics of the power transformers, the flow of the low frequency electric currents may cause serious secondary results, such as high magnetization currents due to saturation, abnormal reactive power requirements, and disruption of operation. Presently, it is not clear which disturbance (the high magnitude short duration MHD-EMP or the low magnitude long duration SS-GIC) is the most severe to a power system. A system approach has been adopted to address these problems, and to determine at what level saturation is reached.

The objectives of the project have been attained with a two step procedure: In the first step a model of an electric power transmission line including grounding and MHD-EMP or solar storm coupling has been developed. The basic methodology utilized for this step is described in Sections 2 and 3. Since the coupling of MHD-EMP or solar storm induced voltages to power lines is mainly through the line grounding system, it is important to accurately model the power line tower grounding as well as the terminal substation grounding system. For this purpose, the EPRI grounding models developed by Georgia Tech have been utilized. The form of the transmission line model is in terms of a multiple input-multiple output linear system.

The second step involves integration of the model developed in the first step into the EPRI computer model ADCFLT. This computer model is a time domain model similar to the EMTP. It allows modeling of an integrated power system, power system grounding, and the nonlinear magnetization characteristics of power transformers. Using this model, system studies have been performed to determine transformer magnetization currents and reactive power requirements. Of special importance is the degree of saturation of power transformers due to these phenomena. This information can be utilized to analyze transformer performance such as eddy losses in steel members, conductors, and leads. A test system has been utilized provided by Minnesota Power Company.

1.2 REPORT OUTLINE AND MAJOR CONCLUSIONS

(to be added)

Section 2

DESIGN WAVEFORMS FOR SOLAR-STORM GEOMAGNETICALLY INDUCED CURRENTS (SS-GIC) AND FOR MAGNETOHYDRODYNAMIC ELECTROMAGNETIC PULSES (MHD-EMP)

2.1 INTRODUCTION

Electric currents that flow in the molten core of the earth cause its dipole-like magnetic field. The magnetic field of the earth interacts with the interplanetary magnetic field which is actually an extension of the magnetic field of the sun due to the solar wind. The solar wind consists of charged particles, mainly electrons and protons (hydrogen ions), emitted from the surface of the sun. Thus, the solar wind acts like an extension of the magnetic field of the sun and interacts with the earth's magnetic field in a complex manner creating the earth's magnetosphere. In addition, interactions of the earth's magnetic field and the solar wind give rise to a vast magnetohydrodynamic generator that converts the kinetic energy of the solar-wind particles in electric energy which powers the auroral currents or auroral electrojets [1,2]. These currents usually follow circular or elliptical paths around the geomagnetic poles at altitudes of 100 kilometers or more and produce fluctuations in the earth's magnetic field that are termed geomagnetic storms. The strength of the geomagnetic storms is strongly related with solar phenomena that affect the solar wind. These phenomena are the solar flares, the coronal holes, and the disappearing filaments. The severity of the geomagnetic storms strongly depends on the intensity of the above mentioned solar effects. Large solar storms can produce large variations of the auroral electrojets which produce large variations of the geomagnetic field on the earth's surface. The earth as a conducting sphere experiences, or portions of it experience, these time varying magnetic fields. Varying magnetic fields induce electric potential gradients which are called earth-surface-potentials (ESP). The earth-surface-potentials can obtain values in the range between 1 and 10 volts/km depending on the severity of the geomagnetic storm and the earth's conductivity [3,4]. The electric power systems are exposed to ESP through the grounding grid. Since the ESP has frequency of one to a few millihertz the resulting geomagnetically-induced-currents (GIC) can be considered quasi-direct currents compared to 50 Hz or 60 Hz of the electrical power system frequency. Geomagnetic field variations caused by magnetosphere phenomena will result in an induced ESP orthogonal to the field changes. Usually, an idealized east-west

auroral current will cause field variations in the north-south component of the earth's magnetic field, resulting in an east-west induced ESP. Thus, transmission lines in the east-west direction are more susceptible to large ESP than transmission lines in the north-south direction. However, the auroral currents are not ideally east-west and consequently large ESP can be observed in any direction. Several analytical methods have been developed to estimate the induced ESP based on different modeling of the auroral currents and the earth's conductivity. Due to the complexity of the geomagnetic phenomena all these models are approximate and direct measurements of the geomagnetic fields seems to be the best choice.

Geomagnetic disturbances and associated induced earth currents can also originate from the explosion of nuclear bombs at high altitude above the earth's surface [5-7]. These explosions result in transient electromagnetic pulses (EMP) which can affect the operation of the power and communications systems. There are two basic types of electromagnetic pulses due to nuclear explosions. The one is the high altitude quick pulse (TEMP) (Tachy-EMP), and the other is the much slower magnetohydrodynamic EMP (MHD-EMP). For this report, only the slow MHD-EMP is of interest since its effect to power system operation is very similar to solar-storm geomagnetically induced currents. Two similar but different magnetic disturbances give rise to the MHD-EMP. The first is called magnetic bubble EMP (BEMP) [8]. The second is called Atmospheric heave EMP (AEMP) [8]. Due to the nuclear explosion a magnetohydrodynamic bubble of ionized conducting debris is formed and expands rapidly. Initially the geomagnetic flux inside the bubble is very small. If the shell of the magnetic bubble were nonconducting, the expansion of the bubble would simply enclose more magnetic flux of the geomagnetic field. However, since the bubble is conducting, currents are induced on the shell which counteract the earth's magnetic field. Thus, even if the bubble increases in volume the geomagnetic flux that encloses remains as small as it was initially. This effect results in a compression of the geomagnetic field around the bubble. These changes of the geomagnetic field can induce electric fields in the earth which can reach a maximum magnitude of 0.1 V/m with periods from 2 to 100 seconds [8]. This pulse occurs at about 2 to 5 seconds after the nuclear explosion. The second component of the MHD-EMP, the atmospheric heave EMP, occurs more than 10 seconds after the explosion. This pulse is caused by the atmospheric heave of the bomb-heated ionized air across the geomagnetic field. This ionization forms current loops which have mirror images in the earth. These perturbations of the geomagnetic field extend out more than 1250 miles from the source point and last approximately 100 sec. The induced electric fields and frequencies are very low between 0.001-0.03 V/m and ~0.01 Hz. Several analytical methods have been developed mainly for the study of the fast

EMP and comparisons of it with the lightning [9-12]. However, there is not much available information for theoretical modeling of MHD-EMP. Most of the analytical studies for the evaluation of the effects of MHD-EMP on power systems are based on measurements of the induced electric field [5,6], or by assuming plane wave excitation [13,14].

In the following subsections, the most common methods used for the evaluation of the ESP due to SS-GIC or MHD-EMP are reviewed. In addition, sample tables of measured data are given to be used as design ESP waveforms for the calculation of the effect of SS-GIC and MHD-EMP on power systems, and for evaluation of several methods proposed for the alleviation of these effects.

2.2 DESIGN EARTH SURFACE POTENTIAL WAVEFORMS DUE TO SOLAR-STORM GEOMAGNETICALLY INDUCED CURRENTS

Several analytical models have been used for the evaluation of the induced electric field on the surface of the earth due to the variations of the geomagnetic field. These models differ in the representation of the auroral currents and the conductivity of the earth. The auroral currents are known to be at altitudes between 100 to 300 km above the earth's surface. These currents can be modeled like current line sources or current sheet sources of infinite extend above a flat earth's surface. However, the auroral currents have such a spatial extension that they can not be considered either a current line or a current sheet. The above assumptions though give some estimate of the induced electric field on the earth's surface. Specifically, the current line model gives a lower limit while the current sheet model gives an upper limit of the induced electric field. Sometimes the auroral currents are assumed to be at an infinite distance from the ground. In this case, the geomagnetic field is modeled as a plane electromagnetic wave. The conductivity of the earth is also difficult to model due to the large variety and inhomogeneity of the earth's surface from place to place. The simplest model assumes a flat earth surface with a uniform effective conductivity. More sophisticated earth models divide the earth's surface in multiple layers, each one having a different conductivity.

The simplest method for modeling the auroral currents is the plane electromagnetic wave model [15]. The earth is modeled as a horizontally stratified medium of one or more layers of differing conductivities. The incident geomagnetic field is assumed to be a linearly polarized, monochromatic plane wave. The electric field on the surface of the earth is computed with usual electromagnetic analysis methods. In addition, using this technique the surface impedance of the earth, Z_s, can be

computed, where $Z_s = E_x/H_y$ (E_x/H_y are the horizontal components of the electric and magnetic field on the earth's surface, respectively). This is useful since from measurement of the magnetic field, the induced electric field can be estimated.

Another widely used technique models the auroral currents as an infinite horizontal current sheet at a height h above the horizontally also stratified earth of one or more layers [15-19]. To solve the problem, the electric and magnetic Hertz vectors are commonly used. For the described geometry, these vectors have only one component which is perpendicular to the earth's surface and to the auroral current sheet. Using the vector Hertz potentials and Maxwell's equations along with the corresponding boundary conditions, the electric field on the earth's surface can be found. This field is a function of (1) the magnitudes along the two horizontal directions of the current sheet (j_x, j_y), (2) the radian frequency ω of the auroral current, (3) the spatial wave numbers of the spectral components of the auroral currents, (4) the altitude h of the auroral current, and (5) the characteristics of the earth. Even if the described analysis considered a single spectral component, there is no loss of generality since by Fourier synthesis any time-dependent source current can be written as a linear combination of its spectral components. Consequently, the resulting induced electric field will be a linear combination of the fields due to the different spectral components. As it was mentioned earlier, the current sheet method overestimates the induced electric field on the earth's surface.

The auroral currents can also be modeled as a line current source parallel to the earth's surface at an altitude h [15,18,20,21]. Usually, the line is positioned in the east-west direction and is assumed positive in the westward direction. Earth's surface is modeled like a horizontally stratified medium. The general methodology used for the solution of these problems is based on Price's analysis [22]. This analysis assumes slow variations of the geomagnetic fields. As a result, the second time derivatives in the wave equation are neglected. This assumption permits solutions of the magnetic field expressed in terms of the gradient of a scalar magnetic potential for the region above the earth, while the electric field solutions are expressed in terms of the time derivative of a vector magnetic potential for the earth region. An equivalent procedure consists of expressing the electric field as $\vec{E} = e^{j\omega t} G(z) \vec{F}(x,y)$, where G and $\vec{F}$ have to be determined for each region from the wave equation and the boundary conditions of the problem [(x,y) correspond to the horizontal plane while z is the perpendicular coordinate]. Using this procedure the resulting electric and magnetic fields on the

earth's surface are calculated as functions of the following parameters: (1) the magnitude of the auroral current, (2) the radian frequency of the auroral current, (3) the altitude h of the auroral current, (4) the difference in latitude between the auroral current and the point for which the calculations are made, and (5) the surface impedance of the earth Z_s [23] which depends on the earth's parameters and modeling. Usually, since the magnitude of the auroral currents is not known, an estimate of $J = 10^5 A$ is used. As it was mentioned previously this method underestimates the induced electric field on the earth's surface due to the modeling of the auroral currents as a horizontal line current.

In the described models the auroral currents are modeled as uniform or sinusoidal distributions. However, none of these assumptions is very accurate. More sophisticated studies include Gaussian modeling of the electrojet [24,25]. In addition, Hibbs et al. have studied nonsymmetric auroral currents distributions [26].

Independently of the used model, the complexity of the physical effect of the auroral electrojet is difficult to represent. In addition, all the described models assume sinusoidal auroral currents. However, if the spectral content of the auroral currents was known, these models along with the superposition principle could be used for the calculation of the induced electric field. Since the spectral content of the auroral currents is not known and, in addition, is varying with time, the geomagnetic field is usually measured in several positions in the areas of interest using magnetometers. By measuring the magnetic field, the induced electric field can be roughly estimated using the plane wave assumption from [4]

$$E(t) = -\frac{1}{(\pi\mu_o\sigma)^{1/2}} \int_0^\infty \frac{g(t-u)}{u^{1/2}}\, du \ , \qquad (2\text{-}1)$$

where E(t) is the horizontal component of the induced electric field, μ_o is the permeability of the freespace, σ is the conductivity of the earth, and g is the time derivative of the horizontal component of the magnetic field. If the measured data are used, the derivative g can be computed numerically and the integral can be approximated using the extended Simpson's rule [27] by the following formula

$$\int_0^\infty \frac{g(t-u)}{u^{1/2}}\, du \approx D^{1/2}\left\{\frac{4}{3}\, g(t)+g(t-D)+\frac{2}{3}\sum_{j=1}^{L}(1+a_j)\,\frac{g[t-(j+1)D]}{(j+1)^{1/2}}\right\} \ , \qquad (2\text{-}2)$$

where D is the data time interval and $a_j = 0$ when j is even and $a_j = 1$ when j is odd; L is the total number of data points that are considered for the calculation of E(t). Using the data measured during May 12-13, 1989, at magnetic Observatory

Furstenfeldbruck (Figure 2-1, Table 2-1, and Eqs. (2-1) and (2-2)), the induced electric field was calculated and its values are summarized in Table 2-2 (Figure 2-2).

2.3 DESIGN EARTH SURFACE POTENTIAL WAVEFORMS DUE TO MAGNETOHYDRODYNAMIC ELECTROMAGNETIC PULSE

The effects of the magnetohydrodynamic electromagnetic pulse (MHD-EMP) on power system grids are very similar to those of geomagnetic storms. More specifically, MHD-EMP generates electric fields on the order of 10^{-1} V/m (about an order of magnitude higher than the geomagnetically-induced electric fields) of frequencies less than 1 Hz and of 100-200 sec duration. As it was described previously, MHD-EMP is due to two distinct physical mechanisms, the magnetic bubble (BEMP) and the atmospheric heave (AEMP). The early portion of the MHD-EMP (less than 10 seconds after the nuclear explosion) is due to BEMP while the rest of MHD-EMP is due to the AEMP [6]. Some estimate of the average induced electric field can be calculated using the following arguments [7]. The magnetic bubble, as it expands, pushes the geomagnetic field out of its way. The bubble obtains its maximum size when the energy of the excluded field equals the initial kinetic energy, T, of the conducting shell of the magnetic bubble, neglecting all other loss mechanisms. Thus, the following equation can be written [7]

$$\frac{1}{2\mu_o}\langle B^2\rangle\left(\frac{4}{3}\pi R^3\right) = T \Rightarrow R = [3\mu_o T/2\pi\langle B^2\rangle]^{1/3}\ , \tag{2-3}$$

where $\langle B^2\rangle$ is the mean squared value of the flux density of the unperturbed geomagnetic field, μ_o is the permeability of freespace, R is the maximum radius of the magnetic bubble (assuming spherical bubble), and T is the initial kinetic energy of the conducting debris of the bomb. The average power, $\langle P\rangle$, of the MHD-EMP can be estimated from

$$\langle P\rangle = \frac{fT}{\Delta t}\ , \tag{2-4}$$

where f is the conversion efficiency of the kinetic energy, T, in electromagnetic power, and Δt is the duration of the produced electromagnetic pulse. The average power density near the bubble can then be found from $\langle P\rangle/4\pi R^2$. Using the Poynting vector, the power density is $E^2/2\eta$, where η is the intrinsic impedance of freespace. Using the above arguments, an estimate of the induced electric field can be found from

$$E = \left[\frac{2fT^{1/3}\eta}{4\pi\Delta t[3\mu_o/2\pi\langle B^2\rangle]^{2/3}}\right]^{1/2}\ . \tag{2-5}$$

Using $f \approx 10^{-5}$, $T \approx 1.76 \cdot 10^{15}$ J (for a 30% yield of a 1.4 Mt bomb [7]), $\eta \approx 377\ \Omega$, $\Delta t \approx 100$ sec, and $B \approx 5 \cdot 10^{-5}$ wb/m^2, an electric field of 0.1 V/m can be estimated. The above estimate is based only on the BEMP effect under the rough assumptions made above. However, the atmospheric currents due to air ionization produce significant portion of the induced electric field. Thus, the most valuable information about a MHD induced EMP is empirically known from the magnetometer data acquired during actual nuclear events as the "Starfish" test conducted in the Pacific. The design waveform for the simulation of MHD-EMP is the one measured during the Starfish test. The magnetometer data [6] have been used along with Eq. (2-1) to calculate the induced electric field that appears in Figure 1 of Reference 5. This electric field has been sampled and linearly approximated and is tabulated in Table 2-3 (Figure 2-3).

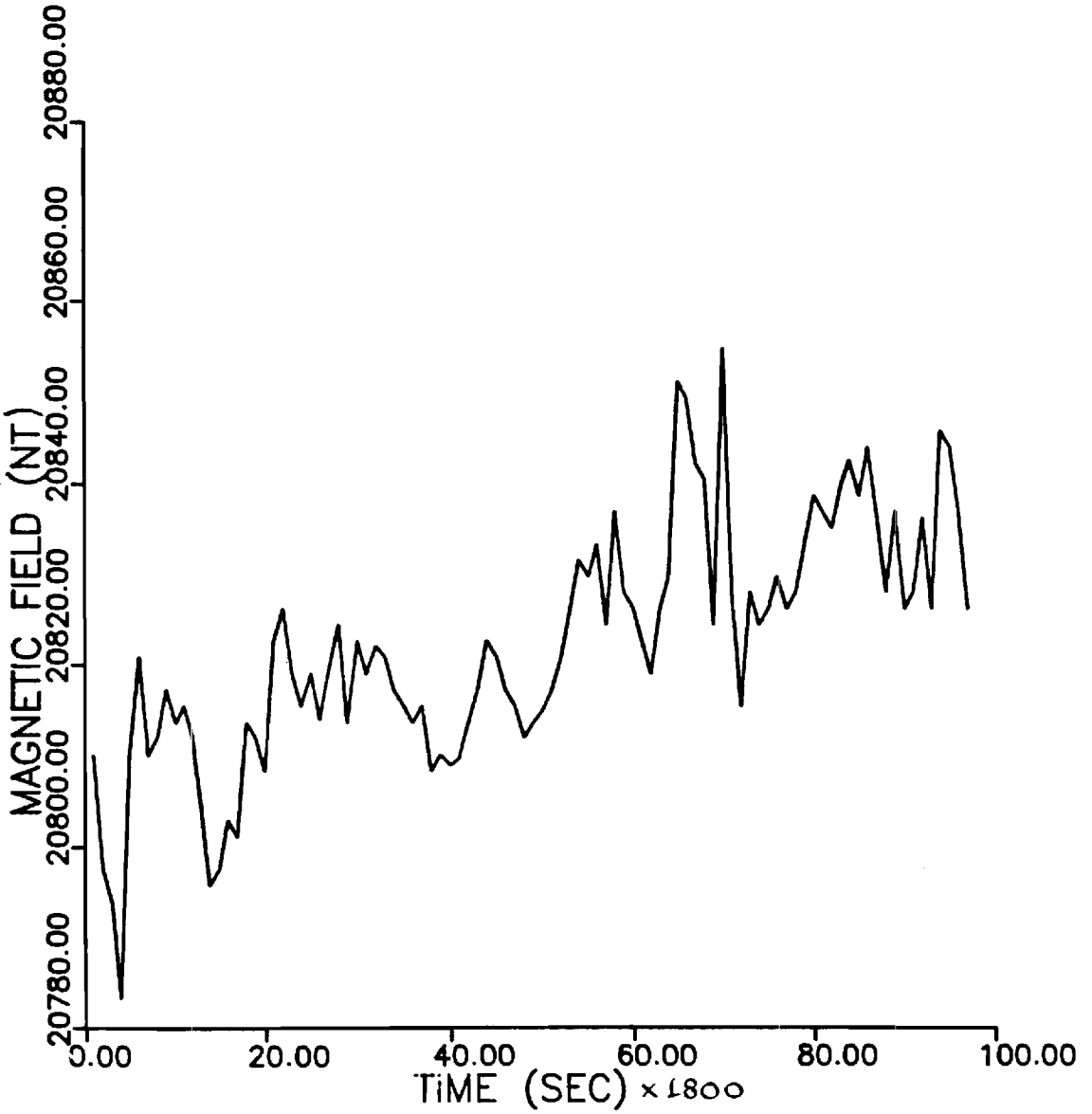

Figure 2-1. Horizontal Component of Magnetic Field.
Magnetic Observatory Fürstenfeldbruck, May 13, 1989

Fig. 2-1

Fig. 1

Horizontal component of ~~magnetic~~ field

2.1

TABLE I

Measurements of the Horizontal Component of the Magnetic Flux Density of the Geomagnetic Field at the Fürstenfeldbruck Station in 30 Minute Intervals Between May 12-13, 1989

Time (sec)	Horizontal Component of Geomagnetic Field (nT)
.0	20810.00
1800.0	20797.60
3600.0	20794.00
5400.0	20783.30
7200.0	20811.10
9000.0	20820.80
10800.0	20810.00
12600.0	20811.90
14400.0	20817.20
16200.0	20813.60
18000.0	20815.40
19800.0	20811.90
21600.0	20804.70
23400.0	20795.80
25200.0	20797.60
27000.0	20802.90
28800.0	20801.10
30600.0	20813.60
32400.0	20811.90
34200.0	20808.30
36000.0	20822.60
37800.0	20826.10
39600.0	20819.00
41400.0	20815.40
43200.0	20819.00
45000.0	20814.00
46800.0	20819.70
48600.0	20824.30
50400.0	20813.60
52200.0	20822.50
54000.0	20819.00
55800.0	20822.00
57600.0	20820.80
59400.0	20817.20
61200.0	20815.40
63000.0	20813.60
64800.0	20815.40
66600.0	20808.30
68400.0	20810.10
70200.0	20809.00
72000.0	20809.70
73800.0	20813.60
75600.0	20817.20
77400.0	20822.60
79200.0	20820.80
81000.0	20817.20

82800.0	20815.40
84600.0	20811.90
86400.0	20813.60
88200.0	20815.00
90000.0	20817.20
91800.0	20820.80
93600.0	20826.10
95400.0	20831.50
97200.0	20829.70
99000.0	20833.20
100800.0	20824.30
102600.0	20836.80
104400.0	20827.90
106200.0	20826.10
108000.0	20822.60
109800.0	20819.00
111600.0	20826.10
113400.0	20829.70
115200.0	20851.10
117000.0	20849.30
118800.0	20842.20
120600.0	20840.40
122400.0	20824.30
124200.0	20854.70
126000.0	20827.90
127800.0	20815.40
129600.0	20827.90
131400.0	20824.30
133200.0	20826.10
135000.0	20829.70
136800.0	20826.10
138600.0	20827.90
140400.0	20833.20
142200.0	20838.60
144000.0	20836.80
145800.0	20835.00
147600.0	20839.50
149400.0	20842.50
151200.0	20838.60
153000.0	20843.90
154800.0	20836.10
156600.0	20827.90
158400.0	20836.80
160200.0	20826.10
162000.0	20827.90
163800.0	20836.10
165600.0	20826.10
167400.0	20845.70
169200.0	20843.90
171000.0	20836.80
172800.0	20826.10

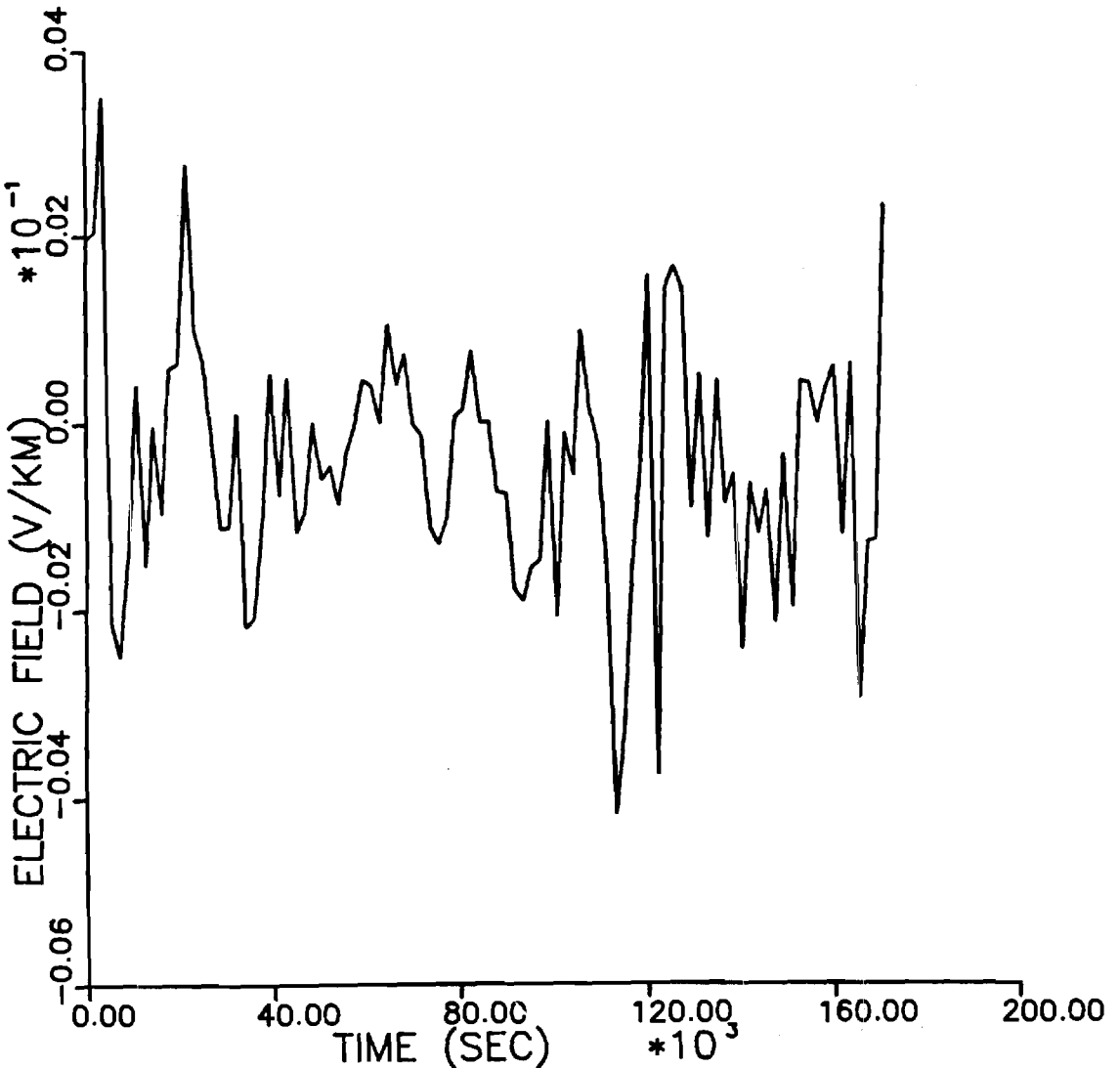

Figure 2-2. SS-GIC Electric Field. Magnetic Observatory Fürstenfeldbruck, May 13, 1989

Fig. 2-2

~~Fig 2~~

SS-GIC precedent field in V/km

TABLE II

Calculated Induced Electric Field (SS-GIC) Using the Measurements of Table I and Eqs. (1) and (2)

Time (sec)	Induced Electric Field (V/km)
.0	.19613E-02
1800.0	.20404E-02
3600.0	.35063E-02
5400.0	-.21590E-02
7200.0	-.24903E-02
9000.0	-.13399E-02
10800.0	.40067E-03
12600.0	-.15157E-02
14400.0	-.37079E-04
16200.0	-.97319E-03
18000.0	.58856E-03
19800.0	.64136E-03
21600.0	.27804E-02
23400.0	.97135E-03
25200.0	.68159E-03
27000.0	-.12122E-03
28800.0	-.11203E-02
30600.0	-.11249E-02
32400.0	.91153E-04
34200.0	-.21800E-02
36000.0	-.20967E-02
37800.0	-.10255E-02
39600.0	.52078E-03
41400.0	-.78152E-03
43200.0	.47075E-03
45000.0	-.11750E-02
46800.0	-.95832E-03
48600.0	-.61076E-05
50400.0	-.60230E-03
52200.0	-.46227E-03
54000.0	-.87251E-03
55800.0	-.33812E-03
57600.0	-.25453E-04
59400.0	.45499E-03
61200.0	.39364E-03
63000.0	.41640E-05
64800.0	.10508E-02
66600.0	.40856E-03
68400.0	.73819E-03
70200.0	-.12803E-04
72000.0	-.12281E-03
73800.0	-.11164E-02
75600.0	-.12954E-02
77400.0	-.10285E-02
79200.0	.67825E-04
81000.0	.14286E-03
82800.0	.76736E-03

84600.0	.62566E-05
86400.0	.17448E-04
88200.0	-.73720E-03
90000.0	-.75860E-03
91800.0	-.17937E-02
93600.0	-.19081E-02
95400.0	-.15541E-02
97200.0	-.14738E-02
99000.0	.79403E-06
100800.0	-.20720E-02
102600.0	-.11190E-03
104400.0	-.56233E-03
106200.0	.98050E-03
108000.0	.13813E-03
109800.0	-.22304E-03
111600.0	-.16265E-02
113400.0	-.41819E-02
115200.0	-.32840E-02
117000.0	-.14967E-02
118800.0	-.50570E-03
120600.0	.15648E-02
122400.0	-.37526E-02
124200.0	.14089E-02
126000.0	.16592E-02
127800.0	.14355E-02
129600.0	-.91577E-03
131400.0	.50753E-03
133200.0	-.12444E-02
135000.0	.44008E-03
136800.0	-.87843E-03
138600.0	-.55878E-03
140400.0	-.24192E-02
142200.0	-.66480E-03
144000.0	-.11979E-02
145800.0	-.73047E-03
147600.0	-.21370E-02
149400.0	-.35746E-03
151200.0	-.19755E-02
153000.0	.43395E-03
154800.0	.41453E-03
156600.0	-.62593E-05
158400.0	.35518E-03
160200.0	.59024E-03
162000.0	-.12100E-02
163800.0	.62786E-03
165600.0	-.29351E-02
167400.0	-.12896E-02
169200.0	-.12626E-02
171000.0	.23348E-02

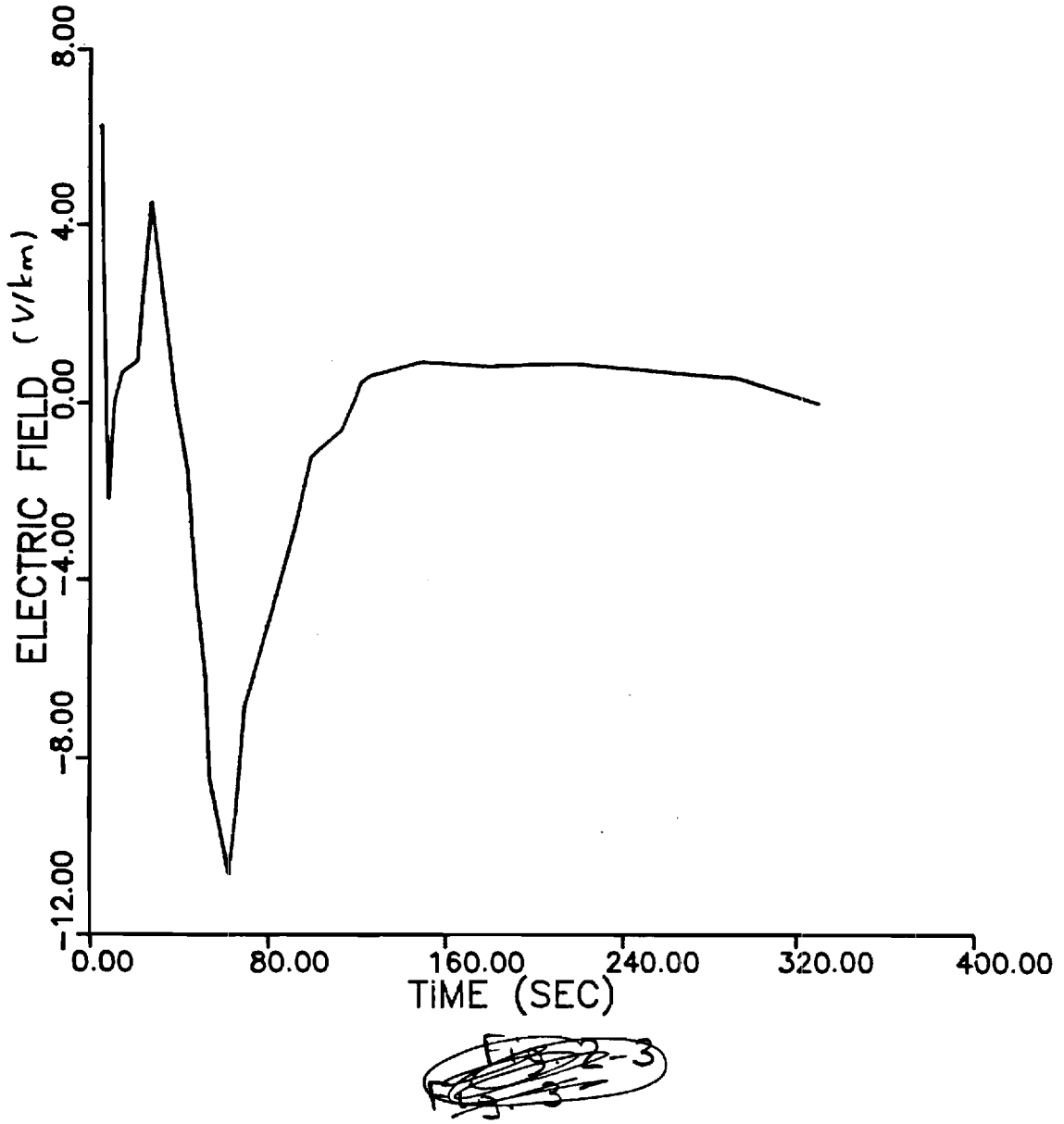

Figure 2-3. MHD-EMP induced electric field.

TABLE III

Measured Induced Electric Field (MHD-EMP)
During the "Starfish" Test

Time (sec)	Electric Field (V/km)
0.0	.00000E+00
5.0	.62500E+01
7.0	.00000E+00
8.0	-.21900E+01
10.5	.00000E+00
13.9	.69000E+00
20.9	.94000E+00
27.8	.45300E+01
38.3	.00000E+00
43.5	-.15600E+01
47.0	-.40600E+01
52.2	-.62500E+01
53.9	-.84400E+01
62.6	-.10630E+02
66.0	-.90600E+01
69.6	-.68800E+01
83.5	-.43800E+01
92.2	-.28100E+01
99.1	-.12500E+01
113.0	-.63000E+00
118.3	.00000E+00
121.7	.47000E+00
127.0	.63000E+00
149.6	.94000E+00
180.9	.84000E+00
217.4	.90000E+00
280.0	.63000E+00
292.2	.59000E+00
330.4	.00000E+00

Section 3

TRANSMISSION SYSTEM MODEL

3.1 INTRODUCTION

This section describes the transmission system model for the study of geomagnetic disturbances. The model is based on a time domain simulation algorithm similar to the EMTP. Each power system element is modeled with a set of differential equations which are solved in the time domain. For the study of geomagnetic disturbances, two power system elements are very important: (1) magnetic core transformers and (2) long transmission lines. Specifically, long transmission lines provide the gate for geomagnetically induced currents to enter the power system. On the other hand, magnetic core transformers reach saturation when geomagnetically induced currents flow in their windings and cause most of the undesirable effects. This section describes in detail these two models.

3.2 MAGNETIC CORE TRANSFORMERS

Magnetic core transformers are highly nonlinear devices due to their saturable magnetic core. A typical iron core magnetization curve is illustrated in Figure 3-1. For practical reasons, power transformers are designed in such a way that the maximum operating magnetic flux is near the knee of the magnetization curve. During normal operating conditions, the magnetic flux oscillates between $+\lambda_{max}$ and $-\lambda_{max}$ and the magnetization current is symmetric about the zero axis. When a DC current is injected through the transformer winding, this symmetry is destroyed. In this case, the transformer may operate past the magnetization curve knee for portions of the cycle, requiring a high magnetization current to maintain the applied voltage.

This phenomena is modeled as follows. Consider a single phase transformer as it is illustrated in Figure 3-2. The equations describing the transformer are:

$$v_{1u}(t) = r_{1u} i_{1u}(t) + d\lambda(t)/dt$$

$$v_{2u}(t) = r_{2u} i_{2u}(t) + d\lambda(t)/dt$$

$$\lambda(t) = g(i_m(t))$$

$$i_{m(t)} = i_{1u}(t) + i_{2u}(t)$$

where

$v_{1u}(t), v_{2u}(t)$ are the voltages in per unit

$i_{1u}(t), i_{2u}(t)$ are the currents in per unit

$g(\cdot)$ is the magnetization curve

$i_m(t)$ is the magnetization current in per unit.

Three single phase transformers, appropriately connected (wye-delta, etc.), provide the model of a three phase transformer. The equations of the power transformers are integrated in the time domain.

3.3 TRANSMISSION LINE MODEL WITH GIC COUPLING

The transmission line model used in this study is a time domain state space model based on the methodology described in Reference 29. It is capable of representing transmission line parameter frequency dependence, line tower grounding, as well as effects of geomagnetically induced currents (GIC).

The model is easily interfaced with other time domain models of power system components (such as transformers, loads, and generators). Thus the effect of GIC phenomena on the integrated power system can be assessed.

The transmission line model involves two components:

(1) Overhead conductors and earth return

(2) Grounding system.

Consider the transmission line shown in Figure 3-3. The section of overhead conductors between any two consecutive towers comprise a "conductor component" while each tower with its grounding systems is a component of the grounding system. Each component is modeled by an equivalent admittance matrix (which is a function of frequency) and equivalent current sources. Then, using nodal analysis, the equivalent circuit of the entire transmission line and GIC coupling is formed. The resulting model is in the form of a passive circuit of known admittance matrix and lumped current sources connected at the line terminals. This model is finally converted to the time domain using Fourier techniques.

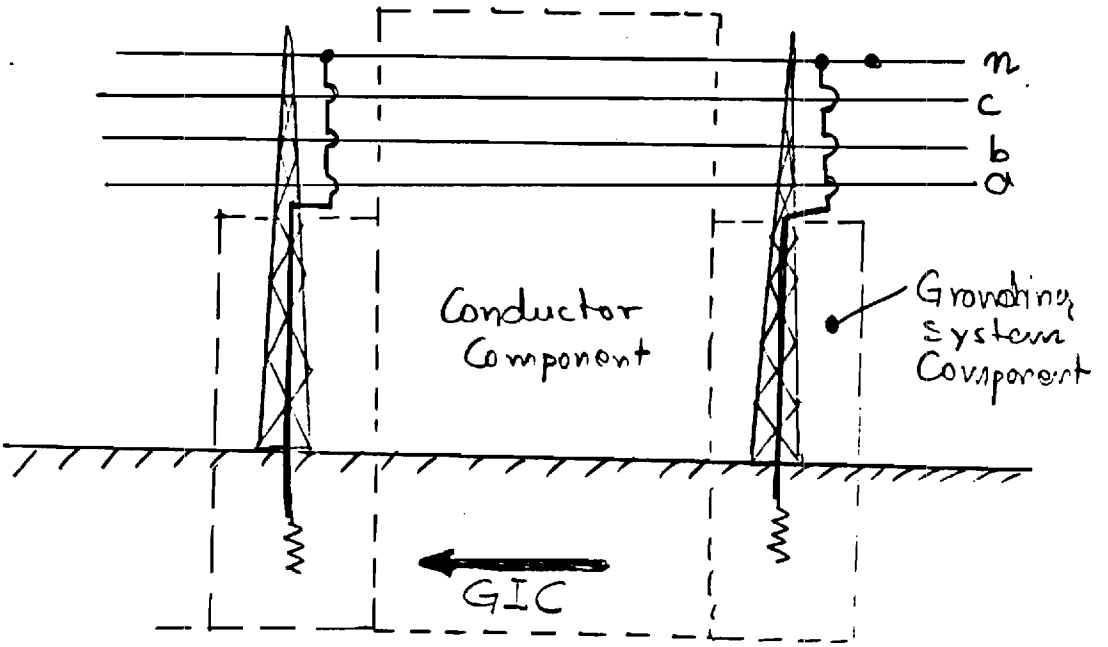

(a)

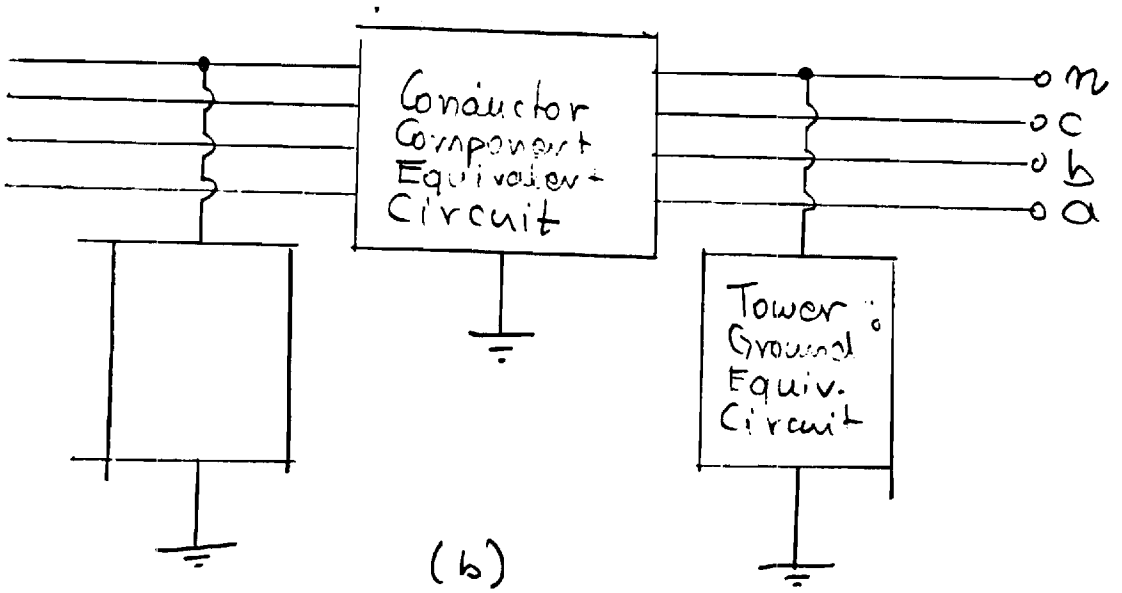

(b)

Figure 3.2 : Transmission Line Section
(a) Physical Configuration
(b) Equivalent Circuits

The derivation of the conductor and grounding system equivalent circuits are presented in the following sections.

3.3.1 Overhead Conductor Model

An overhead transmission line conductor section, in the presence of geomagnetically induced currents is represented by the equations

$$\frac{\partial v(x,t)}{\partial x} = -Ri(x,t) - L\frac{\partial i(x,t)}{\partial t} + v_g(x,t) \quad , \tag{3-1}$$

$$\frac{\partial i(x,t)}{\partial x} = -Gv(x,t) - C\frac{\partial v(x,t)}{\partial t} \quad ,$$

where

- v : line voltage with respect to remote earth (v)
- i : line current (A)
- R : line series resistance (Ohms/meter)
- L : line series inductance (Henries/meter)
- G : line shunt conductance (Siemens/meter)
- C : line shunt capacitance (Farads/meter)
- v_g : component of voltage due to GIC in the direction of the line (volts/meter).

(See Appendix A for a derivation of Eq. (3-1).)

Since the line parameters are frequency dependent, the solution of the above equation is computed in the frequency domain. The Fourier transform of the above equations ~~are~~ *is*

$$\frac{\partial V(x,\omega)}{\partial x} = -Z(\omega)I(x,\omega) + V_g(x,\omega) \quad , \tag{3-2}$$

$$\frac{\partial I(x,\omega)}{\partial x} = -Y(\omega)V(x,\omega) \quad , \tag{3-3}$$

where

$$Z(\omega) = R(\omega) + j\omega L(\omega)$$

$$Y(\omega) = G(\omega) + j\omega C(\omega) \quad .$$

For overhead transmission lines, several simplifications can be made:

(1) The conductance term is negligible and thus

$$Y(\omega) = j\omega C(\omega) \ .$$

(2) For a short line span, V_g is assumed constant with respect to position, thus

$$V_g(x,\omega) = V_g(\omega) \ .$$

(3) The resistance and inductance are computed using the complex depth of return method.

(4) The capacitance matrix is independent of frequency.

For a multiphase line the voltage due to GIC, V_g appears in series with every conductor. Thus it is replaced by the vector of the form

$$\begin{matrix} 1 \\ 1 \\ \vdots \\ 1 \end{matrix} \cdot V_g(x,\omega)$$

In order to compute the conductor section equivalent circuit, the current is eliminated in the equation system (3-2), (3-3), by differentiating Eq. (3-2) with respect to x and substituting current with voltage from Eq. (3-3)

$$\frac{\partial^2 V(x,\omega)}{\partial x^2} = K(\omega)V(x,\omega) \qquad (3\text{-}4)$$

where

$$K(\omega) = Z(\omega)Y(\omega) \ . \qquad (3\text{-}5)$$

The solution to the above equation (3-4) is obtained using eigenvalue analysis of the matrix K. Specifically, the system is decoupled by the transformation

$$V'(x,\omega) = W^{-1}(\omega)V(x,\omega) \qquad (3\text{-}6)$$

where

$$K(\omega) = W(\omega)D(\omega)W(\omega)^{-1} \qquad (3\text{-}7)$$

where $D(\omega)$ is a diagonal matrix containing the eigenvalues of matrix K, and $W(\omega)$ the eigenvector matrix of $K(\omega)$.

Applying transformation (3-7) to Eq. (3-4) yields

$$\frac{\partial^2 V'(x,\omega)}{\partial x^2} = D(\omega)V'(x,\omega) \ . \tag{3-8}$$

The general solution to the above equation is

$$V'(x,\omega) = e^{x\sqrt{D(\omega)}} \cdot C_1(\omega) + e^{-x\sqrt{D(\omega)}} \cdot C_2(\omega) \ , \tag{3-9}$$

where C_1, C_2 are constants to be determined by boundary conditions. Specifically,

$$V'(o,\omega) = C_1(\omega) + C_2(\omega) \tag{3-10}$$

$$V'(\ell,\omega) = e^{\ell\sqrt{D(\omega)}} C_1(\omega) + e^{-\ell\sqrt{D(\omega)}} C_2(\omega) \ .$$

Solving for C_1 and C_2 yields

$$C_1(\omega) = \left[e^{2\ell\sqrt{D(\omega)}} - I\right]^{-1} \left(e^{\ell\sqrt{D(\omega)}} V_2' - V_1'\right) \tag{3-11}$$

$$C_2(\omega) = \left[e^{-2\pi\sqrt{D(\omega)}} - I\right]^{-1} \left(e^{-\ell\sqrt{D(\omega)}} V_2' - V_1'\right) \ ,$$

where

$$V_1' = V'(o,\omega) = W^{-1} V(o,\omega)$$
$$V_2' = V'(\ell,\omega) = W^{-1} V(\ell,\omega)$$

and ℓ is the line length.

Thus, Eqs. (3-9) and (3-11) define the voltage at any point of the line given the voltages at the line ends. Now, using (3-2), the current is also computed as a function of the terminal voltages yielding

$$I(x,\omega) = Z^{-1}(\omega) V_g(\omega) = Z(\omega)^{-1} \frac{\partial V(x,\omega)}{\partial x} \ . \tag{3-12}$$

Evaluating the above at the line terminals, ($x = 0$, and $x = \ell$) yields

$$I_1(\omega) = Z(\omega)^{-1} V_g(\omega) - Z(\omega)^{-1} W(\omega) \left\{\sqrt{D(\omega)}\ C_1(\omega) - \sqrt{D(\omega)}\ C_2(\omega)\right\}$$

$$I_2(\omega) = Z(\omega)^{-1} V_g(\omega) - Z^{-1}(\omega) W(\omega) \left\{\sqrt{D(\omega)}\ E^{\ell\sqrt{D(\omega)}} C_1(\omega) - \sqrt{D(\omega)}\ e^{-\ell\sqrt{D(\omega)}} C_2(\omega)\right\} \ . \tag{3-13}$$

The above can be rewritten in matrix form as follows

$$\begin{bmatrix} I_1(\omega) \\ I_2(\omega) \end{bmatrix} = \left[\begin{array}{c|c} Z^{-1}(\omega) & 0 \\ \hline 0 & Z^{-1}(\omega) \end{array}\right] \cdot \begin{bmatrix} V_g(\omega) \\ V_g(\omega) \end{bmatrix} + \begin{bmatrix} Y_1(\omega) & Y_2(\omega) \\ Y_2(\omega) & Y_1(\omega) \end{bmatrix} \begin{bmatrix} V_1(\omega) \\ V_2(\omega) \end{bmatrix} \tag{3-14}$$

where

$$\begin{aligned} Y_1(\omega) &= -Z^{-1}(\omega)W(\omega)\left[\sqrt{D(\omega)}\left[-e^{2\ell\sqrt{D(\omega)}}+I\right]^{-1}+\sqrt{D(\omega)}\left[e^{-2\ell\sqrt{D(\omega)}}-I\right]^{-1}\right]W^{-1}(\omega) \\ &= Z^{-1}(\omega)W(\omega)\sqrt{D(\omega)}\left[\left(e^{2\ell\sqrt{D(\omega)}}-I\right)^{-1}-\left(e^{-2\ell\sqrt{D(\omega)}}-I\right)^{-1}\right]W^{-1}(\omega) \\ &= Z^{-1}(\omega)W(\omega)H_1(\omega)W^{-1}(\omega) \\ Y_2(\omega) &= Z^{-1}(\omega)W(\omega)\sqrt{D(\omega)}\left[\left[e^{2\ell\sqrt{D(\omega)}}-I\right]^{-1}e^{\ell\sqrt{D(\omega)}}-\left[e^{-2\ell\sqrt{D(\omega)}}-I\right]^{-1}e^{-\ell\sqrt{D(\omega)}}\right]W^{-1}(\omega) \\ &= Z^{-1}(\omega)W(\omega)\sqrt{D(\omega)}\left[e\left(e^{\ell\sqrt{D(\omega)}}-e^{-\ell\sqrt{D(\omega)}}\right)^{-1}\right]W^{-1}(\omega) \\ &= Z^{-1}(\omega)W(\omega)H_2(\omega)W^{-1}(\omega)\ , \end{aligned} \tag{3-15}$$

where $H_1(\omega)$, $H_2(\omega)$ are diagonal matrices of which the diagonal elements are

$$\begin{aligned} H_{1_{ii}} &= \frac{\sqrt{e_i}}{\tanh(\ell\sqrt{e_i})} \\ H_{2_{ii}} &= \frac{\sqrt{e_i}}{\sinh(\ell\sqrt{e_i})}\ , \end{aligned} \tag{3-16}$$

where e_i is the ith eigenvalue of matrix $K(\omega)$.

From Eq. (3-14), an equivalent circuit can be derived representing a multiphase transmission line section in the presence of GIC. Figure 3-4 illustrates the equivalent circuit. It consists of a passive circuit whose admittance matrix is known and current sources connected at each terminal representing GIC coupling. Note that all parameters of the equivalent circuit are frequency dependent. Thus the admittance matrix and current source values have to be computed explicitly at each frequency of interest.

3.3.2 Tower Grounding Model

Each tower and its grounding structure are represented by a step response. It is defined as the current flowing into the tower from the neutral wire support point when a unit step voltage is applied at the same point.

The step response of the tower and its grounding system can be determined experimentally [30] or analytically [31,32]. When computed analytically, finite element analysis is utilized to solve for the flow of currents in the earth. Then a convolution algorithm is utilized to evaluate the tower and ground step response [31].

The tower model has been validated with data obtained by Bonneville Power Administration (BPA). The validation of this model is reported in Reference 32.

The admittance of the tower and grounding system at any given frequency is computed from the step response with an appropriate Fourier transform.

3.3.3 Integrated Model

The equivalent circuit of the entire transmission line is constructed by combining the equivalent circuits of each conductor section and tower grounding systems. The procedure is based on nodal analysis method, where all internal node voltages and currents are eliminated, and all internal current sources are represented by equivalent current sources at the terminals of the line. The resulting equivalent circuit has the same topology as the one for a single line section as illustrated in Figure 3-4.

In order to utilize the developed model in time domain simulation, the equivalent circuit parameters are transformed into the time domain. Specifically, the admittance matrix of the passive part of the equivalent circuit is transformed to an impulse response, and the equivalent current sources (which are also computed as functions of frequency) are transformed into time domain waveforms. A discrete Fourier transform method is used for this purpose.

The Snelson transformation is applied before Fourier transformation to minimize resulting time domain waveform durations (see Reference 33). Specifically, the voltage and current variables are replaced by B and F as follows

$$F(\omega) = V(\omega) + G^{-1} I(\omega) \qquad (3\text{-}17)$$

$$B(\omega) = V(\omega) - G^{-1} I(\omega)$$

where G is a real nxn matrix (n = number of conductors), and

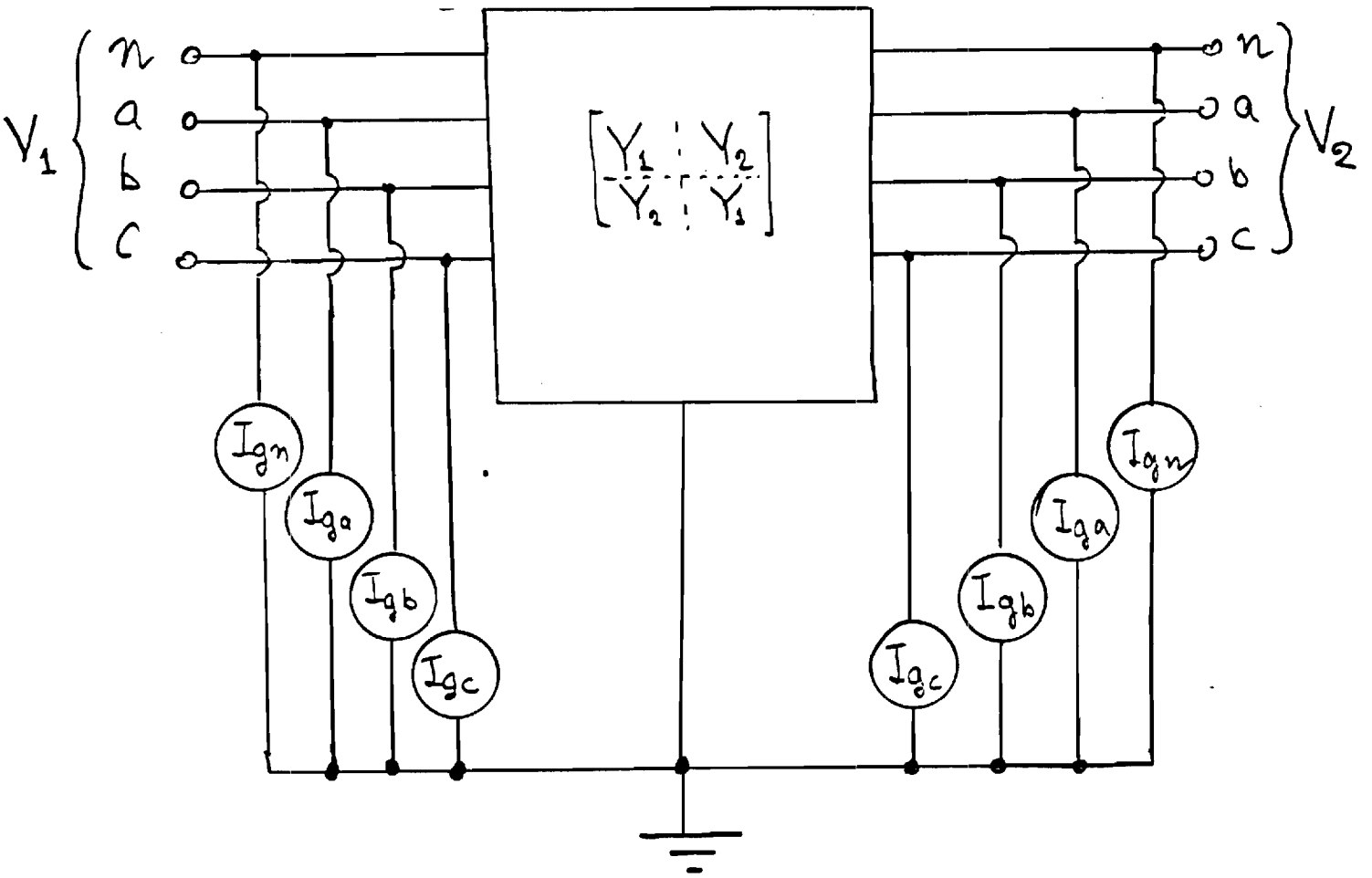

Figure 3.4 : Equivalent Circuit of a Transmission Line Section with GIC coupling

$$V(\omega) = \begin{matrix} V_1(\omega) \\ V_2(\omega) \end{matrix} \quad , \quad I(\omega) = \begin{matrix} I_1(\omega) \\ I_2(\omega) \end{matrix} .$$

Applying the above transformation to Eq. (3-14) yields

$$\frac{1}{2} G\big(F(\omega)-B(\omega)\big) = \begin{matrix} Z^{-1}(\omega)V_g(\omega) \\ -Z^{-1}(\omega)V_g(\omega) \end{matrix} + \frac{1}{2} Y(\omega)\big(F(\omega)+B(\omega)\big) . \tag{3-18}$$

Solving for $B(\omega)$ yields

$$B(\omega) = M(\omega)F(\omega) + A_g(\omega) , \tag{3-19}$$

where

$$M(\omega) = \big(G(\omega)+Y(\omega)\big)^{-1}\big(G(\omega)-Y(\omega)\big)F(\omega)$$

$$A_g(\omega) = -2\big(Y(\omega)+G(\omega)\big)^{-1} \begin{matrix} Z(\omega)V_g(\omega) \\ Z^{-1}(\omega)V_g(\omega) \end{matrix}$$

The matrix $M(\omega)$ and the vector $A_g(\omega)$ are next transformed into time domain functions using the FFT algorithms

$$m(t) = F^{-1}\{M(\omega)\}$$
$$a_g(t) = F^{-1}\{A_g(\omega)\} \tag{3-20}$$

The functions matrices $m(t)$ and $a_g(t)$ comprise a time domain model of the entire transmission line with GIC coupling. Specifically, $m(t)$ contains the impulse response of the transmission line (based on Snelson's transformation) and the functions $a_g(t)$ represent the GIC effects. These functions are utilized in a convolution based algorithm, in order to simulate the operation of transmission lines with GIC coupling in the integrated power system. This algorithm is described in the following section.

3.3.4 Convolution Algorithm

The transmission line model is cast into the resistive companion form via a discrete convolution scheme. This technique allows the model to be interfaced with models of other power system components, thus forming a model of an integrated power system. (This is the standard methodology followed by several time domain simulation programs such as the EMTP and the PSTS programs.) Specifically, the model of a transmission line with GIC coupling is represented by the equivalent circuit shown in Figure 3-5. The voltage vector v and current vector i represent the voltages and current injections on each conductor at the ends of the line. The following equation holds for these voltages and currents:

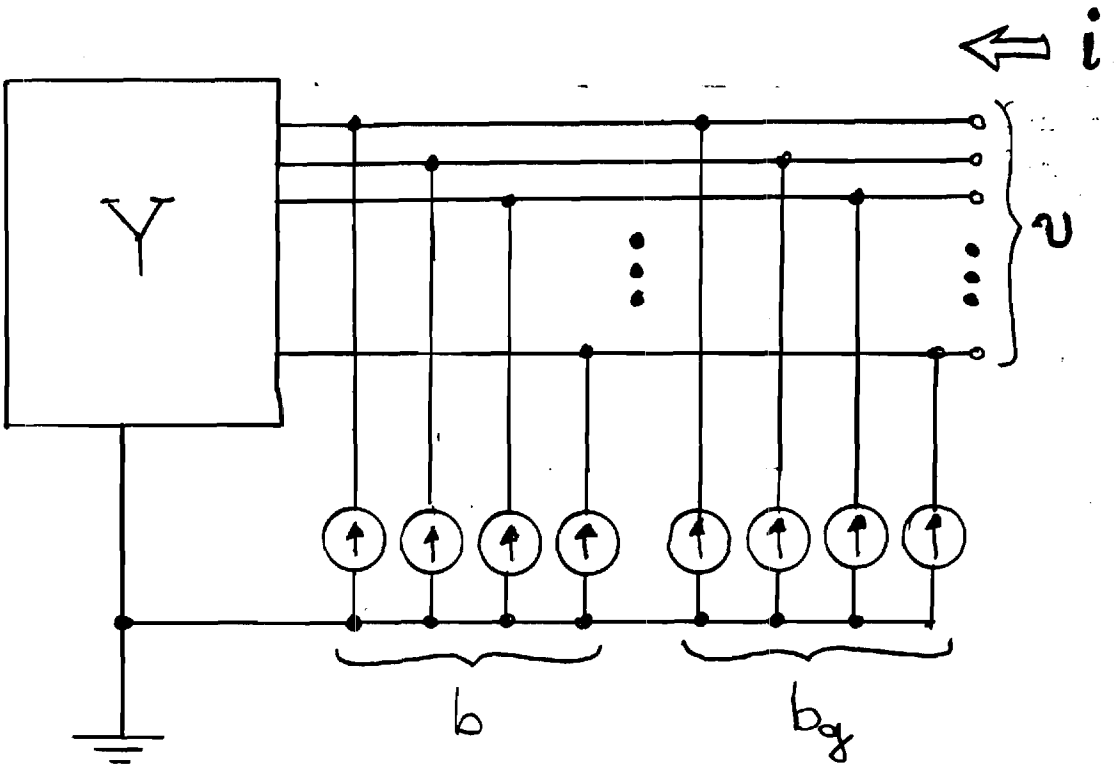

Figure 3-5: Model of Transmission Line with GIC coupling in the Resistive Companion Form.

$$Y \cdot v = b + b_g + i \tag{3-21}$$

where Y is the transmission line characteristic impedance, b is the vector of currents depending on past history voltages and currents, and b_g is the vector of currents representing GIC effects. The above equation can be solved by discrete time techniques in terms of the impulse response model defined in the previous section. Specifically, let v_n and i_n represent the values of the voltage and current vectors at the line ends at the n-th time step. Then:

$$Yv_n = b_{n-1} + b_{g_n} + i_n \tag{3-22}$$

where

$$Y = G[I+S_o]^{-1}[I-S_o]$$

$$b_{n-1} = G[I+S_o]^{-1}\Sigma(S_k-S_{k-1})(v_{n-k}-G^{-1}i_{n-k})$$

$$b_{g_n} = G[I+S_o]^{-1}a_{g_n}$$

where S_i represents the transmission line step respone (at the ith time interval), i.e. it is the integral of the impulse response m(t), performed in discrete time.

The above equation (3-22) is a resistive companion form representation of a transmission line with GIC coupling. Specifically, the real matrix Y is the admittance matrix of a resistive network (block Y in Figure 3-5). The vector b_{n-1} represents the past history dependent current sources. The entries of the current source vector b_{n-1} are computed by discrete convolution as shown in Eq. (3-22). The vector b_{g_n} are the independent current sources (b_g in Figure 3-5), representing the effects of GIC.

Using these equations, a transmission line with GIC coupling and its interaction with the integrated power system is simulated using the standard methodology for power system transient simulation employed by the EMTP and PSTS programs.

Section 4

PRELIMINARY MODEL EVALUATION

(to be added)

Section 5

REFERENCES

1. Syun-Ichi Akasofu, "The Dynamic Aurora," Scientific American, pp. 90-97, May 1989.

2. S. Chapman, Solar Plarma, Geomagnetism and Aurora, Gordon and Breach Science Publishers, New York, 1968.

3. V. D. Albertson, "Geomagnetic Disturbance Causes and Power System Effects," 1989 IEEE PES Summer Meeting, Long Beach, California, July 12, 1989.

4. R. Pirjola, "On Currents Induced in Power Transmission Systems During Geomagnetic Variations," IEEE Transactions on Power Apparatus and Systems, vol. PAS-104, no. 10, pp. 2825-2830, October 1985.

5. G. B. Rackliffe, J. C. Crouse, J. R. Legro, and V. J. Kruse, "Simulation of Geomagnetic Currents Induced in a Power System by Magnetohydrodynamic Electromagnetic Pulses," IEEE Transactions on Power Delivery, vol. PWRD-3, no. 1, pp. 392-397, January 1988.

6. J. R. Legro, N. C. Abi-Samra, J. C. Crouse, and F. M. Tesche, "A Methodology to Assess the Effects of Magnetohydrodynamic Electromagnetic Pulse (MHD-EMP) on Power Systems," IEEE Transactions on Power Delivery, vol. PWRD-1, no. 3, pp. 203-209, July 1986.

7. M. Rabinowitz, "Magnetohydrodynamic EMP, Solar Storm GIC, and Substorms," Conference on Geomagnetically Induced Currents, sponsored by Electric Power Research Institute, Burlingame, California, November 8-10, 1989.

8. M. Rabinowitz, "Nuclear Electromagnetic Pulse," Encyclopedia of Science and Technology, 1986 Yearbook, McGraw Hill, New York, pp. 34-47, 1985.

9. C. N. Vittitoe and M. Rabinowitz, "Radiative Reactions and Coherency Modeling in the High-Altitude Electromagnetic Pulse," Physical Review A, vol. 37, no. 6, pp. 1969-1977, March 15, 1988.

10. M. Rabinowitz, "Effect of the Fast Nuclear Electromagnetic Pulse on the Electric Power Grid Nationwide: A Different View," IEEE Transactions on Power Delivery, vol. PWRD-2, no. 4, pp. 1199-1222, October 1987.

11. K. W. Klein, P. R. Barnes, and H. W. Zaininger, "Electromagnetic Pulse and the Electric Power Network," IEEE Transactions on Power Apparatus and Systems, vol. PAS-104, pp. 1571-1577, 1985.

12. C. L. Longmire, "On the Electromagnetic Pulse Produced by Nuclear Explosions," IEEE Transactions on Electromagnetic Compatibility, vol. EMC-20, no. 1, pp. 3-13, February 1978.

13. C. N. Vittitoe, "Did High-Altitude EMP Cause the Hawaiian Streetlights Incident?", Sandia National Labs, Albuquerque, New Mexico, SAND88-00430, 1988.

14. D. P. Millard, A. P. Sakis Meliopoulos, and G. J. Cokkinides, "Parametric Analysis of EMP Induced Overvoltages on Power Lines," IEEE Transactions on Power Delivery, vol. PWRD-3, no. 3, pp. 1224-1231, July 1988.

15. J. R. Wait, Geo-Electromagnetism, Academic Press, Inc., New York, Chapter VI, pp. 184-208, 1982.

16. A. A. Kaufman and George V. Keller, The Magnetotelluric Sounding Method, Elsevier Scientific Publishing Company, New York, Chapter 5, pp. 113-155, 1981.

17. T. Rikitake and Y. Honkura, Solid Earth Geomagnetism, Terra Scientific Publishing Company, Tokyo, Japan, and D. Reidel Publishing Company, Boston, Chapter 11, pp. 267-292, 1985.

18. V. D. Albertson and J. A. Van Ballen, "Electric and Magnetic Fields at the Earth's Surface Due to Auroral Currents," IEEE Transactions on Power Apparatus and Systems, vol. PAS-89, no. 4, pp. 578-584, April 1970.

19. J. R. Wait, "Electromagnetic Surface Impedance for a Layered Earth for General Excitation," Radio Science, vol. 15, no. 1, pp. 129-134, January-February 1980.

20. R. Pirjola and A. Viljanen, "On Geomagnetically-Induced Currents in the Finnish 400 kV Power System by an Auroral Electrojet Current," IEEE Transactions on Power Delivery, vol. PWRD-4, no. 2, pp. 1239-1245, April 1989.

21. D. Park, "Magnetic Field of a Horizontal Current Above a Conducting Earth," Journal of Geophysical Research, vol. 78, no. 16, pp. 3040-3043, June 1, 1973.

22. A. T. Price, "Electromagnetic Induction in a Semi-Infinite Conductor with a Plane Boundary," Quart. J. Mech. and Appl. Math., vol. 3, pt. 4, pp. 385-410, 1950.

23. S. P. Srivastava, "Method of Interpretation of Magnetotelluric Data when Source Field is Considered," Journal of Geophysical Research, vol. 70, no. 4, pp. 945-954, February 15, 1965.

24. R. D. Hibbs and F. W. Jones, "The Calculation of the Electromagnetic Fields of a Sheet Current Source with Arbitrary Spatial Intensity Distribution over a Layered Half Space - I, The General Method and Results," Geophys. J. R. Astr. Soc., vol. 46, pp. 433-452, 1976.

25. W. R. Peltier and J. F. Hermance, "Magnetotelluric Fields of a Gaussian Electrojet," Can. J. Earth Sci., vol. 8, pp. 338-346, 1971.

26. R. D. Hibbs, Jr. and F. W. Jones, "Electromagnetic Induction in the Earth by a Non-Symmetric Non-Uniform Source," J. Geomag. Geoelectr., vol. 25, pp. 75-86, 1973.

27. M. Abramowitz and J. A. Stegun (eds.), Handbook of Mathematical Functions, U.S. Department of Commerce, National Bureau of Standards, 10th ed., pg. 886, 1972.

28. D. Larose, "The Hydro-Québec System Blackout of 13 March 1989," Conference on Geomagnetically Induced Currents, sponsored by Electric Power Research Institute, Burlingame, California, November 8-10, 1989.

29. G. J. Cokkinides and A. P. Meliopoulos, "Transmission Line Modeling with Explicit Grounding Representation," Electric Power Systems Research, vol. 14, no. 2, pp. 109-119, April 1988.

30. W. A. Chisholm and Y. L. Chow, "Travel Time of Transmission Towers," IEEE Transactions on Power Apparatus and Systems, vol. PAS-104, no. 10, pp. 2922-2928, October 1985.

31. A. P. Meliopoulos and M. G. Moharem, "Transient Analysis of Grounding Systems," IEEE Transactions on Power Apparatus and Systems, vol. PAS-102, no. 2, pp. 389-397, February 1983.

32. A. Paplexopoulos and A. P. Meliopoulos, "Frequency Dependent Modeling of Grounding Systems," Proc. Midwest Power Symposium, pp. VI.E. 1-13, 1985.

33. J. K. Snelson, "Propagation of Traveling Waves on Transmission Lines-Frequency Dependent Parameters," IEEE Transactiosn of Power Apparatus and Systems, vol. PAS-91, pp. 85-91, January/February 1972.

Appendix A

DERIVATION OF TRANSMISSION LINE EQUATIONS IN THE PRESENCE OF GIC

Consider an infinitesimal segment of overhead conductor Δx. It is characterized by an inductance, $L' = L\Delta x$, resistance, $R' = R\Delta x$, and shunt capacitance, $C' = C\Delta x$. Assuming that EMP/GIC related electromagnetic fields are slowly varying their direct effect on the line is negligible. However, a substantial voltage can develop along the line direction on the earth, due to GIC. Assume that the earth potential difference across the line length, Δx, due to GIC is $V_g \cdot \Delta x$. The equivalent circuit of the line segment is shown in Figure A-1.

$$v_2 - v_1 = -R'i_2 - L' \frac{di_2}{dt} + v_g \cdot \Delta x$$

$$i_2 - i_1 = -G'v_1 - C' \frac{du_1}{dt}$$

let

$$v_2 - v_1 = \Delta v$$

$$i_2 - i_1 = \Delta i$$

then

$$\frac{\Delta u}{\Delta x} = -Ri_2 = L' \frac{di_2}{dt} + v_g$$

$$\frac{\Delta i}{\Delta x} = -Gv_1 - C \frac{du_1}{dt}$$

taking limit as

$$\Delta x \to 0$$

$$i_1 \to i_2 \triangleq i$$

$$v_1 - v_2 \triangleq v$$

results in the differential equations

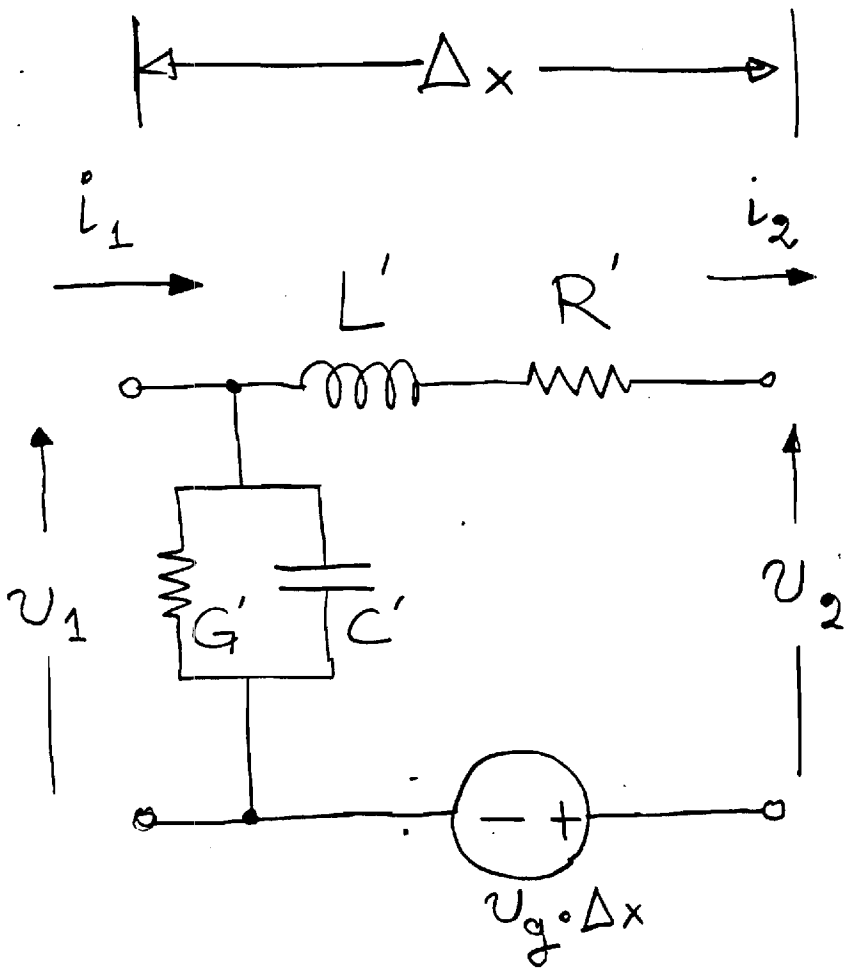

Figure A-1 : Equivalent circuit of a short line segment in the presence of GIC

$$\frac{\partial v}{\partial x} = -Ri - L\frac{di}{dt} + v_g$$

$$\frac{\partial i}{\partial x} = -Gv - C\frac{du}{dt} .$$

E-21-666

EFFECTS OF GEOMAGNETIC DISTURBANCES ON ELECTRIC POWER TRANSMISSION SYSTEMS

Prepared for

ELECTRIC POWER RESEARCH INSTITUTE
3412 Hillview Avenue
Palo Alto, California 94304

EPRI Project Manager
Dr. Mario Rabinowitz

Prepared by

A. P. Sakis Meliopoulos
E. N. Glytsis
Electric Power Laboratory
School of Electrical Engineering
Georgia Institute of Technology
Atlanta, Georgia 30332-0250

G. J. Cokkinides
Department of Electrical Engineering
University of South Carolina
Columbia, South Carolina 29208

February 1990
Revised June 1990

EPRI PERSPECTIVE

(to be added)

ABSTRACT

(to be added)

SUMMARY

(to be added)

ACKNOWLEDGEMENTS

(to be added)

TABLE OF CONTENTS

LIST OF ILLUSTRATIONS

(to be added)

LIST OF TABLES

(to be added)

Section 1

INTRODUCTION AND OBJECTIVE

1.1 INTRODUCTION

The objective of this project is to investigate the level of induced and/or transferred voltages and currents to an electric power system from (1) geomagnetic disturbances due to MHD-EMP and (2) GIC due to solar storms, SS-GIC. Subsequently, a comparison of the effects of MHD-EMP and SS-GIC have been performed.

MHD-EMP is an electromagnetic pulse with very low amplitude which results from geomagnetic disturbances caused by high altitude nuclear detonation. The electric field magnitude is on the order of 100 V/km, low frequency and lasts for several minutes. Similar geomagnetic disturbances are caused by solar storms and result in electric field magnitudes on the order of 10 V/km, low frequency and last from minutes to an hour. Both phenomena cause the flow of almost DC current in the windings of power transformers through the grounding system. Because of the nonlinear magnetization characteristics of the power transformers, the flow of the low frequency electric currents may cause serious secondary results, such as high magnetization currents due to saturation, abnormal reactive power requirements, and disruption of operation. Presently, it is not clear which disturbance (the high magnitude short duration MHD-EMP or the low magnitude long duration SS-GIC) is the most severe to a power system. A system approach has been adopted to address these problems, and to determine at what level saturation is reached.

The objectives of the project have been attained with a two step procedure: In the first step a model of an electric power transmission line including grounding and MHD-EMP or solar storm coupling has been developed. The basic methodology utilized for this step is described in Sections 2 and 3. Since the coupling of MHD-EMP or solar storm induced voltages to power lines is mainly through the line grounding system, it is important to accurately model the power line tower grounding as well as the terminal substation grounding system. For this purpose, the EPRI grounding models developed by Georgia Tech have been utilized. The form of the transmission line model is in terms of a multiple input-multiple output linear system.

The second step involves integration of the model developed in the first step into the EPRI computer model ADCFLT. This computer model is a time domain model similar to the EMTP. It allows modeling of an integrated power system, power system grounding, and the nonlinear magnetization characteristics of power transformers. Using this model, system studies have been performed to determine transformer magnetization currents and reactive power requirements. Of special importance is the degree of saturation of power transformers due to these phenomena. This information can be utilized to analyze transformer performance such as eddy losses in steel members, conductors, and leads. A test system has been utilized provided by Minnesota Power Company.

1.2 REPORT OUTLINE AND MAJOR CONCLUSIONS

(to be added)

Section 2

DESIGN WAVEFORMS FOR SOLAR-STORM GEOMAGNETICALLY INDUCED CURRENTS (SS-GIC) AND FOR MAGNETOHYDRODYNAMIC ELECTROMAGNETIC PULSES (MHD-EMP)

2.1 INTRODUCTION

Electric currents that flow in the molten core of the earth cause its dipole-like magnetic field. The magnetic field of the earth interacts with the interplanetary magnetic field which is actually an extension of the magnetic field of the sun due to the solar wind. The solar wind consists of charged particles, mainly electrons and protons (hydrogen ions), emitted from the surface of the sun. Thus, the solar wind acts like an extension of the magnetic field of the sun and interacts with the earth's magnetic field in a complex manner creating the earth's magnetosphere. In addition, interactions of the earth's magnetic field and the solar wind give rise to a vast magnetohydrodynamic generator that converts the kinetic energy of the solar-wind particles in electric energy which powers the auroral currents or auroral electrojets [1,2]. These currents usually follow circular or elliptical paths around the geomagnetic poles at altitudes of 100 kilometers or more and produce fluctuations in the earth's magnetic field that are termed geomagnetic storms. The strength of the geomagnetic storms is strongly related with solar phenomena that affect the solar wind. These phenomena are the solar flares, the coronal holes, and the disappearing filaments. The severity of the geomagnetic storms strongly depends on the intensity of the above mentioned solar effects. Large solar storms can produce large variations of the auroral electrojets which produce large variations of the geomagnetic field on the earth's surface. The earth as a conducting sphere experiences, or portions of it experience, these time varying magnetic fields. Varying magnetic fields induce electric potential gradients which are called earth-surface-potentials (ESP). The earth-surface-potentials can obtain values in the range between 1 and 10 volts/km depending on the severity of the geomagnetic storm and the earth's conductivity [3,4]. The electric power systems are exposed to ESP through the grounding grid. Since the ESP has frequency of one to a few millihertz the resulting geomagnetically-induced-currents (GIC) can be considered quasi-direct currents compared to 50 Hz or 60 Hz of the electrical power system frequency. Geomagnetic field variations caused by magnetosphere phenomena will result in an induced ESP orthogonal to the field changes. Usually, an idealized east-west

auroral current will cause field variations in the north-south component of the earth's magnetic field, resulting in an east-west induced ESP. Thus, transmission lines in the east-west direction are more susceptible to large ESP than transmission lines in the north-south direction. However, the auroral currents are not ideally east-west and consequently large ESP can be observed in any direction. Several analytical methods have been developed to estimate the induced ESP based on different modeling of the auroral currents and the earth's conductivity. Due to the complexity of the geomagnetic phenomena all these models are approximate and direct measurements of the geomagnetic fields seems to be the best choice.

Geomagnetic disturbances and associated induced earth currents can also originate from the explosion of nuclear bombs at high altitude above the earth's surface [5-7]. These explosions result in transient electromagnetic pulses (EMP) which can affect the operation of the power and communications systems. There are two basic types of electromagnetic pulses due to nuclear explosions. The one is the high altitude quick pulse (TEMP) (Tachy-EMP), and the other is the much slower magnetohydrodynamic EMP (MHD-EMP). For this report, only the slow MHD-EMP is of interest since its effect to power system operation is very similar to solar-storm geomagnetically induced currents. Two similar but different magnetic disturbances give rise to the MHD-EMP. The first is called magnetic bubble EMP (BEMP) [8]. The second is called Atmospheric heave EMP (AEMP) [8]. Due to the nuclear explosion a magnetohydrodynamic bubble of ionized conducting debris is formed and expands rapidly. Initially the geomagnetic flux inside the bubble is very small. If the shell of the magnetic bubble were nonconducting, the expansion of the bubble would simply enclose more magnetic flux of the geomagnetic field. However, since the bubble is conducting, currents are induced on the shell which counteract the earth's magnetic field. Thus, even if the bubble increases in volume the geomagnetic flux that encloses remains as small as it was initially. This effect results in a compression of the geomagnetic field around the bubble. These changes of the geomagnetic field can induce electric fields in the earth which can reach a maximum magnitude of 0.1 V/m with periods from 2 to 100 seconds [8]. This pulse occurs at about 2 to 5 seconds after the nuclear explosion. The second component of the MHD-EMP, the atmospheric heave EMP, occurs more than 10 seconds after the explosion. This pulse is caused by the atmospheric heave of the bomb-heated ionized air across the geomagnetic field. This ionization forms current loops which have mirror images in the earth. These perturbations of the geomagnetic field extend out more than 1250 miles from the source point and last approximately 100 sec. The induced electric fields and frequencies are very low between 0.001-0.03 V/m and ~0.01 Hz. Several analytical methods have been developed mainly for the study of the fast

EMP and comparisons of it with the lightning [9-12]. However, there is not much available information for theoretical modeling of MHD-EMP. Most of the analytical studies for the evaluation of the effects of MHD-EMP on power systems are based on measurements of the induced electric field [5,6], or by assuming plane wave excitation [13,14].

In the following subsections, the most common methods used for the evaluation of the ESP due to SS-GIC or MHD-EMP are reviewed. In addition, sample tables of measured data are given to be used as design ESP waveforms for the calculation of the effect of SS-GIC and MHD-EMP on power systems, and for evaluation of several methods proposed for the alleviation of these effects.

2.2 DESIGN EARTH SURFACE POTENTIAL WAVEFORMS DUE TO SOLAR-STORM GEOMAGNETICALLY INDUCED CURRENTS

Several analytical models have been used for the evaluation of the induced electric field on the surface of the earth due to the variations of the geomagnetic field. These models differ in the representation of the auroral currents and the conductivity of the earth. The auroral currents are known to be at altitudes between 100 to 300 km above the earth's surface. These currents can be modeled like current line sources or current sheet sources of infinite extend above a flat earth's surface. However, the auroral currents have such a spatial extension that they can not be considered either a current line or a current sheet. The above assumptions though give some estimate of the induced electric field on the earth's surface. Specifically, the current line model gives a lower limit while the current sheet model gives an upper limit of the induced electric field. Sometimes the auroral currents are assumed to be at an infinite distance from the ground. In this case, the geomagnetic field is modeled as a plane electromagnetic wave. The conductivity of the earth is also difficult to model due to the large variety and inhomogeneity of the earth's surface from place to place. The simplest model assumes a flat earth surface with a uniform effective conductivity. More sophisticated earth models divide the earth's surface in multiple layers, each one having a different conductivity.

The simplest method for modeling the auroral currents is the plane electromagnetic wave model [15]. The earth is modeled as a horizontally stratified medium of one or more layers of differing conductivities. The incident geomagnetic field is assumed to be a linearly polarized, monochromatic plane wave. The electric field on the surface of the earth is computed with usual electromagnetic analysis methods. In addition, using this technique the surface impedance of the earth, Z_s, can be

computed, where $Z_s = E_x/H_y$ (E_x/H_y are the horizontal components of the electric and magnetic field on the earth's surface, respectively). This is useful since from measurement of the magnetic field, the induced electric field can be estimated.

Another widely used technique models the auroral currents as an infinite horizontal current sheet at a height h above the horizontally also stratified earth of one or more layers [15-19]. To solve the problem, the electric and magnetic Hertz vectors are commonly used. For the described geometry, these vectors have only one component which is perpendicular to the earth's surface and to the auroral current sheet. Using the vector Hertz potentials and Maxwell's equations along with the corresponding boundary conditions, the electric field on the earth's surface can be found. This field is a function of (1) the magnitudes along the two horizontal directions of the current sheet (j_x,j_y), (2) the radian frequency ω of the auroral current, (3) the spatial wave numbers of the spectral components of the auroral currents, (4) the altitude h of the auroral current, and (5) the characteristics of the earth. Even if the described analysis considered a single spectral component, there is no loss of generality since by Fourier synthesis any time-dependent source current can be written as a linear combination of its spectral components. Consequently, the resulting induced electric field will be a linear combination of the fields due to the different spectral components. As it was mentioned earlier, the current sheet method overestimates the induced electric field on the earth's surface.

The auroral currents can also be modeled as a line current source parallel to the earth's surface at an altitude h [15,18,20,21]. Usually, the line is positioned in the east-west direction and is assumed positive in the westward direction. Earth's surface is modeled like a horizontally stratified medium. The general methodology used for the solution of these problems is based on Price's analysis [22]. This analysis assumes slow variations of the geomagnetic fields. As a result, the second time derivatives in the wave equation are neglected. This assumption permits solutions of the magnetic field expressed in terms of the gradient of a scalar magnetic potential for the region above the earth, while the electric field solutions are expressed in terms of the time derivative of a vector magnetic potential for the earth region. An equivalent procedure consists of expressing the electric field as $\vec{E} = e^{j\omega t}G(z)\vec{F}(x,y)$, where G and $\vec{F}$ have to be determined for each region from the wave equation and the boundary conditions of the problem [(x,y) correspond to the horizontal plane while z is the perpendicular coordinate]. Using this procedure the resulting electric and magnetic fields on the

earth's surface are calculated as functions of the following parameters: (1) the magnitude of the auroral current, (2) the radian frequency of the auroral current, (3) the altitude h of the auroral current, (4) the difference in latitude between the auroral current and the point for which the calculations are made, and (5) the surface impedance of the earth Z_s [23] which depends on the earth's parameters and modeling. Usually, since the magnitude of the auroral currents is not known, an estimate of $J = 10^5 A$ is used. As it was mentioned previously this method underestimates the induced electric field on the earth's surface due to the modeling of the auroral currents as a horizontal line current.

In the described models the auroral currents are modeled as uniform or sinusoidal distributions. However, none of these assumptions is very accurate. More sophisticated studies include Gaussian modeling of the electrojet [24,25]. In addition, Hibbs et al. have studied nonsymmetric auroral currents distributions [26].

Independently of the used model, the complexity of the physical effect of the auroral electrojet is difficult to represent. In addition, all the described models assume sinusoidal auroral currents. However, if the spectral content of the auroral currents was known, these models along with the superposition principle could be used for the calculation of the induced electric field. Since the spectral content of the auroral currents is not known and, in addition, is varying with time, the geomagnetic field is usually measured in several positions in the areas of interest using magnetometers. By measuring the magnetic field, the induced electric field can be roughly estimated using the plane wave assumption from [4]

$$E(t) = -\frac{1}{(\pi\mu_o\sigma)^{1/2}} \int_0^\infty \frac{g(t-u)}{u^{1/2}}\, du \ , \qquad (2\text{-}1)$$

where E(t) is the horizontal component of the induced electric field, μ_o is the permeability of the freespace, σ is the conductivity of the earth, and g is the time derivative of the horizontal component of the magnetic field. If the measured data are used, the derivative g can be computed numerically and the integral can be approximated using the extended Simpson's rule [27] by the following formula

$$\int_0^\infty \frac{g(t-u)}{u^{1/2}}\, du \approx D^{1/2}\left\{\frac{4}{3}\, g(t)+g(t-D)+\frac{2}{3}\sum_{j=1}^{L}(1+a_j)\,\frac{g[t-(j+1)D]}{(j+1)^{1/2}}\right\} \ , \qquad (2\text{-}2)$$

where D is the data time interval and $a_j = 0$ when j is even and $a_j = 1$ when j is odd; L is the total number of data points that are considered for the calculation of E(t). Using the data measured during May 12-13, 1989, at magnetic Observatory

Furstenfeldbruck (Figure 2-1, Table 2-1, and Eqs. (2-1) and (2-2)), the induced electric field was calculated and its values are summarized in Table 2-2 (Figure 2-2).

2.3 DESIGN EARTH SURFACE POTENTIAL WAVEFORMS DUE TO MAGNETOHYDRODYNAMIC ELECTROMAGNETIC PULSE

The effects of the magnetohydrodynamic electromagnetic pulse (MHD-EMP) on power system grids are very similar to those of geomagnetic storms. More specifically, MHD-EMP generates electric fields on the order of 10^{-1} V/m (about an order of magnitude higher than the geomagnetically-induced electric fields) of frequencies less than 1 Hz and of 100-200 sec duration. As it was described previously, MHD-EMP is due to two distinct physical mechanisms, the magnetic bubble (BEMP) and the atmospheric heave (AEMP). The early portion of the MHD-EMP (less than 10 seconds after the nuclear explosion) is due to BEMP while the rest of MHD-EMP is due to the AEMP [6]. Some estimate of the average induced electric field can be calculated using the following arguments [7]. The magnetic bubble, as it expands, pushes the geomagnetic field out of its way. The bubble obtains its maximum size when the energy of the excluded field equals the initial kinetic energy, T, of the conducting shell of the magnetic bubble, neglecting all other loss mechanisms. Thus, the following equation can be written [7]

$$\frac{1}{2\mu_o}\langle B^2\rangle\left(\frac{4}{3}\pi R^3\right) = T \Rightarrow R = [3\mu_o T/2\pi\langle B^2\rangle]^{1/3}\ , \tag{2-3}$$

where $\langle B^2\rangle$ is the mean squared value of the flux density of the unperturbed geomagnetic field, μ_o is the permeability of freespace, R is the maximum radius of the magnetic bubble (assuming spherical bubble), and T is the initial kinetic energy of the conducting debris of the bomb. The average power, $\langle P\rangle$, of the MHD-EMP can be estimated from

$$\langle P\rangle = \frac{fT}{\Delta t}\ , \tag{2-4}$$

where f is the conversion efficiency of the kinetic energy, T, in electromagnetic power, and Δt is the duration of the produced electromagnetic pulse. The average power density near the bubble can then be found from $\langle P\rangle/4\pi R^2$. Using the Poynting vector, the power density is $E^2/2\eta$, where η is the intrinsic impedance of freespace. Using the above arguments, an estimate of the induced electric field can be found from

$$E = \left[\frac{2fT^{1/3}\eta}{4\pi\Delta t[3\mu_o/2\pi\langle B^2\rangle]^{2/3}}\right]^{1/2}\ . \tag{2-5}$$

Using $f \simeq 10^{-5}$, $T \simeq 1.76 \cdot 10^{15}$ J (for a 30% yield of a 1.4 Mt bomb [7]), $\eta = 377\ \Omega$, $\Delta t \simeq 100$ sec, and $B \simeq 5 \cdot 10^{-5}$ wb/m^2, an electric field of 0.1 V/m can be estimated. The above estimate is based only on the BEMP effect under the rough assumptions made above. However, the atmospheric currents due to air ionization produce significant portion of the induced electric field. Thus, the most valuable information about a MHD induced EMP is empirically known from the magnetometer data acquired during actual nuclear events as the "Starfish" test conducted in the Pacific. The design waveform for the simulation of MHD-EMP is the one measured during the Starfish test. The magnetometer data [6] have been used along with Eq. (2-1) to calculate the induced electric field that appears in Figure 1 of Reference 5. This electric field has been sampled and linearly approximated and is tabulated in Table 2-3 (Figure 2-3).

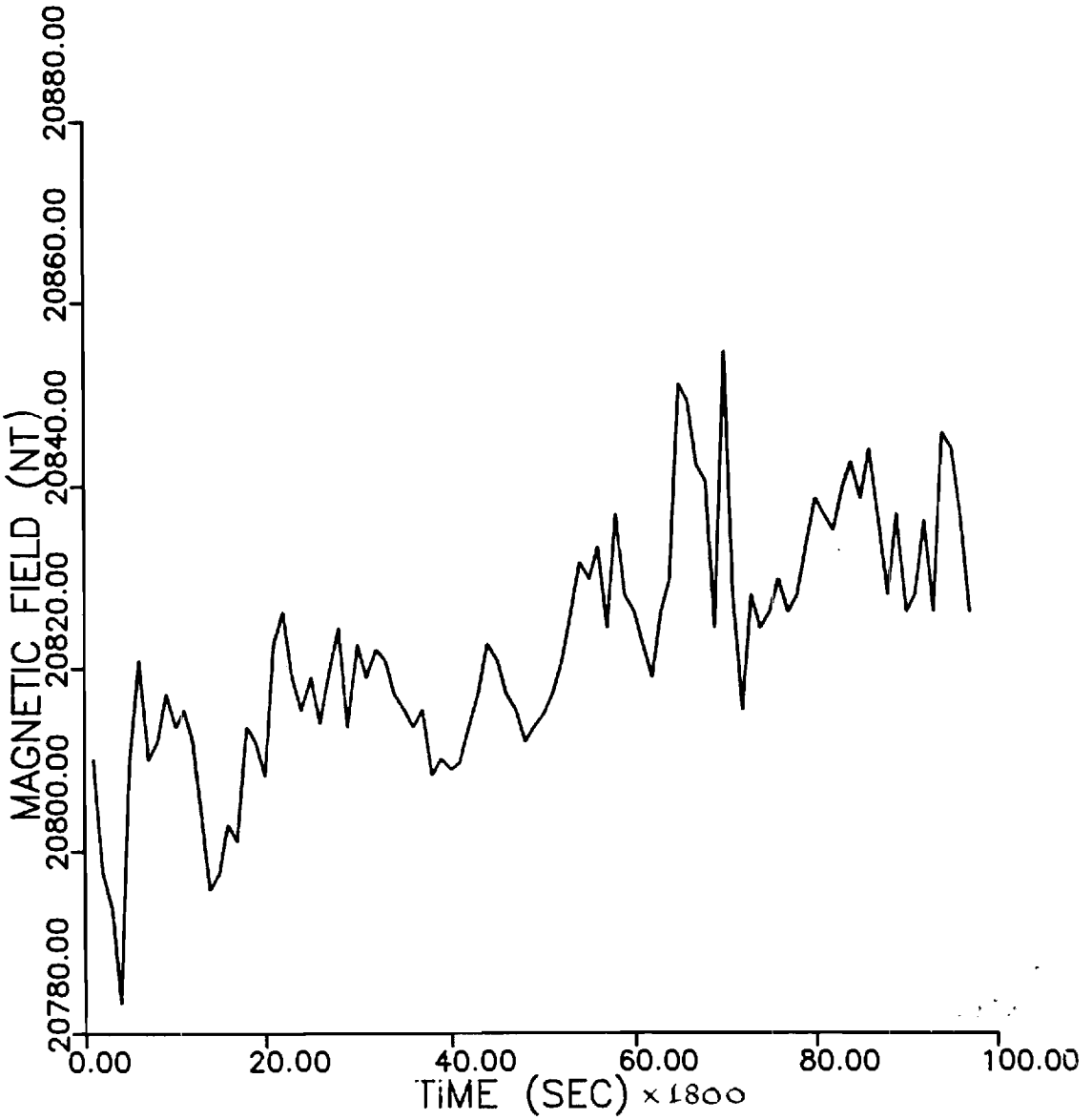

Figure 2-1. Horizontal Component of Magnetic Field. Magnetic Observatory Fürstenfeldbruck, May 13, 1989

~~Fig. 2-1~~

~~Fig. 1~~

~~Horizontal component of magnetic field~~

TABLE I

Measurements of the Horizontal Component of the Magnetic Flux Density of the Geomagnetic Field at the Fürstenfeldbruck Station in 30 Minute Intervals Between May 12-13, 1989

Time (sec)	Horizontal Component of Geomagnetic Field (nT)
.0	20810.00
1800.0	20797.60
3600.0	20794.00
5400.0	20783.30
7200.0	20811.10
9000.0	20820.80
10800.0	20810.00
12600.0	20811.90
14400.0	20817.20
16200.0	20813.60
18000.0	20815.40
19800.0	20811.90
21600.0	20804.70
23400.0	20795.80
25200.0	20797.60
27000.0	20802.90
28800.0	20801.10
30600.0	20813.60
32400.0	20811.90
34200.0	20808.30
36000.0	20822.60
37800.0	20826.10
39600.0	20819.00
41400.0	20815.40
43200.0	20819.00
45000.0	20814.00
46800.0	20819.70
48600.0	20824.30
50400.0	20813.60
52200.0	20822.50
54000.0	20819.00
55800.0	20822.00
57600.0	20820.80
59400.0	20817.20
61200.0	20815.40
63000.0	20813.60
64800.0	20815.40
66600.0	20808.30
68400.0	20810.10
70200.0	20809.00
72000.0	20809.70
73800.0	20813.60
75600.0	20817.20
77400.0	20822.60
79200.0	20820.80
81000.0	20817.20

82800.0	20815.40
84600.0	20811.90
86400.0	20813.60
88200.0	20815.00
90000.0	20817.20
91800.0	20820.80
93600.0	20826.10
95400.0	20831.50
97200.0	20829.70
99000.0	20833.20
100800.0	20824.30
102600.0	20836.80
104400.0	20827.90
106200.0	20826.10
108000.0	20822.60
109800.0	20819.00
111600.0	20826.10
113400.0	20829.70
115200.0	20851.10
117000.0	20849.30
118800.0	20842.20
120600.0	20840.40
122400.0	20824.30
124200.0	20854.70
126000.0	20827.90
127800.0	20815.40
129600.0	20827.90
131400.0	20824.30
133200.0	20826.10
135000.0	20829.70
136800.0	20826.10
138600.0	20827.90
140400.0	20833.20
142200.0	20838.60
144000.0	20836.80
145800.0	20835.00
147600.0	20839.50
149400.0	20842.50
151200.0	20838.60
153000.0	20843.90
154800.0	20836.10
156600.0	20827.90
158400.0	20836.80
160200.0	20826.10
162000.0	20827.90
163800.0	20836.10
165600.0	20826.10
167400.0	20845.70
169200.0	20843.90
171000.0	20836.80
172800.0	20826.10

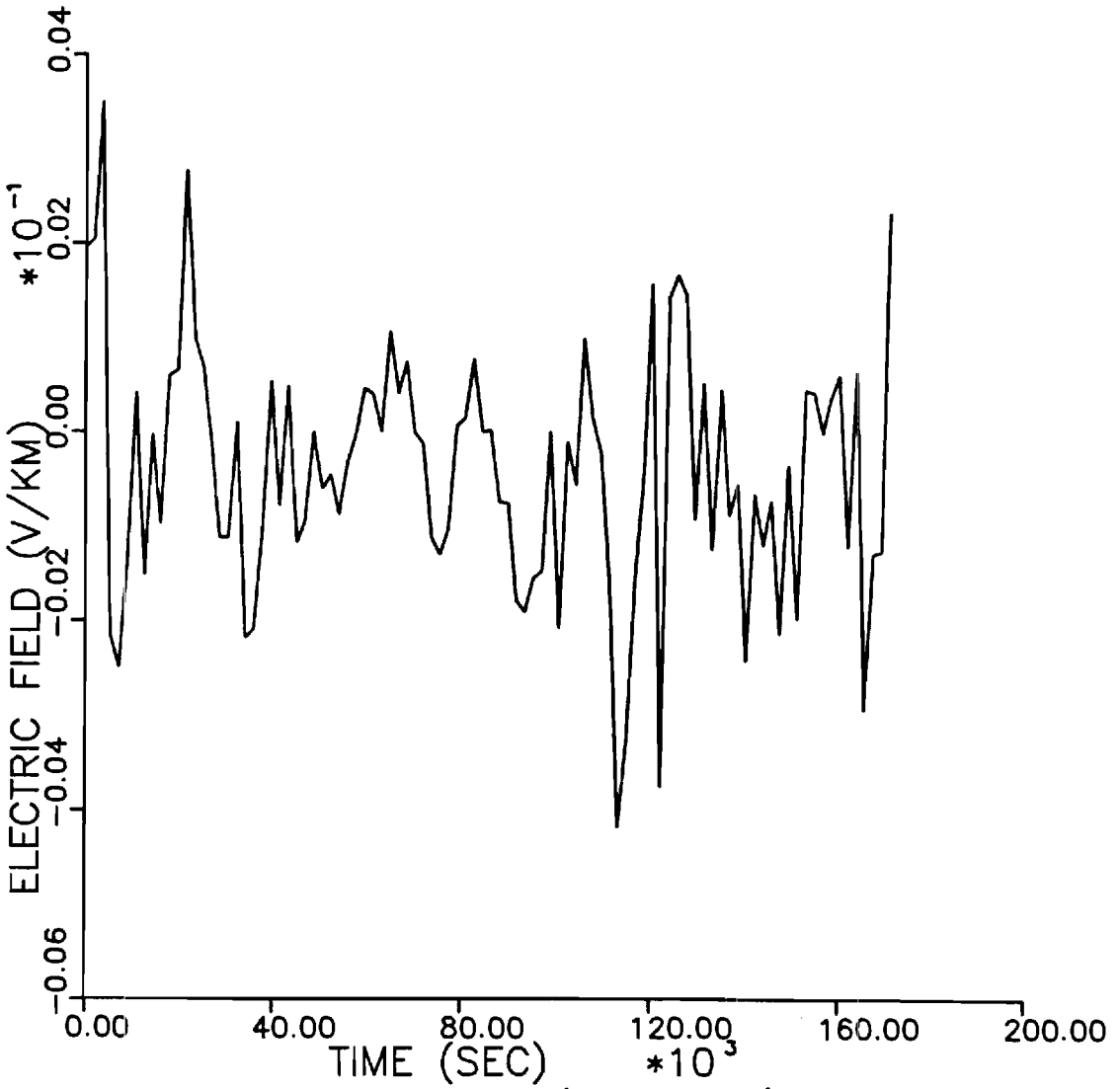

Figure 2-2. SS-GIC Electric Field. Magnetic Observatory Fürstenfeldbruck, May 13, 1989

Fig. 2-2

~~Fig. 2~~

SS-GIC electric field in V/km

TABLE II

Calculated Induced Electric Field (SS-GIC) Using the Measurements of Table I and Eqs. (1) and (2)

Time (sec)	Induced Electric Field (V/km)
.0	.19613E-02
1800.0	.20404E-02
3600.0	.35063E-02
5400.0	-.21590E-02
7200.0	-.24903E-02
9000.0	-.13399E-02
10800.0	.40067E-03
12600.0	-.15157E-02
14400.0	-.37079E-04
16200.0	-.97319E-03
18000.0	.58856E-03
19800.0	.64136E-03
21600.0	.27804E-02
23400.0	.97135E-03
25200.0	.68159E-03
27000.0	-.12122E-03
28800.0	-.11203E-02
30600.0	-.11249E-02
32400.0	.91153E-04
34200.0	-.21800E-02
36000.0	-.20967E-02
37800.0	-.10255E-02
39600.0	.52078E-03
41400.0	-.78152E-03
43200.0	.47075E-03
45000.0	-.11750E-02
46800.0	-.95832E-03
48600.0	-.61076E-05
50400.0	-.60230E-03
52200.0	-.46227E-03
54000.0	-.87251E-03
55800.0	-.33812E-03
57600.0	-.25453E-04
59400.0	.45499E-03
61200.0	.39364E-03
63000.0	.41640E-05
64800.0	.10508E-02
66600.0	.40856E-03
68400.0	.73819E-03
70200.0	-.12803E-04
72000.0	-.12281E-03
73800.0	-.11164E-02
75600.0	-.12954E-02
77400.0	-.10285E-02
79200.0	.67825E-04
81000.0	.14286E-03
82800.0	.76736E-03

84600.0	.62566E-05
86400.0	.17448E-04
88200.0	-.73720E-03
90000.0	-.75860E-03
91800.0	-.17937E-02
93600.0	-.19081E-02
95400.0	-.15541E-02
97200.0	-.14738E-02
99000.0	.79403E-06
100800.0	-.20720E-02
102600.0	-.11190E-03
104400.0	-.56233E-03
106200.0	.98050E-03
108000.0	.13813E-03
109800.0	-.22304E-03
111600.0	-.16265E-02
113400.0	-.41819E-02
115200.0	-.32840E-02
117000.0	-.14967E-02
118800.0	-.50570E-03
120600.0	.15648E-02
122400.0	-.37526E-02
124200.0	.14089E-02
126000.0	.16592E-02
127800.0	.14355E-02
129600.0	-.91577E-03
131400.0	.50753E-03
133200.0	-.12444E-02
135000.0	.44008E-03
136800.0	-.87843E-03
138600.0	-.55878E-03
140400.0	-.24192E-02
142200.0	-.66480E-03
144000.0	-.11979E-02
145800.0	-.73047E-03
147600.0	-.21370E-02
149400.0	-.35746E-03
151200.0	-.19755E-02
153000.0	.43395E-03
154800.0	.41453E-03
156600.0	-.62593E-05
158400.0	.35518E-03
160200.0	.59024E-03
162000.0	-.12100E-02
163800.0	.62786E-03
165600.0	-.29351E-02
167400.0	-.12896E-02
169200.0	-.12626E-02
171000.0	.23348E-02

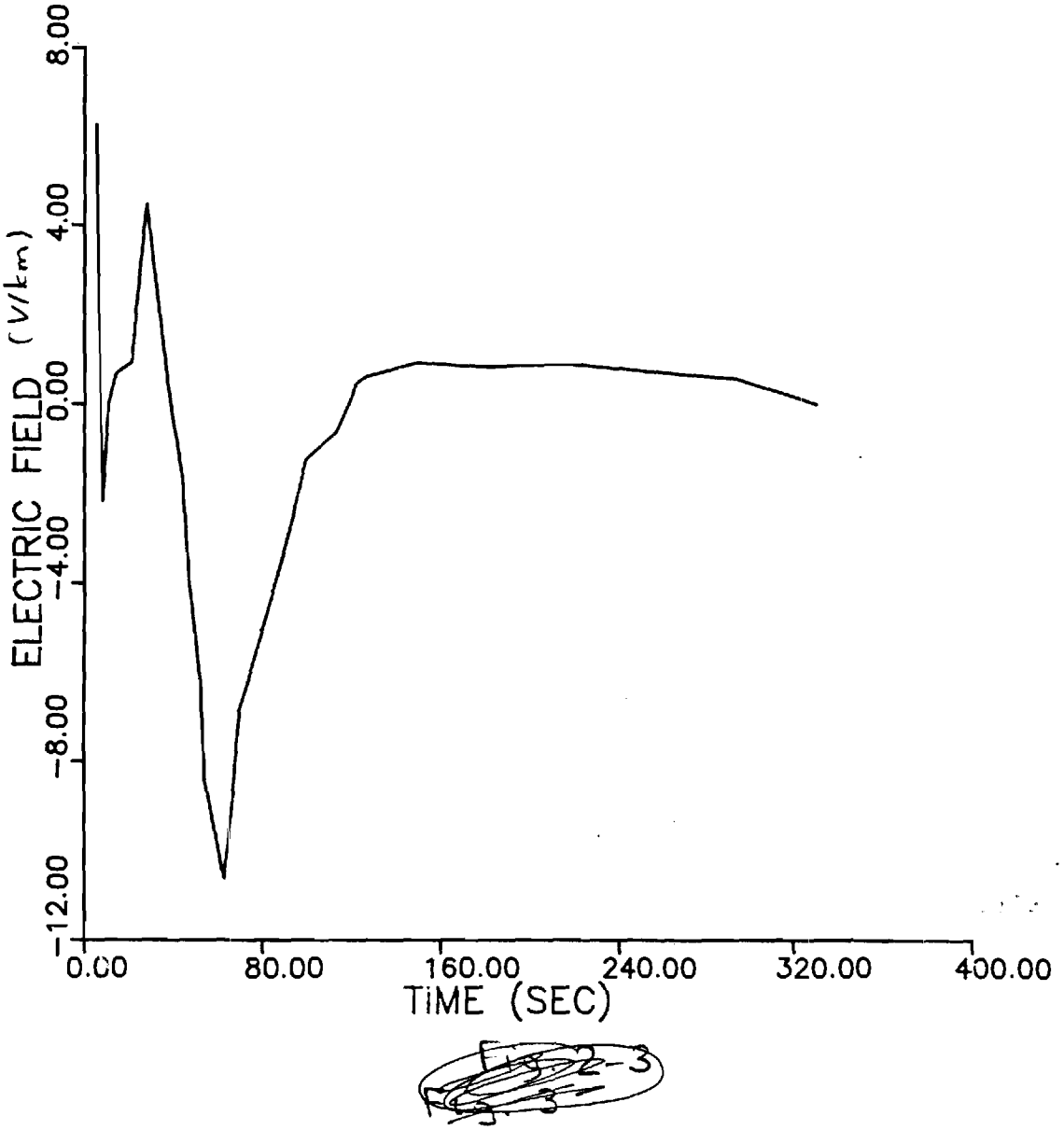

Figure 2-3. MHD-EMP induced electric field.

2-3

TABLE ~~LXI~~

Measured Induced Electric Field (MHD-EMP)
During the "Starfish" Test

Time (sec)	Electric Field (V/km)
0.0	.00000E+00
5.0	.62500E+01
7.0	.00000E+00
8.0	-.21900E+01
10.5	.00000E+00
13.9	.69000E+00
20.9	.94000E+00
27.8	.45300E+01
38.3	.00000E+00
43.5	-.15600E+01
47.0	-.40600E+01
52.2	-.62500E+01
53.9	-.84400E+01
62.6	-.10630E+02
66.0	-.90600E+01
69.6	-.68800E+01
83.5	-.43800E+01
92.2	-.28100E+01
99.1	-.12500E+01
113.0	-.63000E+00
118.3	.00000E+00
121.7	.47000E+00
127.0	.63000E+00
149.6	.94000E+00
180.9	.84000E+00
217.4	.90000E+00
280.0	.63000E+00
292.2	.59000E+00
330.4	.00000E+00

Section 3

TRANSMISSION SYSTEM MODEL

3.1 INTRODUCTION

This section describes the transmission system model for the study of geomagnetic disturbances. The model is based on a time domain simulation algorithm similar to the EMTP. Each power system element is modeled with a set of differential equations which are solved in the time domain. For the study of geomagnetic disturbances, two power system elements are very important: (1) magnetic core transformers and (2) long transmission lines. Specifically, long transmission lines provide the gate for geomagnetically induced currents to enter the power system. On the other hand, magnetic core transformers reach saturation when geomagnetically induced currents flow in their windings and cause most of the undesirable effects. This section describes in detail these two models.

3.2 MAGNETIC CORE TRANSFORMERS

Magnetic core transformers are highly nonlinear devices due to their saturable magnetic core. A typical iron core magnetization curve is illustrated in Figure 3-1. For practical reasons, power transformers are designed in such a way that the maximum operating magnetic flux is near the knee of the magnetization curve. During normal operating conditions, the magnetic flux oscillates between $+\lambda_{max}$ and $-\lambda_{max}$ and the magnetization current is symmetric about the zero axis. When a DC current is injected through the transformer winding, this symmetry is destroyed. In this case, the transformer may operate past the magnetization curve knee for portions of the cycle, requiring a high magnetization current to maintain the applied voltage.

This phenomenon is modeled as follows. Consider a single phase transformer as it is illustrated in Figure 3-2. The equations describing the transformer are:

$$v_{1u}(t) = r_{1u} i_{1u}(t) + L_{1u} di_{1u}/dt + d\lambda(t)/dt$$

$$v_{2u}(t) = r_{2u} i_{2u}(t) + L_{2u} di_{2u}/dt + d\lambda(t)/dt$$

$$\lambda(t) = g(i_m(t))$$

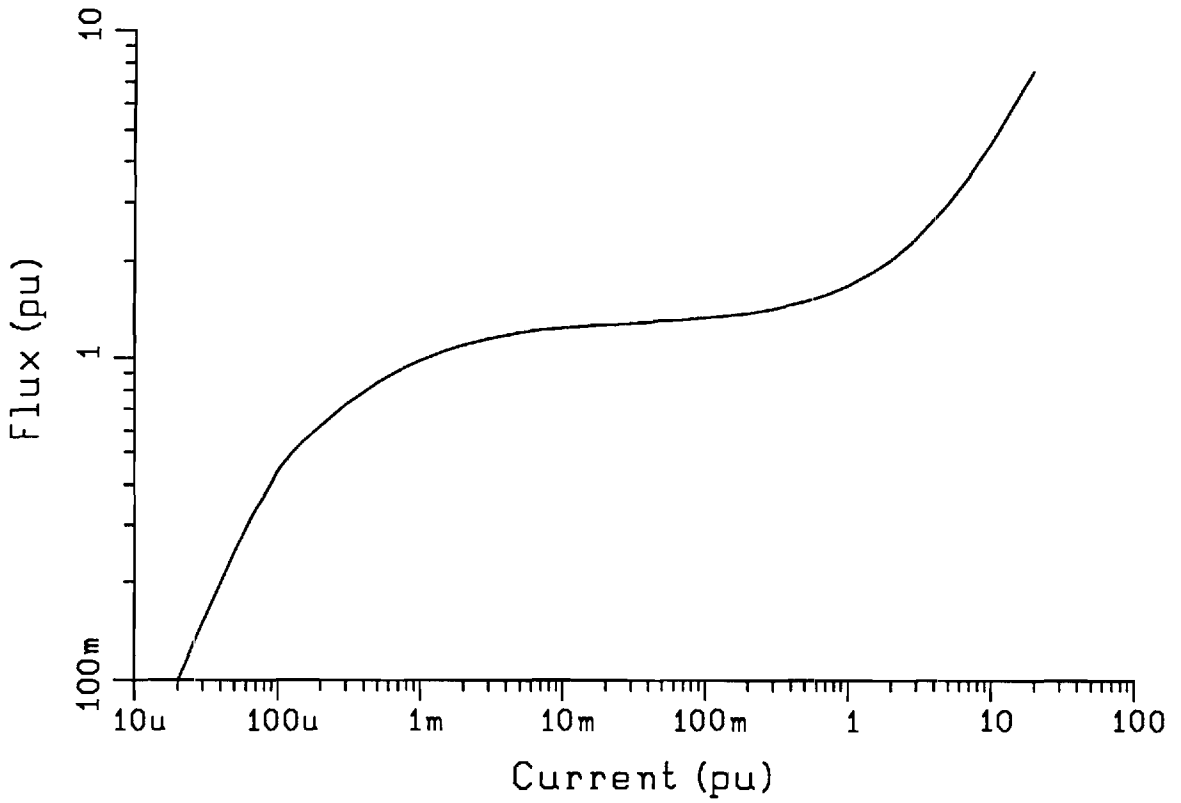

Figure 3-1 : Typical Iron Core Magnetization Curve

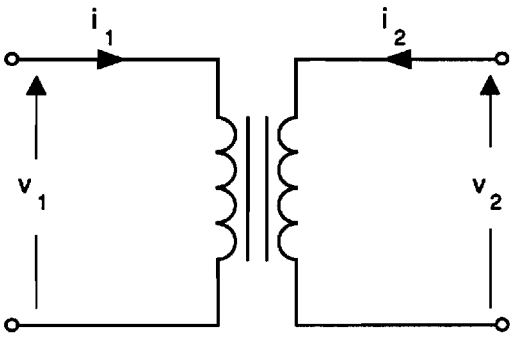

(a)

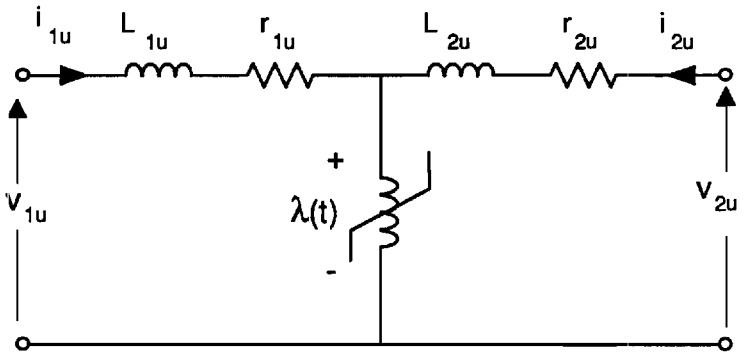

(b)

Figure 3-2 : Single Phase Transformer & equivalent Circuit
(a) Transformer
(b) Per Unit Equivalent Circuit

$$i_{m(t)} = i_{1u}(t) + i_{2u}(t)$$

where

$v_{1u}(t), v_{2u}(t)$ are the voltages in per unit

$i_{1u}(t), i_{2u}(t)$ are the currents in per unit

$g(\cdot)$ is the magnetization curve

$i_m(t)$ is the magnetization current in per unit.

Three single phase transformers, appropriately connected (wye-delta, etc.), provide the model of a three phase transformer. The equations of the power transformer are integrated in the time domain.

3.3 TRANSMISSION LINE MODEL WITH GIC COUPLING

The transmission line model used in this study is a time domain state space model based on the methodology described in Reference 29. It is capable of representing transmission line parameter frequency dependence, line tower grounding, as well as effects of geomagnetically induced currents (GIC).

The model is easily interfaced with other time domain models of power system components (such as transformers, loads, and generators). Thus the effect of GIC phenomena on the integrated power system can be assessed.

The transmission line model involves two components:

(1) Overhead conductors and earth return

(2) Grounding system.

Consider the transmission line shown in Figure 3-3. The section of overhead conductors between any two consecutive towers comprise a "conductor component" while each tower with its grounding systems is a component of the grounding system. Each component is modeled by an equivalent admittance matrix (which is a function of frequency) and equivalent current sources. Then, using nodal analysis, the equivalent circuit of the entire transmission line and GIC coupling is formed. The resulting model is in the form of a passive circuit of known admittance matrix and lumped current sources connected at the line terminals. This model is finally converted to the time domain using Fourier techniques.

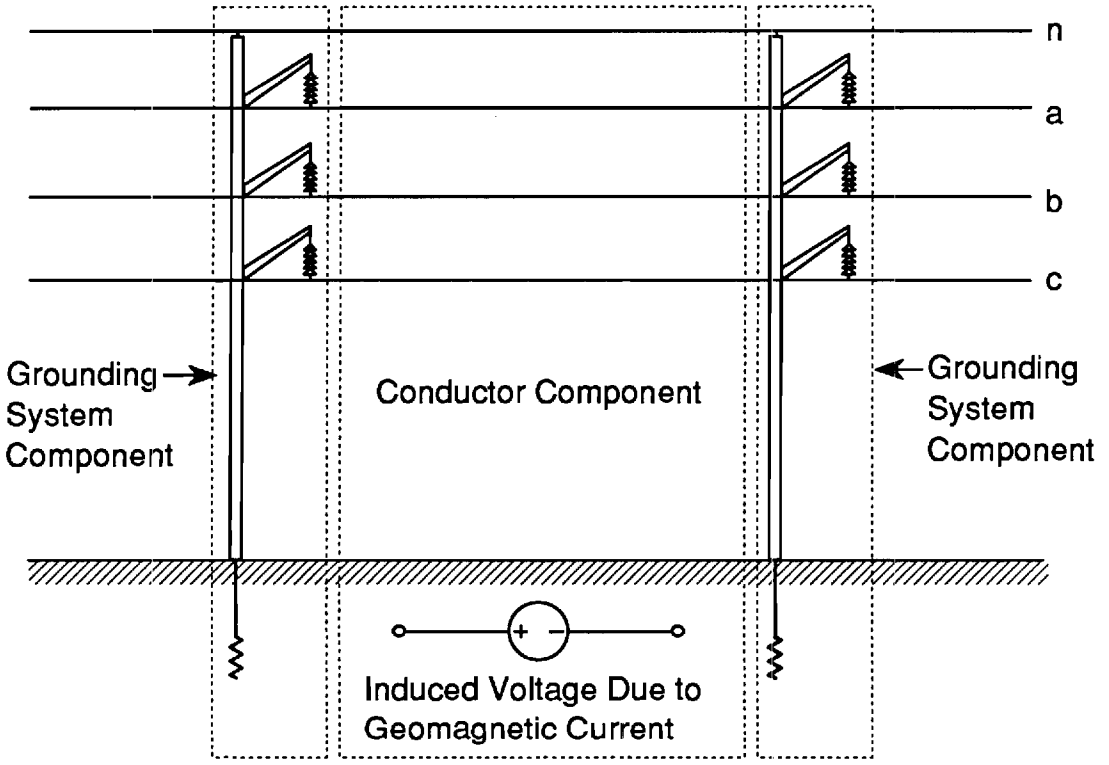

(a)

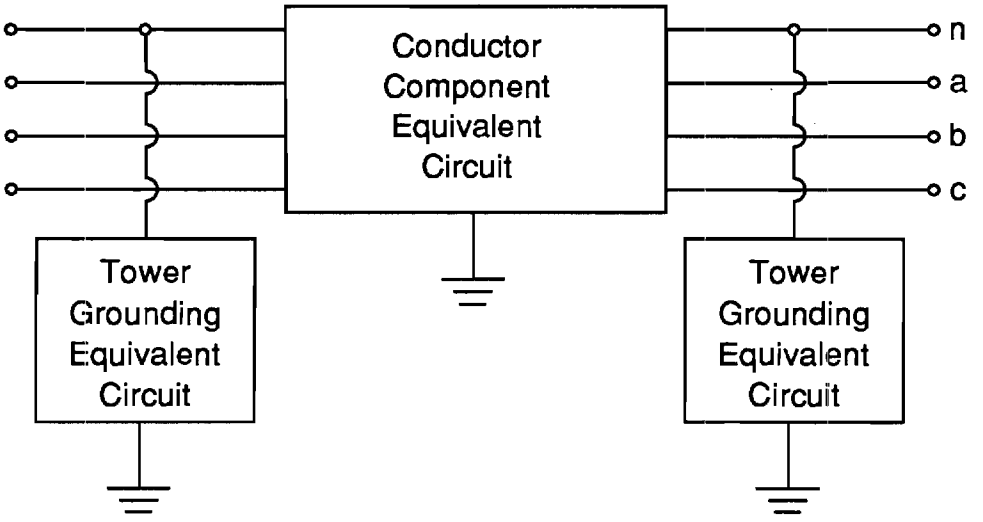

(b)

Figure 3-3 : Transmissin Line Section
(a) Physical Configuration
(b) Equivalent Circuit

The derivation of the conductor and grounding system equivalent circuits are presented in the following sections.

3.3.1 Overhead Conductor Model

An overhead transmission line conductor section, in the presence of geomagnetically induced currents is represented by the equations

$$\frac{\partial v(x,t)}{\partial x} = -Ri(x,t) - L\frac{\partial i(x,t)}{\partial t} + v_g(x,t) \quad , \tag{3-1}$$

$$\frac{\partial i(x,t)}{\partial x} = -Gv(x,t) - C\frac{\partial v(x,t)}{\partial t} \quad ,$$

where

- v : line voltage with respect to remote earth (v)
- i : line current (A)
- R : line series resistance (Ohms/meter)
- L : line series inductance (Henries/meter)
- G : line shunt conductance (Siemens/meter)
- C : line shunt capacitance (Farads/meter)
- v_g : component of voltage due to GIC in the direction of the line (volts/meter).

(See Appendix A for a derivation of Eq. (3-1).)

Since the line parameters are frequency dependent, the solution of the above equation is computed in the frequency domain. The Fourier transform of the above equations is

$$\frac{\partial V(x,\omega)}{\partial x} = -Z(\omega)I(x,\omega) + V_g(x,\omega) \quad , \tag{3-2}$$

$$\frac{\partial I(x,\omega)}{\partial x} = -Y(\omega)V(x,\omega) \quad , \tag{3-3}$$

where

$$Z(\omega) = R(\omega) + j\omega L(\omega)$$

$$Y(\omega) = G(\omega) + j\omega C(\omega) \quad .$$

For overhead transmission lines, several simplifications can be made:

(1) The conductance term is negligible and thus

$$Y(\omega) = j\omega C(\omega) \ .$$

(2) For a short line span, V_g is assumed constant with respect to position, thus

$$V_g(x,\omega) = V_g(\omega) \ .$$

(3) The resistance and inductance are computed using the complex depth of return method.

(4) The capacitance matrix is independent of frequency.

For a multiphase line the voltage due to GIC, V_g appears in series with every conductor. Thus it is replaced by the vector of the form

$$\begin{bmatrix} 1 \\ 1 \\ \vdots \\ 1 \end{bmatrix} \cdot V_g(x,\omega)$$

In order to compute the conductor section equivalent circuit, the current is eliminated in the equation system (3-2), (3-3), by differentiating Eq. (3-2) with respect to x and substituting current with voltage from Eq. (3-3)

$$\frac{\partial^2 V(x,\omega)}{\partial x^2} = K(\omega)V(x,\omega) \qquad (3\text{-}4)$$

where

$$K(\omega) = Z(\omega)Y(\omega) \ . \qquad (3\text{-}5)$$

The solution to the above equation (3-4) is obtained using eigenvalue analysis of the matrix K. Specifically, the system is decoupled by the transformation

$$V'(x,\omega) = W^{-1}(\omega)V(x,\omega) \qquad (3\text{-}6)$$

where

$$K(\omega) = W(\omega)D(\omega)W(\omega)^{-1} \qquad (3\text{-}7)$$

where $D(\omega)$ is a diagonal matrix containing the eigenvalues of matrix K, and $W(\omega)$ the eigenvector matrix of $K(\omega)$.

Applying transformation (3-7) to Eq. (3-4) yields

$$\frac{\partial^2 V'(x,\omega)}{\partial x^2} = D(\omega)V'(x,\omega) \ . \tag{3-8}$$

The general solution to the above equation is

$$V'(x,\omega) = e^{x\sqrt{D(\omega)}} \cdot A_1(\omega) + e^{-x\sqrt{D(\omega)}} \cdot A_2(\omega) \ , \tag{3-9}$$

where A_1, A_2 are constants to be determined by boundary conditions. Specifically,

$$V'(o,\omega) = A_1(\omega) + A_2(\omega) \tag{3-10}$$

$$V'(\ell,\omega) = e^{\ell\sqrt{D(\omega)}} A_1(\omega) + e^{-\ell\sqrt{D(\omega)}} A_2(\omega) \ .$$

Solving for A_1 and A_2 yields

$$A_1(\omega) = \left[e^{2\ell\sqrt{D(\omega)}} - I\right]^{-1} \left(e^{\ell\sqrt{D(\omega)}} V_2' - V_1'\right) \tag{3-11}$$

$$A_2(\omega) = \left[e^{-2\pi\sqrt{D(\omega)}} - I\right]^{-1} \left(e^{-\ell\sqrt{D(\omega)}} V_2' - V_1'\right) \ ,$$

where

$$V_1' = V'(o,\omega) = W^{-1} V(o,\omega)$$
$$V_2' = V'(\ell,\omega) = W^{-1} V(\ell,\omega)$$

and ℓ is the line length.

Thus, Eqs. (3-9) and (3-11) define the voltage at any point of the line given the voltages at the line ends. Now, using (3-2), the current is also computed as a function of the terminal voltages yielding

$$I(x,\omega) = Z^{-1}(\omega) V_g(\omega) = Z(\omega)^{-1} \frac{\partial V(x,\omega)}{\partial x} \ . \tag{3-12}$$

Evaluating the above at the line terminals, ($x = 0$, and $x = \ell$) yields

$$I_1(\omega) = Z(\omega)^{-1} V_g(\omega) - Z(\omega)^{-1} W(\omega) \left\{\sqrt{D(\omega)}\ A_1(\omega) - \sqrt{D(\omega)}\ A_2(\omega)\right\}$$

$$I_2(\omega) = Z(\omega)^{-1} V_g(\omega) - Z^{-1}(\omega) W(\omega) \left\{\sqrt{D(\omega)}\ E^{\ell\sqrt{D(\omega)}} A_1(\omega) - \sqrt{D(\omega)}\ e^{-\ell\sqrt{D(\omega)}} A_2(\omega)\right\} \ . \tag{3-13}$$

The above can be rewritten in matrix form as follows

$$\begin{bmatrix} I_1(\omega) \\ I_2(\omega) \end{bmatrix} = \left[\begin{array}{c|c} Z^{-1}(\omega) & 0 \\ \hline 0 & Z^{-1}(\omega) \end{array}\right] \cdot \begin{bmatrix} V_g(\omega) \\ V_g(\omega) \end{bmatrix} + \begin{bmatrix} Y_1(\omega) & Y_2(\omega) \\ Y_2(\omega) & Y_1(\omega) \end{bmatrix} \begin{bmatrix} V_1(\omega) \\ V_2(\omega) \end{bmatrix} \tag{3-14}$$

where

$$\begin{aligned} Y_1(\omega) &= -Z^{-1}(\omega)W(\omega)\left[\sqrt{D(\omega)}\left[-e^{2\ell\sqrt{D(\omega)}}+I\right]^{-1}+\sqrt{D(\omega)}\left[e^{-2\ell\sqrt{D(\omega)}}-I\right]^{-1}\right]W^{-1}(\omega) \\ &= Z^{-1}(\omega)W(\omega)\sqrt{D(\omega)}\left[\left(e^{2\ell\sqrt{D(\omega)}}-I\right)^{-1}-\left(e^{-2\ell\sqrt{D(\omega)}}-I\right)^{-1}\right]W^{-1}(\omega) \\ &= Z^{-1}(\omega)W(\omega)H_1(\omega)W^{-1}(\omega) \\ Y_2(\omega) &= Z^{-1}(\omega)W(\omega)\sqrt{D(\omega)}\left[\left[e^{2\ell\sqrt{D(\omega)}}-I\right]^{-1}e^{\ell\sqrt{D(\omega)}}-\left[e^{-2\ell\sqrt{D(\omega)}}-I\right]^{-1}e^{-\ell\sqrt{D(\omega)}}\right]W^{-1}(\omega) \\ &= Z^{-1}(\omega)W(\omega)\sqrt{D(\omega)}\left[2\left(e^{\ell\sqrt{D(\omega)}}-e^{-\ell\sqrt{D(\omega)}}\right)^{-1}\right]W^{-1}(\omega) \\ &= Z^{-1}(\omega)W(\omega)H_2(\omega)W^{-1}(\omega)\ , \end{aligned} \tag{3-15}$$

where $H_1(\omega)$,$H_2(\omega)$ are diagonal matrices of which the diagonal elements are

$$\begin{aligned} H_{1_{ii}} &= \frac{\sqrt{D_i}}{\tanh(\ell\sqrt{D_i})} \\ H_{2_{ii}} &= \frac{\sqrt{D_i}}{\sinh(\ell\sqrt{D_i})}\ , \end{aligned} \tag{3-16}$$

where D_i is the ith eigenvalue of matrix $K(\omega)$.

From Eq. (3-14), an equivalent circuit can be derived representing a multiphase transmission line section in the presence of GIC. Figure 3-4 illustrates the equivalent circuit. It consists of a passive circuit whose admittance matrix is known and current sources connected at each terminal representing GIC coupling. Note that all parameters of the equivalent circuit are frequency dependent. Thus the admittance matrix and current source values have to be computed explicitly at each frequency of interest.

3.3.2 Tower Grounding Model

Each tower and its grounding structure are represented by a step response. It is defined as the current flowing into the tower from the neutral wire support point when a unit step voltage is applied at the same point.

The step response of the tower and its grounding system can be determined experimentally [30] or analytically [31,32]. When computed analytically, finite element analysis is utilized to solve for the flow of currents in the earth. Then a convolution algorithm is utilized to evaluate the tower and ground step response [31].

The tower model has been validated with data obtained by Bonneville Power Administration (BPA). The validation of this model is reported in Reference 32.

The admittance of the tower and grounding system at any given frequency is computed from the step response with an appropriate Fourier transform.

3.3.3 Integrated Model

The equivalent circuit of the entire transmission line is constructed by combining the equivalent circuits of each conductor section and tower grounding systems. The procedure is based on nodal analysis method, where all internal node voltages and currents are eliminated, and all internal current sources are represented by equivalent current sources at the terminals of the line. The resulting equivalent circuit has the same topology as the one for a single line section as illustrated in Figure 3-4.

In order to utilize the developed model in time domain simulation, the equivalent circuit parameters are transformed into the time domain. Specifically, the admittance matrix of the passive part of the equivalent circuit is transformed to an impulse response, and the equivalent current sources (which are also computed as functions of frequency) are transformed into time domain waveforms. A discrete Fourier transform method is used for this purpose.

The Snelson transformation is applied before Fourier transformation to minimize resulting time domain waveform durations (see Reference 33). Specifically, the voltage and current variables are replaced by B and F as follows

$$F(\omega) = V(\omega) + G^{-1} I(\omega) \qquad (3\text{-}17)$$

$$B(\omega) = V(\omega) - G^{-1} I(\omega)$$

where G is a real nxn matrix (n = number of conductors), and

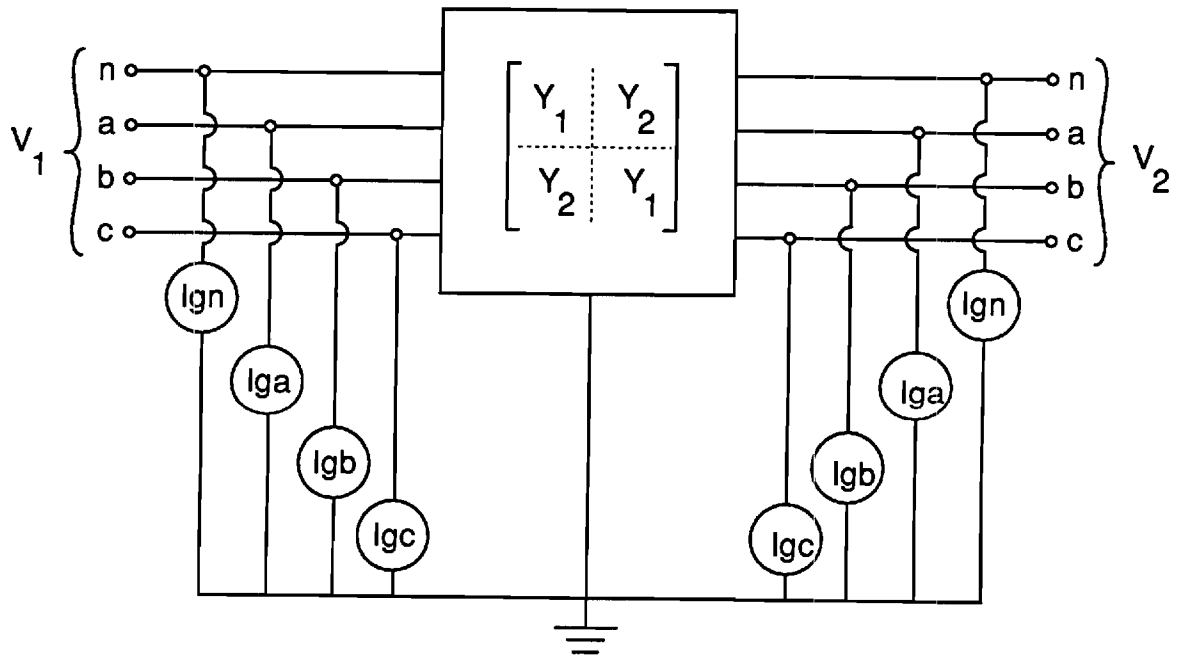

Figure 3-4 : Equivalent Circuit of a Transmission Line Section with GIC Coupling

$$V(\omega) = \begin{bmatrix} V_1(\omega) \\ V_2(\omega) \end{bmatrix} , \quad I(\omega) = \begin{bmatrix} I_1(\omega) \\ I_2(\omega) \end{bmatrix}.$$

Applying the above transformation to Eq. (3-14) yields

$$\frac{1}{2} G\big(F(\omega)-B(\omega)\big) = \begin{bmatrix} Z^{-1}(\omega)V_g(\omega) \\ -Z^{-1}(\omega)V_g(\omega) \end{bmatrix} + \frac{1}{2} Y(\omega)\big(F(\omega)+B(\omega)\big) \quad . \tag{3-18}$$

Solving for $B(\omega)$ yields

$$B(\omega) = M(\omega)F(\omega) + A_g(\omega) \quad , \tag{3-19}$$

where

$$M(\omega) = \big(G(\omega)+Y(\omega)\big)^{-1}\big(G(\omega)-Y(\omega)\big)F(\omega)$$

$$A_g(\omega) = -2\big(Y(\omega)+G(\omega)\big)^{-1} \begin{bmatrix} Z(\omega)V_g(\omega) \\ Z^{-1}(\omega)V_g(\omega) \end{bmatrix}$$

The matrix $M(\omega)$ and the vector $A_g(\omega)$ are next transformed into time domain functions using the FFT algorithm

$$m(t) = \mathbf{F}^{-1}\{M(\omega)\}$$

$$a_g(t) = \mathbf{F}^{-1}\{A_g(\omega)\} \tag{3-20}$$

The function matrices $m(t)$ and $a_g(t)$ comprise a time domain model of the entire transmission line with GIC coupling. Specifically, $m(t)$ contains the impulse response of the transmission line (based on Snelson's transformation) and the functions $a_g(t)$ represent the GIC effects. These functions are utilized in a convolution based algorithm, in order to simulate the operation of transmission lines with GIC coupling in the integrated power system. This algorithm is described in the following section.

3.3.4 Convolution Algorithm

The transmission line model is cast into the resistive companion form via a discrete convolution scheme. This technique allows the model to be interfaced with models of other power system components, thus forming a model of an integrated power system. (This is the standard methodology followed by several time domain simulation programs such as the EMTP and the PSTS programs.) Specifically, the model of a transmission line with GIC coupling is represented by the equivalent circuit shown in Figure 3-5. The voltage vector v and current vector i represent the voltages and

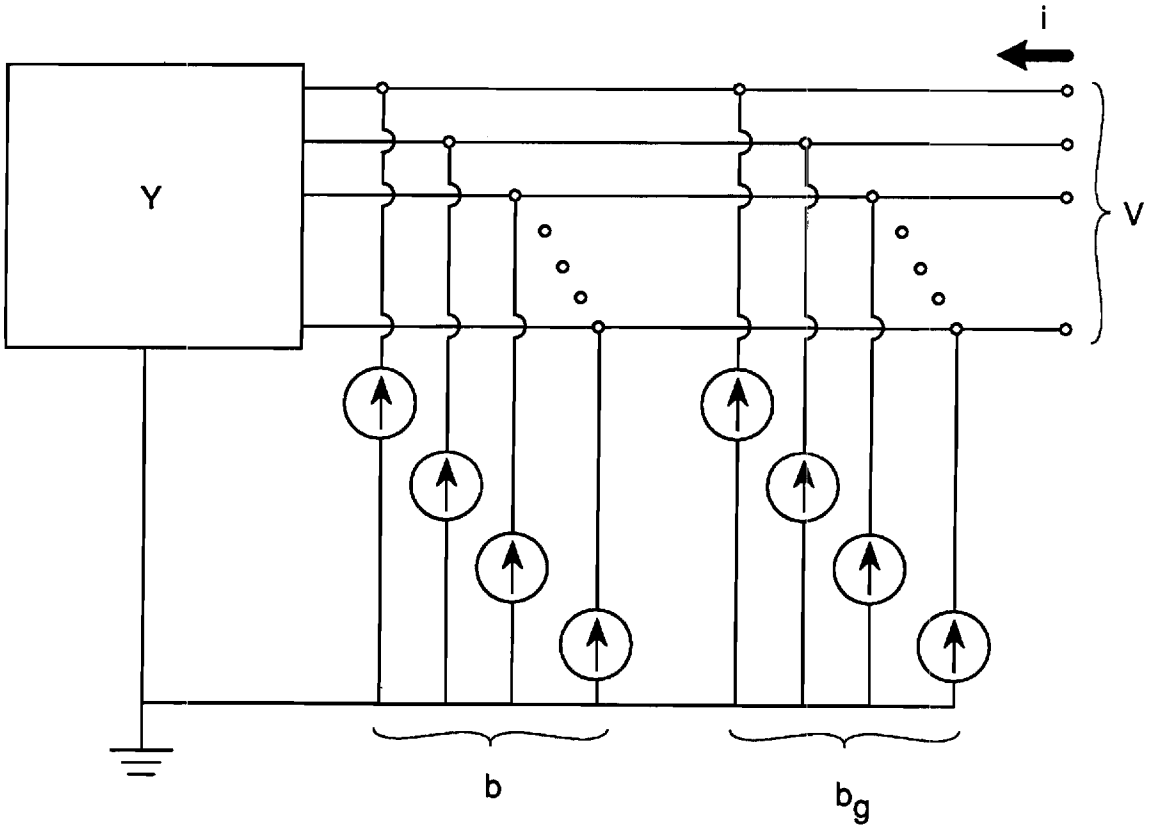

Figure 3-5 : Model of Transmission with GIC Coupling
in the Resistive Companion Form

current injections on each conductor at the ends of the line. The following equation holds for these voltages and currents:

$$Y \cdot v(t) = b(t) + b_g(t) + i(t) \tag{3-21}$$

where Y is the transmission line characteristic admittance matrix, b is the vector of currents depending on past history voltages and currents, and b_g is the vector of currents representing GIC effects. The above equation can be solved by discrete time techniques in terms of the impulse response model defined in the previous section. Specifically, let v_n and i_n represent the values of the voltage and current vectors at the line ends at the n-th time step. Then:

$$Yv_n = b_{n-1} + b_{g_n} + i_n \tag{3-22}$$

where

$$\begin{aligned} Y &= G[I+S_o]^{-1}[I-S_o] \\ b_{n-1} &= G[I+S_o]^{-1} \sum_{k=0}^{N} (S_k - S_{k-1})(v_{n-k} - G^{-1} i_{n-k}) \\ b_{g_n} &= G[I+S_o]^{-1} a_{g_n} \end{aligned}$$

where S_i represents the transmission line step respone (at the ith time interval), i.e. it is the integral of the impulse response m(t), performed in discrete time.

The above equation (3-22) is a resistive companion form representation of a transmission line with GIC coupling. Specifically, the real matrix Y is the admittance matrix of a resistive network (block Y in Figure 3-5). The vector b_{n-1} represents the past history dependent current sources. The entries of the current source vector b_{n-1} are computed by discrete convolution as shown in Eq. (3-22). The vector b_{g_n} are the independent current sources (b_g in Figure 3-5), representing the effects of GIC.

Using these equations, a transmission line with GIC coupling and its interaction with the integrated power system is simulated using the standard methodology for power system transient simulation employed by the EMTP and PSTS programs.

Section 4

PRELIMINARY MODEL EVALUATION

4.1 INTRODUCTION

This section describes the application and preliminary evaluation of the power transmission system model, for the study of geomagnetic disturbances. The evaluation approach is based on the computation of the response of a simplified power system to a set of step functions of geomagnetically induced earth surface potential. The simulation results are compared to results from a study of the same system, which was performed by General Electric.

4.2 DESCRIPTION OF THE TEST SYSTEM

The test system is a simplification of the Minnesota Power Company 500 kV line between Dorsey and Minneapolis. Specifically it consists of a 500 kV transmission line, terminated by three phase transformer banks at both ends. Figure 4-1 illustrates a single line diagram of the test system.

The transmission line data are listed in Table 4-1. During normal operation, the sky wires are not electrically connected to the transmission line towers. Tower configuration data specifies the location of the center of each phase bundle and each sky wire with respect to a Cartesian coordinate system with its origin located at the center of the tower base.

Each of the three phase transformer banks consists of three single phase transformers connected DELTA/GROUNDED Y. The grounded Y side is connected on the 500 kV transmission line (see Figure 4-1). The characteristics of each single phase transformer are as follows:

Voltage	115/288 kV
Power Rating	350 MVA
Leakage Reactance	0.10 pu
Magnetizing Current	0.01 pu
Winding Resistance (high V. side)	1.5 ohms

Transformer saturation is modeled as described in Section 3.2. The transformer core magnetization characteristics are described by a piecewise-linear function which is tabulated in Table 4-2. (The same data are plotted in Figure 3-1.)

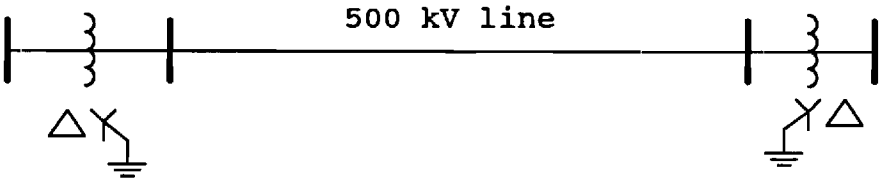

(a)

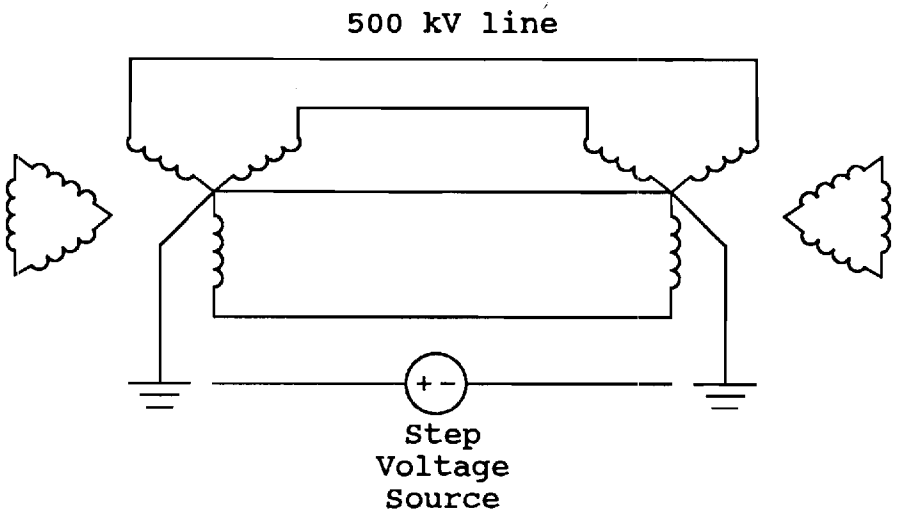

(b)

Figure 4-1 :Test System
a) Single Line Diagram
b) Three Phase Diagram

Table 4-1

Transmission Line Data

GENERAL DATA

Line Length	473 miles
Configuration	3 conductor bundle per phase
Bundle Spacing	18 inches
Tower Spacing	0.25 miles
Tower Footing Resistance	30 Ohms

CONDUCTOR DATA

Conductor	Type	O.D inches	Resistance (Ohms/mile)
Ground Conductors	7/16 steel	0.4375	4.435
Phase Conductors	1192 ACSR	1.3020	0.080

TOWER CONFIGURATION DATA

Conductor	x - coordinate (feet)	y - coordinate (feet)
Phase A	-32.0	97.5
Phase B	0.0	97.5
Phase C	32.0	97.5
Sky Wire 1	-35.0	129.5
Sky Wire 2	35.0	129.5

Table 4-2
Transformer Magnetization Characteristics
(High Voltage Side)

Current (kiloamperes)	Flux Linkage (kilowebers-turns)
.00000000	.00000000
.00003429	.10829000
.00005144	.16243500
.00006858	.21603860
.00008573	.26855920
.00010288	.31837260
.00012002	.36363780
.00013717	.40381350
.00017146	.47052010
.00025719	.58990980
.00034292	.67004440
.00051438	.78022940
.00085730	.91104380
.00120022	.98717160
.00171460	1.06189200
.00257190	1.13823600
.00342920	1.18398900
.00514380	1.23965000
.00857300	1.29379500
.01200220	1.31696900
.01714600	1.33564900
.02571900	1.35427500
.03429200	1.36621400
.05143800	1.38240300
.08573000	1.40297800
.12002200	1.41748900
.17146000	1.43548700
.25719000	1.46136800
.34292000	1.48486700
.51438000	1.52867100
.85730000	1.60999600
1.20022000	1.68764000
1.71460000	1.80183200
2.57190000	1.98619600
3.42920000	2.16433300
5.14380000	2.51356800
8.57300000	3.19796100
12.00220000	3.86935900
17.14600000	4.86183700
34.29200000	8.12678100

The response of the described system is computed assuming a geomagnetically induced voltage (GIV) of step function waveform. Three cases are simulated with different GIV levels as follows:

1. 1.0 volts per mile
2. 10.0 volts per mile
3. 100.0 volts per mile.

The effects of GIV to the test system are assessed in two steps: First, the steady state direct current through the transformer is computed for the above GIV levels and various values of line parameters. Next, the transient response of the transformer excitation current is completed for the above GIV levels to determine the time constants involved to reach saturation. The results of this study are described in the next section.

4.3 COMPUTATION OF STEADY STATE RESPONSE

This section presents the computation of the steady state response of the test system under GIC excitation. In order to gain insight in the system parameters that determine the system behavior under GIC excitation, a simple approach is used first. Specifically, an equivalent DC model of the system is constructed. Using, this simple model, the magnitude and distribution of geomagnetically induced currents are evaluated. The effect of the neutral wire of the transmission line to GIC response is assessed. Furthermore, the results of this analysis are used to validate the detailed (transient) model.

The DC model of the test system is constructed by considering only the resistances of each system component. Specifically, an equivalent circuit is constructed containing the DC models of the transformers, transmission line, grounding system, and geomagnetic voltage. This circuit is illustrated in Figure 4-2. The equivalent circuits of each component are described next.

The transformers are represented by their winding resistances. Specifically, the windings of the Y connected (high voltage) side of the transformer exhibit three parallel paths to the flow of the electric current injected at the transformer neutral. Assuming that the windings are identical, the equivalent resistance is 1/3 of the winding resistance of each high voltage winding.

The transmission line is represented by a DC equivalent circuit. Each of the phase wires is represented by a resistance equal to the total DC resistance of the phase conductor.

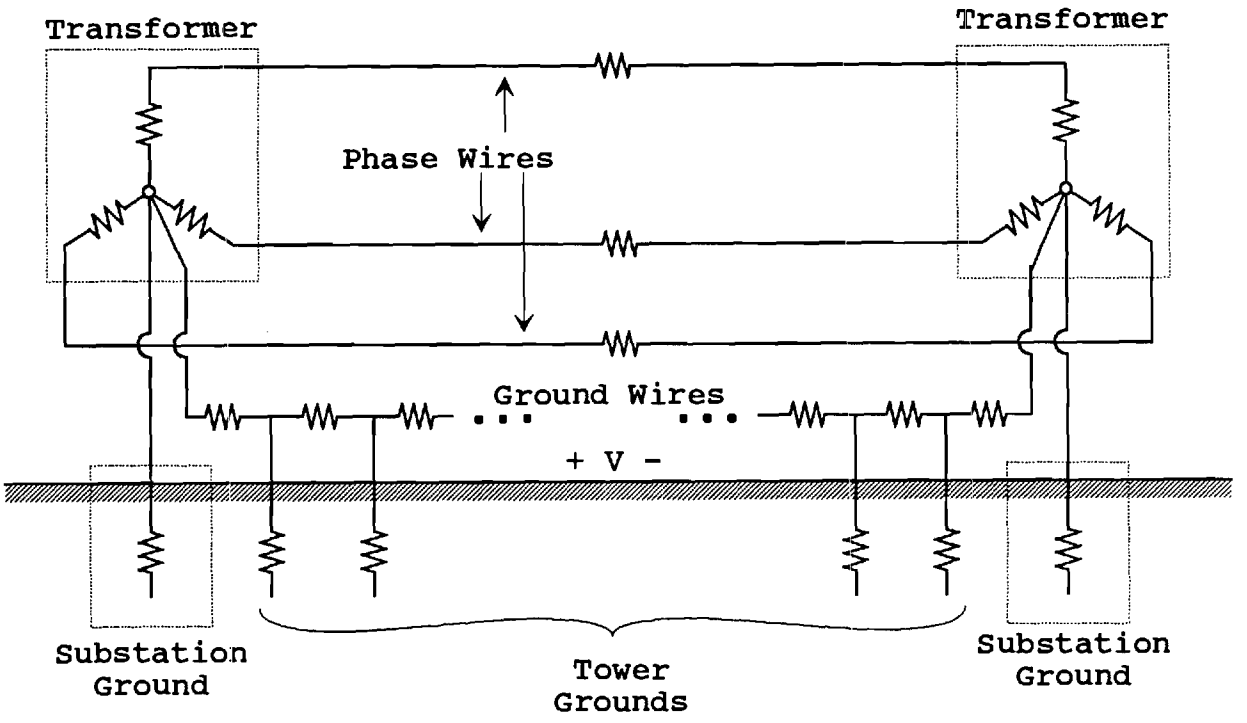

Figure 4-2 : DC Equivalent Circuit of Test System

The neutral wire is represented by its DC resistance. The neutral wire may or may not be multiply grounded. Figure 4-2 illustrates the tower footing grounding which is represented by its DC resistance.

The substation grounds at each line end are represented by 1 Ohm resistances, connected from the transformer Y side neutral to remote earth.

Finally, the equivalent circuit of the earth containing the geomagnetically induced voltage is represented by a series of Thevenin equivalent circuits connected between consecutive tower grounds and substation grounds. Thus, for each line segment, a separate Thevenin equivalent of the earth is used. Each Thevenin equivalent consists of a voltage source representing the geomagnetically induced voltage, and a resistor representing the earth path resistance. The earth path resistance is highly dependent on frequency. The earth path resistance computed at 0.6 Hz was used.

The above model was employed to study the effects of multiply grounded ground wires on the steady state direct current through the transformer winding. The following values were used for the parametric study:

GIV	1 Volt/mile
Earth path resistance	0.001Ohm/mile
Tower footing resistance	5, 30, 100, & infinite Ohms
Tower spacing	0.25 mile
Equivalent phase ~~condition~~ conductor resistance	0.00889 Ohms/mile
Ground conductor resistance	4.435 & 1.240 Ohms/mile
Total line length	473 miles

The results of the parametric study are illustrated in Figure 4-3. The Figure is self explanatory. Note that there is a substantial effect of the line grounding parameters on the steady state value of the direct current through the transformer.

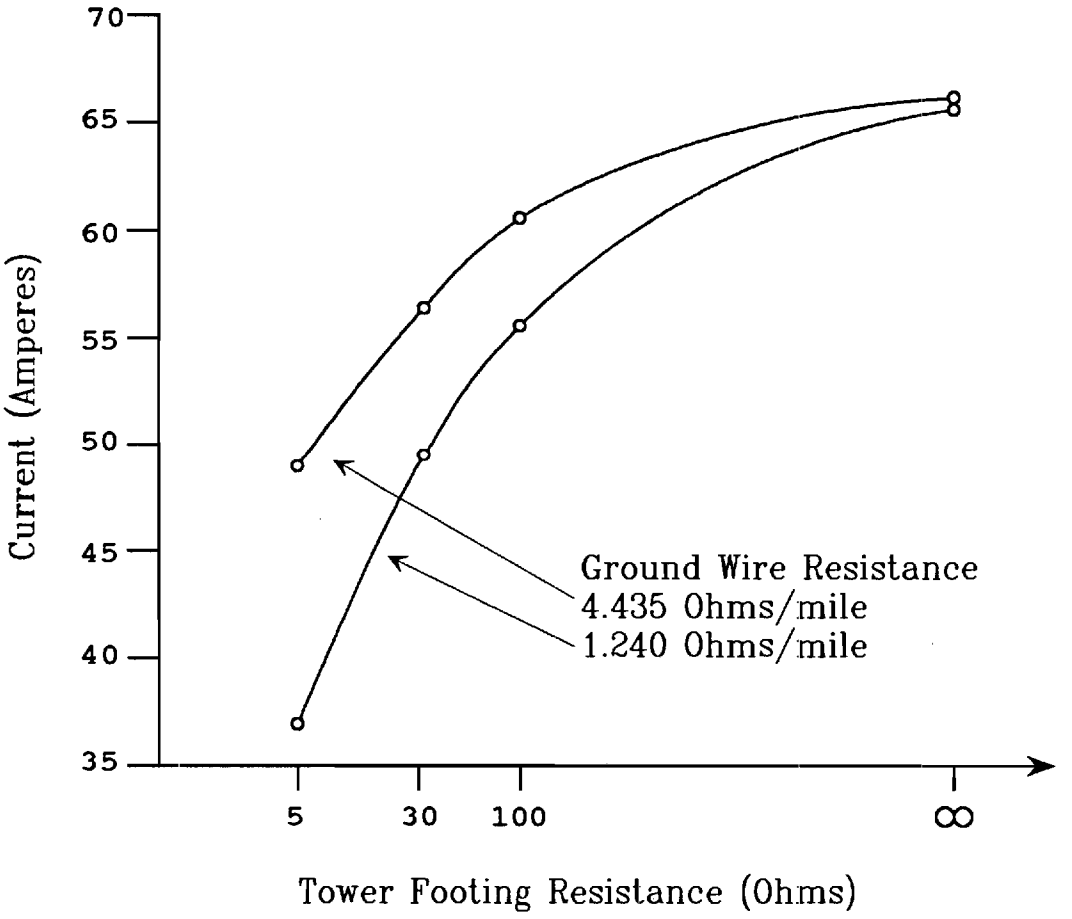

Figure 4-3 : Steady State Direct Current through Transformer Winding

4.4. Computation of Time Constants to Saturation.

The described model of the test system was simulated in the time domain to determine the time constants involved to reach steady state operation. Specifically, the time constants were defined as the time required for the dc current in the windings of the transformer to reach 63% of its steady state value. Figure 4-4 illustrates a typical simulation and the definition of the time constant. The Figure also illustrates the parameters of the simulation as well.

The time constants were computed for various parameters as follows:

GIV	1, 10, 100 Volts/mile
Earth path resistance	0.001 ohms/mile
Tower Footing Resistance	5, 30, 100, infinite ohms
Tower Spacing	0.25 miles
Equivalent Phase Conductor Resistance	0.00889 ohms/mile
Ground Conductor Resistance	4.435 & 1.240 ohms/mile
Total Line Length.	473 miles

The results of the parametric study are illustrated in Table 4.3. Note the wide variation of time constants (145 seconds to 2.3 seconds) System parameters drastically affect time constants.

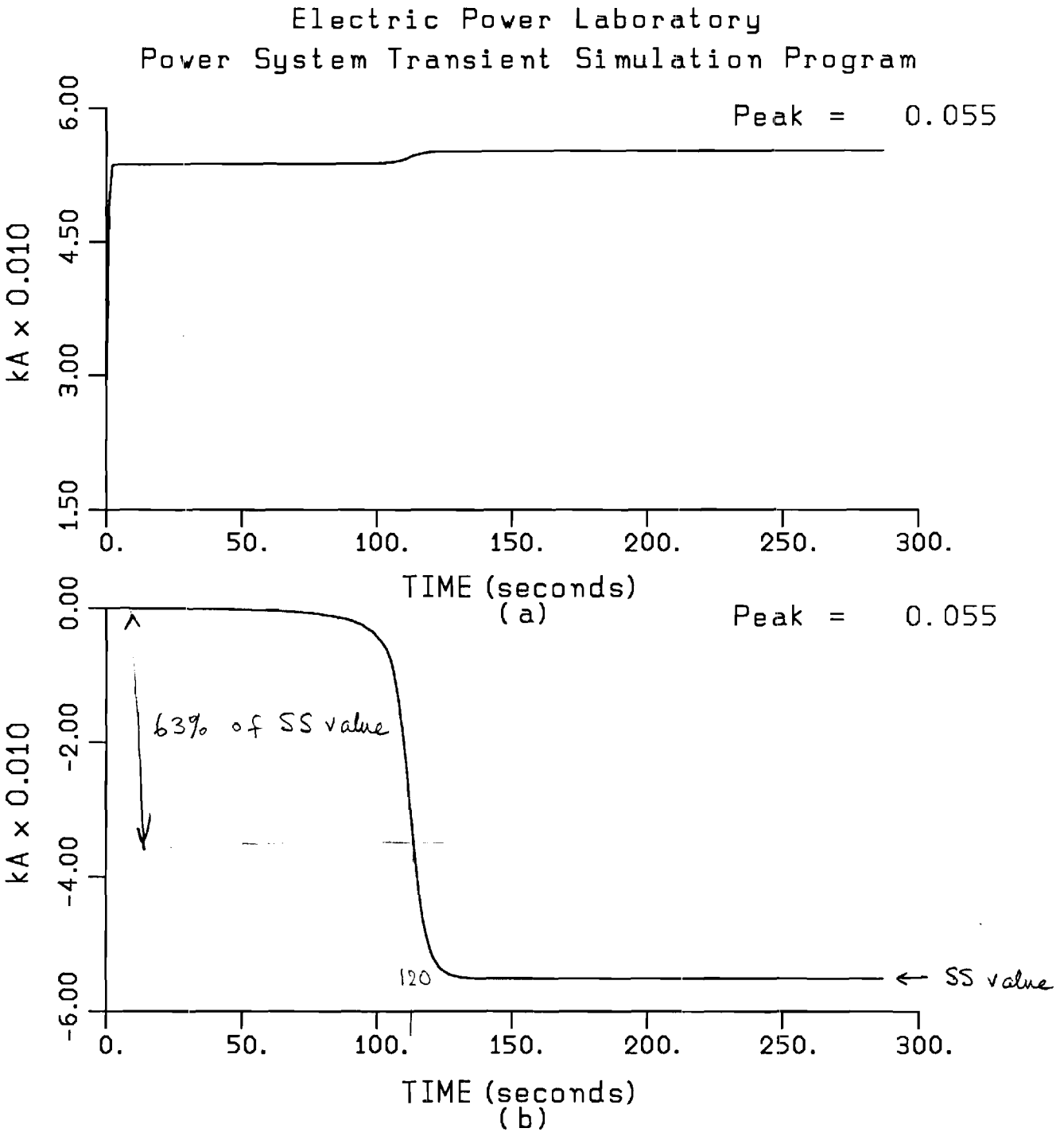

GIV = 1 V/mi, Rtf = 5 Ohms, Rg = 4.435 Ohms/mi
(a) Line Zero Sequence Current
(b) Transformer Magnetization Current

Figure 4-4. Typical Results of Time Domain Simulation of the Test System.

Table 4.3 : Test System Time Constant to Saturation* (in seconds) Versus GIV Level, Tower Footing Resistance (R_t), and Ground Wire Resistance (R_g)

	G.I.V.					
	1 V / mile		10 V / mile		100 V / mile	
R_t \ R_g	4.435	1.24	4.435	1.24	4.435	1.24
5	120	145	13.0	16.0	2.8	3.1
30	98	109	11.2	12.5	2.5	2.6
100	93	96	10.6	11.4	2.4	2.5
inf	85	85	10.0	10.0	2.3	2.3

* Time Constant to Saturation is defined as the time required for the transformer magnetization current to reach 63.2% of its steady state value.

Section 5

REFERENCES

1. Syun-Ichi Akasofu, "The Dynamic Aurora," Scientific American, pp. 90-97, May 1989.

2. S. Chapman, Solar Plarma, Geomagnetism and Aurora, Gordon and Breach Science Publishers, New York, 1968.

3. V. D. Albertson, "Geomagnetic Disturbance Causes and Power System Effects," 1989 IEEE PES Summer Meeting, Long Beach, California, July 12, 1989.

4. R. Pirjola, "On Currents Induced in Power Transmission Systems During Geomagnetic Variations," IEEE Transactions on Power Apparatus and Systems, vol. PAS-104, no. 10, pp. 2825-2830, October 1985.

5. G. B. Rackliffe, J. C. Crouse, J. R. Legro, and V. J. Kruse, "Simulation of Geomagnetic Currents Induced in a Power System by Magnetohydrodynamic Electromagnetic Pulses," IEEE Transactions on Power Delivery, vol. PWRD-3, no. 1, pp. 392-397, January 1988.

6. J. R. Legro, N. C. Abi-Samra, J. C. Crouse, and F. M. Tesche, "A Methodology to Assess the Effects of Magnetohydrodynamic Electromagnetic Pulse (MHD-EMP) on Power Systems," IEEE Transactions on Power Delivery, vol. PWRD-1, no. 3, pp. 203-209, July 1986.

7. M. Rabinowitz, "Magnetohydrodynamic EMP, Solar Storm GIC, and Substorms," Conference on Geomagnetically Induced Currents, sponsored by Electric Power Research Institute, Burlingame, California, November 8-10, 1989.

8. M. Rabinowitz, "Nuclear Electromagnetic Pulse," Encyclopedia of Science and Technology, 1986 Yearbook, McGraw Hill, New York, pp. 34-47, 1985.

9. C. N. Vittitoe and M. Rabinowitz, "Radiative Reactions and Coherency Modeling in the High-Altitude Electromagnetic Pulse," Physical Review A, vol. 37, no. 6, pp. 1969-1977, March 15, 1988.

10. M. Rabinowitz, "Effect of the Fast Nuclear Electromagnetic Pulse on the Electric Power Grid Nationwide: A Different View," IEEE Transactions on Power Delivery, vol. PWRD-2, no. 4, pp. 1199-1222, October 1987.

11. K. W. Klein, P. R. Barnes, and H. W. Zaininger, "Electromagnetic Pulse and the Electric Power Network," IEEE Transactions on Power Apparatus and Systems, vol. PAS-104, pp. 1571-1577, 1985.

12. C. L. Longmire, "On the Electromagnetic Pulse Produced by Nuclear Explosions," IEEE Transactions on Electromagnetic Compatibility, vol. EMC-20, no. 1, pp. 3-13, February 1978.

13. C. N. Vittitoe, "Did High-Altitude EMP Cause the Hawaiian Streetlights Incident?", Sandia National Labs, Albuquerque, New Mexico, SAND88-00430, 1988.

14. D. P. Millard, A. P. Sakis Meliopoulos, and G. J. Cokkinides, "Parametric Analysis of EMP Induced Overvoltages on Power Lines," IEEE Transactions on Power Delivery, vol. PWRD-3, no. 3, pp. 1224-1231, July 1988.

15. J. R. Wait, Geo-Electromagnetism, Academic Press, Inc., New York, Chapter VI, pp. 184-208, 1982.

16. A. A. Kaufman and George V. Keller, The Magnetotelluric Sounding Method, Elsevier Scientific Publishing Company, New York, Chapter 5, pp. 113-155, 1981.

17. T. Rikitake and Y. Honkura, Solid Earth Geomagnetism, Terra Scientific Publishing Company, Tokyo, Japan, and D. Reidel Publishing Company, Boston, Chapter 11, pp. 267-292, 1985.

18. V. D. Albertson and J. A. Van Ballen, "Electric and Magnetic Fields at the Earth's Surface Due to Auroral Currents," IEEE Transactions on Power Apparatus and Systems, vol. PAS-89, no. 4, pp. 578-584, April 1970.

19. J. R. Wait, "Electromagnetic Surface Impedance for a Layered Earth for General Excitation," Radio Science, vol. 15, no. 1, pp. 129-134, January-February 1980.

20. R. Pirjola and A. Viljanen, "On Geomagnetically-Induced Currents in the Finnish 400 kV Power System by an Auroral Electrojet Current," IEEE Transactions on Power Delivery, vol. PWRD-4, no. 2, pp. 1239-1245, April 1989.

21. D. Park, "Magnetic Field of a Horizontal Current Above a Conducting Earth," Journal of Geophysical Research, vol. 78, no. 16, pp. 3040-3043, June 1, 1973.

22. A. T. Price, "Electromagnetic Induction in a Semi-Infinite Conductor with a Plane Boundary," Quart. J. Mech. and Appl. Math., vol. 3, pt. 4, pp. 385-410, 1950.

23. S. P. Srivastava, "Method of Interpretation of Magnetotelluric Data when Source Field is Considered," Journal of Geophysical Research, vol. 70, no. 4, pp. 945-954, February 15, 1965.

24. R. D. Hibbs and F. W. Jones, "The Calculation of the Electromagnetic Fields of a Sheet Current Source with Arbitrary Spatial Intensity Distribution over a Layered Half Space - I, The General Method and Results," Geophys. J. R. Astr. Soc., vol. 46, pp. 433-452, 1976.

25. W. R. Peltier and J. F. Hermance, "Magnetotelluric Fields of a Gaussian Electrojet," Can. J. Earth Sci., vol. 8, pp. 338-346, 1971.

26. R. D. Hibbs, Jr. and F. W. Jones, "Electromagnetic Induction in the Earth by a Non-Symmetric Non-Uniform Source," J. Geomag. Geoelectr., vol. 25, pp. 75-86, 1973.

27. M. Abramowitz and J. A. Stegun (eds.), Handbook of Mathematical Functions, U.S. Department of Commerce, National Bureau of Standards, 10th ed., pg. 886, 1972.

28. D. Larose, "The Hydro-Quebec System Blackout of 13 March 1989," Conference on Geomagnetically Induced Currents, sponsored by Electric Power Research Institute, Burlingame, California, November 8-10, 1989.

29. G. J. Cokkinides and A. P. Meliopoulos, "Transmission Line Modeling with Explicit Grounding Representation," Electric Power Systems Research, vol. 14, no. 2, pp. 109-119, April 1988.

30. W. A. Chisholm and Y. L. Chow, "Travel Time of Transmission Towers," IEEE Transactions on Power Apparatus and Systems, vol. PAS-104, no. 10, pp. 2922-2928, October 1985.

31. A. P. Meliopoulos and M. G. Moharem, "Transient Analysis of Grounding Systems," IEEE Transactions on Power Apparatus and Systems, vol. PAS-102, no. 2, pp. 389-397, February 1983.

32. A. Paplexopoulos and A. P. Meliopoulos, "Frequency Dependent Modeling of Grounding Systems," Proc. Midwest Power Symposium, pp. VI.E. 1-13, 1985.

33. J. K. Snelson, "Propagation of Traveling Waves on Transmission Lines-Frequency Dependent Parameters," IEEE Transactiosn of Power Apparatus and Systems, vol. PAS-91, pp. 85-91, January/February 1972.

Appendix A

DERIVATION OF TRANSMISSION LINE EQUATIONS IN THE PRESENCE OF GIC

Consider an infinitesimal segment of overhead conductor Δx. It is characterized by an inductance, $L' = L\Delta x$, resistance, $R' = R\Delta x$, and shunt capacitance, $C' = C\Delta x$. Assuming that EMP/GIC related electromagnetic fields are slowly varying their direct effect on the line is negligible. However, a substantial voltage can develop along the line direction on the earth surface, due to GIC. Assume that the earth potential difference across the line length, Δx, due to GIC is $V_g \cdot \Delta x$. The equivalent circuit of the line segment is shown in Figure A-1.

$$v_2 - v_1 = -R'i_2 - L' \frac{di_2}{dt} + v_g \cdot \Delta x$$

$$i_2 - i_1 = -G'v_1 - C' \frac{dv_1}{dt}$$

let

$$v_2 - v_1 = \Delta v$$

$$i_2 - i_1 = \Delta i$$

then

$$\frac{\Delta v}{\Delta x} = -Ri_2 - L' \frac{di_2}{dt} + v_g$$

$$\frac{\Delta i}{\Delta x} = -Gv_1 - C \frac{du_1}{dt}$$

taking limit as

$$\Delta x \to 0$$

$$i_1 \to i_2 \triangleq i$$

$$v_1 \to v_2 \triangleq v$$

results in the differential equations

$$\frac{\partial v}{\partial x} = -Ri - L\frac{di}{dt} + v_g$$

$$\frac{\partial i}{\partial x} = -Gv - C\frac{dv}{dt} .$$

where:

$v = v(x,t)$: voltage of point on transmission line located at ~~disturbance~~ distance x from line end, with respect to remote earth voltage

$i = i(x,t)$: current at point of transmission line located at distance x from line end

R = line series resistance per unit of length

L = line series inductance per unit of length

C = line shunt capacitance per unit of length

G = line shunt conductance per unit of length

v_g = geomagnetically induced earth surface voltage component along the direction of the line, per unit of length

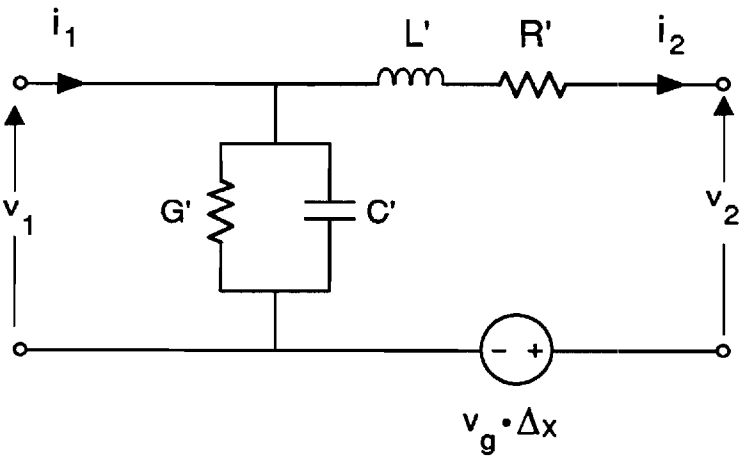

Figure A-1 : Equivalent Circuit of Short Line Segment in the Presence of Geomagneticaly Induced Voltage on the Earth Surface.

E-21-666

GEORGIA INSTITUTE OF TECHNOLOGY
SCHOOL OF ELECTRICAL ENGINEERING
ATLANTA, GEORGIA 30332

TELEPHONE: (404) 894-

Kathy
FYI
Sakis

October 15, 1990

Dr. Mario Rabinowitz
Electric Power Research Institute
P.O. Box 10412
Palo Alto, CA 94303

Dear Mario,

Enclosed please find the third quarterly technical report on "Effects of Geomagnetic Disturbances on Electric Power Transmission Systems."

Sincerely,

A. P. Sakis Meliopoulos

APM/pk
Enclosure
cc: Mrs. Kathy Knighton, GIT

EFFECTS OF GEOMAGNETIC DISTURBANCES ON ELECTRIC POWER TRANSMISSION SYSTEMS

Prepared for

ELECTRIC POWER RESEARCH INSTITUTE
3412 Hillview Avenue
Palo Alto, California 94304

EPRI Project Manager
Dr. Mario Rabinowitz

Prepared by

A. P. Sakis Meliopoulos
E. N. Glytsis
Electric Power Laboratory
School of Electrical Engineering
Georgia Institute of Technology
Atlanta, Georgia 30332-0250

G. J. Cokkinides
Department of Electrical Engineering
University of South Carolina
Columbia, South Carolina 29208

February 1990
Last Revision September 1990

EPRI PERSPECTIVE

(to be added)

ABSTRACT

(to be added)

SUMMARY

(to be added)

ACKNOWLEDGEMENTS

(to be added)

TABLE OF CONTENTS

LIST OF ILLUSTRATIONS

LIST OF TABLES

Section 1

INTRODUCTION AND OBJECTIVE

1.1 INTRODUCTION

The objective of this project is to investigate the level of induced and/or transferred voltages and currents to an electric power system from (1) geomagnetic disturbances due to MHD-EMP and (2) GIC due to solar storms, SS-GIC. Subsequently, a comparison of the effects of MHD-EMP and SS-GIC have been performed.

MHD-EMP is an electromagnetic pulse with very low amplitude which results from geomagnetic disturbances caused by high altitude nuclear detonation. The electric field magnitude is on the order of 100 V/km, low frequency and lasts for several minutes. Similar geomagnetic disturbances are caused by solar storms and result in electric field magnitudes on the order of 10 V/km, low frequency and last from minutes to an hour. Both phenomena cause the flow of almost DC current in the windings of power transformers through the grounding system. Because of the nonlinear magnetization characteristics of the power transformers, the flow of the low frequency electric currents may cause serious secondary results, such as high magnetization currents due to saturation, abnormal reactive power requirements, and disruption of operation. Presently, it is not clear which disturbance (the high magnitude short duration MHD-EMP or the low magnitude long duration SS-GIC) is the most severe to a power system. A system approach has been adopted to address these problems, and to determine at what level saturation is reached.

The objectives of the project have been attained with a two step procedure: In the first step a model of an electric power transmission line including grounding and MHD-EMP or solar storm coupling has been developed. The basic methodology utilized for this step is described in Sections 2 and 3. Since the coupling of MHD-EMP or solar storm induced voltages to power lines is mainly through the line grounding system, it is important to accurately model the power line tower grounding as well as the terminal substation grounding system. For this purpose, the EPRI grounding models developed by Georgia Tech have been utilized. The form of the transmission line model is in terms of a multiple input-multiple output linear system.

The second step involves integration of the model developed in the first step into the EPRI computer model ADCFLT. This computer model is a time domain model similar to the EMTP. It allows modeling of an integrated power system, power system grounding, and the nonlinear magnetization characteristics of power transformers. Using this model, system studies have been performed to determine transformer magnetization currents and reactive power requirements. Of special importance is the degree of saturation of power transformers due to these phenomena. This information can be utilized to analyze transformer performance such as eddy losses in steel members, conductors, and leads. A test system has been utilized provided by Minnesota Power Company.

1.2 REPORT OUTLINE AND MAJOR CONCLUSIONS

Section 2 describes the investigation of the waveforms of geomagnetically induced voltages (GIV) resulting from solar storms (SS) and nuclear bomb explosions (MHD-EMP). The mechanism associated with the generation of GIV is briefly described. Next, models for predicting GIV waveforms from magnetic field measurements are discussed. Measured magnetic field data, collected during SS and MHD-EMP phenomena are presented. Finally, the GIV waveforms computed from magnetic field measurements are presented. These waveforms are used to compare the effects of MHD-EMP and SS-GIV on electric power systems in Section 4.

Section 3 presents the modeling techniques used to simulate the power system in the presence of GIV. Specifically, a model for iron core transformers and a model for multiphase transmission lines are presented. These models are based on a time domain simulation algorithm similar to the EMTP. The transformer model accurately represents magnetic core saturation effects. The transmission line model represents effects of tower grounding and substation grounding at the line ends. These model characteristics are essential for the accurate simulation of GIV effects.

Section 4 describes the application of the models (presented in Section 3) for the study of the effects of GIV on power systems. The test system selected for this study is described first. This system is a simplification of a 500 kV, 473 mile long line. Data for this system were provided by Minnesota Power Company. The performance of this system in the presence of GIV is studied via parametric analysis. Specifically, the steady state currents through the transformer windings are computed for different values of tower footing resistance and ground wire resistances.

Next the time constants associated with magnetic core saturation are parametrically computed with respect to GIV level, ground wire resistance, and tower footing resistance. The results of this study indicate that the transmission line grounding parameters have a substantial effect on both steady state currents and saturation time constants. Finally, the relative effects of MHD-EMP and SS-GIV are compared. For this study, the design waveforms for MHD-EMP-GIV and SS-GIV, described in Section 2, are used. The level of transformer saturation reached in each case is parametrically computed with respect to ground wire and tower footing resistance. The following conclusions were reached from this study.

- For low levels of GIV or short transmission lines, MHD-EMP-GIV and SS-GIV have comparable effects on power systems when the level of MHD-EMP-GIV is 10 times the level of SS-GIV.

- For high levels of GIV, the short duration of the MHD-EMP-GIV mitigates the results only marginally.

- Thermal effects on power transformers due to MHD-EMP-GIV are less severe than those due to SS-GIV.

Section 2

DESIGN WAVEFORMS OF GEOMAGNETICALLY INDUCED VOLTAGES FROM SOLAR STORMS (SS-GIV) AND FROM MAGNETOHYDRODYNAMIC ELECTROMAGNETIC PULSES (MHD-EMP-GIV)

2.1 INTRODUCTION

Electric currents that flow in the molten core of the earth cause its dipole-like magnetic field. The magnetic field of the earth interacts with the interplanetary magnetic field which is actually an extension of the magnetic field of the sun due to the solar wind. The solar wind consists of charged particles, mainly electrons and protons (hydrogen ions), emitted from the surface of the sun. Thus, the solar wind acts like an extension of the magnetic field of the sun and interacts with the earth's magnetic field in a complex manner creating the earth's magnetosphere. In addition, interactions of the earth's magnetic field and the solar wind give rise to a vast magnetohydrodynamic generator that converts the kinetic energy of the solar-wind particles in electric energy which powers the auroral currents or auroral electrojets [1,2]. These currents usually follow circular or elliptical paths around the geomagnetic poles at altitudes of 100 kilometers or more and produce fluctuations in the earth's magnetic field that are termed geomagnetic storms. The strength of the geomagnetic storms is strongly related with solar phenomena that affect the solar wind. These phenomena are the solar flares, the coronal holes, and the disappearing filaments. The severity of the geomagnetic storms strongly depends on the intensity of the above mentioned solar effects. Large solar storms can produce large variations of the auroral electrojets which produce large variations of the geomagnetic field on the earth's surface. The earth as a conducting sphere experiences, or portions of it experience, these time varying magnetic fields. Varying magnetic fields induce electric potential gradients which are called earth-surface-potentials (ESP). The earth-surface-potentials can obtain values in the range between 1 and 10 volts/km depending on the severity of the geomagnetic storm and the earth's conductivity [3,4]. The electric power systems are exposed to ESP through the grounding grid. Since the ESP has frequency of one to a few millihertz the resulting geomagnetically-induced-currents (GIC) can be considered quasi-direct currents compared to 50 Hz or 60 Hz of the electrical power system frequency. Geomagnetic field variations caused by magnetosphere phenomena will result in an induced ESP orthogonal to the field changes. Usually, an idealized east-west

auroral current will cause field variations in the north-south component of the earth's magnetic field, resulting in an east-west induced ESP. Thus, transmission lines in the east-west direction are more susceptible to large ESP than transmission lines in the north-south direction. However, the auroral currents are not ideally east-west and consequently large ESP can be observed in any direction. Several analytical methods have been developed to estimate the induced ESP based on different modeling of the auroral currents and the earth's conductivity. Due to the complexity of the geomagnetic phenomena all these models are approximate and direct measurements of the geomagnetic fields seems to be the best choice.

Geomagnetic disturbances and associated induced earth currents can also originate from the explosion of nuclear bombs at high altitude above the earth's surface [5-7]. These explosions result in transient electromagnetic pulses (EMP) which can affect the operation of the power and communications systems. There are two basic types of electromagnetic pulses due to nuclear explosions. The one is the high altitude quick pulse (TEMP) (Tachy-EMP), and the other is the much slower magnetohydrodynamic EMP (MHD-EMP). For this report, only the slow MHD-EMP is of interest since its effect to power system operation is very similar to solar-storm geomagnetically induced currents. Two similar but different magnetic disturbances give rise to the MHD-EMP. The first is called magnetic bubble EMP (BEMP) [8]. The second is called Atmospheric heave EMP (AEMP) [8]. Due to the nuclear explosion a magnetohydrodynamic bubble of ionized conducting debris is formed and expands rapidly. Initially the geomagnetic flux inside the bubble is very small. If the shell of the magnetic bubble were nonconducting, the expansion of the bubble would simply enclose more magnetic flux of the geomagnetic field. However, since the bubble is conducting, currents are induced on the shell which counteract the earth's magnetic field. Thus, even if the bubble increases in volume the geomagnetic flux that encloses remains as small as it was initially. This effect results in a compression of the geomagnetic field around the bubble. These changes of the geomagnetic field can induce electric fields in the earth which can reach a maximum magnitude of 0.1 V/m with periods from 2 to 100 seconds [8]. This pulse occurs at about 2 to 5 seconds after the nuclear explosion. The second component of the MHD-EMP, the atmospheric heave EMP, occurs more than 10 seconds after the explosion. This pulse is caused by the atmospheric heave of the bomb-heated ionized air across the geomagnetic field. This ionization forms current loops which have mirror images in the earth. These perturbations of the geomagnetic field extend out more than 1250 miles from the source point and last approximately 100 sec. The induced electric fields and frequencies are very low between 0.001-0.03 V/m and ~0.01 Hz. Several analytical methods have been developed mainly for the study of the fast

EMP and comparisons of it with the lightning [9-12]. However, there is not much available information for theoretical modeling of MHD-EMP. Most of the analytical studies for the evaluation of the effects of MHD-EMP on power systems are based on measurements of the induced electric field [5,6], or by assuming plane wave excitation [13,14].

In the following subsections, the most common methods used for the evaluation of the ESP due to SS-GIC or MHD-EMP are reviewed. In addition, sample tables of measured data are given to be used as design ESP waveforms for the calculation of the effect of SS-GIC and MHD-EMP on power systems, and for evaluation of several methods proposed for the alleviation of these effects.

2.2 DESIGN EARTH SURFACE POTENTIAL WAVEFORMS DUE TO SOLAR-STORMS

Several analytical models have been used for the evaluation of the induced electric field on the surface of the earth due to the variations of the geomagnetic field. These models differ in the representation of the auroral currents and the conductivity of the earth. The auroral currents are known to be at altitudes between 100 to 300 km above the earth's surface. These currents can be modeled like current line sources or current sheet sources of infinite extend above a flat earth's surface. However, the auroral currents have such a spatial extension that they can not be considered either a current line or a current sheet. The above assumptions though give some estimate of the induced electric field on the earth's surface. Specifically, the current line model gives a lower limit while the current sheet model gives an upper limit of the induced electric field. Sometimes the auroral currents are assumed to be at an infinite distance from the ground. In this case, the geomagnetic field is modeled as a plane electromagnetic wave. The conductivity of the earth is also difficult to model due to the large variety and inhomogeneity of the earth's surface from place to place. The simplest model assumes a flat earth surface with a uniform effective conductivity. More sophisticated earth models divide the earth's surface in multiple layers, each one having a different conductivity.

The simplest method for modeling the auroral currents is the plane electromagnetic wave model [15]. The earth is modeled as a horizontally stratified medium of one or more layers of differing conductivities. The incident geomagnetic field is assumed to be a linearly polarized, monochromatic plane wave. The electric field on the surface of the earth is computed with usual electromagnetic analysis methods. In addition, using this technique the surface impedance of the earth, Z_g, can be

computed, where $Z_s = E_x/H_y$ (E_x/H_y are the horizontal components of the electric and magnetic field on the earth's surface, respectively). This is useful since from measurement of the magnetic field, the induced electric field can be estimated.

Another widely used technique models the auroral currents as an infinite horizontal current sheet at a height h above the horizontally also stratified earth of one or more layers [15-19]. To solve the problem, the electric and magnetic Hertz vectors are commonly used. For the described geometry, these vectors have only one component which is perpendicular to the earth's surface and to the auroral current sheet. Using the vector Hertz potentials and Maxwell's equations along with the corresponding boundary conditions, the electric field on the earth's surface can be found. This field is a function of (1) the magnitudes along the two horizontal directions of the current sheet (j_x,j_y), (2) the radian frequency ω of the auroral current, (3) the spatial wave numbers of the spectral components of the auroral currents, (4) the altitude h of the auroral current, and (5) the characteristics of the earth. Even if the described analysis considered a single spectral component, there is no loss of generality since by Fourier synthesis any time-dependent source current can be written as a linear combination of its spectral components. Consequently, the resulting induced electric field will be a linear combination of the fields due to the different spectral components. As it was mentioned earlier, the current sheet method overestimates the induced electric field on the earth's surface.

The auroral currents can also be modeled as a line current source parallel to the earth's surface at an altitude h [15,18,20,21]. Usually, the line is positioned in the east-west direction and is assumed positive in the westward direction. Earth's surface is modeled like a horizontally stratified medium. The general methodology used for the solution of these problems is based on Price's analysis [22]. This analysis assumes slow variations of the geomagnetic fields. As a result, the second time derivatives in the wave equation are neglected. This assumption permits solutions of the magnetic field expressed in terms of the gradient of a scalar magnetic potential for the region above the earth, while the electric field solutions are expressed in terms of the time derivative of a vector magnetic potential for the earth region. An equivalent procedure consists of expressing the electric field as $\vec{E} = e^{j\omega t}G(z)\vec{F}(x,y)$, where G and $\vec{F}$ have to be determined for each region from the wave equation and the boundary conditions of the problem [(x,y) correspond to the horizontal plane while z is the perpendicular coordinate]. Using this procedure the resulting electric and magnetic fields on the

earth's surface are calculated as functions of the following parameters: (1) the magnitude of the auroral current, (2) the radian frequency of the auroral current, (3) the altitude h of the auroral current, (4) the difference in latitude between the auroral current and the point for which the calculations are made, and (5) the surface impedance of the earth Z_s [23] which depends on the earth's parameters and modeling. Usually, since the magnitude of the auroral currents is not known, an estimate of $J = 10^5 A$ is used. As it was mentioned previously this method underestimates the induced electric field on the earth's surface due to the modeling of the auroral currents as a horizontal line current.

In the described models the auroral currents are modeled as uniform or sinusoidal distributions. However, none of these assumptions is very accurate. More sophisticated studies include Gaussian modeling of the electrojet [24,25]. In addition, Hibbs et al. have studied nonsymmetric auroral currents distributions [26].

Independently of the used model, the complexity of the physical effect of the auroral electrojet is difficult to represent. In addition, all the described models assume sinusoidal auroral currents. However, if the spectral content of the auroral currents was known, these models along with the superposition principle could be used for the calculation of the induced electric field. Since the spectral content of the auroral currents is not known and, in addition, is varying with time, the geomagnetic field is usually measured in several positions in the areas of interest using magnetometers. By measuring the magnetic field, the induced electric field can be roughly estimated using the plane wave assumption from [4]

$$E(t) = -\frac{1}{(\pi \mu_o \sigma)^{1/2}} \int_0^\infty \frac{g(t-u)}{u^{1/2}}\, du \,, \qquad (2\text{-}1)$$

where E(t) is the horizontal component of the induced electric field, μ_o is the permeability of the freespace, σ is the conductivity of the earth, and g is the time derivative of the horizontal component of the magnetic field. If the measured data are used, the derivative g can be computed numerically and the integral can be approximated using the extended Simpson's rule [27] by the following formula

$$\int_0^\infty \frac{g(t-u)}{u^{1/2}}\, du \approx D^{1/2}\left\{\frac{4}{3}\, g(t)+g(t-D)+\frac{2}{3}\sum_{j=1}^{L}(1+a_j)\,\frac{g[t-(j+1)D]}{(j+1)^{1/2}}\right\} \,, \qquad (2\text{-}2)$$

where D is the data time interval and $a_j = 0$ when j is even and $a_j = 1$ when j is odd; L is the total number of data points that are considered for the calculation of E(t). Using the data measured during May 12-13, 1989, at magnetic Observatory

Furstenfeldbruck (Figure 2-1, Table 2-1, and Eqs. (2-1) and (2-2)), the induced electric field was calculated and its values are summarized in Table 2-2 (Figure 2-2).

2.3 DESIGN EARTH SURFACE POTENTIAL WAVEFORMS DUE TO MAGNETOHYDRODYNAMIC ELECTROMAGNETIC PULSES

The effects of the magnetohydrodynamic electromagnetic pulse (MHD-EMP) on power system grids are very similar to those of geomagnetic storms. More specifically, MHD-EMP generates electric fields on the order of 10^{-1} V/m (about an order of magnitude higher than the geomagnetically-induced electric fields) of frequencies less than 1 Hz and of 100-200 sec duration. As it was described previously, MHD-EMP is due to two distinct physical mechanisms, the magnetic bubble (BEMP) and the atmospheric heave (AEMP). The early portion of the MHD-EMP (less than 10 seconds after the nuclear explosion) is due to BEMP while the rest of MHD-EMP is due to the AEMP [6]. Some estimate of the average induced electric field can be calculated using the following arguments [7]. The magnetic bubble, as it expands, pushes the geomagnetic field out of its way. The bubble obtains its maximum size when the energy of the excluded field equals the initial kinetic energy, T, of the conducting shell of the magnetic bubble, neglecting all other loss mechanisms. Thus, the following equation can be written [7]

$$\frac{1}{2\mu_o}\langle B^2\rangle\left(\frac{4}{3}\pi R^3\right) = T \qquad R = [3\mu_o T/2\pi\langle B^2\rangle]^{1/3}\ , \tag{2-3}$$

where $\langle B^2\rangle$ is the mean squared value of the flux density of the unperturbed geomagnetic field, μ_o is the permeability of freespace, R is the maximum radius of the magnetic bubble (assuming spherical bubble), and T is the initial kinetic energy of the conducting debris of the bomb. The average power, $\langle P\rangle$, of the MHD-EMP can be estimated from

$$\langle P\rangle = \frac{fT}{\Delta t}\ , \tag{2-4}$$

where f is the conversion efficiency of the kinetic energy, T, in electromagnetic power, and Δt is the duration of the produced electromagnetic pulse. The average power density near the bubble can then be found from $\langle P\rangle/4\pi R^2$. Using the Poynting vector, the power density is $E^2/2\eta$, where η is the intrinsic impedance of freespace. Using the above arguments, an estimate of the induced electric field can be found from

$$E = \left[\frac{2fT^{1/3}\eta}{4\pi\Delta t[3\mu_o/2\pi\langle B^2\rangle]^{2/3}}\right]^{1/2}\ . \tag{2-5}$$

Using $f \approx 10^{-5}$, $T \approx 1.76 \cdot 10^{15}$ J (for a 30% yield of a 1.4 Mt bomb [7]), $\eta = 377\ \Omega$, $\Delta t \approx 100$ sec, and $B \approx 5 \cdot 10^{-5}$ wb/m^2, an electric field of 0.1 V/m can be estimated. The above estimate is based only on the BEMP effect under the rough assumptions made above. However, the atmospheric currents due to air ionization produce significant portion of the induced electric field. Thus, the most valuable information about a MHD induced EMP is empirically known from the magnetometer data acquired during actual nuclear events as the "Starfish" test conducted in the Pacific. The design waveform for the simulation of MHD-EMP is the one measured during the Starfish test. The magnetometer data [6] have been used along with Eq. (2-1) to calculate the induced electric field that appears in Figure 1 of Reference 5. This electric field has been sampled and linearly approximated and is tabulated in Table 2-3 (Figure 2-3).

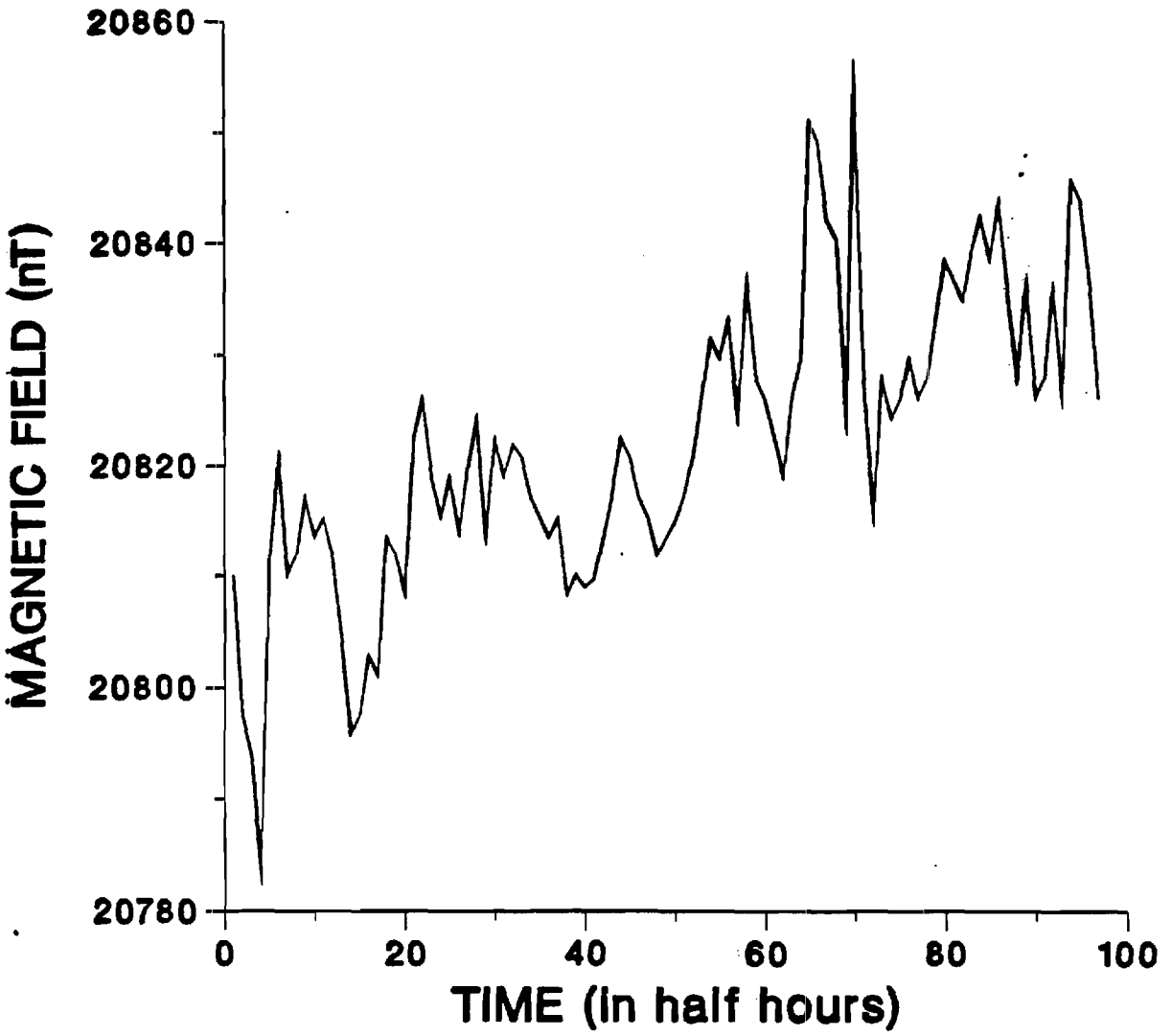

Figure 2-1: Horizontal Component of Magnetic Field.
Magnetic Observatory Fürstenfeldbruck, May 12-13, 1989.

TABLE 2.1

Measurements of the Horizontal Component of the Magnetic Flux Density of the Geomagnetic Field at the Fürstenfeldbruck Station in 30 Minute Intervals Between May 12-13, 1989

Time (sec)	Horizontal Component of Geomagnetic Field (nT)
.0	20810.00
1800.0	20797.60
3600.0	20794.00
5400.0	20783.30
7200.0	20811.10
9000.0	20820.80
10800.0	20810.00
12600.0	20811.90
14400.0	20817.20
16200.0	20813.60
18000.0	20815.40
19800.0	20811.90
21600.0	20804.70
23400.0	20795.80
25200.0	20797.60
27000.0	20802.90
28800.0	20801.10
30600.0	20813.60
32400.0	20811.90
34200.0	20808.30
36000.0	20822.60
37800.0	20826.10
39600.0	20819.00
41400.0	20815.40
43200.0	20819.00
45000.0	20814.00
46800.0	20819.70
48600.0	20824.30
50400.0	20813.60
52200.0	20822.50
54000.0	20819.00
55800.0	20822.00
57600.0	20820.80
59400.0	20817.20
61200.0	20815.40
63000.0	20813.60
64800.0	20815.40
66600.0	20808.30
68400.0	20810.10
70200.0	20809.00
72000.0	20809.70
73800.0	20813.60
75600.0	20817.20

TABLE 2.1 (continued)

Time (sec)	Horizontal Component of Geomagnetic Field (nT)
77400.0	20822.60
79200.0	20820.80
81000.0	20817.20
82800.0	20815.40
84600.0	20811.90
86400.0	20813.60
88200.0	20815.00
90000.0	20817.20
91800.0	20820.80
93600.0	20826.10
95400.0	20831.50
97200.0	20829.70
99000.0	20833.20
100800.0	20824.30
102600.0	20836.80
104400.0	20827.90
106200.0	20826.10
108000.0	20822.60
109800.0	20819.00
111600.0	20826.10
113400.0	20829.70
115200.0	20851.10
117000.0	20849.30
118800.0	20842.20
120600.0	20840.40
122400.0	20824.30
124200.0	20854.70
126000.0	20827.90
127800.0	20815.40
129600.0	20827.90
131400.0	20824.30
133200.0	20826.10
135000.0	20829.70
136800.0	20826.10
138600.0	20827.90
140400.0	20833.20
142200.0	20838.60
144000.0	20836.80
145800.0	20835.00
147600.0	20839.50
149400.0	20842.50
151200.0	20838.60
153000.0	20843.90
154800.0	20836.10
156600.0	20827.90
158400.0	20836.80
160200.0	20826.10
162000.0	20827.90

TABLE 2.1 (continued)

Time (sec)	Horizontal Component of Geomagnetic Field (nT)
163800.0	20836.10
165600.0	20826.10
167400.0	20845.70
169200.0	20843.90
171000.0	20836.80
172800.0	20826.10

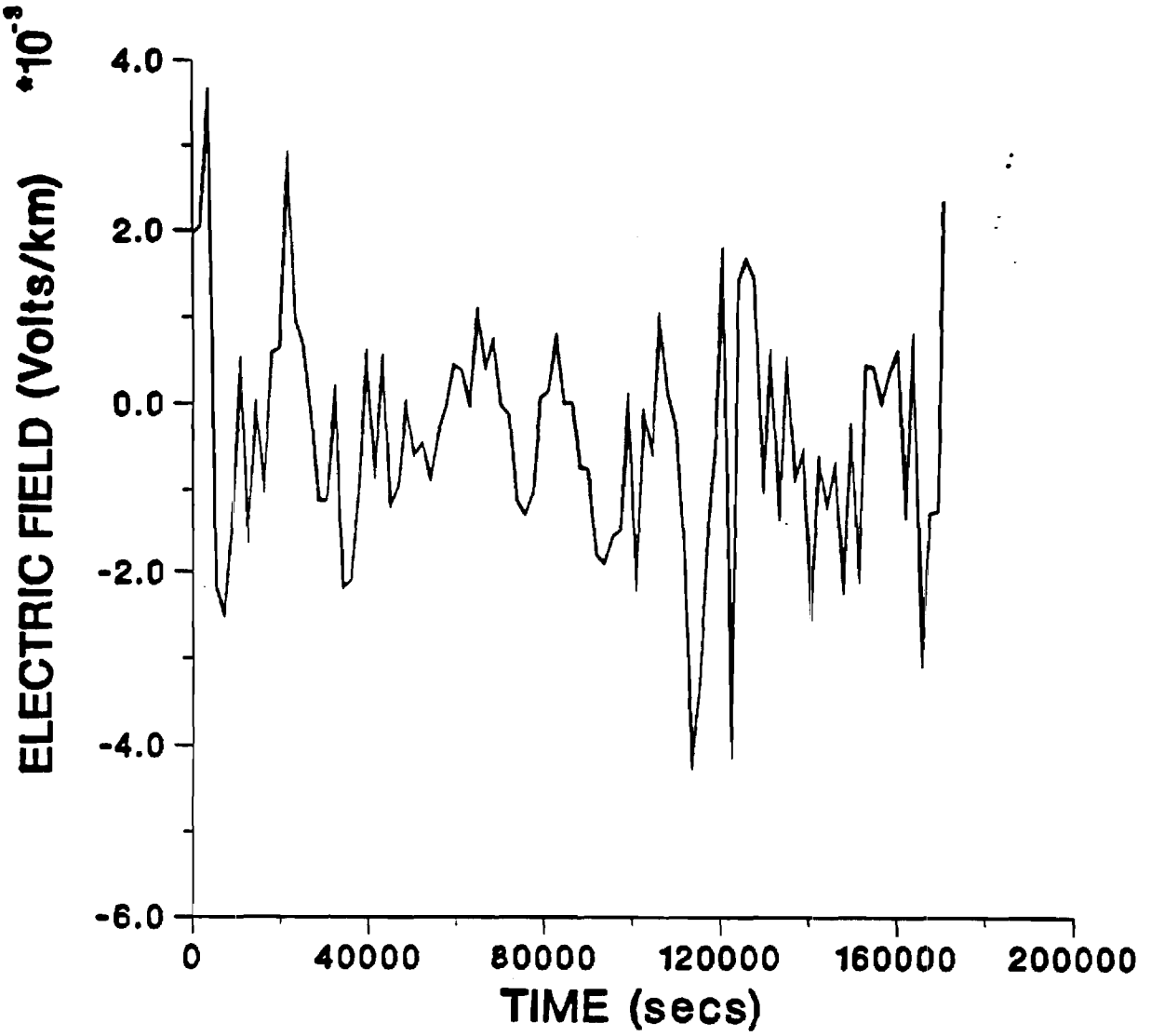

Figure 2-2: SS-GIC Electric Field.
Magnetic Observatory Fürstenfeldbruck, May 12-13, 1989.

TABLE 2.2

Calculated Induced Electric Field (SS-GIC) Using the Measurements of Table I and Eqs. (1) and (2)

Time (sec)	Induced Electric Field (V/km)
.0	.19613E-02
1800.0	.20404E-02
3600.0	.35063E-02
5400.0	-.21590E-02
7200.0	-.24903E-02
9000.0	-.13399E-02
10800.0	.40067E-03
12600.0	-.15157E-02
14400.0	-.37079E-04
16200.0	-.97319E-03
18000.0	.58856E-03
19800.0	.64136E-03
21600.0	.27804E-02
23400.0	.97135E-03
25200.0	.68159E-03
27000.0	-.12122E-03
28800.0	-.11203E-02
30600.0	-.11249E-02
32400.0	.91153E-04
34200.0	-.21800E-02
36000.0	-.20967E-02
37800.0	-.10255E-02
39600.0	.52078E-03
41400.0	-.78152E-03
43200.0	.47075E-03
45000.0	-.11750E-02
46800.0	-.95832E-03
48600.0	-.61076E-05
50400.0	-.60230E-03
52200.0	-.46227E-03
54000.0	-.87251E-03
55800.0	-.33812E-03
57600.0	-.25453E-04
59400.0	.45499E-03
61200.0	.39364E-03
63000.0	.41640E-05
64800.0	.10508E-02
66600.0	.40856E-03
68400.0	.73819E-03
70200.0	-.12803E-04
72000.0	-.12281E-03
73800.0	-.11164E-02
75600.0	-.12954E-02
77400.0	-.10285E-02
79200.0	.67825E-04

TABLE 2.2 (continued)

Calculated Induced Electric Field (SS-GIC) Using the Measurements of Table I and Eqs. (1) and (2)

Time (sec)	Induced Electric Field (V/km)
81000.0	.14286E-03
82800.0	.76736E-03
84600.0	.62566E-05
86400.0	.17448E-04
88200.0	-.73720E-03
90000.0	-.75860E-03
91800.0	-.17937E-02
93600.0	-.19081E-02
95400.0	-.15541E-02
97200.0	-.14738E-02
99000.0	.79403E-06
100800.0	-.20720E-02
102600.0	-.11190E-03
104400.0	-.56233E-03
106200.0	.98050E-03
108000.0	.13813E-03
109800.0	-.22304E-03
111600.0	-.16265E-02
113400.0	-.41819E-02
115200.0	-.32840E-02
117000.0	-.14967E-02
118800.0	-.50570E-03
120600.0	.15648E-02
122400.0	-.37526E-02
124200.0	.14089E-02
126000.0	.16592E-02
127800.0	.14355E-02
129600.0	-.91577E-03
131400.0	.50753E-03
133200.0	-.12444E-02
135000.0	.44008E-03
136800.0	-.87843E-03
138600.0	-.55878E-03
140400.0	-.24192E-02
142200.0	-.66480E-03
144000.0	-.11979E-02
145800.0	-.73047E-03
147600.0	-.21370E-02
149400.0	-.35746E-03
151200.0	-.19755E-02
153000.0	.43395E-03
154800.0	.41453E-03
156600.0	-.62593E-05
158400.0	.35518E-03
160200.0	.59024E-03
162000.0	-.12100E-02

TABLE 2.2 (continued)

Calculated Induced Electric Field (SS-GIC) Using the Measurements of Table I and Eqs. (1) and (2)

Time (sec)	Induced Electric Field (V/km)
163800.0	.62786E-03
165600.0	-.29351E-02
167400.0	-.12896E-02
169200.0	-.12626E-02
171000.0	.23348E-02

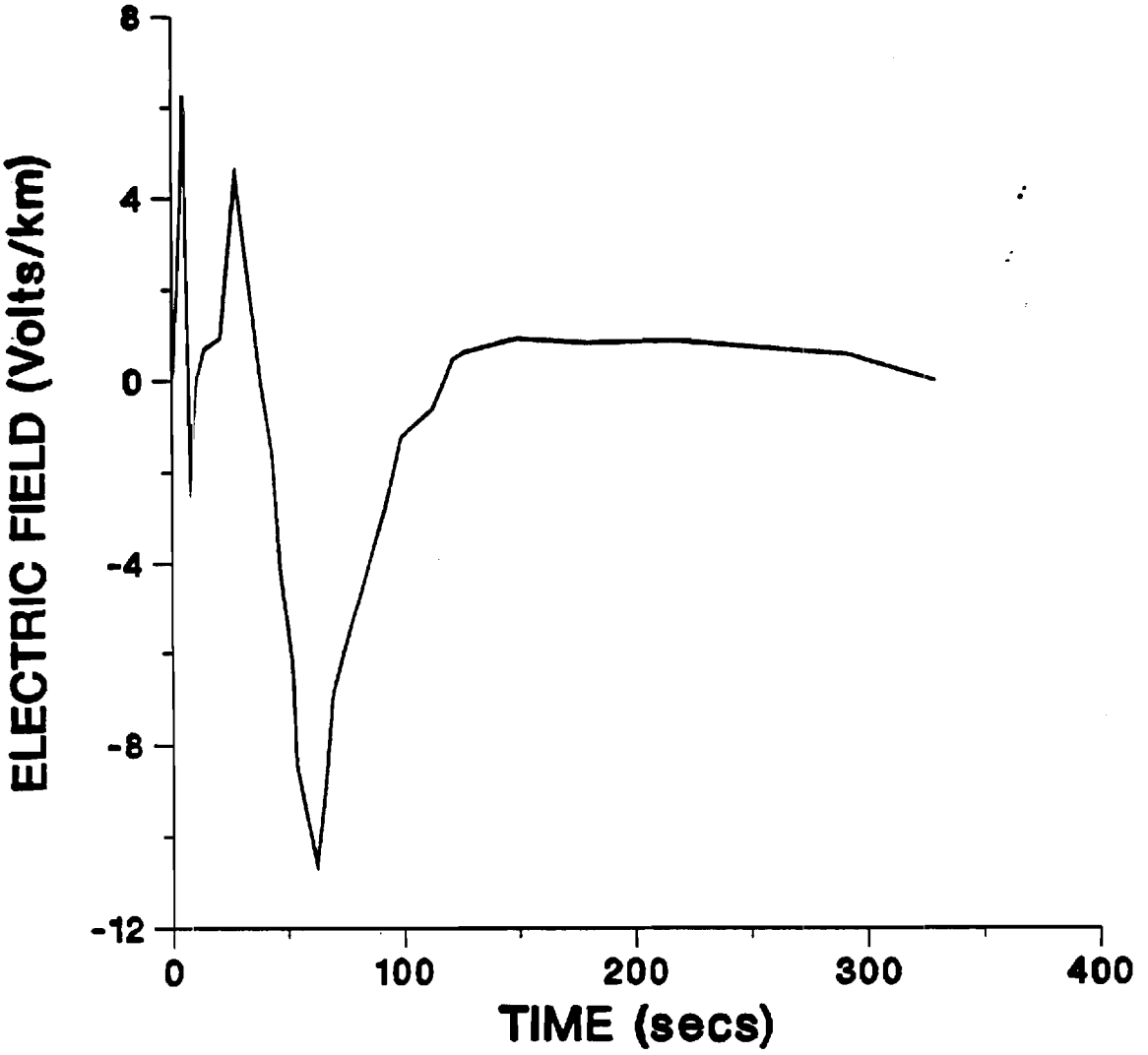

Figure 2-3: MHD-EMP Induced Electric Field.

TABLE 2.3

Measured Induced Electric Field (MHD-EMP)
During the "Starfish" Test

Time (sec)	Electric Field (V/km)
0.0	.00000E+00
5.0	.62500E+01
7.0	.00000E+00
8.0	-.21900E+01
10.5	.00000E+00
13.9	.69000E+00
20.9	.94000E+00
27.8	.45300E+01
38.3	.00000E+00
43.5	-.15600E+01
47.0	-.40600E+01
52.2	-.62500E+01
53.9	-.84400E+01
62.6	-.10630E+02
66.0	-.90600E+01
69.6	-.68800E+01
83.5	-.43800E+01
92.2	-.28100E+01
99.1	-.12500E+01
113.0	-.63000E+00
118.3	.00000E+00
121.7	.47000E+00
127.0	.63000E+00
149.6	.94000E+00
180.9	.84000E+00
217.4	.90000E+00
280.0	.63000E+00
292.2	.59000E+00
330.4	.00000E+00

Section 3

TRANSMISSION SYSTEM MODEL

3.1 INTRODUCTION

This section describes the transmission system model for the study of geomagnetic disturbances. The model is based on a time domain simulation algorithm similar to the EMTP. Each power system element is modeled with a set of differential equations which are solved in the time domain. For the study of geomagnetic disturbances, two power system elements are very important: (1) magnetic core transformers and (2) long transmission lines. Specifically, long transmission lines provide the gate for geomagnetically induced currents to enter the power system. On the other hand, magnetic core transformers reach saturation when geomagnetically induced currents flow in their windings and cause most of the undesirable effects. This section describes in detail these two models.

3.2 IRON CORE TRANSFORMERS

Iron core transformers are highly nonlinear devices due to their saturable iron magnetic core. A typical iron core magnetization curve is illustrated in Figure 3-1. For practical reasons, power transformers are designed in such a way that the maximum operating magnetic flux is near the knee of the magnetization curve. During normal operating conditions, the magnetic flux oscillates between $+\lambda_{max}$ and $-\lambda_{max}$ and the magnetization current is symmetric about the zero axis. When a DC current is injected through the transformer winding, this symmetry is destroyed. In this case, the transformer may operate past the magnetization curve knee for portions of the cycle, requiring a high magnetization current to maintain the applied voltage.

This phenomenon is modeled as follows. Consider a single phase transformer as it is illustrated in Figure 3-2. The equations describing the transformer are:

$$v_{1u}(t) = r_{1u} i_{1u}(t) + L_{1u} du_{1u}/dt + d\lambda(t)/dt$$

$$v_{2u}(t) = r_{2u} i_{2u}(t) + L_{2u} di_{2u}/dt + d\lambda(t)/dt$$

$$\lambda(t) = g(i_m(t))$$

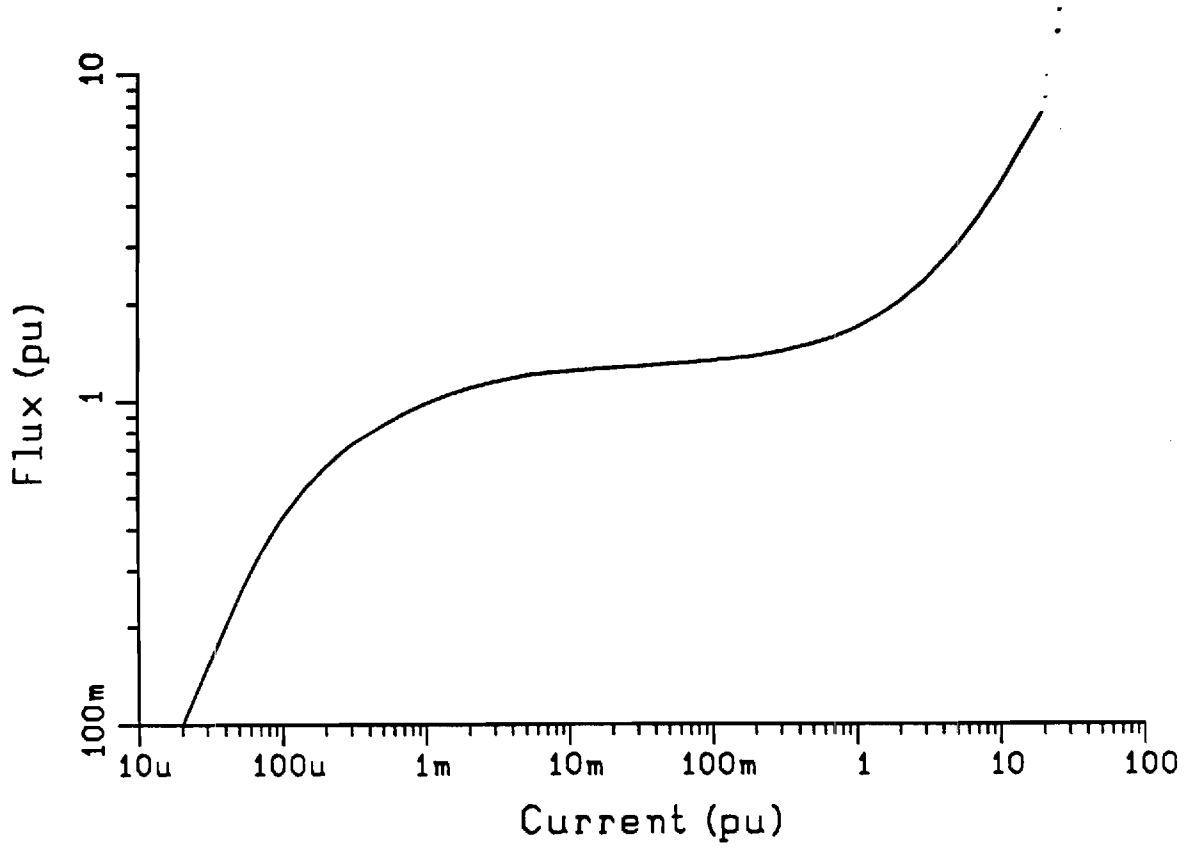

Figure 3-1 : Typical Iron Core Magnetization Curve

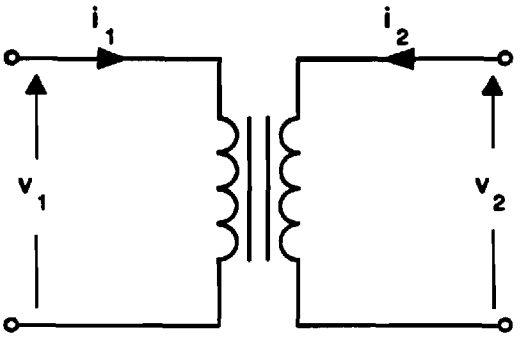

(a)

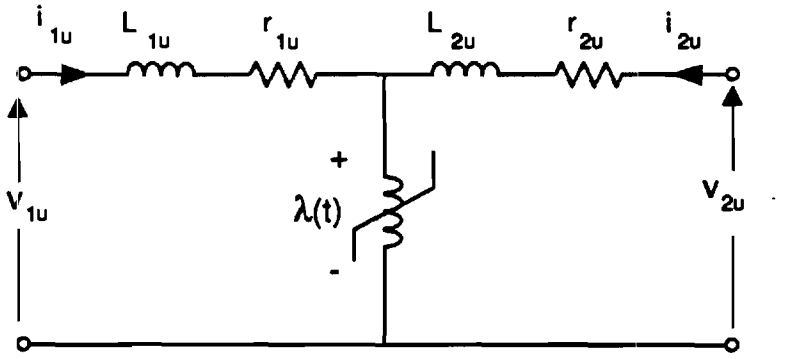

(b)

Figure 3-2 : Single Phase Transformer & equivalent Circuit
(a) Transformer
(b) Per Unit Equivalent Circuit

$$i_{m(t)} = i_{1u}(t) + i_{2u}(t)$$

where

$v_{1u}(t), v_{2u}(t)$ are the voltages in per unit

$i_{1u}(t), i_{2u}(t)$ are the currents in per unit

$g(\cdot)$ is the magnetization curve

$i_m(t)$ is the magnetization current in per unit.

Three single phase transformers, appropriately connected (wye-delta, etc.), provide the model of a three phase transformer. The equations of the power transformer are integrated in the time domain.

3.3 TRANSMISSION LINE MODEL WITH GIV COUPLING

The transmission line model used in this study is a time domain state space model based on the methodology described in Reference 29. It is capable of representing transmission line parameter frequency dependence, line tower grounding, as well as effects of geomagnetically induced currents (GIC).

The model is easily interfaced with other time domain models of power system components (such as transformers, loads, and generators). Thus the effect of GIC phenomena on the integrated power system can be assessed.

The transmission line model involves two components:

(1) Overhead conductors and earth return

(2) Grounding system.

Consider the transmission line shown in Figure 3-3. The section of overhead conductors between any two consecutive towers comprise a "conductor component" while each tower with its grounding systems is a component of the grounding system. Each component is modeled by an equivalent admittance matrix (which is a function of frequency) and equivalent current sources. Then, using nodal analysis, the equivalent circuit of the entire transmission line and GIC coupling is formed. The resulting model is in the form of a passive circuit of known admittance matrix and lumped current sources connected at the line terminals. This model is finally converted to the time domain using Fourier techniques.

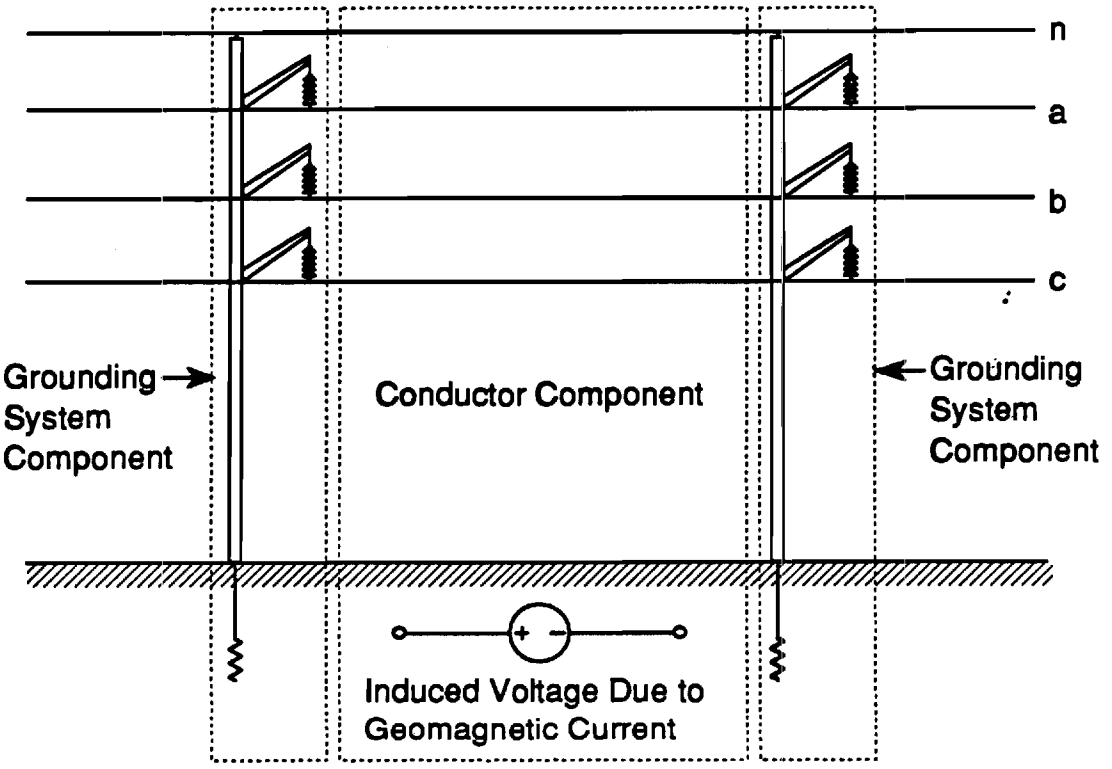

(a)

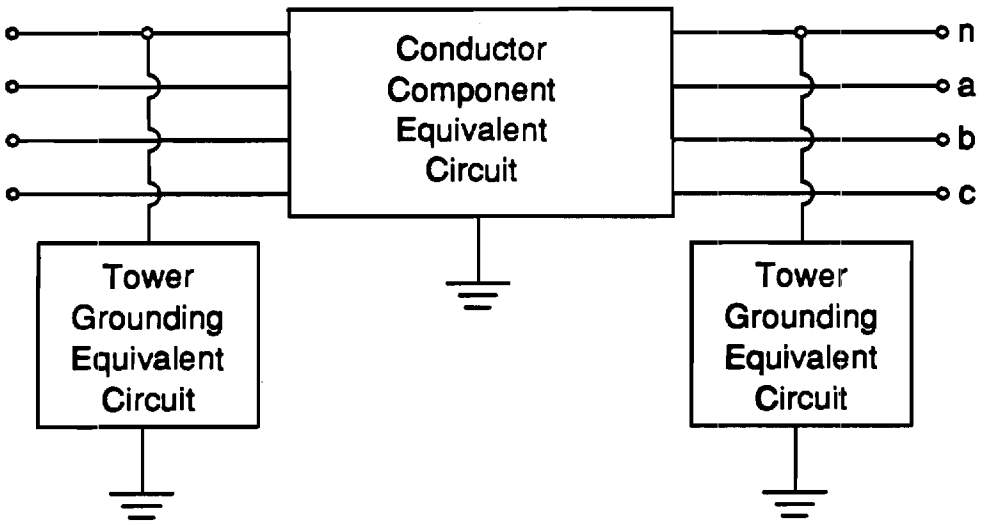

(b)

Figure 3-3 : Transmissin Line Section
(a) Physical Configuration
(b) Equivalent Circuit

The derivation of the conductor and grounding system equivalent circuits are presented in the following sections.

3.3.1 Overhead Conductor Model

An overhead transmission line conductor section, in the presence of geomagnetically induced currents is represented by the equations

$$\frac{\partial v(x,t)}{\partial x} = -Ri(x,t) - L\frac{\partial i(x,t)}{\partial t} + v_g(x,t) \quad , \tag{3-1}$$

$$\frac{\partial i(x,t)}{\partial x} = -Gv(x,t) - C\frac{\partial v(x,t)}{\partial t} \quad ,$$

where

- v : line voltage with respect to remote earth (v)
- i : line current (A)
- R : line series resistance (Ohms/meter)
- L : line series inductance (Henries/meter)
- G : line shunt conductance (Siemens/meter)
- C : line shunt capacitance (Farads/meter)
- v_g : component of voltage due to GIC in the direction of the line (volts/meter).

(See Appendix A for a derivation of Eq. (3-1).)

Since the line parameters are frequency dependent, the solution of the above equation is computed in the frequency domain. The Fourier transform of the above equations is

$$\frac{\partial V(x,\omega)}{\partial x} = -Z(\omega)I(x,\omega) + V_g(x,\omega) \quad , \tag{3-2}$$

$$\frac{\partial I(x,\omega)}{\partial x} = -Y(\omega)V(x,\omega) \quad , \tag{3-3}$$

where

$$Z(\omega) = R(\omega) + j\omega L(\omega)$$

$$Y(\omega) = G(\omega) + j\omega C(\omega) \quad .$$

For overhead transmission lines, several simplifications can be made:

(1) The conductance term is negligible and thus

$$Y(\omega) = j\omega C(\omega) \ .$$

(2) For a short line span, V_g is assumed constant with respect to position, thus

$$V_g(x,\omega) = V_g(\omega) \ .$$

(3) The resistance and inductance are computed using the complex depth of return method.

(4) The capacitance matrix is independent of frequency.

For a multiphase line the voltage due to GIC, V_g appears in series with every conductor. Thus it is replaced by the vector of the form

$$\begin{bmatrix} 1 \\ 1 \\ \vdots \\ 1 \end{bmatrix} \cdot V_g(x,\omega)$$

In order to compute the conductor section equivalent circuit, the current is eliminated in the equation system (3-2), (3-3), by differentiating Eq. (3-2) with respect to x and substituting current with voltage from Eq. (3-3)

$$\frac{\partial^2 V(x,\omega)}{\partial x^2} = K(\omega)V(x,\omega) \qquad (3\text{-}4)$$

where

$$K(\omega) = Z(\omega)Y(\omega) \ . \qquad (3\text{-}5)$$

The solution to the above equation (3-4) is obtained using eigenvalue analysis of the matrix K. Specifically, the system is decoupled by the transformation

$$V'(x,\omega) = W^{-1}(\omega)V(x,\omega) \qquad (3\text{-}6)$$

where

$$K(\omega) = W(\omega)D(\omega)W(\omega)^{-1} \qquad (3\text{-}7)$$

where $D(\omega)$ is a diagonal matrix containing the eigenvalues of matrix K, and $W(\omega)$ the eigenvector matrix of $K(\omega)$.

Applying transformation (3-7) to Eq. (3-4) yields

$$\frac{\partial^2 V'(x,\omega)}{\partial x^2} = D(\omega)V'(x,\omega) \ . \tag{3-8}$$

The general solution to the above equation is

$$V'(x,\omega) = e^{x\sqrt{D(\omega)}} \cdot A_1(\omega) + e^{-x\sqrt{D(\omega)}} \cdot A_2(\omega) \ , \tag{3-9}$$

where A_1, A_2 are constants to be determined by boundary conditions. Specifically,

$$V'(o,\omega) = A_1(\omega) + A_2(\omega) \tag{3-10}$$

$$V'(\ell,\omega) = e^{\ell\sqrt{D(\omega)}} A_1(\omega) + e^{-\ell\sqrt{D(\omega)}} A_2(\omega) \ .$$

Solving for A_1 and A_2 yields

$$A_1(\omega) = \left[e^{2\ell\sqrt{D(\omega)}} - I\right]^{-1} \left(e^{\ell\sqrt{D(\omega)}} V_2' - V_1'\right) \tag{3-11}$$

$$A_2(\omega) = \left[e^{-2\pi\sqrt{D(\omega)}} - I\right]^{-1} \left(e^{-\ell\sqrt{D(\omega)}} V_2' - V_1'\right) \ ,$$

where

$$V_1' = V'(o,\omega) = W^{-1} V(o,\omega)$$
$$V_2' = V'(\ell,\omega) = W^{-1} V(\ell,\omega)$$

and ℓ is the line length.

Thus, Eqs. (3-9) and (3-11) define the voltage at any point of the line given the voltages at the line ends. Now, using (3-2), the current is also computed as a function of the terminal voltages yielding

$$I(x,\omega) = Z^{-1}(\omega) V_g(\omega) = Z(\omega)^{-1} \frac{\partial V(x,\omega)}{\partial x} \ . \tag{3-12}$$

Evaluating the above at the line terminals, ($x = 0$, and $x = \ell$) yields

$$I_1(\omega) = Z(\omega)^{-1} V_g(\omega) - Z(\omega)^{-1} W(\omega) \left\{\sqrt{D(\omega)}\ A_1(\omega) - \sqrt{D(\omega)}\ A_2(\omega)\right\}$$

$$I_2(\omega) = Z(\omega)^{-1} V_g(\omega) - Z^{-1}(\omega) W(\omega) \left\{\sqrt{D(\omega)}\ E^{\ell\sqrt{D(\omega)}} A_1(\omega) - \sqrt{D(\omega)}\ e^{-\ell\sqrt{D(\omega)}} A_2(\omega)\right\} \ . \tag{3-13}$$

The above can be rewritten in matrix form as follows

$$\begin{bmatrix} I_1(\omega) \\ I_2(\omega) \end{bmatrix} = \left[\begin{array}{c|c} Z^{-1}(\omega) & 0 \\ \hline 0 & Z^{-1}(\omega) \end{array}\right] \cdot \begin{bmatrix} V_g(\omega) \\ V_g(\omega) \end{bmatrix} + \begin{bmatrix} Y_1(\omega) & Y_2(\omega) \\ Y_2(\omega) & Y_1(\omega) \end{bmatrix} \begin{bmatrix} V_1(\omega) \\ V_2(\omega) \end{bmatrix} \tag{3-14}$$

where

$$\begin{aligned} Y_1(\omega) &= -Z^{-1}(\omega)W(\omega)\left[\sqrt{D(\omega)}\left[-e^{2\ell\sqrt{D(\omega)}}+I\right]^{-1}+\sqrt{D(\omega)}\left[e^{-2\ell\sqrt{D(\omega)}}-I\right]^{-1}\right]W^{-1}(\omega) \\ &= Z^{-1}(\omega)W(\omega)\sqrt{D(\omega)}\left[\left(e^{2\ell\sqrt{D(\omega)}}-I\right)^{-1}-\left(e^{-2\ell\sqrt{D(\omega)}}-I\right)^{-1}\right]W^{-1}(\omega) \\ &= Z^{-1}(\omega)W(\omega)H_1(\omega)W^{-1}(\omega) \\ Y_2(\omega) &= Z^{-1}(\omega)W(\omega)\sqrt{D(\omega)}\left[\left[e^{2\ell\sqrt{D(\omega)}}-I\right]^{-1}e^{\ell\sqrt{D(\omega)}}-\left[e^{-2\ell\sqrt{D(\omega)}}-I\right]^{-1}e^{-\ell\sqrt{D(\omega)}}\right]W^{-1}(\omega) \\ &= Z^{-1}(\omega)W(\omega)\sqrt{D(\omega)}\left[2\left(e^{\ell\sqrt{D(\omega)}}-e^{-\ell\sqrt{D(\omega)}}\right)^{-1}\right]W^{-1}(\omega) \\ &= Z^{-1}(\omega)W(\omega)H_2(\omega)W^{-1}(\omega)\ , \end{aligned} \tag{3-15}$$

where $H_1(\omega), H_2(\omega)$ are diagonal matrices of which the diagonal elements are

$$\begin{aligned} H_{1_{ii}} &= \frac{\sqrt{D_i}}{\tanh(\ell\sqrt{D_i})} \\ H_{2_{ii}} &= \frac{\sqrt{D_i}}{\sinh(\ell\sqrt{D_i})}\ , \end{aligned} \tag{3-16}$$

where D_i is the ith eigenvalue of matrix $K(\omega)$.

From Eq. (3-14), an equivalent circuit can be derived representing a multiphase transmission line section in the presence of GIC. Figure 3-4 illustrates the equivalent circuit. It consists of a passive circuit whose admittance matrix is known and current sources connected at each terminal representing GIC coupling. Note that all parameters of the equivalent circuit are frequency dependent. Thus the admittance matrix and current source values have to be computed explicitly at each frequency of interest.

3.3.2 Tower Grounding Model

Each tower and its grounding structure are represented by a step response. It is defined as the current flowing into the tower from the neutral wire support point when a unit step voltage is applied at the same point.

The step response of the tower and its grounding system can be determined experimentally [30] or analytically [31,32]. When computed analytically, finite element analysis is utilized to solve for the flow of currents in the earth. Then a convolution algorithm is utilized to evaluate the tower and ground step response [31].

The tower model has been validated with data obtained by Bonneville Power Administration (BPA). The validation of this model is reported in Reference 32.

The admittance of the tower and grounding system at any given frequency is computed from the step response with an appropriate Fourier transform.

3.3.3 Integrated Model

The equivalent circuit of the entire transmission line is constructed by combining the equivalent circuits of each conductor section and tower grounding systems. The procedure is based on nodal analysis method, where all internal node voltages and currents are eliminated, and all internal current sources are represented by equivalent current sources at the terminals of the line. The resulting equivalent circuit has the same topology as the one for a single line section as illustrated in Figure 3-4.

In order to utilize the developed model in time domain simulation, the equivalent circuit parameters are transformed into the time domain. Specifically, the admittance matrix of the passive part of the equivalent circuit is transformed to an impulse response, and the equivalent current sources (which are also computed as functions of frequency) are transformed into time domain waveforms. A discrete Fourier transform method is used for this purpose.

The Snelson transformation is applied before Fourier transformation to minimize resulting time domain waveform durations (see Reference 33). Specifically, the voltage and current variables are replaced by B and F as follows

$$F(\omega) = V(\omega) + G^{-1} I(\omega) \qquad (3\text{-}17)$$

$$B(\omega) = V(\omega) - G^{-1} I(\omega)$$

where G is a real nxn matrix (n = number of conductors), and

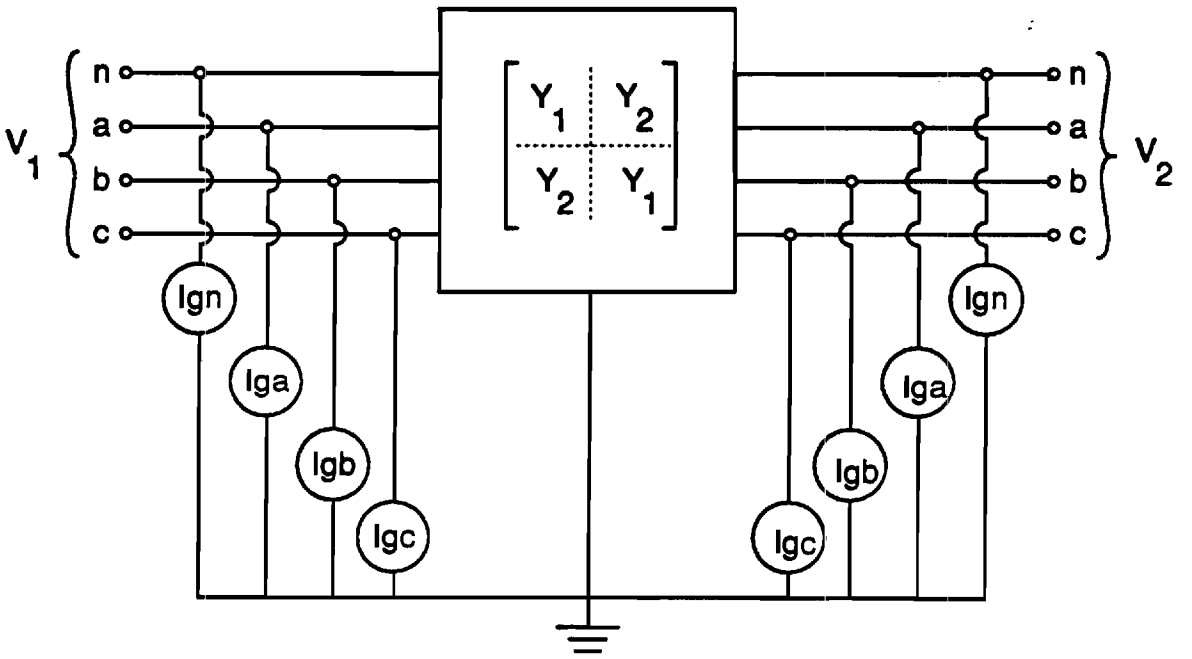

Figure 3-4 : Equivalent Circuit of a Transmission Line Section with GIC Coupling

$$V(\omega) = \begin{bmatrix} V_1(\omega) \\ V_2(\omega) \end{bmatrix}, \quad I(\omega) = \begin{bmatrix} I_1(\omega) \\ I_2(\omega) \end{bmatrix}.$$

Applying the above transformation to Eq. (3-14) yields

$$\frac{1}{2} G\big(F(\omega)-B(\omega)\big) = \begin{bmatrix} Z^{-1}(\omega)V_g(\omega) \\ \hline Z^{-1}(\omega)V_g(\omega) \end{bmatrix} + \frac{1}{2} Y(\omega)\big(F(\omega)+B(\omega)\big) \ . \tag{3-18}$$

Solving for $B(\omega)$ yields

$$B(\omega) = M(\omega)F(\omega) + A_g(\omega) \ , \tag{3-19}$$

where

$$M(\omega) = \big(G(\omega)+Y(\omega)\big)^{-1}\big(G(\omega)-Y(\omega)\big)F(\omega)$$

$$A_g(\omega) = -2\big(Y(\omega)+G(\omega)\big)^{-1} \begin{bmatrix} Z(\omega)V_g(\omega) \\ Z^{-1}(\omega)V_g(\omega) \end{bmatrix}$$

The matrix $M(\omega)$ and the vector $A_g(\omega)$ are next transformed into time domain functions using the FFT algorithm

$$m(t) = F^{-1}\{M(\omega)\}$$

$$a_g(t) = F^{-1}\{A_g(\omega)\} \tag{3-20}$$

The function matrices $m(t)$ and $a_g(t)$ comprise a time domain model of the entire transmission line with GIC coupling. Specifically, $m(t)$ contains the impulse response of the transmission line (based on Snelson's transformation) and the functions $a_g(t)$ represent the GIC effects. These functions are utilized in a convolution based algorithm, in order to simulate the operation of transmission lines with GIC coupling in the integrated power system. This algorithm is described in the following section.

3.3.4 Convolution Algorithm

The transmission line model is cast into the resistive companion form via a discrete convolution scheme. This technique allows the model to be interfaced with models of other power system components, thus forming a model of an integrated power system. (This is the standard methodology followed by several time domain simulation programs such as the EMTP and the PSTS programs.) Specifically, the model of a transmission line with GIC coupling is represented by the equivalent circuit shown in Figure 3-5. The voltage vector v and current vector i represent the voltages and

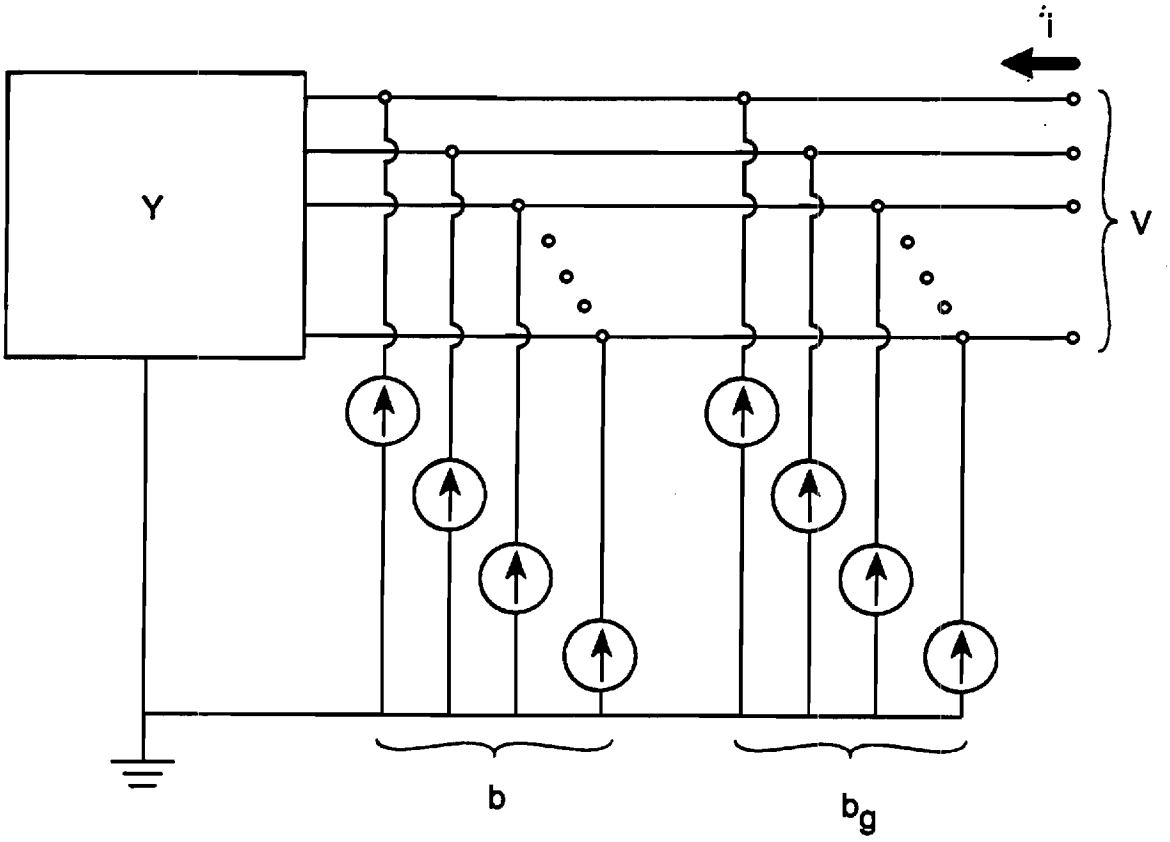

Figure 3-5 : Model of Transmission with GIC Coupling
in the Resistive Companion Form

current injections on each conductor at the ends of the line. The following equation holds for these voltages and currents:

$$Y \cdot v(t) = b(t) + b_g(t) + i(t) \tag{3-21}$$

where Y is the transmission line characteristic admittance matrix, b is the vector of currents depending on past history voltages and currents, and b_g is the vector of currents representing GIC effects. The above equation can be solved by discrete time techniques in terms of the impulse response model defined in the previous section. Specifically, let v_n and i_n represent the values of the voltage and current vectors at the line ends at the n-th time step. Then:

$$Yv_n = b_{n-1} + b_{g_n} + i_n \tag{3-22}$$

where

$$\begin{aligned} Y &= G[I+S_o]^{-1}[I-S_o] \\ b_{n-1} &= G[I+S_o]^{-1} \sum_{k=0}^{N} (S_k - S_{k-1})(v_{n-k} - G^{-1} i_{n-k}) \\ b_{g_n} &= G[I+S_o]^{-1} a_{g_n} \end{aligned}$$

where S_i represents the transmission line step respone (at the ith time interval), i.e. it is the integral of the impulse response m(t), performed in discrete time.

The above equation (3-22) is a resistive companion form representation of a transmission line with GIC coupling. Specifically, the real matrix Y is the admittance matrix of a resistive network (block Y in Figure 3-5). The vector b_{n-1} represents the past history dependent current sources. The entries of the current source vector b_{n-1} are computed by discrete convolution as shown in Eq. (3-22). The vector b_{g_n} are the independent current sources (b_g in Figure 3-5), representing the effects of GIC.

Using these equations, a transmission line with GIC coupling and its interaction with the integrated power system is simulated using the standard methodology for power system transient simulation employed by the EMTP and PSTS programs.

Section 4

INVESTIGATION OF GEOMAGNETICALLY INDUCED EFFECTS ON POWER SYSTEMS

4.1 INTRODUCTION

This section describes the application of the power transmission system model, for the study of geomagnetic disturbances. A test system is selected consisting of a 500 kV transmission line terminated by delta-wye connected transformers at both ends. The response of this system under geomagnetically induced voltages (GIV) is investigated. Specifically, a parametric analysis of the system steady state and transient response to GIV is performed. The effects of GIV level, duration, and transmission system parameters are examined. Finally, the design GIV waveforms corresponding to MHD-EMP and SS are applied to the test system and the resulting system responses are compared.

4.2 DESCRIPTION OF THE TEST SYSTEM

The test system is a simplification of the Minnesota Power Company 500 kV line between Dorsey and Minneapolis. Specifically it consists of a 500 kV transmission line, terminated by three phase transformer banks at both ends. Figure 4-1 illustrates a single line diagram of the test system.

The transmission line data are listed in Table 4-1. During normal operation, the sky wires are not electrically connected to the transmission line towers. Tower configuration data specifies the location of the center of each phase bundle and each sky wire with respect to a Cartesian coordinate system with its origin located at the center of the tower base.

Each of the three phase transformer banks consists of three single phase transformers connected DELTA/GROUNDED Y. The grounded Y side is connected on the 500 kV transmission line (see Figure 4-1). The characteristics of each single phase transformer are as follows:

Voltage 115/288 kV	
Power Rating	350 MVA
Leakage Reactance	0.10 pu
Magnetizing Current	0.01 pu
Winding Resistance (high V. side)	1.5 ohms

Table 4-1

Transmission Line Data

GENERAL DATA

Line Length	473 miles
Configuration	3 conductor bundle per phase
Bundle Spacing	18 inches
Tower Spacing	0.25 miles
Tower Footing Resistance	30 Ohms

CONDUCTOR DATA

Conductor	Type	O.D inches	Resistance (Ohms/mile)
Ground Conductors	7/16 steel	0.4375	4.435
Phase Conductors	1192 ACSR	1.3020	0.080

TOWER CONFIGURATION DATA

Conductor	x - coordinate (feet)	y - coordinate (feet)
Phase A	-32.0	97.5
Phase B	0.0	97.5
Phase C	32.0	97.5
Sky Wire 1	-35.0	129.5
Sky Wire 2	35.0	129.5

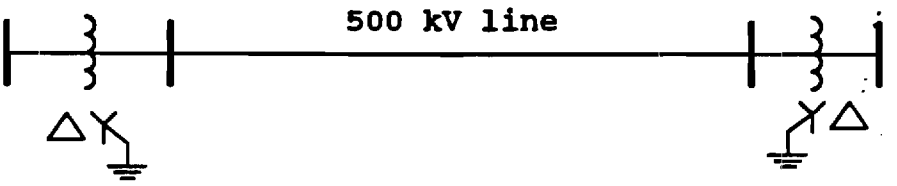

(a)

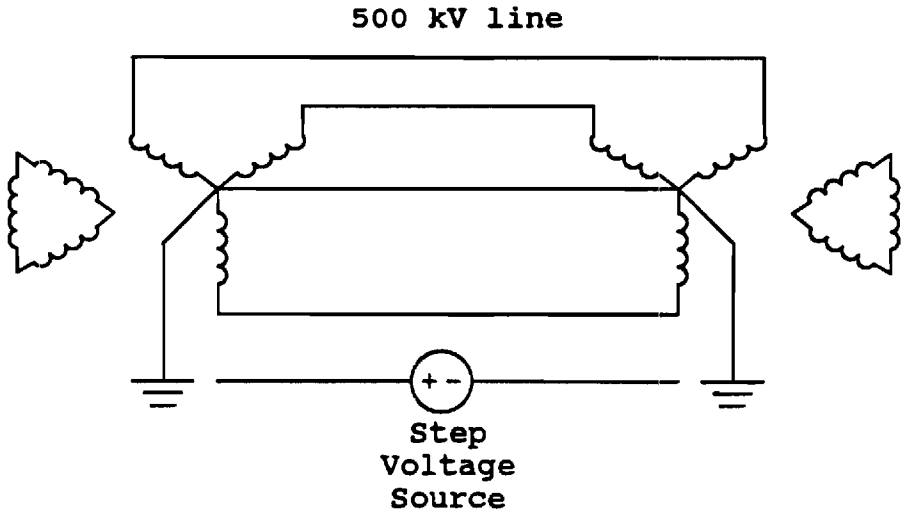

(b)

Figure 4-1 :Test System
a) Single Line Diagram
b) Three Phase Diagram

Transformer saturation is modeled as described in Section 3.2. The transformer core magnetization characteristics are described by a piecewise-linear function which is tabulated in Table 4-2. (The same data are plotted in Figure 3-1.)

The response of the described system is computed assuming a geomagnetically induced voltage (GIV) of step function waveform. Three cases are simulated with different GIV levels as follows:

1. 1.0 volts per mile
2. 10.0 volts per mile
3. 100.0 volts per mile.

The effects of GIV to the test system are assessed as follows: First, the steady state direct current through the transformer is computed for the above GIV levels and various values of line parameters. Next, the transient response of the transformer excitation current is computed for the above GIV levels to determine the time constants involved to reach saturation. Finally, the design GIV waveform from MHD-EMP and solar storms are applied to the test system to determine the relative effects. The results of this study are described in the following sections.

4.3 COMPUTATION OF STEADY STATE RESPONSE

This section presents the computation of the steady state response of the test system under GIC excitation. In order to gain insight in the system parameters that determine the system behavior under GIC excitation, a simple approach is used first. Specifically, an equivalent DC model of the system is constructed. Using, this simple model, the magnitude and distribution of geomagnetically induced currents are evaluated.

The DC model of the test system is constructed by considering only the resistances of each system component. Specifically, an equivalent circuit is constructed containing the DC models of the transformers, transmission line, grounding system, and geomagnetic voltage. This circuit is illustrated in Figure 4-2. The equivalent circuits of each component are described next.

The transformers are represented by their winding resistances. Specifically, the windings of the Y connected (high voltage) side of the transformer exhibit three parallel paths to the flow of the electric current injected at the transformer neutral. Assuming that the windings are identical, the equivalent resistance is 1/3 of the winding resistance of each high voltage winding.

Table 4-2
Transformer Magnetization Characteristics
(High Voltage Side)

Current (kiloamperes)	Flux Linkage (kilowebers-turns)
.00000000	.00000000
.00003429	.10829000
.00005144	.16243500
.00006858	.21603860
.00008573	.26855920
.00010288	.31837260
.00012002	.36363780
.00013717	.40381350
.00017146	.47052010
.00025719	.58990980
.00034292	.67004440
.00051438	.78022940
.00085730	.91104380
.00120022	.98717160
.00171460	1.06189200
.00257190	1.13823600
.00342920	1.18398900
.00514380	1.23965000
.00857300	1.29379500
.01200220	1.31696900
.01714600	1.33564900
.02571900	1.35427500
.03429200	1.36621400
.05143800	1.38240300
.08573000	1.40297800
.12002200	1.41748900
.17146000	1.43548700
.25719000	1.46136800
.34292000	1.48486700
.51438000	1.52867100
.85730000	1.60999600
1.20022000	1.68764000
1.71460000	1.80183200
2.57190000	1.98619600
3.42920000	2.16433300
5.14380000	2.51356800
8.57300000	3.19796100
12.00220000	3.86935900
17.14600000	4.86183700
34.29200000	8.12678100

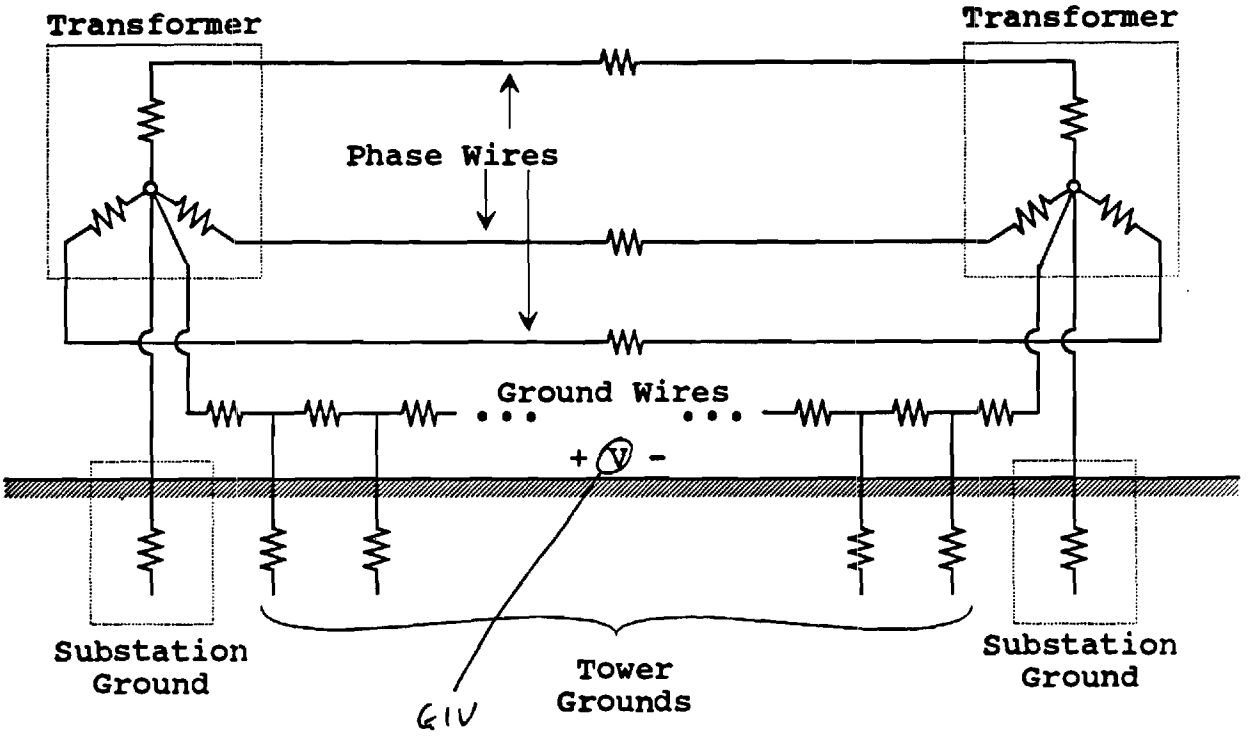

Figure 4-2 : DC Equivalent Circuit of Test System

The transmission line is represented by a DC equivalent circuit. Each of the phase wires is represented by a resistance equal to the total DC resistance of the phase conductor.

The neutral wire is represented by its DC resistance. The neutral wire may or may not be multiply grounded. Figure 4-2 illustrates the tower footing grounding which is represented by its DC resistance.

The substation grounds at each line end are represented by 1 Ohm resistances, connected from the transformer Y side neutral to remote earth.

Finally, the equivalent circuit of the earth containing the geomagnetically induced voltage is represented by a series of Thevenin equivalent circuits connected between consecutive tower grounds and substation grounds. Thus, for each line segment, a separate Thevenin equivalent of the earth is used. Each Thevenin equivalent consists of a voltage source representing the geomagnetically induced voltage, and a resistor representing the earth path resistance. The earth path resistance is highly dependent on frequency. The earth path resistance computed at 0.6 Hz was used.

The above model was employed to study the effects of multiply grounded ground wires on the steady state direct current through the transformer winding. The following values were used for the parametric study:

GIV	1 Volt/mile
Earth path resistance	0.001 Ohm/mile
Tower footing resistance	5, 30, 100, & infinite Ohms
Tower spacing	0.25 mile
Equivalent phase conductor resistance	0.00889 Ohms/mile
Ground conductor resistance	4.435 & 1.240 Ohms/mile
Total line length	473 miles

The results of the parametric study are illustrated in Figure 4-3. The figure is self explanatory. Note that there is a substantial effect of the line grounding parameters on the steady state value of the direct current through the transformer. A well grounded transmission line will mitigate the DC current through the transformer by 50%.

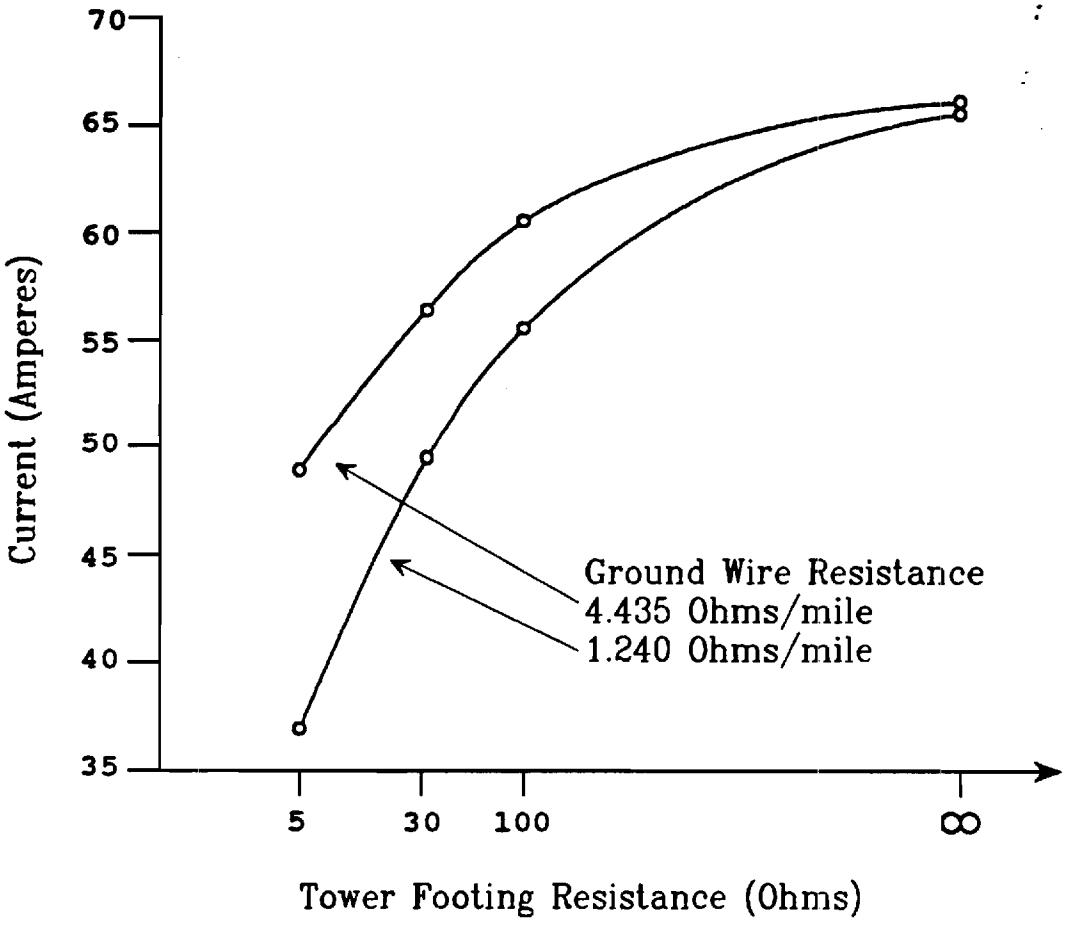

Figure 4-3 : Steady State Direct Current through Transformer Winding

4.4 COMPUTATION OF TIME CONSTANTS TO SATURATION

The described model of the test system was simulated in the time domain to determine the time constants involved to reach steady state operation. Specifically, the time constants were defined as the time required to reach 63% of its steady state value. Figure 4-4 illustrates a typical simulation and the definition of the time constant. The figure also illustrates the parameters of the simulation as well.

The time constants were computed for various parameters as follows:

GIV	1, 10, 100 Volts/mile
Earth Path Resistance	0.001 ohms/mile
Tower Footing Resistance	5, 30, 100 infinite ohms
Tower Spacing	0.25 miles
Equivalent Phase Conductor Resistance	0.00889 ohms/mile
Ground Conductor Resistance	4.435 & 1.240 ohms/mile
Total Line Length	473 miles

The results of the parametric study are illustrated in Table 4-3. Note the wide variation of time constants (145 seconds to 2.3 seconds). System parameters drastically affect time constants.

4.5 COMPARISON OF SATURATION LEVELS DUE TO MHD-EMP AND SS-GIC

An important test which determines the relative effects of MHD-EMP and SS-GIC on power systems is the level of saturation reached due to typical values of GIV from MHD-EMP or SS. For this test the following two comparable strength MHD-EMP and SS-GIV will be assumed:

Case 1. The geomagnetically induced voltage due to MHD-EMP has a time variation as in Figure 2-3 and a peak value of 100 volts/mile.

The geomagnetically induced voltage due to a solar storm is practically DC and has a maximum value of 10 volts/mile.

Case 2. Same as in Case 1 except that the peak values are 10 and 1 volt(s)/mile, respectively.

The maximum levels of saturation were computed for the following range of parameters.

Tower footing resistance	5, 30, 100 & infinite ohms
Tower spacing	0.25 mile
Equivalent phase conductor resistance	0.00889 ohms/mile
Ground conductor resistance	4.435 & 1.240 ohms/mile
Total line length	473 miles

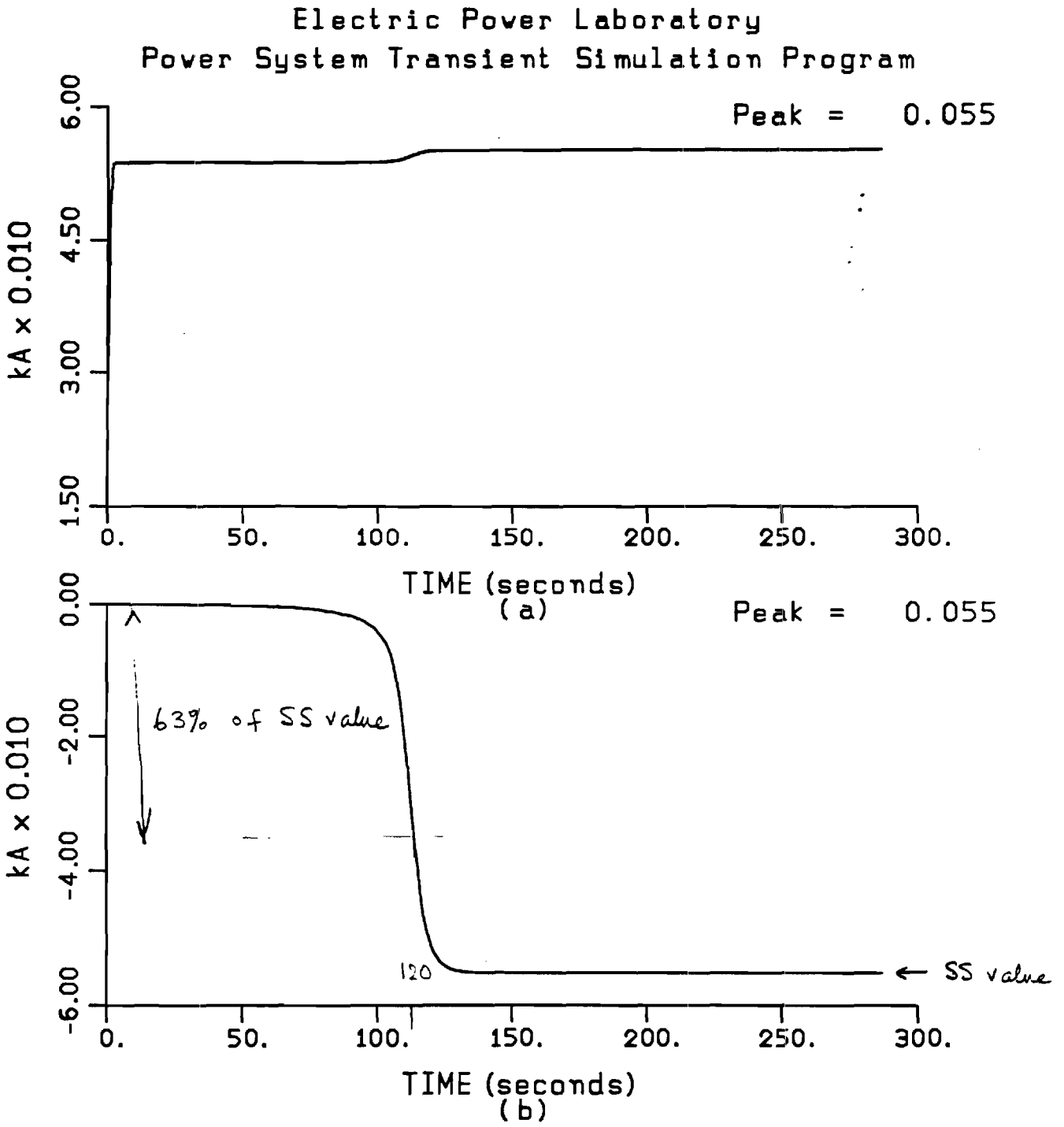

GIV = 1 V/mi, Rtf = 5 Ohms, Rg = 4.435 Ohms/mi
(a) Line Zero Sequence Current
(b) Transformer Magnetization Current

Figure 4-4. Typical Results of Time Domain Simulation of the Test System.

Table 4-3: Test System Time Constant to Saturation* (in seconds) Versus GIV Level, Tower Footing Resistance (R_t), and Ground Wire Resistance (R_g)

	G.I.V.					
	1 V	/ mile	10 V	/ mile	100 V	/ mile
R_g \ R_t	4.435	1.24	4.435	1.24	4.435	1.24
5	120	145	13.0	16.0	2.8	3.1
30	98	109	11.2	12.5	2.5	2.6
100	93	96	10.6	11.4	2.4	2.5
inf	85	85	10.0	10.0	2.3	2.3

* Time Constant to Saturation is defined as the time required for the transformer magnetization current to reach 63.2% of its steady state value.

The results are illustrated in Tables 4-4 and 4-5. Note that for Case 2, even if the MHD-EMP-GIV is ten times higher than SS-GIV, the maximum saturation level is comparable. For Case 1, the saturation level is much higher for MHD-EMP excitation. The implication of these results are as follows:

Heating: Transformer thermal time constants are on the order of hours [33]. Specifically, Reference 33 reports on measured thermal time constants of a distribution transformer. The time constants have been measured by applying step loads on the transformer. Figure 4-5 is reproduced from Reference 53. It clearly illustrates the relatively long thermal time constants. Thus, thermal heating is probably not a major consideration for GIV excitation due to MHD-EMP because of its relatively short duration of high DC offset flux. As a matter of fact, simulations show that saturation in this case lasts several hours. In this case, heating becomes a major consideration.

Loss of Equipment: Due to GIV excitation (SS or MHD-EMP), transformers become generators of harmonics and absorbers of reactive power. Protective relaying, sensing this situation, may trip the transformer. In this case, irrespective of the duration of the GIV excitation, loss of equipment will occur with possibly major consequences such as the Hydro-Quebec blackout.

4.6 CONCLUSIONS

A comprehensive model for studying the effects of geomagnetically induced voltages on power systems has been developed. The model has been used to study the time constants involved in reaching transformer saturation due to GIV and the saturation level versus system parameters.

The most important parameters determining the effects of GIV on power systems are:

1. Level of GIV
2. Duration of GIV
3. Tower grounding impedance
4. Ground wire resistance.

Comparative studies of MHD-EMP-GIV and SS-GIV indicate that (1) for low values of GIV, an MHD-EMP level of 10 times the SS-GIV will cause comparable effects, and (2) for high values of GIV, the short duration of the MHD-EMP mitigates the results only marginally. Since transformer thermal constants are much larger than the duration of MHD-EMP, the general conclusion is that the thermal effects due to MHD-EMP induced voltages on power systems are less severe than those due to solar storm GIV.

Table 4-4: Maximum DC Offset Magnetic Flux (in pu)

in Transformer Core.

Case 1

	SS-GIV = 1V / mile		MHD-EMP	GIV = 10V/mi
R_t \ R_g	4.435	1.25	4.435	1.25
5	0.129	0.128	0.142	0.136
30	0.130	0.129	0.143	0.140
100	0.130	0.130	0.144	0.143
inf	0.130	0.130	0.146	0.146

Table 4-5: Maximum DC Offset Magnetic Flux (in pu) in Transformer Core.

Case 2

	SS-GIV = 10 V / mile		MHD-EMP	GIV = 100 V/mi
R_t \ R_g	4.435	1.25	4.435	1.25
5	0.147	0.143		
30	0.150	0.147	0.300	0.281
100	0.151	0.149		0.298
inf	0.153	0.153	0.325	0.325

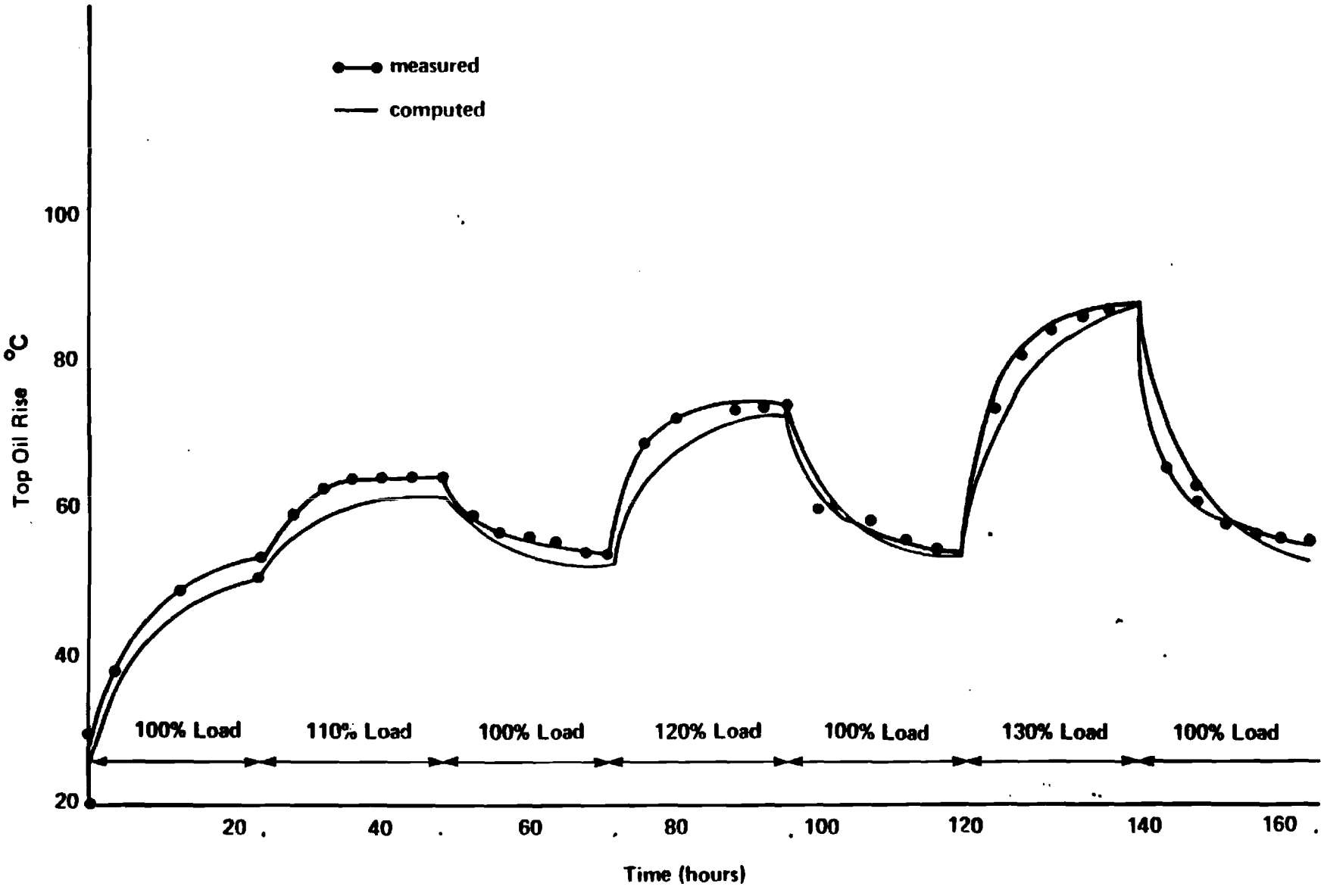

Figure 4. Simulated and Measured Top Oil Temperature Rise.

Section 5

REFERENCES

1. Syun-Ichi Akasofu, "The Dynamic Aurora," Scientific American, pp. 90-97, May 1989.

2. S. Chapman, Solar Plarma, Geomagnetism and Aurora, Gordon and Breach Science Publishers, New York, 1968.

3. V. D. Albertson, "Geomagnetic Disturbance Causes and Power System Effects," 1989 IEEE PES Summer Meeting, Long Beach, California, July 12, 1989.

4. R. Pirjola, "On Currents Induced in Power Transmission Systems During Geomagnetic Variations," IEEE Transactions on Power Apparatus and Systems, vol. PAS-104, no. 10, pp. 2825-2830, October 1985.

5. G. B. Rackliffe, J. C. Crouse, J. R. Legro, and V. J. Kruse, "Simulation of Geomagnetic Currents Induced in a Power System by Magnetohydrodynamic Electromagnetic Pulses," IEEE Transactions on Power Delivery, vol. PWRD-3, no. 1, pp. 392-397, January 1988.

6. J. R. Legro, N. C. Abi-Samra, J. C. Crouse, and F. M. Tesche, "A Methodology to Assess the Effects of Magnetohydrodynamic Electromagnetic Pulse (MHD-EMP) on Power Systems," IEEE Transactions on Power Delivery, vol. PWRD-1, no. 3, pp. 203-209, July 1986.

7. M. Rabinowitz, "Magnetohydrodynamic EMP, Solar Storm GIC, and Substorms," Conference on Geomagnetically Induced Currents, sponsored by Electric Power Research Institute, Burlingame, California, November 8-10, 1989.

8. M. Rabinowitz, "Nuclear Electromagnetic Pulse," Encyclopedia of Science and Technology, 1986 Yearbook, McGraw Hill, New York, pp. 34-47, 1985.

9. C. N. Vittitoe and M. Rabinowitz, "Radiative Reactions and Coherency Modeling in the High-Altitude Electromagnetic Pulse," Physical Review A, vol. 37, no. 6, pp. 1969-1977, March 15, 1988.

10. M. Rabinowitz, "Effect of the Fast Nuclear Electromagnetic Pulse on the Electric Power Grid Nationwide: A Different View," IEEE Transactions on Power Delivery, vol. PWRD-2, no. 4, pp. 1199-1222, October 1987.

11. K. W. Klein, P. R. Barnes, and H. W. Zaininger, "Electromagnetic Pulse and the Electric Power Network," IEEE Transactions on Power Apparatus and Systems, vol. PAS-104, pp. 1571-1577, 1985.

12. C. L. Longmire, "On the Electromagnetic Pulse Produced by Nuclear Explosions," IEEE Transactions on Electromagnetic Compatibility, vol. EMC-20, no. 1, pp. 3-13, February 1978.

13. C. N. Vittitoe, "Did High-Altitude EMP Cause the Hawaiian Streetlights Incident?", Sandia National Labs, Albuquerque, New Mexico, SAND88-00430, 1988.

14. D. P. Millard, A. P. Sakis Meliopoulos, and G. J. Cokkinides, "Parametric Analysis of EMP Induced Overvoltages on Power Lines," IEEE Transactions on Power Delivery, vol. PWRD-3, no. 3, pp. 1224-1231, July 1988.

15. J. R. Wait, Geo-Electromagnetism, Academic Press, Inc., New York, Chapter VI, pp. 184-208, 1982.

16. A. A. Kaufman and George V. Keller, The Magnetotelluric Sounding Method, Elsevier Scientific Publishing Company, New York, Chapter 5, pp. 113-155, 1981.

17. T. Rikitake and Y. Honkura, Solid Earth Geomagnetism, Terra Scientific Publishing Company, Tokyo, Japan, and D. Reidel Publishing Company, Boston, Chapter 11, pp. 267-292, 1985.

18. V. D. Albertson and J. A. Van Ballen, "Electric and Magnetic Fields at the Earth's Surface Due to Auroral Currents," IEEE Transactions on Power Apparatus and Systems, vol. PAS-89, no. 4, pp. 578-584, April 1970.

19. J. R. Wait, "Electromagnetic Surface Impedance for a Layered Earth for General Excitation," Radio Science, vol. 15, no. 1, pp. 129-134, January-February 1980.

20. R. Pirjola and A. Viljanen, "On Geomagnetically-Induced Currents in the Finnish 400 kV Power System by an Auroral Electrojet Current," IEEE Transactions on Power Delivery, vol. PWRD-4, no. 2, pp. 1239-1245, April 1989.

21. D. Park, "Magnetic Field of a Horizontal Current Above a Conducting Earth," Journal of Geophysical Research, vol. 78, no. 16, pp. 3040-3043, June 1, 1973.

22. A. T. Price, "Electromagnetic Induction in a Semi-Infinite Conductor with a Plane Boundary," Quart. J. Mech. and Appl. Math., vol. 3, pt. 4, pp. 385-410, 1950.

23. S. P. Srivastava, "Method of Interpretation of Magnetotelluric Data when Source Field is Considered," Journal of Geophysical Research, vol. 70, no. 4, pp. 945-954, February 15, 1965.

24. R. D. Hibbs and F. W. Jones, "The Calculation of the Electromagnetic Fields of a Sheet Current Source with Arbitrary Spatial Intensity Distribution over a Layered Half Space - I, The General Method and Results," Geophys. J. R. Astr. Soc., vol. 46, pp. 433-452, 1976.

25. W. R. Peltier and J. F. Hermance, "Magnetotelluric Fields of a Gaussian Electrojet," Can. J. Earth Sci., vol. 8, pp. 338-346, 1971.

26. R. D. Hibbs, Jr. and F. W. Jones, "Electromagnetic Induction in the Earth by a Non-Symmetric Non-Uniform Source," J. Geomag. Geoelectr., vol. 25, pp. 75-86, 1973.

27. M. Abramowitz and J. A. Stegun (eds.), Handbook of Mathematical Functions, U.S. Department of Commerce, National Bureau of Standards, 10th ed., pg. 886, 1972.

28. D. Larose, "The Hydro-Québec System Blackout of 13 March 1989," Conference on Geomagnetically Induced Currents, sponsored by Electric Power Research Institute, Burlingame, California, November 8-10, 1989.

29. G. J. Cokkinides and A. P. Meliopoulos, "Transmission Line Modeling with Explicit Grounding Representation," Electric Power Systems Research, vol. 14, no. 2, pp. 109-119, April 1988.

30. W. A. Chisholm and Y. L. Chow, "Travel Time of Transmission Towers," IEEE Transactions on Power Apparatus and Systems, vol. PAS-104, no. 10, pp. 2922-2928, October 1985.

31. A. P. Meliopoulos and M. G. Moharem, "Transient Analysis of Grounding Systems," IEEE Transactions on Power Apparatus and Systems, vol. PAS-102, no. 2, pp. 389-397, February 1983.

32. A. Papalexopoulos and A. P. Meliopoulos, "Frequency Dependent Modeling of Grounding Systems," Proc. Midwest Power Symposium, pp. VI.E. 1-13, 1985.

33. J. K. Snelson, "Propagation of Traveling Waves on Transmission Lines-Frequency Dependent Parameters," IEEE Transactiosn of Power Apparatus and Systems, vol. PAS-91, pp. 85-91, January/February 1972.

34. A. Semlyen and A. Deri, "Time Domain Modeling of Frequency Dependent Three-Phase Transmission Line Impedance," IEEE Transactions on Power Apparatus and Systems, vol. PAS-104, no. 6, pp. 1549-1555, June 1985.

35. R. P. Webb and A. P. Sakis Meliopoulos, "Transformer Tests and Simulation Results," Report to Southern Company Services, May 1986.

36. A. P. Meliopoulos and G. J. Cokkinides, "Effects of Harmonics on Power Transformers," Proceedings of the 2nd International Conference on Harmonics in Power Systems, Winnipeg, Manitoba, Canada, pp. 201-213, October 1986.

Appendix A

DERIVATION OF TRANSMISSION LINE EQUATIONS IN THE PRESENCE OF GIC

Consider an infinitesimal segment of overhead conductor Δx. It is characterized by an inductance, $L' = L\Delta x$, resistance, $R' = R\Delta x$, and shunt capacitance, $C' = C\Delta x$. Assuming that EMP/GIC related electromagnetic fields are slowly varying their direct effect on the line is negligible. However, a substantial voltage can develop along the line direction on the earth surface, due to GIC. Assume that the earth potential difference across the line length, Δx, due to GIC is $V_g \cdot \Delta x$. The equivalent circuit of the line segment is shown in Figure A-1.

$$v_2 - v_1 = -R'i_2 - L' \frac{di_2}{dt} + v_g \cdot \Delta x$$

$$i_2 - i_1 = -G'v_1 - C' \frac{dv_1}{dt}$$

let

$$v_2 - v_1 = \Delta v$$

$$i_2 - i_1 = \Delta i$$

then

$$\frac{\Delta v}{\Delta x} = -Ri_2 - L' \frac{di_2}{dt} + v_g$$

$$\frac{\Delta i}{\Delta x} = -Gv_1 - C \frac{du_1}{dt}$$

taking limit as

$$\Delta x \to 0$$

$$i_1 \to i_2 \triangleq i$$

$$v_1 \to v_2 \triangleq v$$

results in the differential equations

$$\frac{\partial v}{\partial x} = -Ri - L\frac{di}{dt} + v_g$$

$$\frac{\partial i}{\partial x} = -Gv - C\frac{dv}{dt} .$$

where:

$v = v(x,t)$: voltage of point on transmission line located at distance x from line end, with respect to remote earth voltage

$i = i(x,t)$: current at point of transmission line located at distance x from line end

R = line series resistance per unit of length

L = line series inductance per unit of length

C = line shunt capacitance per unit of length

G = line shunt conductance per unit of length

v_g = geomagnetically induced earth surface voltage component along the direction of the line, per unit of length

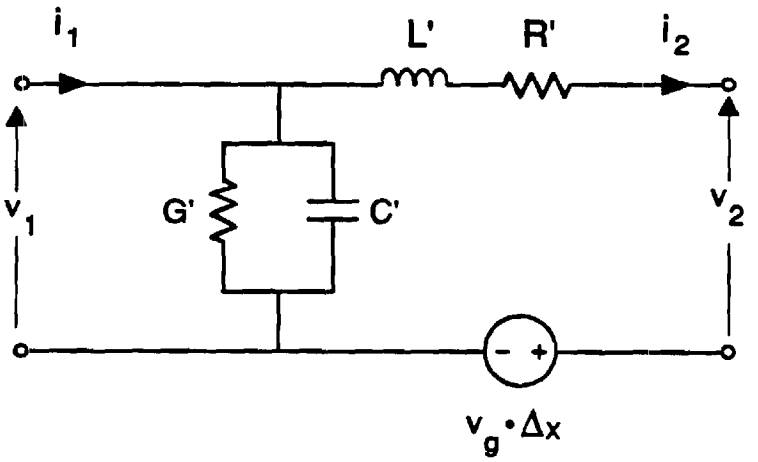

Figure A-1 : Equivalent Circuit of Short Line Segment in the Presence of Geomagneticaly Induced Voltage on the Earth Surface.

E-21-166

GEORGIA INSTITUTE OF TECHNOLOGY
SCHOOL OF ELECTRICAL ENGINEERING
ATLANTA, GEORGIA 30332

TELEPHONE: (404) 894-

February 20, 1991

Dr. Mario Rabinowitz
Electric Power Institute
P.O. Box 10412
Palo Alto, CA 94303

Dear Mario,

Enclosed please find the final technical report on "Effects of Geomagnetic Disturbances on Electric Power Transmission Systems."

Sincerely,

A. P. Sakis Meliopoulos

APM/pk
Enclosure
cc: Mrs. Kathy Knighton, GIT ✓

EFFECTS OF GEOMAGNETIC DISTURBANCES ON ELECTRIC POWER TRANSMISSION SYSTEMS

Prepared for

ELECTRIC POWER RESEARCH INSTITUTE
3412 Hillview Avenue
Palo Alto, California 94304

EPRI Project Manager
Dr. Mario Rabinowitz

Prepared by

A. P. Sakis Meliopoulos
E. N. Glytsis
Electric Power Laboratory
School of Electrical Engineering
Georgia Institute of Technology
Atlanta, Georgia 30332-0250

G. J. Cokkinides
Department of Electrical Engineering
University of South Carolina
Columbia, South Carolina 29208

December 1990

EPRI PERSPECTIVE

(to be added)

ABSTRACT

A comparative sutdy of the effects of solar storm geomagnetically induced currents (SS-GIC) and nuclear detonation induced currents (MHD-EMP-GIC) on the power system is presented. The study is based on the assumption that the earth surface electric field of the MHD electromagnetic pulse is on the order of 100 V/km, with a duration up to several minutes; and the electric field of the solar storms is on the order of 10 V/km, and lasts from several minutes to one hour. Both phenomena cause flow of almost direct current in the windings of power transformers through the grounding system. For long transmission lines, i.e. 300 miles or longer, this DC current offsets the 60 Hz AC and may saturate transformer cores, with secondary results such as high magnetization currents, increased harmonics, and concomitant effect on power system operation. The level of the transformer core saturation depends on the time constant of the saturation process, and on the duration and magnitude of the direct current through the transformer windings. Thus, although the solar storm electric field is much lower than MHD-EMP, the solar storm effects on the power system are comparable due to their long duration. A technique for the computation of the induced and/or transferred voltages and currents to an electric power system from geomagnetic disturbances is presented. Models of transmission lines which explicitly represent grounding, earth potential, and frequency dependent phenomena, and power transformers which explicitly represent nonlinear magnetization characteristics, are utilized.

A parametric analysis of saturation time constants is performed and the effects of MHD-EMP and SS-GIC are compared.

SUMMARY

This study consisted of quantifying typical levels of solar storm (SS) geomagnetically induced currents and those resulting from magnetohydrodynamic electromagnetic pulse (MHD-EMP). The conclusion is that SS-GIC are about one-tenth the magnitude of MHD-EMP-GIC but they last much longer. For the purposes of the study, SS-GIC is considered to be constant (DC) while a design waveform was assumed for MHD-EMP-GIC (see Figure 2-3 of the report).

A model of the electric power system was developed which includes coupling of the electric power system to geomagnetically induced voltages. This model was utilized in the study.

The most important parameters determining the effects of GIV on power systems are:

1. Level of GIV
2. Duration of GIV
3. Tower grounding impedance
4. Ground wire resistance.

Comparative studies of MHD-EMP and SS-GIV indicate that (1) for low values of GIV, an MHD-EMP level of 10 times the SS-GIV will cause comparable effects, and (2) for high values of GIV, the short duration of the MHD-EMP mitigates the results only marginally. Since transformer thermal constants are much larger than the duration of MHD-EMP, the general conclusion is that the thermal effects due to MHD-EMP induced voltages on power systems are less severe than those due to solar storm GIV.

ACKNOWLEDGEMENTS

The authors express their appreciation to Dr. Mario Rabinowitz, project manager, for his support, his stimulating technical discussions, and for providing technical information.

The authors would like to acknowledge the help of Dr. V. Albertson and Mr. John Kappermann for providing the data of the test system. The discussions, input, and suggestions provided by Messrs. R. Barnes, F. Tesche, and R. Walling are appreciated.

TABLE OF CONTENTS

LIST OF ILLUSTRATIONS

LIST OF TABLES

Section 1

INTRODUCTION AND OBJECTIVE

1.1 INTRODUCTION

The objective of this project is to investigate the level of induced and/or transferred voltages and currents to an electric power system from (1) geomagnetic disturbances due to MHD-EMP and (2) GIC due to solar storms, SS-GIC. Subsequently, a comparison of the effects of MHD-EMP and SS-GIC have been performed.

MHD-EMP is an electromagnetic pulse with very low amplitude which results from geomagnetic disturbances caused by high altitude nuclear detonation. The electric field magnitude is on the order of 100 V/km, low frequency and lasts for several minutes. Similar geomagnetic disturbances are caused by solar storms and result in electric field magnitudes on the order of 10 V/km, low frequency and last from minutes to an hour. Both phenomena cause the flow of almost DC current in the windings of power transformers through the grounding system. Because of the nonlinear magnetization characteristics of the power transformers, the flow of the low frequency electric currents may cause serious secondary results, such as high magnetization currents due to saturation, abnormal reactive power requirements, and disruption of operation. Presently, it is not clear which disturbance (the high magnitude short duration MHD-EMP or the low magnitude long duration SS-GIC) is the most severe to a power system. A system approach has been adopted to address these problems, and to determine at what level saturation is reached.

The objectives of the project have been attained with a two step procedure: In the first step a model of an electric power transmission line including grounding and MHD-EMP or solar storm coupling has been developed. The basic methodology utilized for this step is described in Sections 2 and 3. Since the coupling of MHD-EMP or solar storm induced voltages to power lines is mainly through the line grounding system, it is important to accurately model the power line tower grounding as well as the terminal substation grounding system. For this purpose, the EPRI grounding models developed by Georgia Tech have been utilized. The form of the transmission line model is in terms of a multiple input-multiple output linear system.

The second step involves integration of the model developed in the first step into the EPRI computer model ADCFLT. This computer model is a time domain model similar to the EMTP. It allows modeling of an integrated power system, power system grounding, and the nonlinear magnetization characteristics of power transformers. Using this model, system studies have been performed to determine transformer magnetization currents and reactive power requirements. Of special importance is the degree of saturation of power transformers due to these phenomena. This information can be utilized to analyze transformer performance such as eddy losses in steel members, conductors, and leads. A test system has been utilized provided by Minnesota Power Company.

1.2 REPORT OUTLINE AND MAJOR CONCLUSIONS

Section 2 describes the investigation of the waveforms of geomagnetically induced voltages (GIV) resulting from solar storms (SS) and nuclear bomb explosions (MHD-EMP). The mechanism associated with the generation of GIV is briefly described. Next, models for predicting GIV waveforms from magnetic field measurements are discussed. Measured magnetic field data, collected during SS and MHD-EMP phenomena are presented. Finally, the GIV waveforms computed from magnetic field measurements are presented. These waveforms are used to compare the effects of MHD-EMP and SS-GIV on electric power systems in Section 4.

Section 3 presents the modeling techniques used to simulate the power system in the presence of GIV. Specifically, a model for iron core transformers and a model for multiphase transmission lines are presented. These models are based on a time domain simulation algorithm similar to the EMTP. The transformer model accurately represents magnetic core saturation effects. The transmission line model represents effects of tower grounding and substation grounding at the line ends. These model characteristics are essential for the accurate simulation of GIV effects.

Section 4 describes the application of the models (presented in Section 3) for the study of the effects of GIV on power systems. The test system selected for this study is described first. This system is a simplification of a 500 kV, 473 mile long line. Data for this system were provided by Minnesota Power Company. The performance of this system in the presence of GIV is studied via parametric analysis. Specifically, the steady state currents through the transformer windings are computed for different values of tower footing resistance and ground wire resistances.

Next the time constants associated with magnetic core saturation are parametrically computed with respect to GIV level, ground wire resistance, and tower footing resistance. The results of this study indicate that the transmission line grounding parameters have a substantial effect on both steady state currents and saturation time constants. Finally, the relative effects of MHD-EMP and SS-GIV are compared. For this study, the design waveforms for MHD-EMP-GIV and SS-GIV, described in Section 2, are used. The level of transformer saturation reached in each case is parametrically computed with respect to ground wire and tower footing resistance. The following conclusions were reached from this study.

- For low levels of GIV or short transmission lines, MHD-EMP-GIV and SS-GIV have comparable effects on power systems when the level of MHD-EMP-GIV is 10 times the level of SS-GIV.

- For high levels of GIV, the short duration of the MHD-EMP-GIV mitigates the results only marginally.

- Thermal effects on power transformers due to MHD-EMP-GIV are less severe than those due to SS-GIV.

Section 2

DESIGN WAVEFORMS OF GEOMAGNETICALLY INDUCED VOLTAGES FROM SOLAR STORMS (SS-GIV) AND FROM MAGNETOHYDRODYNAMIC ELECTROMAGNETIC PULSES (MHD-EMP-GIV)

2.1 INTRODUCTION

Electric currents that flow in the molten core of the earth cause its dipole-like magnetic field. The magnetic field of the earth interacts with the interplanetary magnetic field which is actually an extension of the magnetic field of the sun due to the solar wind. The solar wind consists of charged particles, mainly electrons and protons (hydrogen ions), emitted from the surface of the sun. Thus, the solar wind acts like an extension of the magnetic field of the sun and interacts with the earth's magnetic field in a complex manner creating the earth's magnetosphere. In addition, interactions of the earth's magnetic field and the solar wind give rise to a vast magnetohydrodynamic generator that converts the kinetic energy of the solar-wind particles in electric energy which powers the auroral currents or auroral electrojets [1,2]. These currents usually follow circular or elliptical paths around the geomagnetic poles at altitudes of 100 kilometers or more and produce fluctuations in the earth's magnetic field that are termed geomagnetic storms. The strength of the geomagnetic storms is strongly related with solar phenomena that affect the solar wind. These phenomena are the solar flares, the coronal holes, and the disappearing filaments. The severity of the geomagnetic storms strongly depends on the intensity of the above mentioned solar effects. Large solar storms can produce large variations of the auroral electrojets which produce large variations of the geomagnetic field on the earth's surface. The earth as a conducting sphere experiences, or portions of it experience, these time varying magnetic fields. Varying magnetic fields induce electric potential gradients which are called earth-surface-potentials (ESP). The earth-surface-potentials can obtain values in the range between 1 and 10 volts/km depending on the severity of the geomagnetic storm and the earth's conductivity [3,4]. The electric power systems are exposed to ESP through the grounding grid. Since the ESP has frequency of one to a few millihertz the resulting geomagnetically-induced-currents (GIC) can be considered quasi-direct currents compared to 50 Hz or 60 Hz of the electrical power system frequency. Geomagnetic field variations caused by magnetosphere phenomena will result in an induced ESP orthogonal to the field changes. Usually, an idealized east-west

auroral current will cause field variations in the north-south component of the earth's magnetic field, resulting in an east-west induced ESP. Thus, transmission lines in the east-west direction are more susceptible to large ESP than transmission lines in the north-south direction. However, the auroral currents are not ideally east-west and consequently large ESP can be observed in any direction. Several analytical methods have been developed to estimate the induced ESP based on different modeling of the auroral currents and the earth's conductivity. Due to the complexity of the geomagnetic phenomena all these models are approximate and direct measurements of the geomagnetic fields seems to be the best choice.

Geomagnetic disturbances and associated induced earth currents can also originate from the explosion of nuclear bombs at high altitude above the earth's surface [5-7]. These explosions result in transient electromagnetic pulses (EMP) which can affect the operation of the power and communications systems. There are two basic types of electromagnetic pulses due to nuclear explosions. The one is the high altitude quick pulse (TEMP) (Tachy-EMP), and the other is the much slower magnetohydrodynamic EMP (MHD-EMP). For this report, only the slow MHD-EMP is of interest since its effect to power system operation is very similar to solar-storm geomagnetically induced currents. Two similar but different magnetic disturbances give rise to the MHD-EMP. The first is called magnetic bubble EMP (BEMP) [8]. The second is called Atmospheric heave EMP (AEMP) [8]. Due to the nuclear explosion a magnetohydrodynamic bubble of ionized conducting debris is formed and expands rapidly. Initially the geomagnetic flux inside the bubble is very small. If the shell of the magnetic bubble were nonconducting, the expansion of the bubble would simply enclose more magnetic flux of the geomagnetic field. However, since the bubble is conducting, currents are induced on the shell which counteract the earth's magnetic field. Thus, even if the bubble increases in volume the geomagnetic flux that encloses remains as small as it was initially. This effect results in a compression of the geomagnetic field around the bubble. These changes of the geomagnetic field can induce electric fields in the earth which can reach a maximum magnitude of 0.1 V/m with periods from 2 to 100 seconds [8]. This pulse occurs at about 2 to 5 seconds after the nuclear explosion. The second component of the MHD-EMP, the atmospheric heave EMP, occurs more than 10 seconds after the explosion. This pulse is caused by the atmospheric heave of the bomb-heated ionized air across the geomagnetic field. This ionization forms current loops which have mirror images in the earth. These perturbations of the geomagnetic field extend out more than 1250 miles from the source point and last approximately 100 sec. The induced electric fields and frequencies are very low between 0.001-0.03 V/m and ~0.01 Hz. Several analytical methods have been developed mainly for the study of the fast

EMP and comparisons of it with the lightning [9-12]. However, there is not much available information for theoretical modeling of MHD-EMP. Most of the analytical studies for the evaluation of the effects of MHD-EMP on power systems are based on measurements of the induced electric field [5,6], or by assuming plane wave excitation [13,14].

In the following subsections, the most common methods used for the evaluation of the ESP due to SS-GIC or MHD-EMP are reviewed. In addition, sample tables of measured data are given to be used as design ESP waveforms for the calculation of the effect of SS-GIC and MHD-EMP on power systems, and for evaluation of several methods proposed for the alleviation of these effects.

2.2 DESIGN EARTH SURFACE POTENTIAL WAVEFORMS DUE TO SOLAR-STORMS

Several analytical models have been used for the evaluation of the induced electric field on the surface of the earth due to the variations of the geomagnetic field. These models differ in the representation of the auroral currents and the conductivity of the earth. The auroral currents are known to be at altitudes between 100 to 300 km above the earth's surface. These currents can be modeled like current line sources or current sheet sources of infinite extend above a flat earth's surface. However, the auroral currents have such a spatial extension that they can not be considered either a current line or a current sheet. The above assumptions though give some estimate of the induced electric field on the earth's surface. Specifically, the current line model gives a lower limit while the current sheet model gives an upper limit of the induced electric field. Sometimes the auroral currents are assumed to be at an infinite distance from the ground. In this case, the geomagnetic field is modeled as a plane electromagnetic wave. The conductivity of the earth is also difficult to model due to the large variety and inhomogeneity of the earth's surface from place to place. The simplest model assumes a flat earth surface with a uniform effective conductivity. More sophisticated earth models divide the earth's surface in multiple layers, each one having a different conductivity.

The simplest method for modeling the auroral currents is the plane electromagnetic wave model [15]. The earth is modeled as a horizontally stratified medium of one or more layers of differing conductivities. The incident geomagnetic field is assumed to be a linearly polarized, monochromatic plane wave. The electric field on the surface of the earth is computed with usual electromagnetic analysis methods. In addition, using this technique the surface impedance of the earth, Z_s, can be

computed, where $Z_s = E_x/H_y$ (E_x/H_y are the horizontal components of the electric and magnetic field on the earth's surface, respectively). This is useful since from measurement of the magnetic field, the induced electric field can be estimated.

Another widely used technique models the auroral currents as an infinite horizontal current sheet at a height h above the horizontally also stratified earth of one or more layers [15-19]. To solve the problem, the electric and magnetic Hertz vectors are commonly used. For the described geometry, these vectors have only one component which is perpendicular to the earth's surface and to the auroral current sheet. Using the vector Hertz potentials and Maxwell's equations along with the corresponding boundary conditions, the electric field on the earth's surface can be found. This field is a function of (1) the magnitudes along the two horizontal directions of the current sheet (j_x,j_y), (2) the radian frequency ω of the auroral current, (3) the spatial wave numbers of the spectral components of the auroral currents, (4) the altitude h of the auroral current, and (5) the characteristics of the earth. Even if the described analysis considered a single spectral component, there is no loss of generality since by Fourier synthesis any time-dependent source current can be written as a linear combination of its spectral components. Consequently, the resulting induced electric field will be a linear combination of the fields due to the different spectral components. As it was mentioned earlier, the current sheet method overestimates the induced electric field on the earth's surface.

The auroral currents can also be modeled as a line current source parallel to the earth's surface at an altitude h [15,18,20,21]. Usually, the line is positioned in the east-west direction and is assumed positive in the westward direction. Earth's surface is modeled like a horizontally stratified medium. The general methodology used for the solution of these problems is based on Price's analysis [22]. This analysis assumes slow variations of the geomagnetic fields. As a result, the second time derivatives in the wave equation are neglected. This assumption permits solutions of the magnetic field expressed in terms of the gradient of a scalar magnetic potential for the region above the earth, while the electric field solutions are expressed in terms of the time derivative of a vector magnetic potential for the earth region. An equivalent procedure consists of expressing the electric field as $\vec{E} = e^{j\omega t}G(z)\vec{F}(x,y)$, where G and $\vec{F}$ have to be determined for each region from the wave equation and the boundary conditions of the problem [(x,y) correspond to the horizontal plane while z is the perpendicular coordinate]. Using this procedure the resulting electric and magnetic fields on the

earth's surface are calculated as functions of the following parameters: (1) the magnitude of the auroral current, (2) the radian frequency of the auroral current, (3) the altitude h of the auroral current, (4) the difference in latitude between the auroral current and the point for which the calculations are made, and (5) the surface impedance of the earth Z_s [23] which depends on the earth's parameters and modeling. Usually, since the magnitude of the auroral currents is not known, an estimate of $J = 10^5 A$ is used. As it was mentioned previously this method underestimates the induced electric field on the earth's surface due to the modeling of the auroral currents as a horizontal line current.

In the described models the auroral currents are modeled as uniform or sinusoidal distributions. However, none of these assumptions is very accurate. More sophisticated studies include Gaussian modeling of the electrojet [24,25]. In addition, Hibbs et al. have studied nonsymmetric auroral currents distributions [26].

Independently of the used model, the complexity of the physical effect of the auroral electrojet is difficult to represent. In addition, all the described models assume sinusoidal auroral currents. However, if the spectral content of the auroral currents was known, these models along with the superposition principle could be used for the calculation of the induced electric field. Since the spectral content of the auroral currents is not known and, in addition, is varying with time, the geomagnetic field is usually measured in several positions in the areas of interest using magnetometers. By measuring the magnetic field, the induced electric field can be roughly estimated using the plane wave assumption from [4]

$$E(t) = -\frac{1}{(\pi\mu_o\sigma)^{1/2}} \int_0^\infty \frac{g(t-u)}{u^{1/2}}\, du \ , \qquad (2\text{-}1)$$

where E(t) is the horizontal component of the induced electric field, μ_o is the permeability of the freespace, σ is the conductivity of the earth, and g is the time derivative of the horizontal component of the magnetic field. If the measured data are used, the derivative g can be computed numerically and the integral can be approximated using the extended Simpson's rule [27] by the following formula

$$\int_0^\infty \frac{g(t-u)}{u^{1/2}}\, du \simeq D^{1/2}\left\{\frac{4}{3}\, g(t)+g(t-D)+\frac{2}{3}\sum_{j=1}^{L}(1+a_j)\,\frac{g[t-(j+1)D]}{(j+1)^{1/2}}\right\} \ , \qquad (2\text{-}2)$$

where D is the data time interval and $a_j = 0$ when j is even and $a_j = 1$ when j is odd; L is the total number of data points that are considered for the calculation of E(t). Using the data measured during May 12-13, 1989, at magnetic Observatory

Furstenfeldbruck (Figure 2-1, Table 2-1, and Eqs. (2-1) and (2-2)), the induced electric field was calculated and its values are summarized in Table 2-2 (Figure 2-2).

2.3 DESIGN EARTH SURFACE POTENTIAL WAVEFORMS DUE TO MAGNETOHYDRODYNAMIC ELECTROMAGNETIC PULSES

The effects of the magnetohydrodynamic electromagnetic pulse (MHD-EMP) on power system grids are very similar to those of geomagnetic storms. More specifically, MHD-EMP generates electric fields on the order of 10^{-1} V/m (about an order of magnitude higher than the geomagnetically-induced electric fields) of frequencies less than 1 Hz and of 100-200 sec duration. As it was described previously, MHD-EMP is due to two distinct physical mechanisms, the magnetic bubble (BEMP) and the atmospheric heave (AEMP). The early portion of the MHD-EMP (less than 10 seconds after the nuclear explosion) is due to BEMP while the rest of MHD-EMP is due to the AEMP [6]. Some estimate of the average induced electric field can be calculated using the following arguments [7]. The magnetic bubble, as it expands, pushes the geomagnetic field out of its way. The bubble obtains its maximum size when the energy of the excluded field equals the initial kinetic energy, T, of the conducting shell of the magnetic bubble, neglecting all other loss mechanisms. Thus, the following equation can be written [7]

$$\frac{1}{2\mu_o}\langle B^2\rangle\left(\frac{4}{3}\pi R^3\right) = T \qquad R = [3\mu_o T/2\pi\langle B^2\rangle]^{1/3}\ , \tag{2-3}$$

where $\langle B^2\rangle$ is the mean squared value of the flux density of the unperturbed geomagnetic field, μ_o is the permeability of freespace, R is the maximum radius of the magnetic bubble (assuming spherical bubble), and T is the initial kinetic energy of the conducting debris of the bomb. The average power, $\langle P\rangle$, of the MHD-EMP can be estimated from

$$\langle P\rangle = \frac{fT}{\Delta t}\ , \tag{2-4}$$

where f is the conversion efficiency of the kinetic energy, T, in electromagnetic power, and Δt is the duration of the produced electromagnetic pulse. The average power density near the bubble can then be found from $\langle P\rangle/4\pi R^2$. Using the Poynting vector, the power density is $E^2/2\eta$, where η is the intrinsic impedance of freespace. Using the above arguments, an estimate of the induced electric field can be found from

$$E = \left[\frac{2fT^{1/3}\eta}{4\pi\Delta t[3\mu_o/2\pi\langle B^2\rangle]^{2/3}}\right]^{1/2}\ . \tag{2-5}$$

Using $f \simeq 10^{-5}$, $T \simeq 1.76 \cdot 10^{15}$J (for a 30% yield of a 1.4 Mt bomb [7]), $\eta = 377\ \Omega$, $\Delta t \simeq 100$ sec, and $B \simeq 5 \cdot 10^{-5}$ wb/m^2, an electric field of 0.1 V/m can be estimated. The above estimate is based only on the BEMP effect under the rough assumptions made above. However, the atmospheric currents due to air ionization produce significant portion of the induced electric field. Thus, the most valuable information about a MHD induced EMP is empirically known from the magnetometer data acquired during actual nuclear events as the "Starfish" test conducted in the Pacific. The design waveform for the simulation of MHD-EMP is the one measured during the Starfish test. The magnetometer data [6] have been used along with Eq. (2-1) to calculate the induced electric field that appears in Figure 1 of Reference 5. This electric field has been sampled and linearly approximated and is tabulated in Table 2-3 (Figure 2-3).

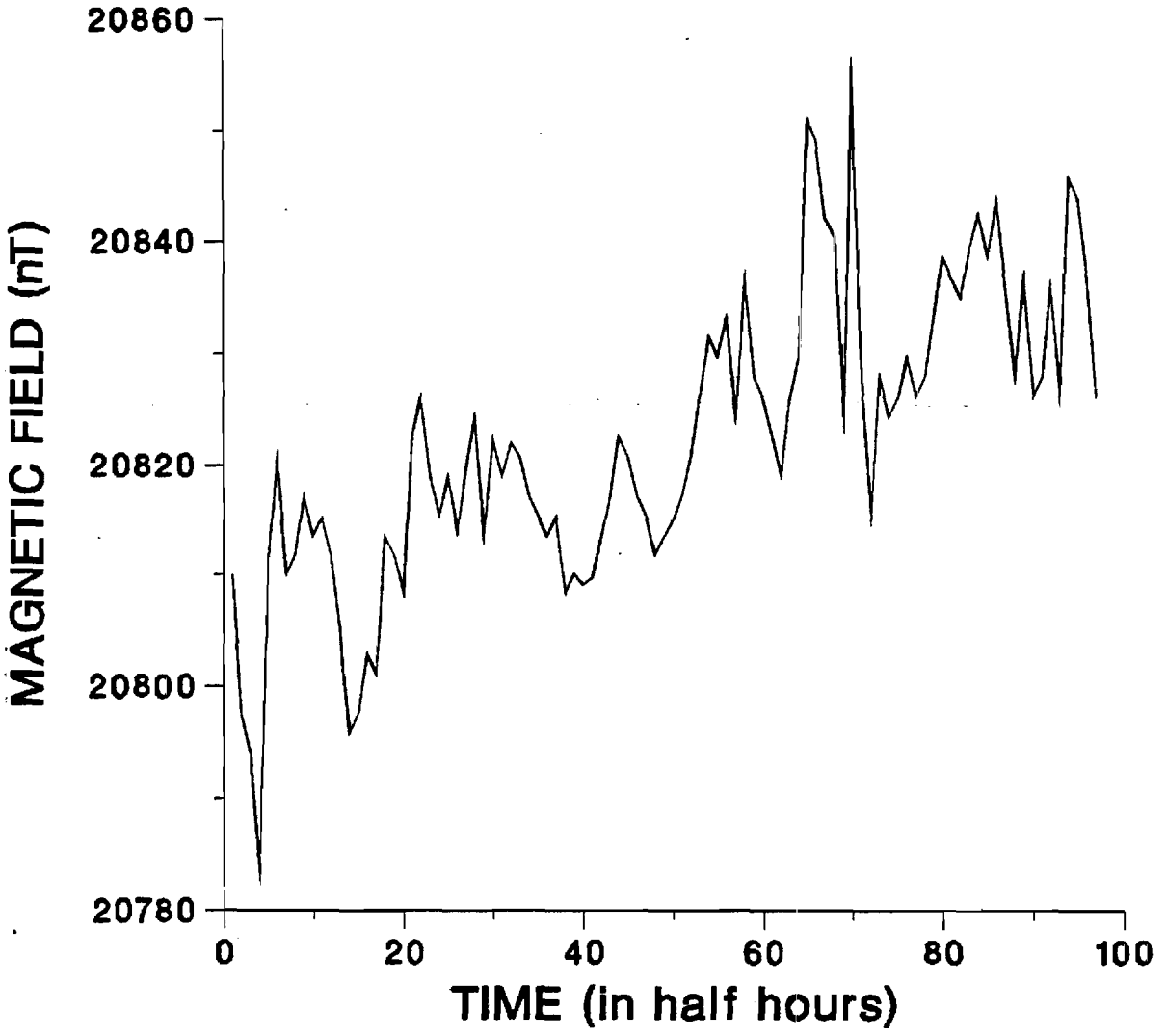

Figure 2-1: Horizontal Component of Magnetic Field.
Magnetic Observatory Fürstenfeldbruck, May 12-13, 1989.

TABLE 2.1

Measurements of the Horizontal Component of the Magnetic Flux Density of the Geomagnetic Field at the Fürstenfeldbruck Station in 30 Minute Intervals Between May 12-13, 1989

Time (sec)	Horizontal Component of Geomagnetic Field (nT)
.0	20810.00
1800.0	20797.60
3600.0	20794.00
5400.0	20783.30
7200.0	20811.10
9000.0	20820.80
10800.0	20810.00
12600.0	20811.90
14400.0	20817.20
16200.0	20813.60
18000.0	20815.40
19800.0	20811.90
21600.0	20804.70
23400.0	20795.80
25200.0	20797.60
27000.0	20802.90
28800.0	20801.10
30600.0	20813.60
32400.0	20811.90
34200.0	20808.30
36000.0	20822.60
37800.0	20826.10
39600.0	20819.00
41400.0	20815.40
43200.0	20819.00
45000.0	20814.00
46800.0	20819.70
48600.0	20824.30
50400.0	20813.60
52200.0	20822.50
54000.0	20819.00
55800.0	20822.00
57600.0	20820.80
59400.0	20817.20
61200.0	20815.40
63000.0	20813.60
64800.0	20815.40
66600.0	20808.30
68400.0	20810.10
70200.0	20809.00
72000.0	20809.70
73800.0	20813.60
75600.0	20817.20

TABLE 2.1 (continued)

Time (sec)	Horizontal Component of Geomagnetic Field (nT)
77400.0	20822.60
79200.0	20820.80
81000.0	20817.20
82800.0	20815.40
84600.0	20811.90
86400.0	20813.60
88200.0	20815.00
90000.0	20817.20
91800.0	20820.80
93600.0	20826.10
95400.0	20831.50
97200.0	20829.70
99000.0	20833.20
100800.0	20824.30
102600.0	20836.80
104400.0	20827.90
106200.0	20826.10
108000.0	20822.60
109800.0	20819.00
111600.0	20826.10
113400.0	20829.70
115200.0	20851.10
117000.0	20849.30
118800.0	20842.20
120600.0	20840.40
122400.0	20824.30
124200.0	20854.70
126000.0	20827.90
127800.0	20815.40
129600.0	20827.90
131400.0	20824.30
133200.0	20826.10
135000.0	20829.70
136800.0	20826.10
138600.0	20827.90
140400.0	20833.20
142200.0	20838.60
144000.0	20836.80
145800.0	20835.00
147600.0	20839.50
149400.0	20842.50
151200.0	20838.60
153000.0	20843.90
154800.0	20836.10
156600.0	20827.90
158400.0	20836.80
160200.0	20826.10
162000.0	20827.90

TABLE 2.1 (continued)

Time (sec)	Horizontal Component of Geomagnetic Field (nT)
163800.0	20836.10
165600.0	20826.10
167400.0	20845.70
169200.0	20843.90
171000.0	20836.80
172800.0	20826.10

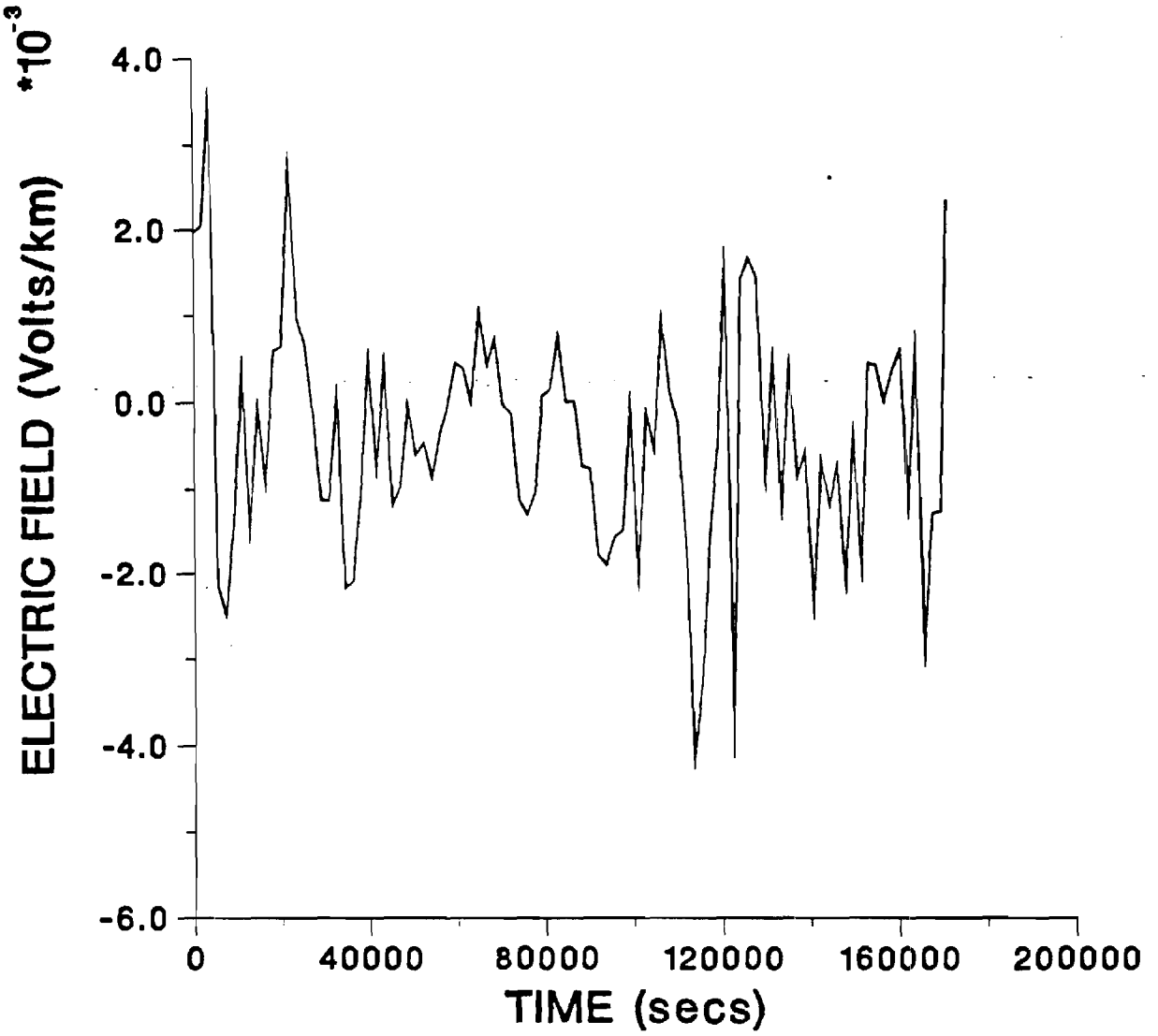

Figure 2-2: SS-GIC Electric Field.
Magnetic Observatory Fürstenfeldbruck, May 12-13, 1989.

TABLE 2.2

Calculated Induced Electric Field (SS-GIC) Using the Measurements of Table I and Eqs. (1) and (2)

Time (sec)	Induced Electric Field (V/km)
.0	.19613E-02
1800.0	.20404E-02
3600.0	.35063E-02
5400.0	-.21590E-02
7200.0	-.24903E-02
9000.0	-.13399E-02
10800.0	.40067E-03
12600.0	-.15157E-02
14400.0	-.37079E-04
16200.0	-.97319E-03
18000.0	.58856E-03
19800.0	.64136E-03
21600.0	.27804E-02
23400.0	.97135E-03
25200.0	.68159E-03
27000.0	-.12122E-03
28800.0	-.11203E-02
30600.0	-.11249E-02
32400.0	.91153E-04
34200.0	-.21800E-02
36000.0	-.20967E-02
37800.0	-.10255E-02
39600.0	.52078E-03
41400.0	-.78152E-03
43200.0	.47075E-03
45000.0	-.11750E-02
46800.0	-.95832E-03
48600.0	-.61076E-05
50400.0	-.60230E-03
52200.0	-.46227E-03
54000.0	-.87251E-03
55800.0	-.33812E-03
57600.0	-.25453E-04
59400.0	.45499E-03
61200.0	.39364E-03
63000.0	.41640E-05
64800.0	.10508E-02
66600.0	.40856E-03
68400.0	.73819E-03
70200.0	-.12803E-04
72000.0	-.12281E-03
73800.0	-.11164E-02
75600.0	-.12954E-02
77400.0	-.10285E-02
79200.0	.67825E-04

TABLE 2.2 (continued)

Calculated Induced Electric Field (SS-GIC) Using the Measurements of Table I and Eqs. (1) and (2)

Time (sec)	Induced Electric Field (V/km)
81000.0	.14286E-03
82800.0	.76736E-03
84600.0	.62566E-05
86400.0	.17448E-04
88200.0	-.73720E-03
90000.0	-.75860E-03
91800.0	-.17937E-02
93600.0	-.19081E-02
95400.0	-.15541E-02
97200.0	-.14738E-02
99000.0	.79403E-06
100800.0	-.20720E-02
102600.0	-.11190E-03
104400.0	-.56233E-03
106200.0	.98050E-03
108000.0	.13813E-03
109800.0	-.22304E-03
111600.0	-.16265E-02
113400.0	-.41819E-02
115200.0	-.32840E-02
117000.0	-.14967E-02
118800.0	-.50570E-03
120600.0	.15648E-02
122400.0	-.37526E-02
124200.0	.14089E-02
126000.0	.16592E-02
127800.0	.14355E-02
129600.0	-.91577E-03
131400.0	.50753E-03
133200.0	-.12444E-02
135000.0	.44008E-03
136800.0	-.87843E-03
138600.0	-.55878E-03
140400.0	-.24192E-02
142200.0	-.66480E-03
144000.0	-.11979E-02
145800.0	-.73047E-03
147600.0	-.21370E-02
149400.0	-.35746E-03
151200.0	-.19755E-02
153000.0	.43395E-03
154800.0	.41453E-03
156600.0	-.62593E-05
158400.0	.35518E-03
160200.0	.59024E-03
162000.0	-.12100E-02

TABLE 2.2 (continued)

Calculated Induced Electric Field (SS-GIC) Using the Measurements of Table I and Eqs. (1) and (2)

Time (sec)	Induced Electric Field (V/km)
163800.0	.62786E-03
165600.0	-.29351E-02
167400.0	-.12896E-02
169200.0	-.12626E-02
171000.0	.23348E-02

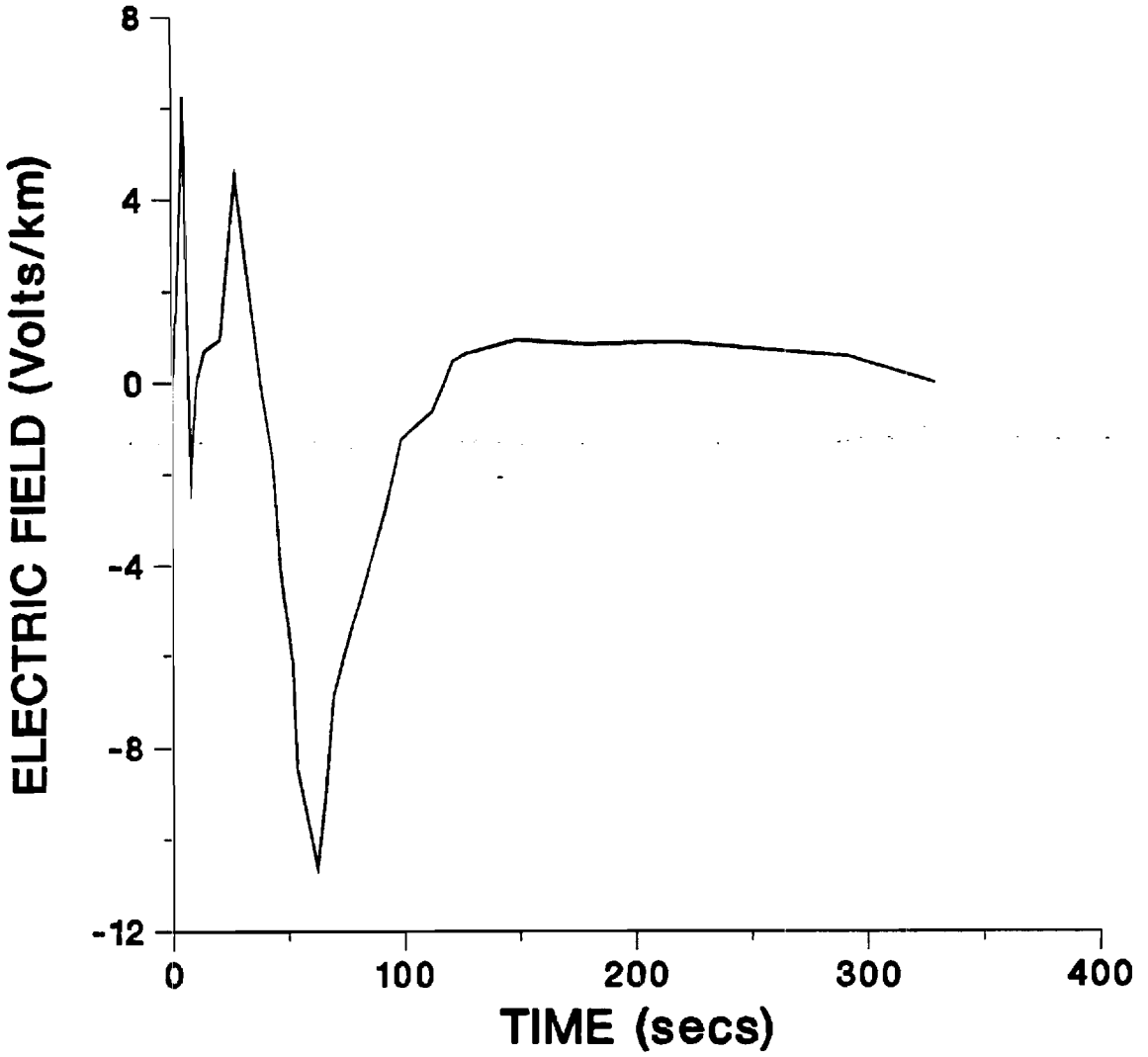

Figure 2-3: MHD-EMP Induced Electric Field.

TABLE 2.3

Measured Induced Electric Field (MHD-EMP)
During the "Starfish" Test

Time (sec)	Electric Field (V/km)
0.0	.00000E+00
5.0	.62500E+01
7.0	.00000E+00
8.0	-.21900E+01
10.5	.00000E+00
13.9	.69000E+00
20.9	.94000E+00
27.8	.45300E+01
38.3	.00000E+00
43.5	-.15600E+01
47.0	-.40600E+01
52.2	-.62500E+01
53.9	-.84400E+01
62.6	-.10630E+02
66.0	-.90600E+01
69.6	-.68800E+01
83.5	-.43800E+01
92.2	-.28100E+01
99.1	-.12500E+01
113.0	-.63000E+00
118.3	.00000E+00
121.7	.47000E+00
127.0	.63000E+00
149.6	.94000E+00
180.9	.84000E+00
217.4	.90000E+00
280.0	.63000E+00
292.2	.59000E+00
330.4	.00000E+00

Section 3

TRANSMISSION SYSTEM MODEL

3.1 INTRODUCTION

This section describes the transmission system model for the study of geomagnetic disturbances. The model is based on a time domain simulation algorithm similar to the EMTP. Each power system element is modeled with a set of differential equations which are solved in the time domain. For the study of geomagnetic disturbances, two power system elements are very important: (1) magnetic core transformers and (2) long transmission lines. Specifically, long transmission lines provide the gate for geomagnetically induced currents to enter the power system. On the other hand, magnetic core transformers reach saturation when geomagnetically induced currents flow in their windings and cause most of the undesirable effects. This section describes in detail these two models.

3.2 IRON CORE TRANSFORMERS

Iron core transformers are highly nonlinear devices due to their saturable iron magnetic core. A typical iron core magnetization curve is illustrated in Figure 3-1. For practical reasons, power transformers are designed in such a way that the maximum operating magnetic flux is near the knee of the magnetization curve. During normal operating conditions, the magnetic flux oscillates between $+\lambda_{max}$ and $-\lambda_{max}$ and the magnetization current is symmetric about the zero axis. When a DC current is injected through the transformer winding, this symmetry is destroyed. In this case, the transformer may operate past the magnetization curve knee for portions of the cycle, requiring a high magnetization current to maintain the applied voltage.

This phenomenon is modeled as follows. Consider a single phase transformer as it is illustrated in Figure 3-2. The equations describing the transformer are:

$$v_{1u}(t) = r_{1u} i_{1u}(t) + L_{1u} di_{1u}/dt + d\lambda(t)/dt$$

$$v_{2u}(t) = r_{2u} i_{2u}(t) + L_{2u} di_{2u}/dt + d\lambda(t)/dt$$

$$\lambda(t) = g\left(i_m(t)\right)$$

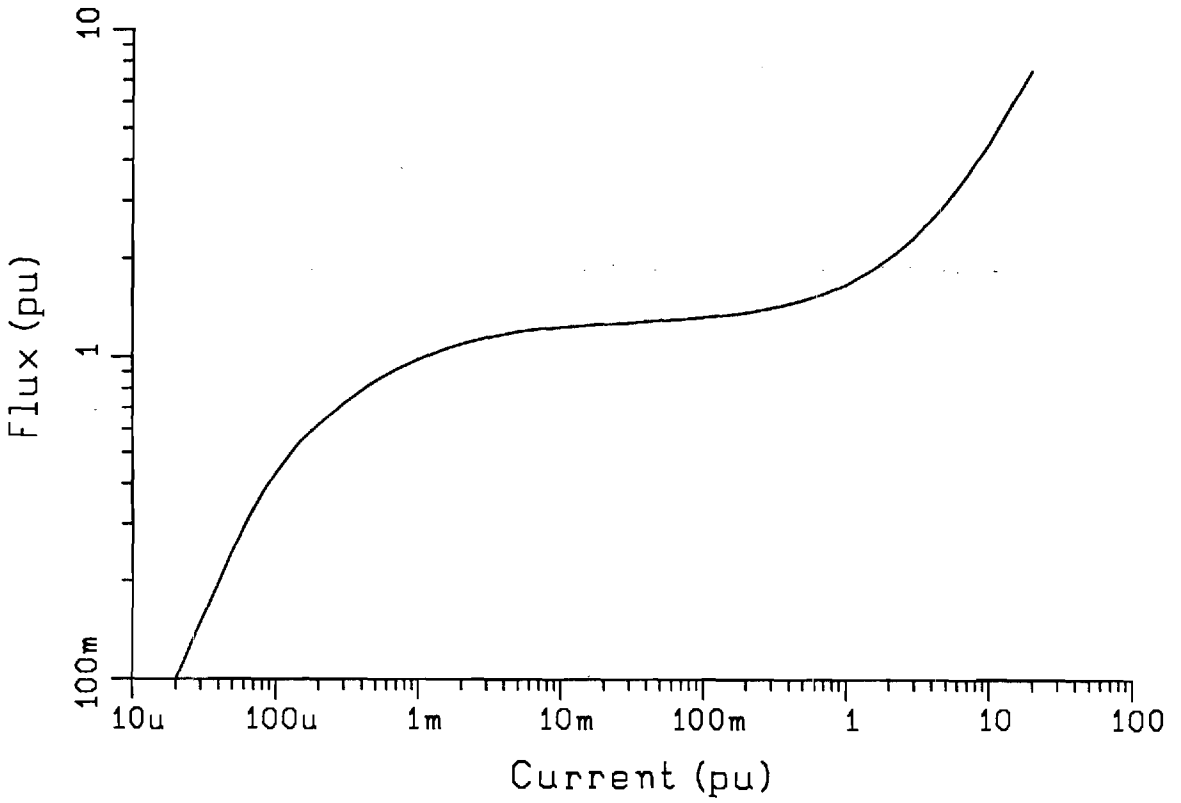

Figure 3-1 : Typical Iron Core Magnetization Curve

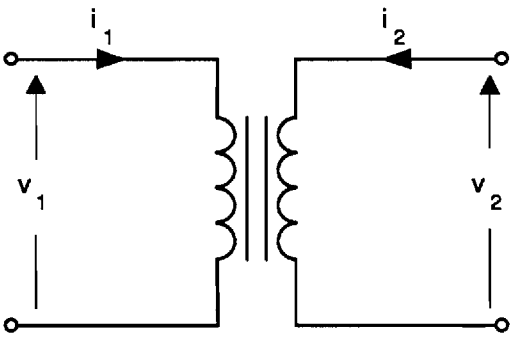

(a)

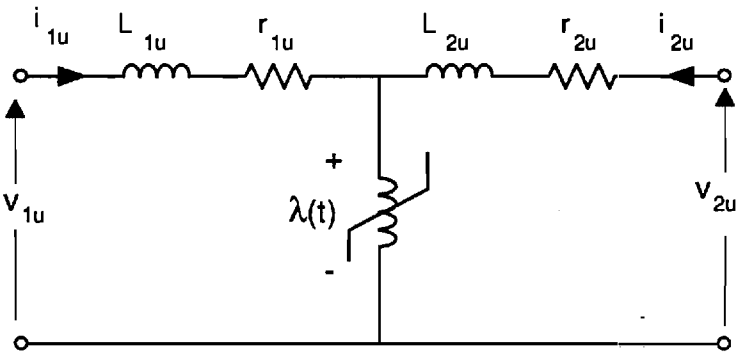

(b)

Figure 3-2 : Single Phase Transformer & equivalent Circuit
(a) Transformer
(b) Per Unit Equivalent Circuit

$$i_{m(t)} = i_{1u}(t) + i_{2u}(t)$$

where

$v_{1u}(t), v_{2u}(t)$ are the voltages in per unit

$i_{1u}(t), i_{2u}(t)$ are the currents in per unit

$g(\cdot)$ is the magnetization curve

$i_m(t)$ is the magnetization current in per unit.

Three single phase transformers, appropriately connected (wye-delta, etc.), provide the model of a three phase transformer. The equations of the power transformer are integrated in the time domain.

3.3 TRANSMISSION LINE MODEL WITH GIV COUPLING

The transmission line model used in this study is a time domain state space model based on the methodology described in Reference 29. It is capable of representing transmission line parameter frequency dependence, line tower grounding, as well as effects of geomagnetically induced currents (GIC).

The model is easily interfaced with other time domain models of power system components (such as transformers, loads, and generators). Thus the effect of GIC phenomena on the integrated power system can be assessed.

The transmission line model involves two components:

(1) Overhead conductors and earth return

(2) Grounding system.

Consider the transmission line shown in Figure 3-3. The section of overhead conductors between any two consecutive towers comprise a "conductor component" while each tower with its grounding systems is a component of the grounding system. Each component is modeled by an equivalent admittance matrix (which is a function of frequency) and equivalent current sources. Then, using nodal analysis, the equivalent circuit of the entire transmission line and GIC coupling is formed. The resulting model is in the form of a passive circuit of known admittance matrix and lumped current sources connected at the line terminals. This model is finally converted to the time domain using Fourier techniques.

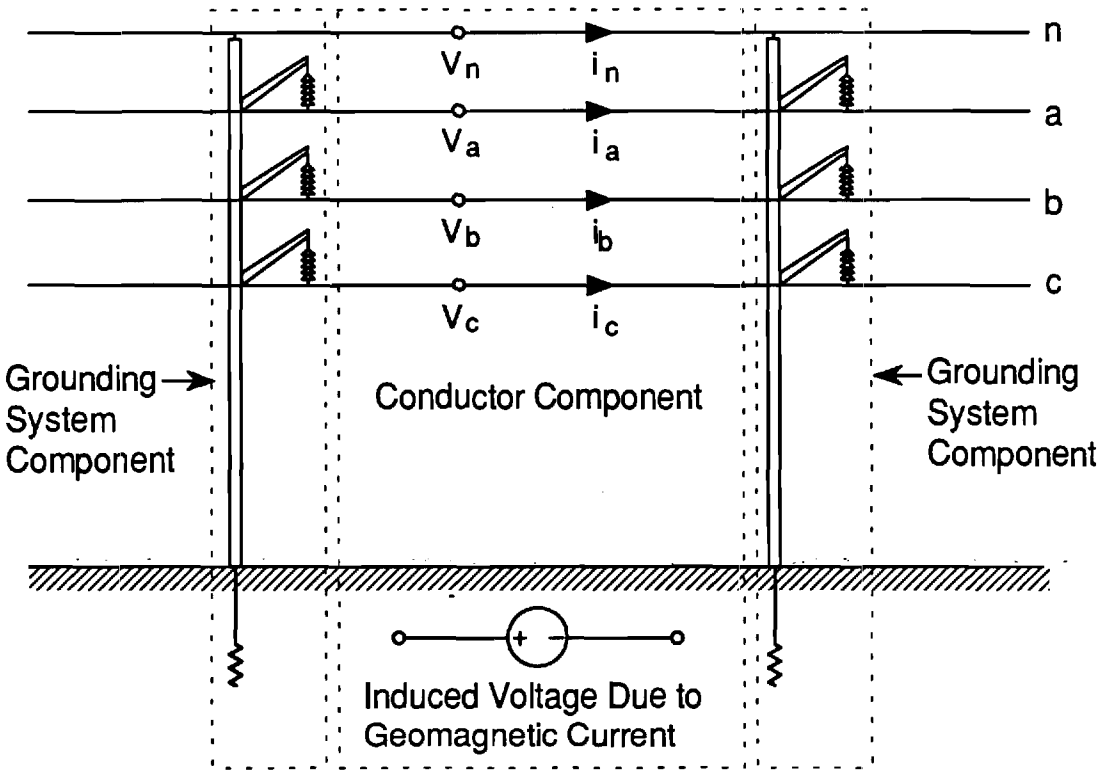

(a)

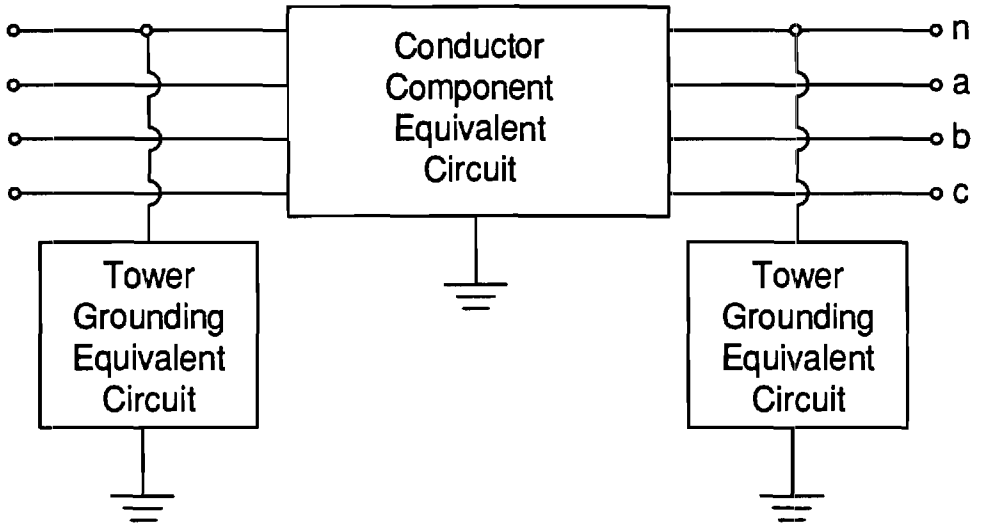

(b)

Figure 3-3 : Transmissin Line Section
(a) Physical Configuration
(b) Equivalent Circuit

The derivation of the conductor and grounding system equivalent circuits are presented in the following sections.

3.3.1 Overhead Conductor Model

An overhead transmission line conductor section, in the presence of geomagnetically induced currents is represented by the equations

$$\frac{\partial v(x,t)}{\partial x} = -Ri(x,t) - L\frac{\partial i(x,t)}{\partial t} + v_g(x,t) \quad , \tag{3-1}$$

$$\frac{\partial i(x,t)}{\partial x} = -Gv(x,t) - C\frac{\partial v(x,t)}{\partial t} \quad ,$$

where

- v : line voltage with respect to remote earth (v)
- i : line current (A)
- R : line series resistance (Ohms/meter)
- L : line series inductance (Henries/meter)
- G : line shunt conductance (Siemens/meter)
- C : line shunt capacitance (Farads/meter)
- v_g : component of voltage due to GIC in the direction of the line (volts/meter).

(See Appendix A for a derivation of Eq. (3-1).)

Since the line parameters are frequency dependent, the solution of the above equation is computed in the frequency domain. The Fourier transform of the above equations is

$$\frac{\partial V(x,\omega)}{\partial x} = -Z(\omega)I(x,\omega) + V_g(x,\omega) \quad , \tag{3-2}$$

$$\frac{\partial I(x,\omega)}{\partial x} = -Y(\omega)V(x,\omega) \quad , \tag{3-3}$$

where

$$Z(\omega) = R(\omega) + j\omega L(\omega)$$

$$Y(\omega) = G(\omega) + j\omega C(\omega) \quad .$$

For overhead transmission lines, several simplifications can be made:

(1) The conductance term is negligible and thus

$$Y(\omega) = j\omega C(\omega) \ .$$

(2) For a short line span, V_g is assumed constant with respect to position, thus

$$V_g(x,\omega) = V_g(\omega) \ .$$

(3) The resistance and inductance are computed using the complex depth of return method.

(4) The capacitance matrix is independent of frequency.

For a multiphase line the voltage due to GIC, V_g appears in series with every conductor. Thus it is replaced by the vector of the form

$$\begin{matrix} 1 \\ 1 \\ \vdots \\ 1 \end{matrix} \cdot V_g(x,\omega)$$

In order to compute the conductor section equivalent circuit, the current is eliminated in the equation system (3-2), (3-3), by differentiating Eq. (3-2) with respect to x and substituting current with voltage from Eq. (3-3)

$$\frac{\partial^2 V(x,\omega)}{\partial x^2} = K(\omega)V(x,\omega) \qquad (3\text{-}4)$$

where

$$K(\omega) = Z(\omega)Y(\omega) \ . \qquad (3\text{-}5)$$

The solution to the above equation (3-4) is obtained using eigenvalue analysis of the matrix K. Specifically, the system is decoupled by the transformation

$$V'(x,\omega) = W^{-1}(\omega)V(x,\omega) \qquad (3\text{-}6)$$

where

$$K(\omega) = W(\omega)D(\omega)W(\omega)^{-1} \qquad (3\text{-}7)$$

where $D(\omega)$ is a diagonal matrix containing the eigenvalues of matrix K, and $W(\omega)$ the eigenvector matrix of $K(\omega)$.

Applying transformation (3-7) to Eq. (3-4) yields

$$\frac{\partial^2 V'(x,\omega)}{\partial x^2} = D(\omega)V'(x,\omega) \ . \tag{3-8}$$

The general solution to the above equation is

$$V'(x,\omega) = e^{x\sqrt{D(\omega)}} \cdot A_1(\omega) + e^{-x\sqrt{D(\omega)}} \cdot A_2(\omega) \ , \tag{3-9}$$

where A_1, A_2 are constants to be determined by boundary conditions. Specifically,

$$V'(o,\omega) = A_1(\omega) + A_2(\omega) \tag{3-10}$$

$$V'(\ell,\omega) = e^{\ell\sqrt{D(\omega)}} A_1(\omega) + e^{-\ell\sqrt{D(\omega)}} A_2(\omega) \ .$$

Solving for A_1 and A_2 yields

$$A_1(\omega) = \left[e^{2\ell\sqrt{D(\omega)}} - I\right]^{-1} \left(e^{\ell\sqrt{D(\omega)}} V_2' - V_1'\right) \tag{3-11}$$

$$A_2(\omega) = \left[e^{-2\pi\sqrt{D(\omega)}} - I\right]^{-1} \left(e^{-\ell\sqrt{D(\omega)}} V_2' - V_1'\right) \ ,$$

where

$$V_1' = V'(o,\omega) = W^{-1} V(o,\omega)$$

$$V_2' = V'(\ell,\omega) = W^{-1} V(\ell,\omega)$$

and ℓ is the line length.

Thus, Eqs. (3-9) and (3-11) define the voltage at any point of the line given the voltages at the line ends. Now, using (3-2), the current is also computed as a function of the terminal voltages yielding

$$I(x,\omega) = Z^{-1}(\omega) V_g(\omega) = Z(\omega)^{-1} \frac{\partial V(x,\omega)}{\partial x} \ . \tag{3-12}$$

Evaluating the above at the line terminals, ($x = 0$, and $x = \ell$) yields

$$I_1(\omega) = Z(\omega)^{-1} V_g(\omega) - Z(\omega)^{-1} W(\omega) \left\{\sqrt{D(\omega)}\ A_1(\omega) - \sqrt{D(\omega)}\ A_2(\omega)\right\}$$

$$I_2(\omega) = Z(\omega)^{-1} V_g(\omega) - Z^{-1}(\omega) W(\omega) \left\{\sqrt{D(\omega)}\ E^{\ell\sqrt{D(\omega)}} A_1(\omega) - \sqrt{D(\omega)}\ e^{-\ell\sqrt{D(\omega)}} A_2(\omega)\right\} \ . \tag{3-13}$$

The above can be rewritten in matrix form as follows

$$\begin{matrix} I_1(\omega) \\ I_2(\omega) \end{matrix} = \left.\begin{matrix} Z^{-1}(\omega) & 0 \\ 0 & Z^{-1}(\omega) \end{matrix}\right| \cdot \begin{matrix} V_g(\omega) \\ V_g(\omega) \end{matrix} + \begin{matrix} Y_1(\omega) & Y_2(\omega) \\ Y_2(\omega) & Y_1(\omega) \end{matrix} \begin{matrix} V_1(\omega) \\ V_2(\omega) \end{matrix} \qquad (3\text{-}14)$$

where

$$\begin{aligned} Y_1(\omega) &= -Z^{-1}(\omega)W(\omega)\left[\sqrt{D(\omega)}\left[-e^{2\ell\sqrt{D(\omega)}}+I\right]^{-1}+\sqrt{D(\omega)}\left[e^{-2\ell\sqrt{D(\omega)}}-I\right]^{-1}\right]W^{-1}(\omega) \\ &= Z^{-1}(\omega)W(\omega)\sqrt{D(\omega)}\left[\left(e^{2\ell\sqrt{D(\omega)}}-I\right)^{-1}-\left(e^{-2\ell\sqrt{D(\omega)}}-I\right)^{-1}\right]W^{-1}(\omega) \\ &= Z^{-1}(\omega)W(\omega)H_1(\omega)W^{-1}(\omega) \\ Y_2(\omega) &= Z^{-1}(\omega)W(\omega)\sqrt{D(\omega)}\left[\left[e^{2\ell\sqrt{D(\omega)}}-I\right]^{-1}e^{\ell\sqrt{D(\omega)}}-\left[e^{-2\ell\sqrt{D(\omega)}}-I\right]^{-1}e^{-\ell\sqrt{D(\omega)}}\right]W^{-1}(\omega) \\ &= Z^{-1}(\omega)W(\omega)\sqrt{D(\omega)}\left[2\left(e^{\ell\sqrt{D(\omega)}}-e^{-\ell\sqrt{D(\omega)}}\right)^{-1}\right]W^{-1}(\omega) \\ &= Z^{-1}(\omega)W(\omega)H_2(\omega)W^{-1}(\omega)\ , \end{aligned} \qquad (3\text{-}15)$$

where $H_1(\omega), H_2(\omega)$ are diagonal matrices of which the diagonal elements are

$$\begin{aligned} H_{1_{ii}} &= \frac{\sqrt{D_i}}{\tanh(\ell\sqrt{D_i})} \\ H_{2_{ii}} &= \frac{\sqrt{D_i}}{\sinh(\ell\sqrt{D_i})}\ , \end{aligned} \qquad (3\text{-}16)$$

where D_i is the ith eigenvalue of matrix $K(\omega)$.

From Eq. (3-14), an equivalent circuit can be derived representing a multiphase transmission line section in the presence of GIC. Figure 3-4 illustrates the equivalent circuit. It consists of a passive circuit whose admittance matrix is known and current sources connected at each terminal representing GIC coupling. Note that all parameters of the equivalent circuit are frequency dependent. Thus the admittance matrix and current source values have to be computed explicitly at each frequency of interest.

3.3.2 Tower Grounding Model

Each tower and its grounding structure are represented by a step response. It is defined as the current flowing into the tower from the neutral wire support point when a unit step voltage is applied at the same point.

The step response of the tower and its grounding system can be determined experimentally [30] or analytically [31,32]. When computed analytically, finite element analysis is utilized to solve for the flow of currents in the earth. Then a convolution algorithm is utilized to evaluate the tower and ground step response [31].

The tower model has been validated with data obtained by Bonneville Power Administration (BPA). The validation of this model is reported in Reference 32.

The admittance of the tower and grounding system at any given frequency is computed from the step response with an appropriate Fourier transform.

3.3.3 Integrated Model

The equivalent circuit of the entire transmission line is constructed by combining the equivalent circuits of each conductor section and tower grounding systems. The procedure is based on nodal analysis method, where all internal node voltages and currents are eliminated, and all internal current sources are represented by equivalent current sources at the terminals of the line. The resulting equivalent circuit has the same topology as the one for a single line section as illustrated in Figure 3-4.

In order to utilize the developed model in time domain simulation, the equivalent circuit parameters are transformed into the time domain. Specifically, the admittance matrix of the passive part of the equivalent circuit is transformed to an impulse response, and the equivalent current sources (which are also computed as functions of frequency) are transformed into time domain waveforms. A discrete Fourier transform method is used for this purpose.

The Snelson transformation is applied before Fourier transformation to minimize resulting time domain waveform durations (see Reference 33). Specifically, the voltage and current variables are replaced by B and F as follows

$$F(\omega) = V(\omega) + G^{-1} I(\omega) \qquad (3\text{-}17)$$

$$B(\omega) = V(\omega) - G^{-1} I(\omega)$$

where G is a real nxn matrix (n = number of conductors), and

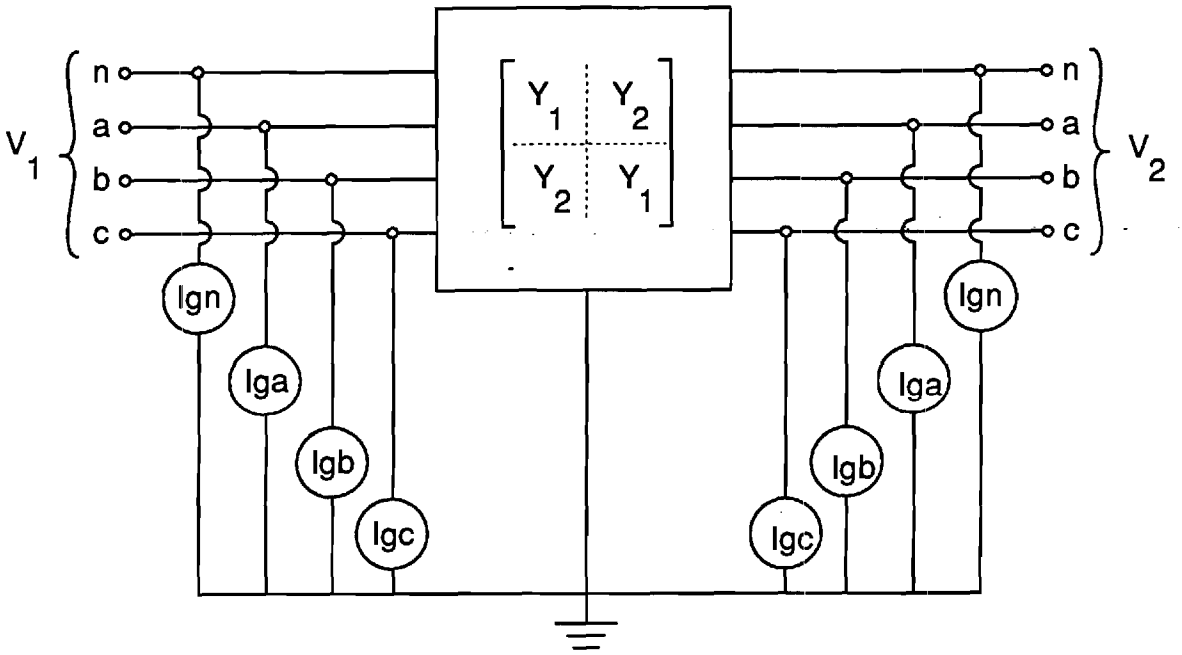

Figure 3-4 : Equivalent Circuit of a Transmission Line Section with GIC Coupling

$$V(\omega) = \begin{matrix} V_1(\omega) \\ V_2(\omega) \end{matrix} \quad , \quad I(\omega) = \begin{matrix} I_1(\omega) \\ I_2(\omega) \end{matrix} .$$

Applying the above transformation to Eq. (3-14) yields

$$\frac{1}{2} G\big(F(\omega)-B(\omega)\big) = \begin{matrix} Z^{-1}(\omega)V_g(\omega) \\ -Z^{-1}(\omega)V_g(\omega) \end{matrix} + \frac{1}{2} Y(\omega)\big(F(\omega)+B(\omega)\big) . \tag{3-18}$$

Solving for $B(\omega)$ yields

$$B(\omega) = M(\omega)F(\omega) + A_g(\omega) , \tag{3-19}$$

where

$$M(\omega) = \big(G(\omega)+Y(\omega)\big)^{-1}\big(G(\omega)-Y(\omega)\big)F(\omega)$$

$$A_g(\omega) = -2\big(Y(\omega)+G(\omega)\big)^{-1} \begin{matrix} Z(\omega)V_g(\omega) \\ Z^{-1}(\omega)V_g(\omega) \end{matrix}$$

The matrix $M(\omega)$ and the vector $A_g(\omega)$ are next transformed into time domain functions using the FFT algorithm

$$m(t) = \mathbb{F}^{-1}\{M(\omega)\}$$
$$a_g(t) = \mathbb{F}^{-1}\{A_g(\omega)\} \tag{3-20}$$

The function matrices $m(t)$ and $a_g(t)$ comprise a time domain model of the entire transmission line with GIC coupling. Specifically, $m(t)$ contains the impulse response of the transmission line (based on Snelson's transformation) and the functions $a_g(t)$ represent the GIC effects. These functions are utilized in a convolution based algorithm, in order to simulate the operation of transmission lines with GIC coupling in the integrated power system. This algorithm is described in the following section.

3.3.4 Convolution Algorithm

The transmission line model is cast into the resistive companion form via a discrete convolution scheme. This technique allows the model to be interfaced with models of other power system components, thus forming a model of an integrated power system. (This is the standard methodology followed by several time domain simulation programs such as the EMTP and the PSTS programs.) Specifically, the model of a transmission line with GIC coupling is represented by the equivalent circuit shown in Figure 3-5. The voltage vector v and current vector i represent the voltages and

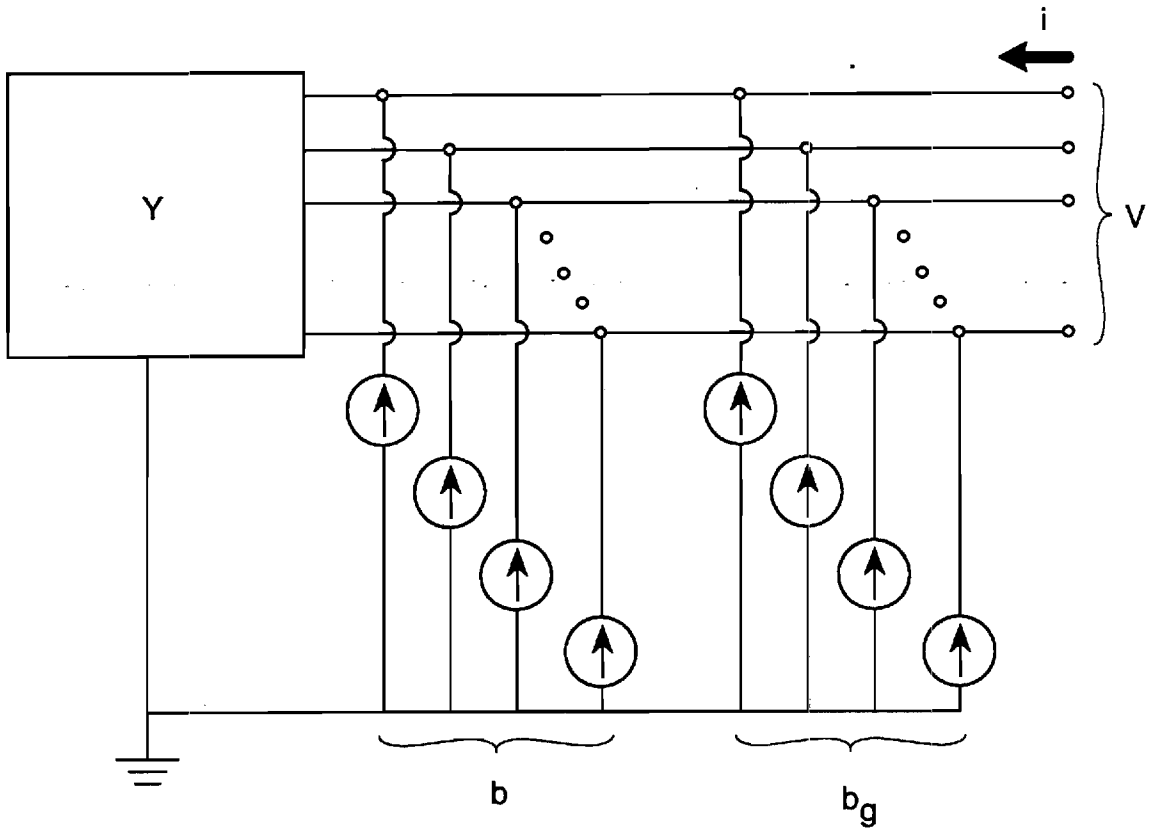

Figure 3-5 : Model of Transmission with GIC Coupling
in the Resistive Companion Form

current injections on each conductor at the ends of the line. The following equation holds for these voltages and currents:

$$Y \cdot v(t) = b(t) + b_g(t) + i(t) \tag{3-21}$$

where Y is the transmission line characteristic admittance matrix, b is the vector of currents depending on past history voltages and currents, and b_g is the vector of currents representing GIC effects. The above equation can be solved by discrete time techniques in terms of the impulse response model defined in the previous section. Specifically, let v_n and i_n represent the values of the voltage and current vectors at the line ends at the n-th time step. Then:

$$Yv_n = b_{n-1} + b_{g_n} + i_n \tag{3-22}$$

where

$$\begin{aligned} Y &= G[I+S_o]^{-1}[I-S_o] \\ b_{n-1} &= G[I+S_o]^{-1} \sum_{k=0}^{N} (S_k - S_{k-1})(v_{n-k} - G^{-1} i_{n-k}) \\ b_{g_n} &= G[I+S_o]^{-1} a_{g_n} \end{aligned}$$

where S_i represents the transmission line step respone (at the ith time interval), i.e. it is the integral of the impulse response m(t), performed in discrete time.

The above equation (3-22) is a resistive companion form representation of a transmission line with GIC coupling. Specifically, the real matrix Y is the admittance matrix of a resistive network (block Y in Figure 3-5). The vector b_{n-1} represents the past history dependent current sources. The entries of the current source vector b_{n-1} are computed by discrete convolution as shown in Eq. (3-22). The vector b_{g_n} are the independent current sources (b_g in Figure 3-5), representing the effects of GIC.

Using these equations, a transmission line with GIC coupling and its interaction with the integrated power system is simulated using the standard methodology for power system transient simulation employed by the EMTP and PSTS programs.

Section 4

INVESTIGATION OF GEOMAGNETICALLY INDUCED EFFECTS ON POWER SYSTEMS

4.1 INTRODUCTION

This section describes the application of the power transmission system model, for the study of geomagnetic disturbances. A test system is selected consisting of a 500 kV transmission line terminated by delta-wye connected transformers at both ends. The response of this system under geomagnetically induced voltages (GIV) is investigated. Specifically, a parametric analysis of the system steady state and transient response to GIV is performed. The effects of GIv level, duration, and transmission system parameters are examined. Finally, the design GIV waveforms corresponding to MHD-EMP and SS are applied to the test system and the resulting system responses are compared.

4.2 DESCRIPTION OF THE TEST SYSTEM

The test system is a simplification of the Minnesota Power Company 500 kV line between Dorsey and Minneapolis. Specifically it consists of a 500 kV transmission line, terminated by three phase transformer banks at both ends. Figure 4-1 illustrates a single line diagram of the test system.

The transmission line data are listed in Table 4-1. During normal operation, the sky wires are not electrically connected to the transmission line towers. Tower configuration data specifies the location of the center of each phase bundle and each sky wire with respect to a Cartesian coordinate system with its origin located at the center of the tower base.

Each of the three phase transformer banks consists of three single phase transformers connected DELTA/GROUNDED Y. The grounded Y side is connected on the 500 kV transmission line (see Figure 4-1). The characteristics of each single phase transformer are as follows:

Voltage	115/288 kV
Power Rating	350 MVA
Leakage Reactance	0.10 pu
Magnetizing Current	0.01 pu
Winding Resistance (high V. side)	1.5 ohms

Table 4-1

Transmission Line Data

GENERAL DATA

Line Length	473 miles
Configuration	3 conductor bundle per phase
Bundle Spacing	18 inches
Tower Spacing	0.25 miles
Tower Footing Resistance	30 Ohms

CONDUCTOR DATA

Conductor	Type	O.D inches	Resistance (Ohms/mile)
Ground Conductors	7/16 steel	0.4375	4.435
Phase Conductors	1192 ACSR	1.3020	0.080

TOWER CONFIGURATION DATA

Conductor	x - coordinate (feet)	y - coordinate (feet)
Phase A	-32.0	97.5
Phase B	0.0	97.5
Phase C	32.0	97.5
Sky Wire 1	-35.0	129.5
Sky Wire 2	35.0	129.5

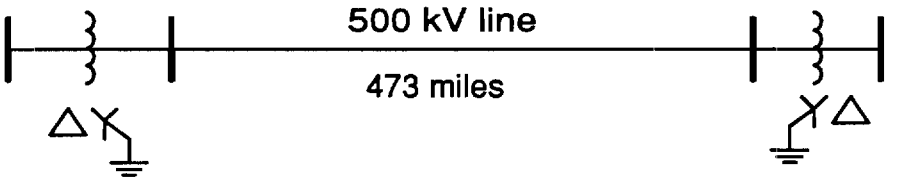

(a)

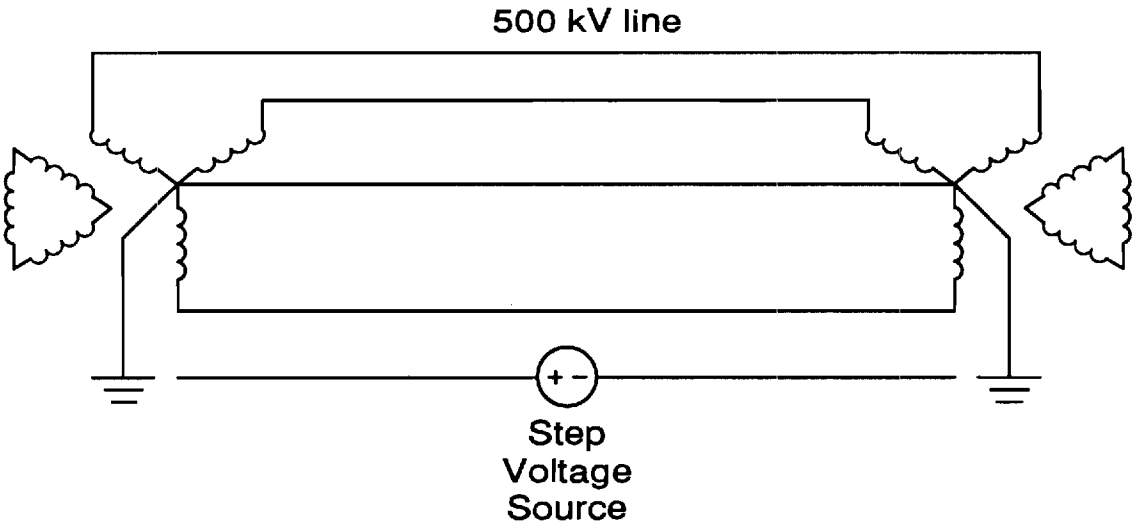

(b)

Figure 4-1 :Test System
a) Single Line Diagram
b) Three Phase Diagram

Transformer saturation is modeled as described in Section 3.2. The transformer core magnetization characteristics are described by a piecewise-linear function which is tabulated in Table 4-2. (The same data are plotted in Figure 3-1.)

The response of the described system is computed assuming a geomagnetically induced voltage (GIV) of step function waveform. Three cases are simulated with different GIV levels as follows:

1. 1.0 volts per mile
2. 10.0 volts per mile
3. 100.0 volts per mile.

The effects of GIV to the test system are assessed as follows: First, the steady state direct current through the transformer is computed for the above GIV levels and various values of line parameters. Next, the transient response of the transformer excitation current is computed for the above GIV levels to determine the time constants involved to reach saturation. Finally, the design GIV waveform from MHD-EMP and solar storms are applied to the test system to determine the relative effects. The results of this study are described in the following sections.

4.3 COMPUTATION OF STEADY STATE RESPONSE

This section presents the computation of the steady state response of the test system under GIC excitation. In order to gain insight in the system parameters that determine the system behavior under GIC excitation, a simple approach is used first. Specifically, an equivalent DC model of the system is constructed. Using, this simple model, the magnitude and distribution of geomagnetically induced currents are evaluated.

The DC model of the test system is constructed by considering only the resistances of each system component. Specifically, an equivalent circuit is constructed containing the DC models of the transformers, transmission line, grounding system, and geomagnetic voltage. This circuit is illustrated in Figure 4-2. The equivalent circuits of each component are described next.

The transformers are represented by their winding resistances. Specifically, the windings of the Y connected (high voltage) side of the transformer exhibit three parallel paths to the flow of the electric current injected at the transformer neutral. Assuming that the windings are identical, the equivalent resistance is 1/3 of the winding resistance of each high voltage winding.

Table 4-2
Transformer Magnetization Characteristics
(High Voltage Side)

Current (kiloamperes)	Flux Linkage (kilowebers-turns)
.00000000	.00000000
.00003429	.10829000
.00005144	.16243500
.00006858	.21603860
.00008573	.26855920
.00010288	.31837260
.00012002	.36363780
.00013717	.40381350
.00017146	.47052010
.00025719	.58990980
.00034292	.67004440
.00051438	.78022940
.00085730	.91104380
.00120022	.98717160
.00171460	1.06189200
.00257190	1.13823600
.00342920	1.18398900
.00514380	1.23965000
.00857300	1.29379500
.01200220	1.31696900
.01714600	1.33564900
.02571900	1.35427500
.03429200	1.36621400
.05143800	1.38240300
.08573000	1.40297800
.12002200	1.41748900
.17146000	1.43548700
.25719000	1.46136800
.34292000	1.48486700
.51438000	1.52867100
.85730000	1.60999600
1.20022000	1.68764000
1.71460000	1.80183200
2.57190000	1.98619600
3.42920000	2.16433300
5.14380000	2.51356800
8.57300000	3.19796100
12.00220000	3.86935900
17.14600000	4.86183700
34.29200000	8.12678100

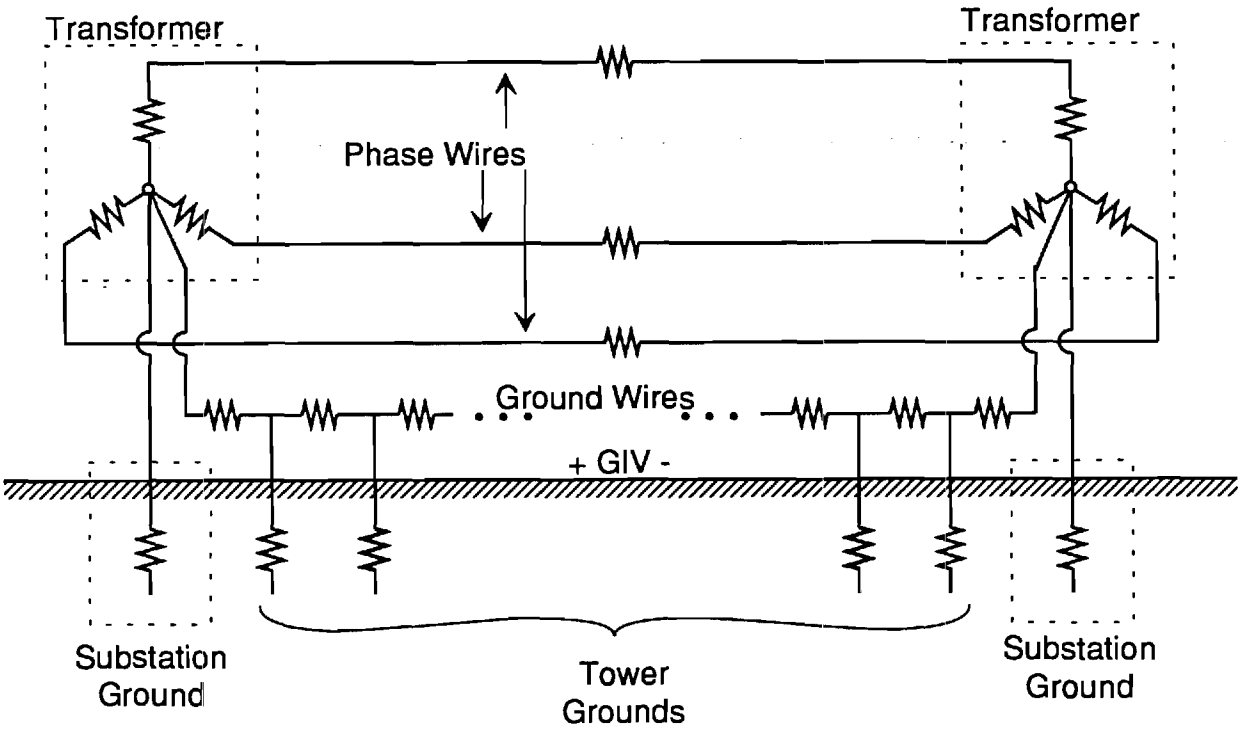

Figure 4-2 : DC Equivalent Circuit of Test System

The transmission line is represented by a DC equivalent circuit. Each of the phase wires is represented by a resistance equal to the total DC resistance of the phase conductor.

The neutral wire is represented by its DC resistance. The neutral wire may or may not be multiply grounded. Figure 4-2 illustrates the tower footing grounding which is represented by its DC resistance.

The substation grounds at each line end are represented by 1 Ohm resistances, connected from the transformer Y side neutral to remote earth.

Finally, the equivalent circuit of the earth containing the geomagnetically induced voltage is represented by a series of Thevenin equivalent circuits connected between consecutive tower grounds and substation grounds. Thus, for each line segment, a separate Thevenin equivalent of the earth is used. Each Thevenin equivalent consists of a voltage source representing the geomagnetically induced voltage, and a resistor representing the earth path resistance. The earth path resistance is highly dependent on frequency. The earth path resistance computed at 0.6 Hz was used.

The above model was employed to study the effects of multiply grounded ground wires on the steady state direct current through the transformer winding. The following values were used for the parametric study:

GIV	1 Volt/mile
Earth path resistance	0.001 Ohm/mile
Tower footing resistance	5, 30, 100, & infinite Ohms
Tower spacing	0.25 mile
Equivalent phase conductor resistance	0.00889 Ohms/mile
Ground conductor resistance	4.435 & 1.240 Ohms/mile
Total line length	473 miles

The results of the parametric study are illustrated in Figure 4-3. The figure is self explanatory. Note that there is a substantial effect of the line grounding parameters on the steady state value of the direct current through the transformer. A well grounded transmission line will mitigate the DC current through the transformer by 50%.

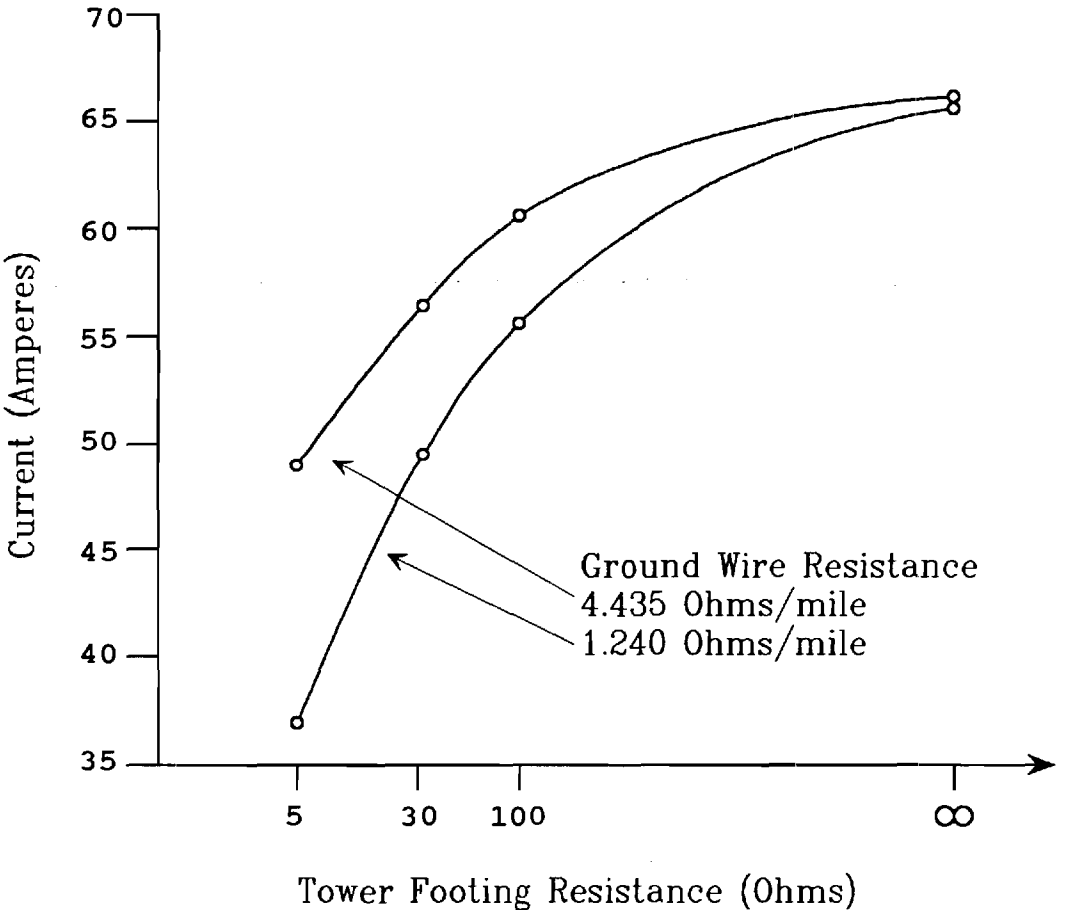

Figure 4-3 : Steady State Direct Current through Transformer Winding

4.4 COMPUTATION OF TIME CONSTANTS TO SATURATION

The described model of the test system was simulated in the time domain to determine the time constants involved to reach steady state operation. Specifically, the time constants were defined as the time required to reach 63% of its steady state value. Figure 4-4 illustrates a typical simulation and the definition of the time constant. The figure also illustrates the parameters of the simulation as well.

The time constants were computed for various parameters as follows:

GIV	1, 10, 100 Volts/mile
Earth Path Resistance	0.001 ohms/mile
Tower Footing Resistance	5, 30, 100 infinite ohms
Tower Spacing	0.25 miles
Equivalent Phase Conductor Resistance	0.00889 ohms/mile
Ground Conductor Resistance	4.435 & 1.240 ohms/mile
Total Line Length	473 miles

The results of the parametric study are illustrated in Table 4-3. Note the wide variation of time constants (145 seconds to 2.3 seconds). System parameters drastically affect time constants.

4.5 COMPARISON OF SATURATION LEVELS DUE TO MHD-EMP AND SS-GIC

An important test which determines the relative effects of MHD-EMP and SS-GIC on power systems is the level of saturation reached due to typical values of GIV from MHD-EMP or SS. For this test the following two comparable strength MHD-EMP and SS-GIV will be assumed:

Case 1. The geomagnetically induced voltage due to MHD-EMP has a time variation as in Figure 2-3 and a peak value of 100 volts/mile.

The geomagnetically induced voltage due to a solar storm is practically DC and has a maximum value of 10 volts/mile.

Case 2. Same as in Case 1 except that the peak values are 10 and 1 volt(s)/mile, respectively.

The maximum levels of saturation were computed for the following range of parameters.

Tower footing resistance	5, 30, 100 & infinite ohms
Tower spacing	0.25 mile
Equivalent phase conductor resistance	0.00889 ohms/mile
Ground conductor resistance	4.435 & 1.240 ohms/mile
Total line length	473 miles

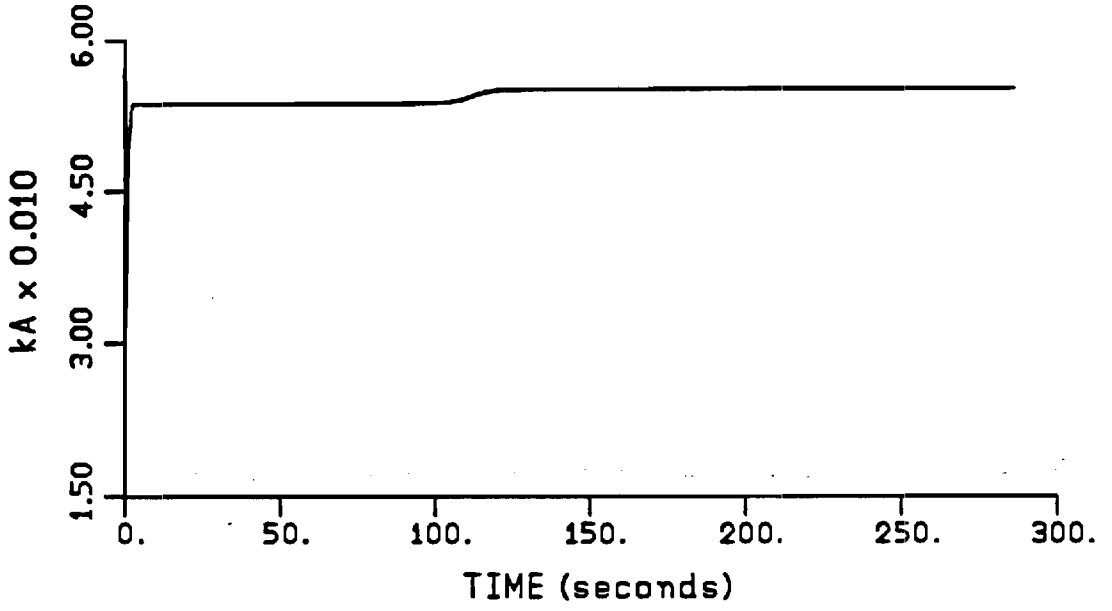

(a) Line Zero Sequence Current

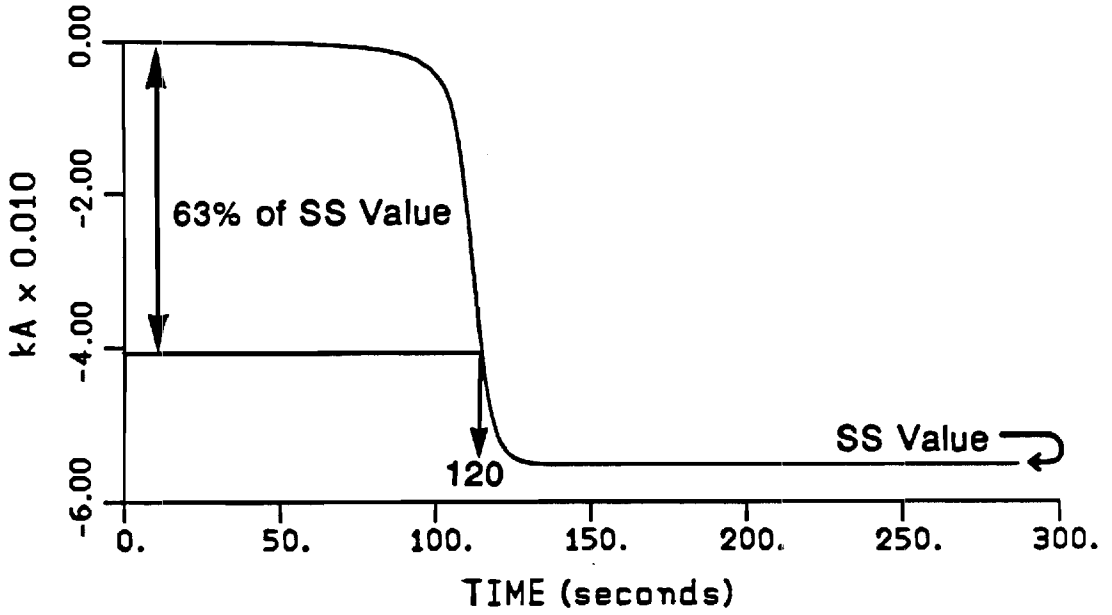

(b) Transformer Magnetization Current

GIV = 1 V/mi, Rtf = 5 Ohms, Rg = 4.435 Ohms/mi

Figure 4-4. Typical Results of the Time Domain Simulation of the Test System.

Table 4-3: Test System Time Constant to Saturation* (in seconds) Versus GIV Level, Tower Footing Resistance (R_t), and Ground Wire Resistance (R_g)

	G.I.V.					
	1 V	/ mile	10 V	/ mile	100 V	/ mile
R_g \ R_t	4.435	1.24	4.435	1.24	4.435	1.24
5	120	145	13.0	16.0	2.8	3.1
30	98	109	11.2	12.5	2.5	2.6
100	93	96	10.6	11.4	2.4	2.5
inf	85	85	10.0	10.0	2.3	2.3

* Time Constant to Saturation is defined as the time required for the transformer magnetization current to reach 63.2% of its steady state value.

The results are illustrated in Tables 4-4 and 4-5. Note that for Case 2, even if the MHD-EMP-GIV is ten times higher than SS-GIV, the maximum saturation level is comparable. For Case 1, the saturation level is much higher for MHD-EMP excitation. The implication of these results are as follows:

Heating: Transformer thermal time constants are on the order of hours [33]. Specifically, Reference 33 reports on measured thermal time constants of a distribution transformer. The time constants have been measured by applying step loads on the transformer. Figure 4-5 is reproduced from Reference 33. It clearly illustrates the relatively long thermal time constants. Thus, thermal heating is probably not a major consideration for GIV excitation due to MHD-EMP because of its relatively short duration of high DC offset flux. On the other hand, heating may be a major consideration for GIV excitation due to solar storms. As a matter of fact, simulations show that saturation in this case lasts several hours. In this case, heating becomes a major consideration.

Loss of Equipment: Due to GIV excitation (SS or MHD-EMP), transformers become generators of harmonics and absorbers of reactive power. Protective relaying, sensing this situation, may trip the transformer. In this case, irrespective of the duration of the GIV excitation, loss of equipment will occur with possibly major consequences such as the Hydro-Quebec blackout.

4.6 CONCLUSIONS

A comprehensive model for studying the effects of geomagnetically induced voltages on power systems has been developed. The model has been used to study the time constants involved in reaching transformer saturation due to GIV and the saturation level versus system parameters.

The most important parameters determining the effects of GIV on power systems are:

1. Level of GIV
2. Duration of GIV
3. Tower grounding impedance
4. Ground wire resistance.

Comparative studies of MHD-EMP-GIV and SS-GIV indicate that (1) for low values of GIV, an MHD-EMP level of 10 times the SS-GIV will cause comparable effects, and (2) for high values of GIV, the short duration of the MHD-EMP mitigates the results only marginally. Since transformer thermal constants are much larger than the duration of MHD-EMP, the general conclusion is that the thermal effects due to MHD-EMP induced voltages on power systems are less severe than those due to solar storm GIV.

Table 4-4: Maximum DC Offset Magnetic Flux (in pu) in Transformer Core Case 1

	SS-GIV = 1V/mile		MHD-EMP-GIV = 10V/mi	
R_t \ R_g	4.435	1.25	4.435	1.25
5	0.129	0.128	0.142	0.136
30	0.130	0.129	0.143	0.140
100	0.130	0.130	0.144	0.143
inf	0.130	0.130	0.146	0.146

Table 4-5: Maximum DC Offset Magnetic Flux (in pu)
in Transformer Core
Case 2

	SS-GIV = 10V/mile		MHD-EMP-GIV=100V/mi	
R_t \ R_g	4.435	1.25	4.435	1.25
5	0.147	0.143	0.292	0.270
30	0.150	0.147	0.300	0.281
100	0.151	0.149	0.310	0.298
inf	0.153	0.153	0.325	0.325

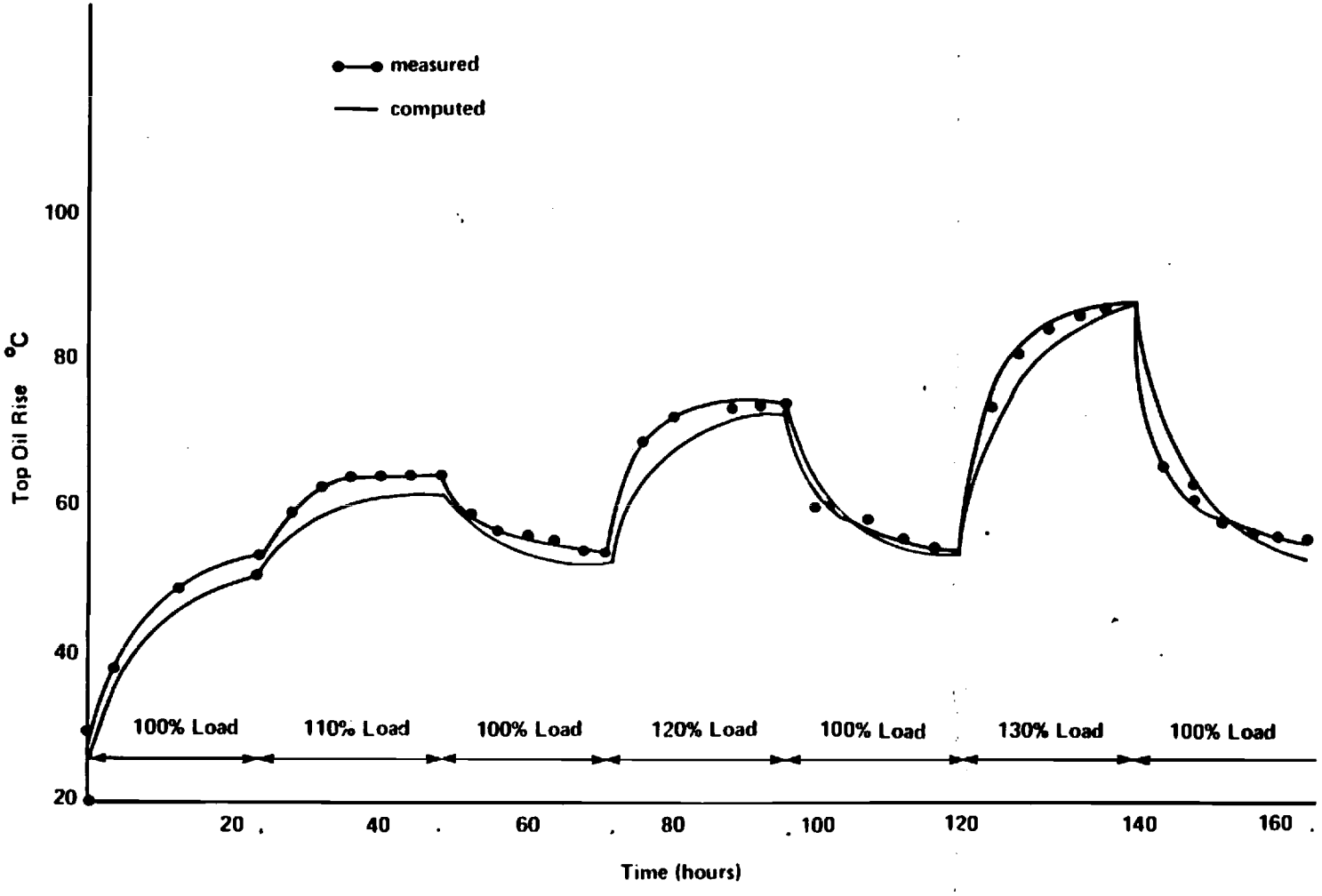

Figure 4-5. Simulated and Measured Top Oil Temperature Rise
(Reproduced from Reference 33)

Section 5

REFERENCES

1. Syun-Ichi Akasofu, "The Dynamic Aurora," Scientific American, pp. 90-97, May 1989.

2. S. Chapman, Solar Plarma, Geomagnetism and Aurora, Gordon and Breach Science Publishers, New York, 1968.

3. V. D. Albertson, "Geomagnetic Disturbance Causes and Power System Effects," 1989 IEEE PES Summer Meeting, Long Beach, California, July 12, 1989.

4. R. Pirjola, "On Currents Induced in Power Transmission Systems During Geomagnetic Variations," IEEE Transactions on Power Apparatus and Systems, vol. PAS-104, no. 10, pp. 2825-2830, October 1985.

5. G. B. Rackliffe, J. C. Crouse, J. R. Legro, and V. J. Kruse, "Simulation of Geomagnetic Currents Induced in a Power System by Magnetohydrodynamic Electromagnetic Pulses," IEEE Transactions on Power Delivery, vol. PWRD-3, no. 1, pp. 392-397, January 1988.

6. J. R. Legro, N. C. Abi-Samra, J. C. Crouse, and F. M. Tesche, "A Methodology to Assess the Effects of Magnetohydrodynamic Electromagnetic Pulse (MHD-EMP) on Power Systems," IEEE Transactions on Power Delivery, vol. PWRD-1, no. 3, pp. 203-209, July 1986.

7. M. Rabinowitz, "Magnetohydrodynamic EMP, Solar Storm GIC, and Substorms," Conference on Geomagnetically Induced Currents, sponsored by Electric Power Research Institute, Burlingame, California, November 8-10, 1989.

8. M. Rabinowitz, "Nuclear Electromagnetic Pulse," Encyclopedia of Science and Technology, 1986 Yearbook, McGraw Hill, New York, pp. 34-47, 1985.

9. C. N. Vittitoe and M. Rabinowitz, "Radiative Reactions and Coherency Modeling in the High-Altitude Electromagnetic Pulse," Physical Review A, vol. 37, no. 6, pp. 1969-1977, March 15, 1988.

10. M. Rabinowitz, "Effect of the Fast Nuclear Electromagnetic Pulse on the Electric Power Grid Nationwide: A Different View," IEEE Transactions on Power Delivery, vol. PWRD-2, no. 4, pp. 1199-1222, October 1987.

11. K. W. Klein, P. R. Barnes, and H. W. Zaininger, "Electromagnetic Pulse and the Electric Power Network," IEEE Transactions on Power Apparatus and Systems, vol. PAS-104, pp. 1571-1577, 1985.

12. C. L. Longmire, "On the Electromagnetic Pulse Produced by Nuclear Explosions," IEEE Transactions on Electromagnetic Compatibility, vol. EMC-20, no. 1, pp. 3-13, February 1978.

13. C. N. Vittitoe, "Did High-Altitude EMP Cause the Hawaiian Streetlights Incident?", Sandia National Labs, Albuquerque, New Mexico, SAND88-00430, 1988.

14. D. P. Millard, A. P. Sakis Meliopoulos, and G. J. Cokkinides, "Parametric Analysis of EMP Induced Overvoltages on Power Lines," IEEE Transactions on Power Delivery, vol. PWRD-3, no. 3, pp. 1224-1231, July 1988.

15. J. R. Wait, Geo-Electromagnetism, Academic Press, Inc., New York, Chapter VI, pp. 184-208, 1982.

16. A. A. Kaufman and George V. Keller, The Magnetotelluric Sounding Method, Elsevier Scientific Publishing Company, New York, Chapter 5, pp. 113-155, 1981.

17. T. Rikitake and Y. Honkura, Solid Earth Geomagnetism, Terra Scientific Publishing Company, Tokyo, Japan, and D. Reidel Publishing Company, Boston, Chapter 11, pp. 267-292, 1985.

18. V. D. Albertson and J. A. Van Ballen, "Electric and Magnetic Fields at the Earth's Surface Due to Auroral Currents," IEEE Transactions on Power Apparatus and Systems, vol. PAS-89, no. 4, pp. 578-584, April 1970.

19. J. R. Wait, "Electromagnetic Surface Impedance for a Layered Earth for General Excitation," Radio Science, vol. 15, no. 1, pp. 129-134, January-February 1980.

20. R. Pirjola and A. Viljanen, "On Geomagnetically-Induced Currents in the Finnish 400 kV Power System by an Auroral Electrojet Current," IEEE Transactions on Power Delivery, vol. PWRD-4, no. 2, pp. 1239-1245, April 1989.

21. D. Park, "Magnetic Field of a Horizontal Current Above a Conducting Earth," Journal of Geophysical Research, vol. 78, no. 16, pp. 3040-3043, June 1, 1973.

22. A. T. Price, "Electromagnetic Induction in a Semi-Infinite Conductor with a Plane Boundary," Quart. J. Mech. and Appl. Math., vol. 3, pt. 4, pp. 385-410, 1950.

23. S. P. Srivastava, "Method of Interpretation of Magnetotelluric Data when Source Field is Considered," Journal of Geophysical Research, vol. 70, no. 4, pp. 945-954, February 15, 1965.

24. R. D. Hibbs and F. W. Jones, "The Calculation of the Electromagnetic Fields of a Sheet Current Source with Arbitrary Spatial Intensity Distribution over a Layered Half Space - I, The General Method and Results," Geophys. J. R. Astr. Soc., vol. 46, pp. 433-452, 1976.

25. W. R. Peltier and J. F. Hermance, "Magnetotelluric Fields of a Gaussian Electrojet," Can. J. Earth Sci., vol. 8, pp. 338-346, 1971.

26. R. D. Hibbs, Jr. and F. W. Jones, "Electromagnetic Induction in the Earth by a Non-Symmetric Non-Uniform Source," J. Geomag. Geoelectr., vol. 25, pp. 75-86, 1973.

27. M. Abramowitz and J. A. Stegun (eds.), Handbook of Mathematical Functions, U.S. Department of Commerce, National Bureau of Standards, 10th ed., pg. 886, 1972.

28. D. Larose, "The Hydro-Québec System Blackout of 13 March 1989," Conference on Geomagnetically Induced Currents, sponsored by Electric Power Research Institute, Burlingame, California, November 8-10, 1989.

29. G. J. Cokkinides and A. P. Meliopoulos, "Transmission Line Modeling with Explicit Grounding Representation," Electric Power Systems Research, vol. 14, no. 2, pp. 109-119, April 1988.

30. W. A. Chisholm and Y. L. Chow, "Travel Time of Transmission Towers," IEEE Transactions on Power Apparatus and Systems, vol. PAS-104, no. 10, pp. 2922-2928, October 1985.

31. A. P. Meliopoulos and M. G. Moharem, "Transient Analysis of Grounding Systems," IEEE Transactions on Power Apparatus and Systems, vol. PAS-102, no. 2, pp. 389-397, February 1983.

32. A. Papalexopoulos and A. P. Meliopoulos, "Frequency Dependent Modeling of Grounding Systems," Proc. Midwest Power Symposium, pp. VI.E. 1-13, 1985.

33. J. K. Snelson, "Propagation of Traveling Waves on Transmission Lines-Frequency Dependent Parameters," IEEE Transactiosn of Power Apparatus and Systems, vol. PAS-91, pp. 85-91, January/February 1972.

34. A. Semlyen and A. Deri, "Time Domain Modeling of Frequency Dependent Three-Phase Transmission Line Impedance," IEEE Transactions on Power Apparatus and Systems, vol. PAS-104, no. 6, pp. 1549-1555, June 1985.

35. R. P. Webb and A. P. Sakis Meliopoulos, "Transformer Tests and Simulation Results," Report to Southern Company Services, May 1986.

36. A. P. Meliopoulos and G. J. Cokkinides, "Effects of Harmonics on Power Transformers," Proceedings of the 2nd International Conference on Harmonics in Power Systems, Winnipeg, Manitoba, Canada, pp. 201-213, October 1986.

Appendix A

DERIVATION OF TRANSMISSION LINE EQUATIONS IN THE PRESENCE OF GIC

Consider an infinitesimal segment of overhead conductor Δx. It is characterized by an inductance, $L' = L\Delta x$, resistance, $R' = R\Delta x$, and shunt capacitance, $C' = C\Delta x$. Assuming that EMP/GIC related electromagnetic fields are slowly varying their direct effect on the line is negligible. However, a substantial voltage can develop along the line direction on the earth surface, due to GIC. Assume that the earth potential difference across the line length, Δx, due to GIC is $V_g \cdot \Delta x$. The equivalent circuit of the line segment is shown in Figure A-1.

$$v_2 - v_1 = -R'i_2 - L' \frac{di_2}{dt} + v_g \cdot \Delta x$$

$$i_2 - i_1 = -G'v_1 - C' \frac{dv_1}{dt}$$

let

$$v_2 - v_1 = \Delta v$$

$$i_2 - i_1 = \Delta i$$

then

$$\frac{\Delta v}{\Delta x} = -Ri_2 - L' \frac{di_2}{dt} + v_g$$

$$\frac{\Delta i}{\Delta x} = -Gv_1 - C \frac{du_1}{dt}$$

taking limit as

$$\Delta x \to 0$$

$$i_1 \to i_2 \stackrel{\Delta}{=} i$$

$$v_1 \to v_2 \stackrel{\Delta}{=} v$$

results in the differential equations

$$\frac{\partial v}{\partial x} = -Ri - L\frac{di}{dt} + v_g$$

$$\frac{\partial i}{\partial x} = -Gv - C\frac{dv}{dt} .$$

where:

$v = v(x,t)$: voltage of point on transmission line located at distance x from line end, with respect to remote earth voltage

$i = i(x,t)$: current at point of transmission line located at distance x from line end

R = line series resistance per unit of length

L = line series inductance per unit of length

C = line shunt capacitance per unit of length

G = line shunt conductance per unit of length

v_g = geomagnetically induced earth surface voltage component along the direction of the line, per unit of length

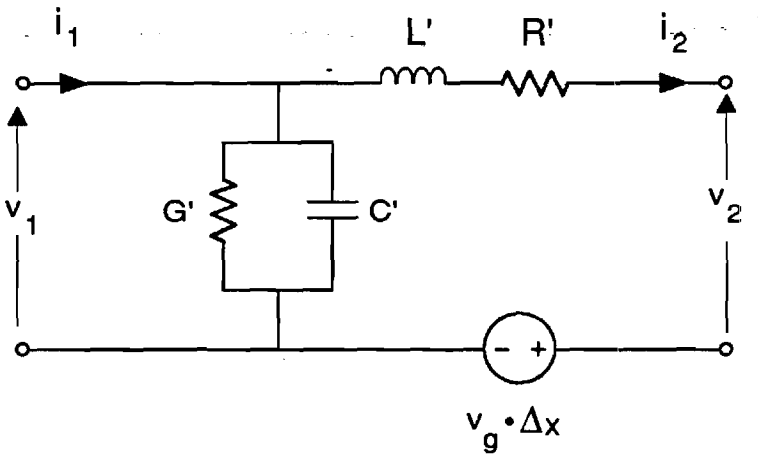

Figure A-1 : Equivalent Circuit of Short Line Segment in the Presence of Geomagnetically Induced Voltage on the Earth Surface.